



HAL
open science

Characterization of the FGFR3 regulatory network in bladder cancer

Aura Ileana Moreno Vega

► **To cite this version:**

Aura Ileana Moreno Vega. Characterization of the FGFR3 regulatory network in bladder cancer. Cancer. Université Paris sciences et lettres, 2020. English. NNT : 2020UPSLOT006 . tel-03778594

HAL Id: tel-03778594

<https://theses.hal.science/tel-03778594>

Submitted on 16 Sep 2022

HAL is a multi-disciplinary open access archive for the deposit and dissemination of scientific research documents, whether they are published or not. The documents may come from teaching and research institutions in France or abroad, or from public or private research centers.

L'archive ouverte pluridisciplinaire **HAL**, est destinée au dépôt et à la diffusion de documents scientifiques de niveau recherche, publiés ou non, émanant des établissements d'enseignement et de recherche français ou étrangers, des laboratoires publics ou privés.



THÈSE DE DOCTORAT
DE L'UNIVERSITÉ PSL

Préparée à l'Institut Curie

**Characterization of the FGFR3 regulatory network
in bladder cancer**

*Caractérisation des réseaux de régulation impliquant FGFR3 dans les
cancers de vessie*

Soutenue par

Aura Ileana

MORENO VEGA

Le 15 septembre 2020

Ecole doctorale n° 582

Cancérologie

Biologie Médecine Santé

Spécialité

**Aspects moléculaires et
cellulaires de la biologie**

Composition du jury :

Daniel METZGER *Président*

Directeur de Recherche,
Institut de Génétique et de Biologie
Moléculaire et Cellulaire (IGBMC)-CNRS

Claude CARON DE FROMENTEL *Rapporteur*

Directeur de Recherche,
Centre de Recherche en Cancérologie de Lyon-INSERM

Céline LEFEBVRE *Rapporteur*

Chef de Projet
Institut de Recherche Servier

Inna KUPERSTEIN *Examineur*

Ingénieur de Recherche
Institut Curie-CNRS

Thomas MERCHER *Examineur*

Directeur de Recherche
Institut Gustave Roussy-INSERM

Isabelle BERNARD-PIERROT *Co-directeur de
thèse*

Chargé de Recherche
Institut Curie-CNRS

François RADVANYI *Directeur de thèse*

Directeur de Recherche
Institut Curie-CNRS



À toi, Jacques

ABSTRACT

Bladder cancer (BLCA) is a frequent cancer in industrialized countries and yet its survival rates have remained largely unchanged for the last three decades. At first diagnosis, the most frequently observed BLCA is non-muscle invasive (NMIBC; 75% of patients). While NMIBC is associated to a good prognosis (88% five-year survival rate), 70% of patients will recur after initial treatment and; depending on tumor grade and stage, 5-75% will progress to muscle invasive disease (MIBC). In contrast to NMIBC, MIBC is life-threatening with a five-year survival of less than 60%, being reduced to less than 6% in presence of metastasis.

One of the two recent promising therapies for BLCA (erdafitinib) is based on the targeting of the frequently altered tyrosine kinase receptor FGFR3 (mutated in 65% of NMIBCs and 15% of MIBCs; translocated in 3% of MIBC). Notwithstanding the positive results observed in clinical trials, the development of drug resistance in patients is anticipated as has been seen in other targeted treatments. A better understanding of the poorly characterized network of FGFR3 is needed to improve current therapies and prevent the onset of resistance mechanisms.

The aims of this thesis project were to: (1) better understand the tumorigenic role and functional consequences of an altered FGFR3 *in vivo*; and (2) identify the master regulators (transcription factors and cofactors; TFs/coTFs) forming part of the gene regulatory network (GRN) of FGFR3 in bladder tumors. The *in vivo* study and characterization of the regulatory network of FGFR3 should enable: 1) a better understanding of the role of FGFR3 in the pathogenesis of BLCA; and 2) the identification of essential network regulators (TFs/coTFs and/or their target genes) with potential therapeutic interest. In particular, the identification of new targets should ameliorate the efficiency of current FGFR3-targeted therapies, and/or reduce the development of drug resistance.

During the first part of my project, we investigated the *in vivo* oncogenic function of an altered FGFR3 through the characterization of a murine model overexpressing a human, frequently mutated FGFR3 (S249C); specifically in the urothelium. Such model represents the first ever demonstration of the oncogenic role of a mutated *FGFR3 in vivo*, with transgenic UPII-hFGFR3-S249C mice developing hyperplasia and low-grade, non-muscle invasive bladder tumors. Moreover, analyses at the histological and transcriptomic level confirmed that tumors from hFGFR3-S249C mice resembled their human counterparts. The characterization of the model further led us to highlight a significantly stronger male dominance in FGFR3 mutated subgroups of human MIBC and NMIBC. As a possible underlying mechanism, we demonstrated androgen receptor (AR) activation by FGFR3 using *in vitro* and *in vivo* models, and its relevance in human tumors was supported by a higher AR activity in FGFR3-mutated NMIBCs and MIBCs.

In a second instance, the combination of a bioinformatic reverse-engineering approach (collaboration with M. Elati) together with experimental validation enabled us to construct a BLCA-GRN that is driven by an altered-FGFR3. Through our inferred BLCA-FGFR3-GRN, we discovered p63, a transcription factor formerly reported to be important in wtFGFR3 MIBCs. In collaboration with the team of C. Lodillinsky, we further corroborated that p63 plays an essential role in the mediation of cell proliferation, migration and invasion of FGFR3-dependent bladder cancer cells. Finally, we showed that FGFR3-mutated NMIBCs exhibited a significantly higher p63 activity compared to wtFGFR3, and this activity was associated with the higher recurrence rate of these tumors. These findings suggest that p63-induced cell migration could participate in enhancing tumor recurrence.

In conclusion, this study has permitted the *in vivo* demonstration that an altered-FGFR3 independently drives bladder tumorigenesis, using a murine model that holds promise for future translational research use. On the other hand, it has provided an altered-FGFR3-driven, BLCA-GRN that could be used by the scientific community for the identification of

essential network regulators. Finally, it has shed-light on an unexpected role of p63 in FGFR3-dependent bladder tumors.

RÉSUMÉ EN FRANÇAIS

Le cancer de la vessie est un cancer fréquent dans les pays industrialisés dont le pronostic a peu changé durant les trente dernières années. Les tumeurs de la vessie sont classées en deux sous-groupes principaux : les tumeurs n'infiltrant pas le muscle vésical (TVNIM ; 75% des cas lors du premier diagnostic) et les tumeurs infiltrant le muscle (TVIM). Les TVNIM sont caractérisées par un taux de survie à 5 ans favorable (88%), mais avec un pourcentage élevé de récurrences (70%) et une progression imprévisible vers une TVIM. Les TVIM sont des tumeurs de pronostic sombre avec un taux de survie à 5 ans de moins de 60%, réduit à 6% en présence de métastases.

Le récepteur aux facteurs de croissance des fibroblastes 3 (FGFR3) est un récepteur à activité tyrosine kinase (RTK) dont le gène est fréquemment altéré dans le cancer de la vessie par des mutations activatrices ponctuelles (65% des TVNIM ; 15% des TVIM) ou par des translocations générant la formation de protéines de fusion (3% des TVIM). En 2019, la Food and Drug Administration a autorisé le premier traitement ciblant les FGFR, notamment pour les patients atteints d'un cancer de la vessie avancé portant une altération génomique de FGFR3. Toutefois, à l'instar de plusieurs thérapies ciblées visant d'autres RTK, des résistances ont déjà été observées lors des essais cliniques utilisant les anti-FGFR et sont probablement la conséquence de mécanismes compensatoires. Ces observations indiquent qu'une meilleure compréhension des mécanismes oncogéniques induits par FGFR3 altéré est requise pour améliorer les traitements actuels et prévenir l'échappement thérapeutique.

Dans ce contexte, les objectifs de cette thèse étaient : (1) d'étudier *in vivo* le rôle tumorigénique et les conséquences fonctionnelles d'une mutation très fréquente de FGFR3, et (2) d'identifier les régulateurs clés (facteurs et cofacteurs de transcription, TFs/coTFs) du réseau de régulation génique contrôlé par FGFR3 dans les tumeurs de vessie.

La première partie de cette thèse a été dédiée à la caractérisation d'un modèle murin surexprimant le gène FGFR3 humain portant une mutation fréquemment observée chez les patients (FGFR3 S249C), via un promoteur spécifique de l'épithélium de vessie. Ce modèle a permis de démontrer pour la première fois *in vivo* le rôle oncogénique de cette mutation conduisant au développement d'hyperplasies puis de tumeurs de type TVNIM de bas grade. Des analyses histologiques et transcriptomiques ont démontré que les tumeurs murines sont comparables aux tumeurs humaines, ouvrant ainsi la possibilité d'utiliser ce modèle en recherche translationnelle. De plus, ce modèle transgénique a permis de mettre en évidence que les patients atteints de TVNIM et TVIM mutées pour FGFR3 sont majoritairement des hommes. En outre, nous avons démontré, *in vitro* et *in vivo*, que FGFR3 activait le récepteur aux androgènes et que l'activité de ce facteur de transcription était plus élevée chez les patients portant une mutation de FGFR3, qu'il s'agisse de TVNIM ou TVIM.

Dans une seconde partie, nous avons construit un réseau de régulation de gènes (GRN) impliquant FGFR3 via un algorithme bioinformatique (collaboration avec M. Elati) et des données transcriptomiques issues de : 1) lignées de cancer de la vessie ou tumeurs de vessie (TVNIM et TVIM) exprimant un FGFR3 muté et 2) modèles précliniques dans lesquels l'expression ou l'activité de FGFR3 a été altérée.

Cette étude a identifié p63, un facteur de transcription préalablement associé à un groupe de tumeurs de vessie présentant un faible taux de mutations de FGFR3, comme un régulateur majeur du GRN contrôlé par FGFR3. Par la suite, le réseau prédit a été validé fonctionnellement en utilisant des données de viabilité cellulaire (criblages à large et petite échelle : CRISPR-Cas9, siRNA). Une étude fonctionnelle, menée en collaboration avec l'équipe de C. Lodillinsky, a permis de déterminer le rôle essentiel de p63 dans le contrôle de la viabilité, la prolifération, la différenciation et la migration des lignées de cancer de vessie exprimant FGFR3 muté. De plus, au sein des TVNIM, les tumeurs mutées FGFR3 présentent une activité plus forte de p63 comparées aux tumeurs non mutées, laquelle est

associée à un taux de récurrence plus élevé. Ces résultats originaux suggèrent que le rôle pro-migratoire de p63 pourrait favoriser la récurrence des tumeurs TVNIM FGFR3 mutées.

En conclusion, ce projet a permis la démonstration *in vivo* du rôle tumorigénique de FGFR3 muté via la mise en place d'un modèle murin qui pourra être utilisé en recherche translationnelle. D'autre part, ces travaux ont contribué à l'identification de régulateurs essentiels faisant partie du réseau de gènes impliquant FGFR3 dans les tumeurs de vessie. Enfin, cette étude a clarifié un rôle inattendu de p63 dans les tumeurs de vessie exprimant un FGFR3 muté.

REMERCIEMENTS

Je souhaite remercier mes directeurs de thèse, François Radvanyi et Isabelle Bernard-Pierrot, de m'avoir accueilli au sein de leur laboratoire et de m'avoir guidé tout le long de ma thèse, me permettant de grandir scientifiquement. Un très grand merci pour votre soutien.

J'aimerais également sincèrement remercier Claude Caron de Fromental (Centre de Recherche en Cancérologie de Lyon) et Céline Lefebvre (Institut de Recherche Servier) d'avoir accepté de consacrer de leur temps pour évaluer mon travail de thèse en tant que rapporteurs, ainsi que Inna Kuperstein (Institut Curie), Thomas Mercher (Institut Gustave Roussy) et Daniel Metzger (Institut de génétique et de biologie moléculaire et cellulaire ; IGBMC) pour leur participation à mon jury de thèse.

J'adresse aussi mes remerciements aux membres de mon comité de thèse, Martin Dutertre (Institut Curie), Thomas Mercher (également dans mon jury de thèse) et Franck Toledo (Institut Curie) pour avoir suivi le progrès de mon projet de thèse et avoir partagé leurs conseils toujours très pertinents.

Je remercie toutes les personnes avec qui j'ai pu collaborer, permettant ainsi l'enrichissement de ce projet : les collaborateurs de l'Université de Lille ; Wajdi Dhifli, Mohamed Elati, Julia Puig, Noémie Oliveira da Costa, et les collaborateurs de l'Instituto de Oncologia Angel H. Roffo (Argentine) ; Catalina Lodillinsky et Macarena Zambrano (a big thank you to our collaborators in Argentina). Un vif merci aux collaborateurs de la plateforme GenomEast de l'IGBMC pour leur aide aux analyses de ChIP-seq : Christelle Tibault-Carpentier, Bernard Jost, Damien Plassard et Tao Ye ; ainsi qu'aux collaborateurs de Medipath et Urosphere et la plateforme de séquençage et l'animalerie de l'Institut Curie.

Un très grand et chaleureux merci à tous les membres (actuels et anciens) de l'équipe d'Oncologie Moléculaire : Hélène pour les conseils sur R et sur ChIP-seq ; Jacqueline, Florent, et Laure pour la bonne ambiance et les rires ; Florent à nouveau pour tous tes conseils et toute ta formation ; Virginia, Daniela et Clémentine pour les soirées LatinOM ; Élodie, merci de m'avoir appris R, Céline, Jing, Elo, Jennifer, Luc, Nanor, Yanish et Linda ; pour les bons moments partagés au labo ou aux afterworks, Mingjun, Xiangyu et Clarice pour tout le travail en équipe pour les articles scientifiques. Enfin, merci à tous les membres de l'équipe pour la bonne ambiance, le soutien et tous les moments conviviaux. Un très grand merci aussi à Michèle, qui a toujours été là pour m'aider.

Merci aussi aux autres doctorants de l'Institut Curie et d'ailleurs, avec qui j'ai participé à différents projets passionnants : YRLS 2019, ADELIIH 2020, Les Petits Déjeuners Professionnels. Gracias Carlos y Maria por los hispanojueves.

Je remercie fortement mes proches : mes amis et ma famille (en France, au Mexique, en Hollande et en Allemagne) pour tout leur soutien et leur aide pendant ces trois ans et demi. Gracias amigos y familia.

Mais, surtout, merci à toi Jacques, pour ton soutien infaillible durant tous les jours de ce long projet.

CONTENTS

INTRODUCTION	1
I. BLADDER CANCER	1
1.1 <i>The urinary bladder</i>	1
1.2 <i>Bladder cancer</i>	2
1.2.1. Epidemiology	2
1.2.2. Risk Factors	3
1.2.3. Clinical Phenotypes and Molecular Pathogenesis	3
1.2.4. Molecular Subtypes	6
1.2.5. Current and emerging therapies	10
II. FGFR3	13
2.1 <i>Structure</i>	13
2.2 <i>Signaling</i>	14
2.3 <i>Deregulation of the FGFR3 signaling and disease</i>	15
2.4 <i>FGFR3 and bladder cancer</i>	16
2.5 <i>FGFR3 as a therapeutic target in bladder cancer</i>	18
2.5.1 Small-molecule tyrosine kinase inhibitors	18
2.5.2 Monoclonal antibodies	19
III. P63	22
3.1 <i>Structure and isoforms</i>	22
3.2 <i>Role in development and disease</i>	24
3.3 <i>P63 and bladder cancer</i>	25
IV. PRECLINICAL MODELS OF BLADDER CANCER	26
4.1 <i>Bladder Cancer Derived Cell Lines</i>	26
4.2 <i>Bladder Cancer Mouse Models</i>	27
4.2.1 Non-Autochthonous Mouse Models	28
4.2.2 Autochthonous Mouse Models	29
V. GENE REGULATORY NETWORKS IN BLADDER CANCER	31
5.1 <i>Main computational methods for GRN inference</i>	33
5.2 <i>Top-down GRN inference</i>	35
5.3 <i>Bottom-up GRN inference</i>	36
5.4 <i>Choice of algorithm for the characterization of the FGFR3 GRN in bladder cancer</i>	38
CoRegNet H-LICORN	38
OBJECTIVES	40
RESULTS	44
CHAPTER 1. TRANSGENIC HFGFR3-S249C MOUSE MODEL	45
1.1 <i>Introduction</i>	45
1.2 <i>Results</i>	47
1.3 <i>Discussion</i>	77

CHAPTER 2. FGFR3 GENE REGULATORY NETWORK IN BLADDER CANCER.....	80
2.1 Introduction.....	80
2.2 Results.....	82
2.3 Discussion.....	117
CONCLUSIONS AND PERSPECTIVES	122
BIBLIOGRAPHY	126
APPENDIX	138
<i>Appendix I. Mahe et al 2018. An FGFR3/MYC positive feedback loop provides new opportunities for targeted therapies in bladder cancers. EMBO Molecular Medicine 2018.</i>	<i>140</i>

FIGURES AND TABLES

Figure 1. Anatomy of the bladder and its tissue layers.....	1
Figure 2. The different cell types of the urothelium.	2
Figure 3. Types of bladder cancer: Staging and grading.....	4
Figure 4. Potential pathways of bladder tumorigenesis.....	6
Figure 5. Molecular classes of non-muscle invasive bladder carcinoma (NMIBC) and possible progression pathways.....	7
Figure 6. Consensus molecular classes of muscle-invasive bladder carcinoma (MIBC).	9
Figure 7. Structure of the fibroblast growth factor receptor proteins (FGFRs).	13
Figure 8. FGFR signal transduction pathway.....	15
Figure 9. Mechanisms of deregulated fibroblast growth factor receptor signaling	16
Figure 10. Localization and frequency of FGFR3 point mutations in bladder cancer.....	17
Figure 11. Mechanisms of acquired resistance to fibroblast growth factor receptor inhibition.	20
Figure 12. Structure of P63 and its protein isoforms.	23
Figure 13. Mouse models of bladder cancer.....	27
Figure 14. Schematic representation of a gene regulatory network (GRN).	31
Figure 15. General approach for inferring a gene regulatory network (GRN) from gene expression data.....	32
Figure 16. Interdisciplinary workflow of gene regulatory network (GRN) inference.	37
Figure 17. Inference of a context-specific cooperativity network using CoRegNet H-LICORN.	39

LIST OF ABBREVIATIONS

Abbreviation	Description
AKT	AKT Serine/Threonine Kinase 1
APOBEC	Apolipoprotein B Mrna Editing Enzyme, Catalytic Polypeptide-Like
AR	Androgen Receptor
ARACNE	Algorithm For The Reconstruction Of Accurate Cellular Networks
ATUB	Alpha tubulin
Ba/sq	Basal Squamous
BAIAP2L1	Bai1 Associated Protein 2 Like 1
BBN	N-Butyl-N-(4 Hydroxybutyl)Nitrosamine)
BCAT	Beta catenin
BCG	Bacille Calmette Guérin
BLCA /Bca	Bladder Cancer
BRAF	B-Raf Proto-Oncogene, Serine/Threonine Kinase
Cas9	CRISPR Associated Protein 9
CDKN2A	Cyclin Dependent Kinase Inhibitor 2A
ChIP	Chromatin Immunoprecipitation
CIS	Carcinoma In Situ
CK	Cytokeratin
coTF	Cofactor
CRISPR	Clustered Regularly Interspaced Short Palindromic Repeats
CRK	CRK Proto-Oncogene, Adaptor Protein
CTLA4	Cytotoxic T-Lymphocyte-Associated Protein 4
DAG	Directed Acyclic Graph
DBD	DNA-Binding Domain
EGFR	Epidermal Growth Factor Receptor
EMT	Epithelial Mesenchymal Transition
ENCODE	Encyclopedia Of DNA Elements
ER	Estrogen Receptor
ERBB2 / HER2	Erb-B2 Receptor Tyrosine Kinase 2
ESR1	Estrogen Receptor 1
FANFT	N-[4-(5-Nitro-2-Furyl)-2-Thiazolyl]Formamide
FANTOM	Functional Annotation Of The Mammalian Genome
FDA	Food And Drug Administration
FGF	Fibroblast Growth Factor
FGFR	Fibroblast Growth Factor Receptor
FGFR3	Fibroblast Growth Factor Receptor 3
FOXA1	Forkhead Box A1
FOXM1	Forkhead Box M1
FRS2	Fibroblast Growth Factor Receptor Substrate 2
GATA3	Gata Binding Protein 3
GC	Gemcitabine
GEM	Genetically Engineered Mice
GENIE3	Gene Network Inference with Ensemble Of Trees
GLOBOCAN	Global Cancer Observatory

GO	Gene Ontology
GRN	Gene Regulatory Network
H-LICORN	Hybrid -Learning Co-Operative Regulation Networks
H-RAS	Harvey Rat Sarcoma
HSPG	Heparan Sulgate Proteoglycan
IPA	Ingenuity Pathway Analysis
ITFP	Integrated TF Platform
JAK	Janus Kinase
JNK	C-Jun N-Terminal Kinase
KD	Knock-Down
KEGG	Kyoto Encyclopedia of Genes and Genomes
KIT	Kit Proto-Oncogene, Receptor Tyrosine Kinase
KLF5	Kruppel Like Factor 5
KMT2C	Lysine Methyltransferase 2c
KMT2D	Lysine Methyltransferase 2d
KO	Knock-Out
K-RAS	Kirsten Rat Sarcoma
KRT	Cytokeratin
LICORN	Learning Co-Operative Regulation Networks
LIMMA	Linear Models For Microarray Data
LumNS	Luminal Non-Specified
LumP	Luminal Papillary
LumU	Luminal Unstable
MAPK	Mitogen-Activated Protein Kinase
MEK	Mitogen-Activated Protein Kinase Kinase 1
MIBC	Muscle Invasive Bladder Carcinoma
mmu	<i>Mus Musculus</i>
MNU	N-Methyl-N-Nitrosourea
MT1-MMP	Membrane-Type I-Matrix Metalloproteinase
mTOR	Mechanistic Target Of Rapamycin
MVAC	Methotrexate, Vinblastine, Doxorubicin, And Cisplatin
MYC	MYC Proto-Oncogene, BHLH Transcription Factor
NE-like	Neuroendocrine-Like
NHU	Normal Human Urothelium
NMIBC	Non-Muscle Invasive Bladder Carcinoma
NOTCH3	Notch Receptor 3
OD	Carboxy-Oligomerization Domain
PCNA	Proliferating Cell Nuclear Antigen
PD1	Programmed Cell Death 1 Protein
PDGFR	Platelet-Derived Growth Factor Receptor
PDL1	Programmed Death-Ligand 1
PDX	Patient-Derived Xenograft
PI3K	Phosphatidylinositol 3-Kinase
PIK3CA	Phosphatidylinositol 4,5-Bisphosphate 3-Kinase Catalytic Subunit Alpha
PLCγ	Phospholipase C Gamma
PPARG	Peroxisome Proliferator-Activator Receptor Gamma

Ppi	Protein-Protein Interaction
PTCH1	Patched 1
RAF	Raf Proto-Oncogene, Serine/Threonine Kinase
RAS	Rat Sarcoma
RB1	Retinoblastoma 1
RHOGDI1- RHO-GDP	Dissociation Inhibitor 2
RPS6	Ribosomal Protein S6
RSK	Ribosomal S6 Kinase
RTK	Receptor Tyrosine Kinase
SADDAN	Severe ACH with Developmental Delay and Acanthosis Nigricans
SAM	Sterile Alpha Motif
SKP	Skin-Derived Precursor Cell
STAT	Signal Transducer and Activator of Transcription
TACC3	Transforming Acidic Coiled-Coil Containing Protein 3
TCGA	The Cancer Genome Atlas
TD	Thanatophoric Dysplasia
TF	Transcription Factor
Tfbs	Transcription Factor Binding Site
TID	Transactivation Inhibitory Domain
TKI	Tyrosine Kinase Inhibitor
TMN	Tumor Node Metastasis
TP53	Tumor Protein P53
TP53	Tumor Protein P63
TRIM29	Tripartite Motif Containing 29
TSC1	Tuberous Sclerosis 1
TSS	Transcriptional Start Site
TURBT	Transurethral Resection of A Bladder Tumor
UCC	Urothelial Cell Carcinoma
UPII /UpkII	Uroplakin II
VEGFR	Vascular Endothelial Growth Factor Receptor
ZEB1	Zinc-Finger E-Box Binding Homeobox 1

INTRODUCTION

I. BLADDER CANCER

1.1 The urinary bladder

The bladder is a hollow muscular organ of the urinary system whose function is to collect urine from the kidneys and temporarily stock it before disposal. The bladder wall is made up of four layers: the urothelium, lamina propria, detrusor muscle (muscularis propria) and adventitia (Figure 1).

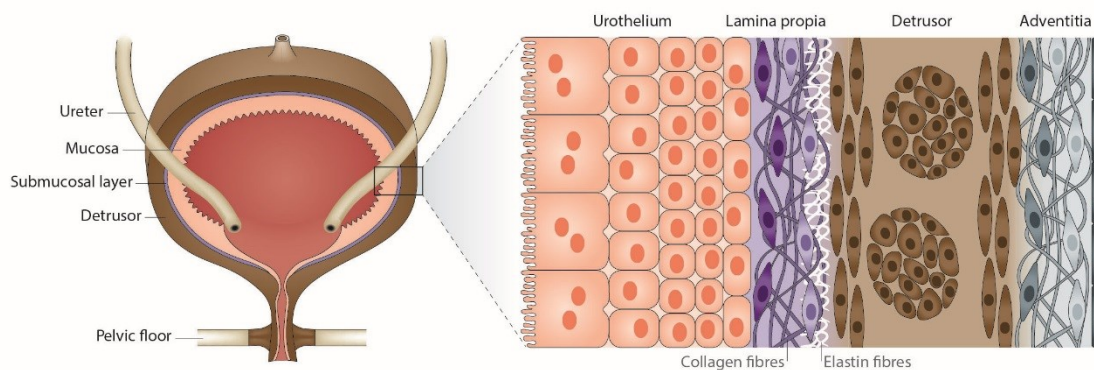


Figure 1. Anatomy of the bladder and its tissue layers.

Left panel. The bladder is an organ of the urinary system composed of four distinct tissue layers: the mucosa (urothelium), the innermost layer lining the hollow lumen; the underlying submucosa (lamina propria), a layer of connective tissue comprised of blood cells, nerves and glands; the thick muscle layer, and the serosa/adventitia; the external layers covering the bladder.

Right Panel. The urothelium is comprised of at least three cell layers including umbrella cells (superficial cells), intermediate cells and basal cells. The lamina propria controls the bladder capacitance and acts as a signal transducer of the central nervous system. The detrusor muscle is a smooth muscle consisting of three layers and constitutes 60-70% of the normal bladder wall. Adapted from Ajalloueiian 2018

Acting as a barrier from toxic urinary substances, the urothelium is a stratified epithelium (transitional epithelium) consisting of at least three cell layers that allow it to contract and expand depending on the amount of urine stored. Three different cell types make up the urothelium and they are characterized based on their size, location and expression of molecular markers. Superficial or umbrella cells are large, terminally differentiated cells that line the lumen of the bladder and express diverse uroplakin proteins and the cytokeratins 18 and 20 (KRT18, KRT20). Intermediate cells are medium sized cuboidal cells which, contrary to the superficial cells, express high-molecular-weight cytokeratins KRT5 and also express the p63 transcription factor. Attached to the basement membrane, basal cells are small cuboidal cells that express KRT14 and the highest levels of p63 and KRT5 (Figure 2)^{1,2}.

INTRODUCTION

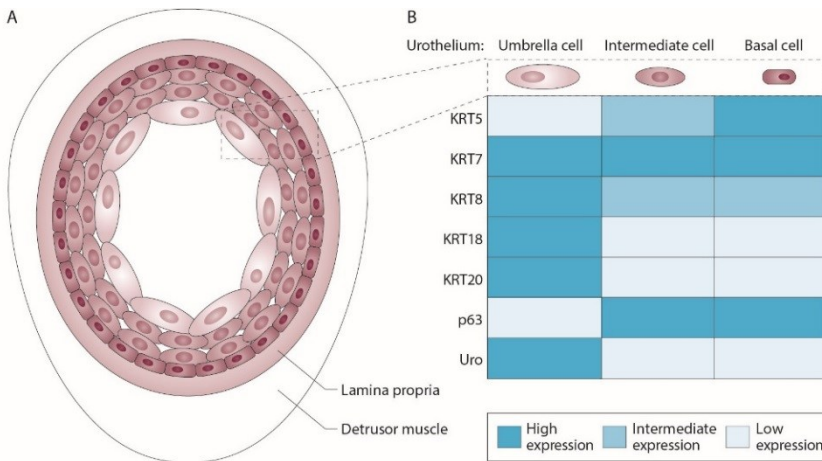


Figure 2. The different cell types of the urothelium.

A. Anatomy of the bladder wall layers and their cellular composition.

B. Outline of the expression levels of cytokeratins (KRTs), the P63 transcription factor and uroplakins (Uro) in the cells of the urothelium. Adapted from Kobayashi 2015 ²

Compared to other epithelia, the urothelium has the lowest rate of cell turnover (3-6 months)³ and yet it is able to rapidly regenerate itself within hours of a pathological or chemically induced injury⁴⁻⁶. Such regeneration process needs to be tightly controlled as an incomplete regeneration could lead to a detrimental barrier breach, whereas an uncontrolled regeneration could result in urothelial hyperplasia and malignant transformation.

1.2 Bladder cancer

1.2.1. Epidemiology

With half a million new cases diagnosed in 2018 and 19.9 million related deaths, bladder cancer is the tenth most common cancer worldwide and it is one of the most frequent cancers in Europe (fourth most common in men). The incidence of bladder cancer is increased with age and there exists a gender disparity with men being three to four-fold more affected than women (Global Cancer Observatory; GLOBOCAN 2018)^{7,8}. Of note, the comparison of bladder cancer incidence in different world populations may result complicated as a result of distinct histopathological definitions. For example, some cancer registries may include non-invasive tumors of tumor stages Tis and Ta (see section 1.2.3 Clinical Phenotypes and Molecular Pathogenesis for further detail on tumor staging) when calculating bladder cancer incidence. As Ta bladder tumors represent 50% of all new bladder cancer diagnoses, the inclusion or omission of such group significantly impacts the calculated incidence (the data here presented is derived from GLOBOCAN 2018, which includes Ta tumors in the analyses).

1.2.2. Risk Factors

Cigarette smoking is the most important risk factor in bladder cancer accounting for approximately 50% of bladder-cancer cases in both men and women⁹. Indeed, high cancer incidences have been observed in certain countries that had elevated smoking rates in the 1980s such as Italy and Spain¹⁰. Of note, risk may be diminished to different degrees depending on the form of tobacco consumption (e.g. pipes, cigar, chewing tobacco)^{11,12}.

Additional risk factors associated to bladder cancer include occupational exposure to carcinogens such as aromatic amines and petroleum products (e.g. polycyclic aromatic hydrocarbons) and can be attributed to less than 8% of bladder-cancer cases. Other bladder-cancer associated environmental risk factors include the consumption of arsenic-contaminated food or water as well as exposure to air pollutants^{13–15}.

Related more closely to the patient, chronic urinary tract infections such as those caused by the parasitic worm *Schistosoma haematobium* (60% prevalence in the Nile Delta, Egypt)¹⁶ have been associated to the development of bladder cancer. Moreover, other studies have reported that there exist genetic predispositions to bladder cancer affecting genes involved in the metabolism of drugs and carcinogens^{17,18}.

1.2.3. Clinical Phenotypes and Molecular Pathogenesis

Clinical Phenotypes

Bladder cancer is a heterogeneous disease with distinct histopathological phenotypes presenting different clinical responses. Transitional cell carcinoma (TCC); now most commonly named urothelial cell carcinoma (UCC)¹, is the most common primary neoplasm (90% of cases). The other less common histological subtypes are squamous cell carcinoma, adenocarcinoma, small-cell carcinoma and sarcoma¹⁰. Bladder cancer is staged according to the TNM (Tumor Node Metastasis) classification system which defines the invasiveness of a tumor based on the depth of penetration of the tumor into the bladder wall and adjacent tissues (T), its spread into regional lymph nodes (N) and the presence or absence of metastases to distant sites (M). Tumors may be further graded into low-grade or high-grade based on basis of architectural and cytological atypia. Grading of tumors; specially NMIBC tumors, is important as it is an independent predictor of disease progression and recurrence^{19,20}.

At diagnosis, the majority of bladder carcinomas (75%) are non-muscle invasive (NMIBC) papillary tumors confined to the urothelium (Ta) or that have invaded the lamina propria (T1).

¹ Urothelial cell carcinomas are the main subject of this thesis and will be referred from here onwards simply as “bladder cancers” or “bladder carcinomas”.

INTRODUCTION

The remaining 25% of cases are tumors that have invaded the different layers of the detrusor muscle and in some cases metastasized to lymph nodes or other organs (MIBC; muscle-invasive bladder cancer) (Figure 3).

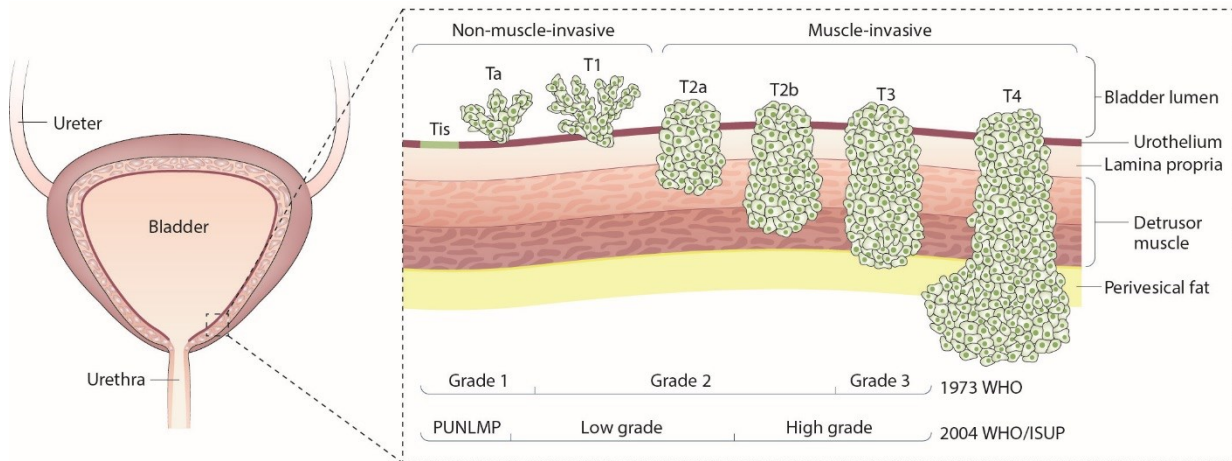


Figure 3. Types of bladder cancer: Staging and grading.

Two major classes of bladder tumors are defined based on their ability to invade the bladder muscle (Non-muscle-invasive versus Muscle-invasive).

Upper right panel part. Staging of bladder cancer based on the Tumor, Node, Metastasis (TNM) system.

Lower right panel part. Histological grading according to the World Health Organization (WHO) classifications published in 1973 and in 2004. Grading allows to give a broad overview of the invasive potential of the tumor. Of note, in spite of being confined to the urothelium, carcinoma in situ (CIS, Tis in the TNM system) is a highly invasive and aggressive cancer. ISUP- International Society of Urological Pathology. PUNLMP- papillary urothelial malignancy of low malignant potential. Adapted from Sanli 2017¹⁰

Molecular Pathogenesis

Two pathways underlying the tumorigenesis of urothelial carcinoma have been described based on clinical and pathological data from human samples and mouse models^{10,21,22}. These distinct but overlapping pathways give rise to papillary NMIBC and non-papillary (solid) MIBC, and comprise distinct molecular alterations such as those affecting the FGFR3/RAS and/or TP53/RB1 signaling (Figure 4). A common, early alteration found in both pathogenesis pathways is the deletion of chromosome 9, found in more than 50% of NMIBC and MIBC tumors^{23–25}. Importantly, such chromosomal alterations impact tumor suppressor genes located on chromosome 9 such as cyclin dependent kinase inhibitor 2A (*CDKN2A*) encoding P16 and P14^{ARF}, patched 1 (*PTCH1*) and tuberous sclerosis 1 (*TSC1*). In NMIBC tumors, our group has reported that loss of *CDKN2A* is associated to a higher progression in the *FGFR3*-mutated tumor subgroup²⁶.

INTRODUCTION

Ta Pathway. Tumors arising through this pathway are non-muscle invasive papillary tumors of stage Ta (accounting for 50% of urothelial tumors) and may develop from simple hyperplasia (flat urothelial hyperplasia) and minimal dysplasia. These tumors are highly recurrent (50-70%) yet few of them progress to muscle-invasive disease²⁰. At the molecular level, low-grade papillary tumors are characterized by activating mutations of *FGFR3*²⁷⁻²⁹, *PIK3CA* (encoding the phosphatidylinositol 4,5-bisphosphate 3-kinase catalytic subunit alpha, p110 α)^{30,31}, and inactivating mutations of the cohesion subunit complex *STAG2*³²⁻³⁴. Within these alterations, the aberrant activation of *FGFR3* constitutes the most common event, observed in approximately 70% of tumors. A functional impact of this alteration (further discussed in section II of this introduction) is the activation of the RAS-MAPK pathway and phospholipase C γ (PLC γ), resulting in increased cell proliferation and survival³⁵. Point mutations impacting *HRAS/KRAS* frequently occur during the development of urothelial hyperplasias and contribute to the progression to non-invasive papillary tumors (Ta-NMIBC). Such mutations (*HRAS/KRAS*) have been revealed to be mutually exclusive with *FGFR3* mutations, and in contrast to *FGFR3* mutations, they are observed at similar frequencies in both NMIBC and MIBC.

Carcinoma *in situ* (CIS) pathway. This pathway is defined by high-grade, muscle-invasive carcinomas (accounting for 20-30% of urothelial carcinomas) that develop from flat CIS/dysplastic lesions or originate *de novo*. Despite the rareness of CIS, most MIBCs are thought to arise from these lesions. Nonetheless, following the discovery of invasive carcinomas harboring *FGFR3* alterations, other models of tumor development have been proposed where low-grade NMIBCs may progress into invasive disease following the loss of *CDKN2A* or inactivation of *TP53/RB1*^{36,37}.

Muscle-invasive carcinomas have a high progression rate (local and distant metastases) and present many genomic alterations. At the molecular level, structural and functional alterations impacting one or both of the tumor suppressor genes *TP53* and *RB1* are frequent³⁸. Other alterations affecting cell proliferation include the upregulated expression of the receptor tyrosine kinase ERBB2 (HER2), and of members of the phosphatidylinositol 3-kinase (PI3K) pathway, pAKT and pRPS6³⁹⁻⁴¹

INTRODUCTION

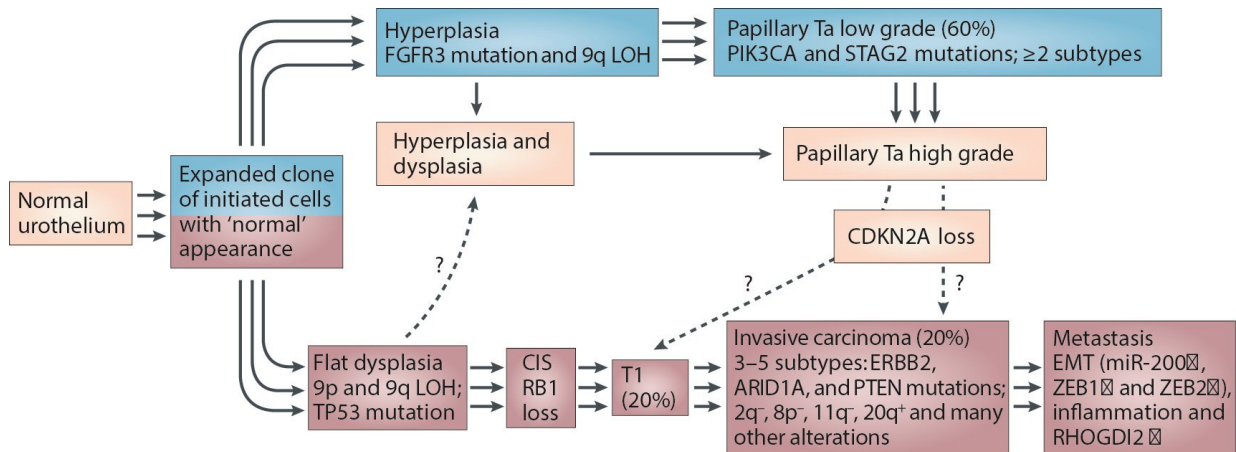


Figure 4. Potential pathways of bladder tumorigenesis.

Histopathological and molecular evidences have highlighted the existence of two possible pathogenesis pathways of papillary non-muscle-invasive bladder cancer (NMIBC low-grade Ta; blue) and solid muscle-invasive bladder cancer (MIBC; red). Percentage of tumors at first diagnosis is indicated. Loss of heterozygosity (LOH) of chromosome 9 is an early event in bladder tumorigenesis, observed in both pathways.

Blue. Low-grade Ta tumors can develop from simple hyperplasia and minimal dysplasia and frequently present activating mutations affecting *FGFR3*. Progression of such tumors into high-grade Ta arises from recurrent mutations in the phosphatidylinositol 4,5-bisphosphate 3-kinase catalytic subunit alpha isoform (*PI3KCA*) and *STAG2* (encoding the cohesin subunit SA-2). *CDKN2A* inactivation suggest a possible progression pathway towards T1 invasive tumors.

Red. MIBCs emerge from flat dysplasias or carcinoma in situ (CIS) presenting *TP53* inactivation and/or *RB1* loss. T1 tumors progress to MIBC (T2) following additional alterations. Dashed arrows represent possible pathways of development. *ARID1A*- AT-rich interactive domain 1A, *EMT*-epithelial-mesenchymal transition, *RHO GDI1*- RHO-GDP dissociation inhibitor 2; *ZEB1*- zinc-finger E-box binding homeobox 1. Adapted from Knowles 2015⁴²

1.2.4. Molecular Subtypes

The grouping of bladder tumors into two categories based on clinical phenotypes and developmental pathways has not sufficed to explain the considerable heterogeneity observed in the clinical response of patients. Consequently, recent efforts have been made to classify bladder tumors using transcriptomic profiles resulting in the identification of multiple molecular subtypes. Being of better prognosis, only three molecular classifications have been derived for NMIBC⁴³⁻⁴⁵. Of those three, the one that is based on the largest set of samples (n=476) is the one by Hedegaard *et al* (Figure 5)⁴³. In contrast, seven independent classifications have been proposed for MIBC⁴⁵⁻⁵².

INTRODUCTION

NMIBC molecular subtypes

Using transcriptomic data from 460 NMIBC patients (low and high-grade Ta, T1 and CIS) and a 117-gene classifier, three major molecular subtypes presenting luminal and basal-like characteristics were identified (Figure 5).

- **Class 1** tumors were composed primarily of non-invasive Ta tumors, characterized by a good prognosis and high expression of early cell-cycle, urothelial differentiation and FGFR3-related genes.
- **Class 2.** Tumors of higher grade and stage, and risk of progression into MIBC were more frequently found in Class 2. Related to this, Class 2 tumors were defined by the expression of late cell-cycle, epithelial mesenchymal transition (EMT)-related and stem-cell-related gene signatures. Interestingly, Class 2 tumors, similar to those of Class 1, expressed KRT20 (CK20) which is normally enriched in the luminal umbrella cells of the urothelium. In this way, Class 2 tumors could represent predecessor tumors of luminal MIBC.
- **Class 3.** Similar to Class 1 tumors, Class 3 tumors exhibited an FGFR3-related gene signature, but also presented markers related to basal-like MIBC (KRT5⁺, KRT14⁺, CD44⁺, KRT20⁻). A high expression of long non-coding RNAs and chromatin remodeling genes, coupled to low expression of cell-cycle genes led to the hypothesis that Class 3 tumors could constitute a subset of dormant NMIBCs. Such tumors would be able to evolve to MIBC after a class shift towards Class 2 tumors (CIS pathway) followed by progression.

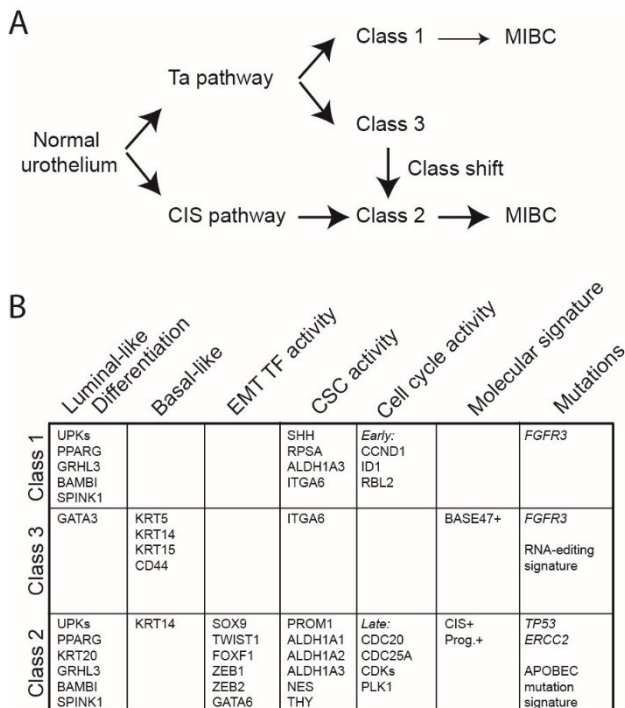


Figure 5. Molecular classes of non-muscle invasive bladder carcinoma (NMIBC) and possible progression pathways.

A. Class 1 and class 3 tumors arise via the Ta pathway, characterized by FGFR3 alterations. Following a shift towards the carcinoma in situ pathway (CIS; class 2), class 3 tumors may further progress into muscle-invasive bladder carcinoma (MIBC).

B. Summary of the different molecular traits defining each of the different classes. Adapted from Hedegaard 2016

INTRODUCTION

MIBC molecular subtypes

The existence of several molecular classifications of MIBC hampered their use for patient stratification in the clinic. For this reason, a consensus classification grouping the previously established signatures was developed (Figure 6)⁴⁸. Six consensus molecular subtypes were established using 1750 MIBC transcriptomic profiles from 18 datasets and the previously published classifiers^{46,47,49–51,53}.

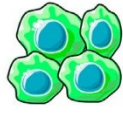
Luminal classes. Three different luminal consensus classes overexpressing an urothelial differentiation signature were identified:

- *Luminal Papillary (LumP)* tumors expressed an activated *FGFR3* gene signature (40% of tumors were enriched in *FGFR3* mutations). As their name indicates it, they were enriched in papillary histomorphology and were associated to the best overall survival. They represented the second largest molecular subtype (24% of samples).
- *Luminal Non-Specified (LumNS)* tumors constituted a small class of tumors (8%) showing a high stromal infiltration. They were the only class of luminal tumors to show an immune infiltration, constituted mainly of B cells. Within the luminal classes, they were of the worst prognosis.
- *Luminal Unstable (LumU)* tumors were the most genomically unstable compared to the other five classes. Contrary to the other luminal subtypes, only LumU tumors presented mutations in *TP53* and *ERCC2*, a gene coding for a protein involved in the nucleotide excision repair pathway.

Other classes

- *Stroma-rich* tumors were characterized by high immune (T and B cells) and stromal (smooth muscle cells, endothelial cells, fibroblasts, myofibroblasts) infiltration. In terms of differentiation, they neither over-express nor under-express a urothelial differentiation signature.
- *Basal-squamous (Ba/sq)* tumors were highly aggressive tumors of poor prognosis, representing the largest class of all (35% of tumors). They were distinguished by alterations of the EGFR signaling pathway (overexpression of the EGFR receptor and its ligands), mutations affecting *TP53* and *RB1*, and a strong immune infiltration.
- *NE-like* tumors displayed a neuroendocrine differentiation and had the worst prognosis of all subtypes.

INTRODUCTION

% of MIBC	24%	8%	15%	15%	35%	3%
Class Name	Luminal Papillary (LumP)	Luminal Non-Specified (LumNS)	Luminal Unstable (LumU)	Stroma-rich	Basal/Squamous (Ba/Sq)	Neuroendocrine-like (NE-like)
						
Differentiation	Urothelial / Luminal				Basal	Neuroendocrine
Oncogenic mechanisms	FGFR3 + PPARG + CDKN2A -	PPARG +	PPARG + E2F3 +, ERBB2 + Genomic instability Cell cycle +		EGFR +	TP53 -, RB1 -, Cell cycle +
Mutations	FGFR3 (40%), KDM6A (38%)	ELF3 (35%)	TP53 (76%), ERCC2 (22%) TMB +, APOBEC +		TP53 (61%), RB1 (25%)	TP53 (94%) RB1 (39%)*
Stromal infiltrate		Fibroblasts		Smooth muscle Fibroblasts Myofibroblasts	Fibroblasts Myofibroblasts	
Immune infiltrate				B cells	CD8 T cells NK cells	
Histology	Papillary morphology (59%)	Micropapillary variant (36%)			Squamous differentiation (42%)	Neuroendocrine differentiation (72%)
Clinical	T2 stage +	Older patients + (80+)			Women + T3/T4 stage +	
Median overall survival (years)	4	1.8	2.9	3.8	1.2	1

* 94% of these tumors present either RB1 mutation or deletion

Figure 6. Consensus molecular classes of muscle-invasive bladder carcinoma (MIBC).

Summary of the molecular and clinicopathological characteristics identified in the different consensus classes of MIBC. The percentage of samples having been assigned to the different classes is represented at the top of the table. Tumor classes are laid out in luminal-to-basal differentiation gradient and neuroendocrine differentiation. Adapted from Kamoun 2019⁴⁸

The molecular classification of bladder tumors has allowed to better understand the complex heterogeneity underlying the disease, but most importantly it has highlighted possible therapeutic targets within the different subtypes. Moreover, distinct responses to treatment have been revealed for each class, meaning that patients may be better stratified in the future, allowing for improved therapy outcomes.

1.2.5. Current and emerging therapies

The choice of primary treatment given to a bladder cancer patient is at present mainly based on the pathological diagnosis and staging of the tumor that is obtained following a transurethral resection (TURBT). Clinical information such as frequency of recurrence, chemotherapy tolerance and tumor multifocality are other important factors that are taken under consideration. Treatment type and efficacy therefore vary greatly depending on the clinical characteristics, stage and associated risk factors of the tumor.

Current therapies

NMIBC Treatment

NMIBC is routinely treated with TURBT. For low-grade Ta tumors (low-risk), TURBT alone (tumor must be completely excised) may suffice although an immediate instillation of chemotherapy is recommended to complete treatment due to an observed variability in tumor recurrence depending on the quality of the surgery⁵⁴⁻⁵⁶. High-risk patients (high-grade Ta and T1) will be treated by a TURBT followed by a single-dose of intravesical immunotherapy with Bacille Calmette Guérin (BCG), a commonly used vaccine against tuberculosis. For tumors presenting an elevated risk of progression or recurrence, intravesical chemotherapy (mitomycin C) is given instead⁵⁶.

MIBC Treatment

Non-metastatic MIBC is managed using multiple approaches involving neo-adjuvant cisplatin-based chemotherapy followed by radical cystectomy (bladder removal) with extended lymphadenectomy. For certain patients, the bladder may be preserved, in which case chemotherapy and radiation are given. Different protocols for the conservative treatment of MIBC exist, and are used differently in diverse countries^{57,58}. Metastatic disease is managed following a combination chemotherapy regimen (GC-gemcitabine and cisplatin or MVAC-methotrexate, vinblastine, doxorubicin, and cisplatin) or checkpoint inhibitors for chemotherapy ineligible patients. Nonetheless, in daily practice the use of cis-platin based chemotherapy has been reported to be limited due to a big percentage of patients (as many as 50%) being ineligible for this kind of treatment⁵⁹. Novel treatments for chemotherapy unfit patients are under investigation, however the clinical outcomes may depend greatly on the population of study (ineligible patients form a very heterogenous group)⁶⁰.

As mentioned before, survival rates vary enormously from one type of bladder cancer to another. In patients with low-grade NMIBC, in spite of a favorable prognosis (10-year recurrence-free survival of ca. 80%), 50-70% of patients will recur and; depending on grade

INTRODUCTION

and stage, from 5% up to 75% of patients will progress to MIBC at 5 years^{54,61,62}. By comparison, MIBC can be life-threatening with 5-year survival rates ranging from less than 50% down to 5% based on lymph node status or distant metastasis^{57,62,63}. The high incidence and recurrence rate of NMIBC, coupled with the poor prognosis of MIBCs make bladder cancer a significant and expensive health problem, necessitating the development of new, more efficient therapies.

Emerging Therapies

For more than two decades the standard care of treatment of bladder cancer remained unchanged, as did its survival rates⁶⁴. Only recently, numerous clinical trials have been put in place to evaluate the therapeutic potential of immunotherapies and targeted therapies in bladder cancer⁶⁵.

Immunotherapies

At present, five immune checkpoint inhibitors (pembrolizumab, nivolumab, atezolizumab, durvalumab and avelumab) have been approved by the Food and Drug Administration (FDA) for use in first or second-line treatment of metastatic MIBC. The main targets of such immunotherapies are programmed cell death 1 protein (PD1) and its ligand (PDL1), however immunotherapies targeting the cytotoxic T-lymphocyte-associated protein 4 (CTLA4) are also being investigated. Based on the observed clinical efficacy in metastatic MIBC, the use of immune check-point inhibitors is being tested in chemotherapy-refractory/ineligible MIBC and BCG-refractory NMIBC⁶⁶⁻⁶⁸.

Targeted therapies

As a result of the molecular characterization of bladder cancer, numerous altered genes/proteins and deregulated signaling pathways of therapeutic interest have been identified^{43,48,50,51,69-71}. Over the past years, several clinical trials in bladder cancer have been established to analyze the efficiency of targeting such molecular alterations. Amongst the most frequently targeted pathways are the PI3K-mTOR signaling or the RTK-RAS-MAPK pathways. Drugs have been developed to target different members of these signaling pathways such as EGFR, FGFR3, PIK3CA, MTOR and ERBB2 (HER2)⁶⁵. Only this year, the FDA approved Balversa (erdafitinib; a pan FGFR inhibitor) as the first targeted therapy in locally advanced or metastatic bladder cancer; reported to have achieved a 40% objective tumor response rate (3% with complete response and 37% with partial response)⁷².

INTRODUCTION

Notwithstanding the promising responses observed for emerging therapies, treatment of MIBC remains challenging. Indeed, only 20% of patients are responsive to immune checkpoint inhibitors and those receiving a targeted therapy eventually become resistant to the treatment^{65,72-74}. A deeper understanding of the underlying molecular mechanisms of bladder cancer is hence essential for the development of better therapeutic strategies.

II. FGFR3

Fibroblast growth factor receptor 3 (FGFR3) belongs to a family of four structurally related, receptor tyrosine kinases (FGFR1-4) playing an important role in embryogenesis and tissue homeostasis. Activating mutations and amplifications affecting *FGFR3* have been associated to a range of developmental and proliferative disorders. In bladder cancer, activating mutations of *FGFR3* are one of the most frequently observed genetic alterations⁷⁵.

2.1 Structure

The FGFR3 protein shares a common structure with the other three members of its family, consisting of an extracellular ligand-binding domain succeeded by a hydrophobic transmembrane domain and an intracellular tyrosine kinase domain. The extracellular domain is composed of an amino terminal hydrophobic signal peptide and three immunoglobulin (Ig) domains that arise by alternative splicing and define the receptor's specificity for its ligands (Figure 7). Many splice isoforms exist for FGFR3. Among them, FGFR3b is expressed in epithelial cells and urothelial carcinoma^{76,77}.

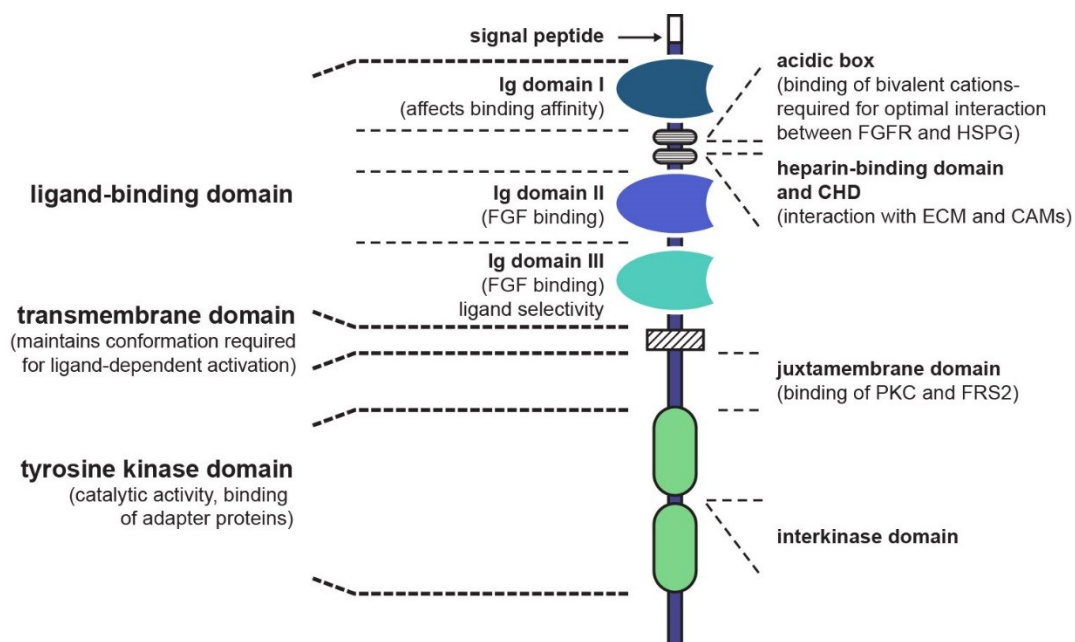


Figure 7. Structure of the fibroblast growth factor receptor proteins (FGFRs).

FGFRs are composed of three major structural domains: the extracellular ligand-binding domain constituted of three immunoglobulin (Ig) domains, a hydrophobic single-transmembrane helix, and an intracellular split tyrosine kinase domain. FGFR-signaling is activated following the binding of FGF to cell surface HSPGs, heparan sulphate proteoglycans that help to stabilize the FGF-FGFR interaction. Ligand-binding specificity is regulated through alternative splicing of the Ig III domain. Transduction of the signaling pathway occurs after a ligand-induced receptor dimerization, followed by the transphosphorylation of the intracellular tyrosine kinases and subsequent binding/phosphorylation of adaptor proteins such as FRS2. Adapted from Iyer 2013⁷⁸

2.2 Signaling

Binding of the fibroblast growth factors (FGFs) to the FGFR extracellular Ig like domains causes the dimerization of the receptor and enables its trans-phosphorylation at key tyrosine residues found in the intracellular domain. Importantly, FGFs do not bind solely to their FGFR receptor, but an additional interaction between FGFs and heparan sulfate proteoglycans (HSPGs) is needed to stabilize the FGF-FGFR complex. Following the activation of the receptor, phosphorylated tyrosine residues function as docking sites for many adaptor proteins that will in turn enable the binding and phosphorylation of other proteins, leading to the transduction of the signaling pathway. There are four main signaling pathways downstream of FGFR activation that are involved in the regulation of cell proliferation, migration and survival: RAS-MAPK, PI3K-AKT, JAK-STAT and PLC γ (Figure 8)^{75,79}. Other signal transduction pathways are activated in a cell-context dependent manner or could arise due to the trafficking of the FGFRs to the nucleus^{75,80}. These include the P38 MAPK (MAPK14), c-Jun N-terminal kinase (JNK), SRC kinase, SHB, CRK and RSK pathways^{79,81}

Because of its role in driving diverse developmental signaling pathways, the FGFR signaling needs to be precisely regulated. Following ligand stimulation, different inhibition mechanisms are deployed and include the endocytosis and degradation of the receptor, inhibition of the receptor's kinase activity and limitation of the accessibility to adaptor proteins.

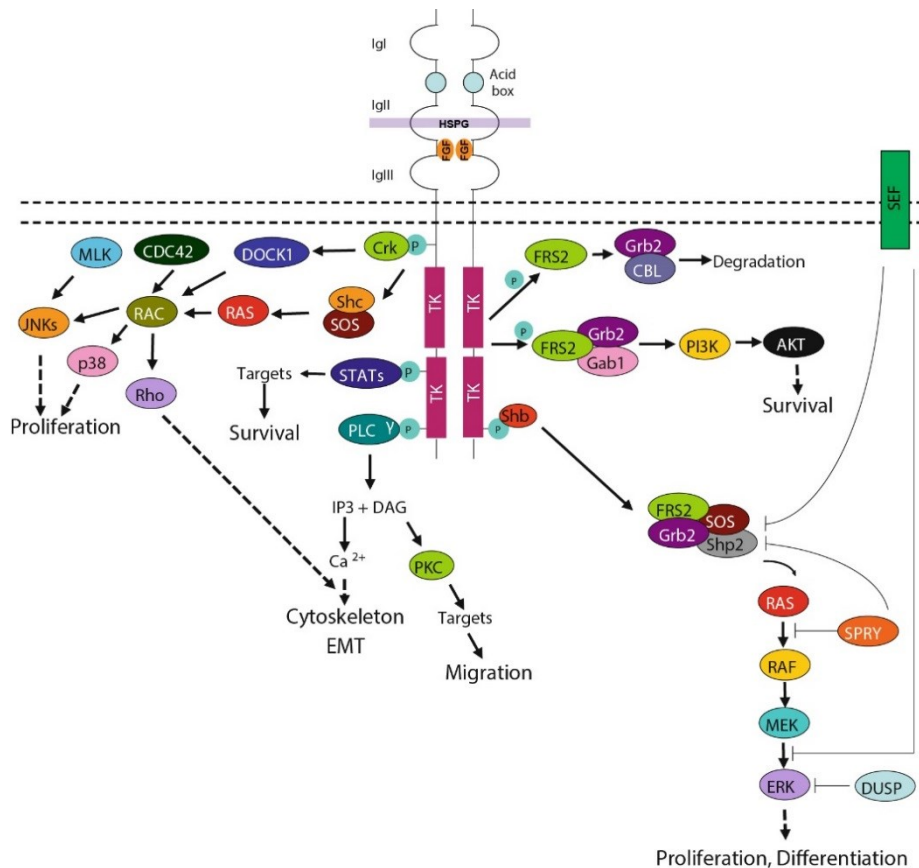


Figure 8

INTRODUCTION

Figure 8. FGFR signal transduction pathway.

Following FGF-ligand binding, signals are transduced to the RAS-MAPK and PI3K-AKT pathways via the FRS2 adaptor protein. Recruitment of PLC γ results in activation of the DAG-PKC and IP $_3$ -Ca $^{2+}$ pathways. Other pathways that may be activated include STATs, P38 MAPKs, JNKs and RSK2 (not shown). Negative regulation occurs at several levels and involves DUSP, SPRY and SEF proteins. FGFR signaling is involved in cell proliferation, survival, differentiation, migration, invasion and epithelial-to-mesenchymal transition (EMT). Adapted from Tiong 2013⁸²

2.3 Deregulation of the FGFR3 signaling and disease

Aberrant activation of the FGFR signaling pathway has been observed in different pathologies including cancer. The mechanisms leading to the alteration of the pathway can originate from genetic alterations or alterations in the signaling of the receptor. Genetic alterations involve the overexpression (due to amplification) or mutation/translocation of the receptor and result in ligand-independent receptor signaling. A deregulation of the autocrine or paracrine signaling of FGF ligands may also result in an abnormally activated FGFR pathway. Other possible disruption mechanisms of the FGFR signaling pathway consist of genetic alterations impacting genes downstream of the receptor (Figure 9).

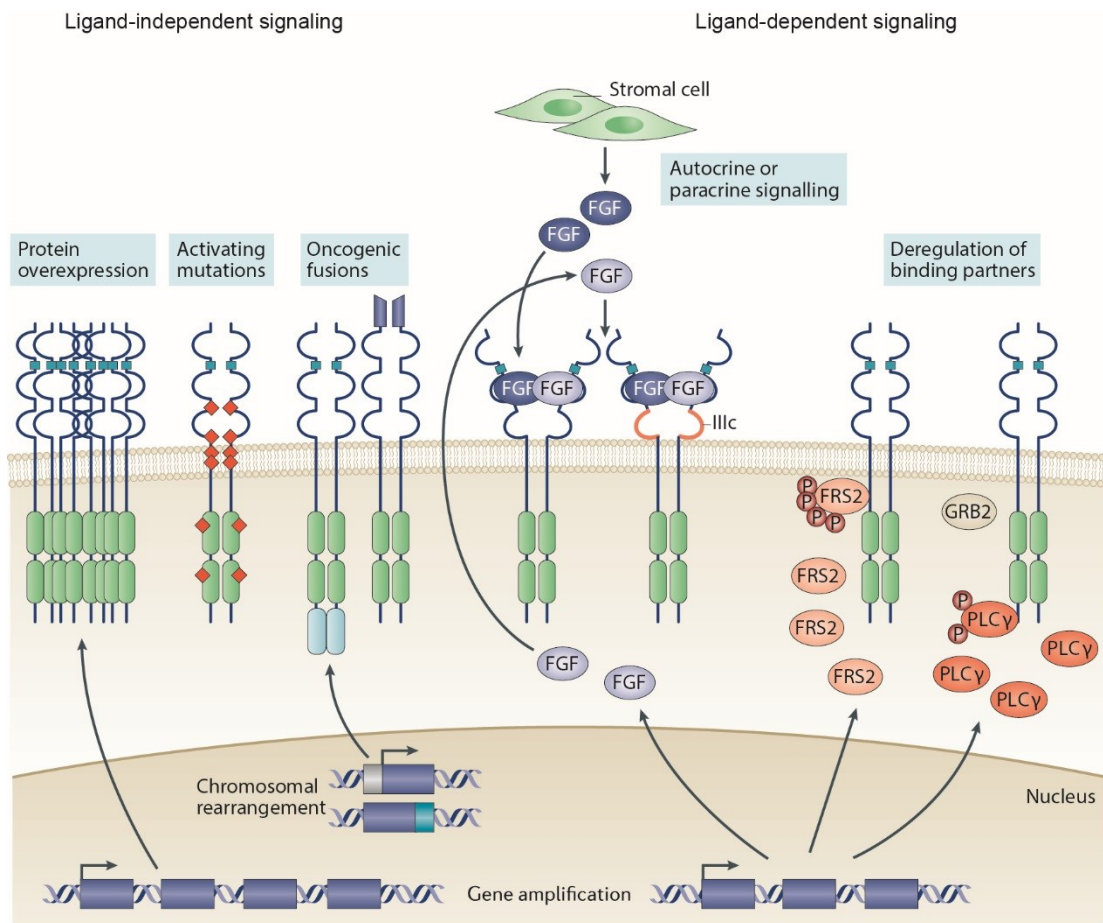


Figure 9

INTRODUCTION

Figure 9. Mechanisms of deregulated fibroblast growth factor receptor signaling

Fibroblast growth factors (FGFs) and the FGF-receptors (FGFRs) may be altered in different ways, deriving in a pathogenic, constitutive FGFR-signaling. Ligand-independent signaling may arise as a result of protein overexpression, often due to gene amplification; activating mutations affecting the dimerization or kinase domain of the receptor; and oncogenic FGFR fusion proteins resulting from chromosomal translocations. Abnormal expression levels of FGF-ligands (produced by the cell or associated stroma) or FGFR-binding partners (FRS2, PLCγ) also lead to a hyperactivated FGFR-signaling. Adapted from Babina 2017⁷³

Just as observed in the normal physiological setting, the cellular context in which an altered FGFR signaling occurs determines its functional outcome. Germline mutations of FGFR3 have been associated to several skeletal disorders where bone growth is severely impacted: hypochondroplasia, achondroplasia, severe achondroplasia with developmental delay and acanthosis nigricans (SADDAN), and thanatophoric dysplasias (TDI, TDII). Functional studies have demonstrated that these mutations lead to a constitutively active receptor, resulting on the inhibition of proliferation and altered differentiation of chondrocytes^{83–85}. Conversely to such inhibitory role, the same activating mutations of FGFR3 have been observed in benign skin epidermal lesions (seborrheic keratoses and epidermal nevi) as well as diverse malignant neoplasms (multiple myeloma, bladder cancer and cervical cancer)^{28,86–90}. The reasons behind such divergent responses remain largely unknown and are probably multi-factorial: cell-type specific expression of adaptor proteins, signal enhancers, transcription factors and co-activators, as well as distinct crosstalk with other signaling pathways.

2.4 FGFR3 and bladder cancer

FGFR3 is one of the most frequently altered genes in bladder cancer. Activating mutations affecting the receptor can be found in 65% of NMIBC and 15% of MIBC^{43,51,91,92}. Moreover, even if mutation rates in MIBC are lower, an overexpression of FGFR3 has been seen in 30% of tumors expressing a wild-type receptor⁹³. Chromosomal translocations that lead to active FGFR3 fusion proteins (FGFR3-TACC3, FGFR3-BAIAP2L1) have also been reported in 3% of MIBC^{51,94}.

The most frequent somatic mutations impacting FGFR3 in bladder cancer are observed at level of the extracellular or transmembrane domain. These mutations cause a cysteine amino-acid substitution that allows for constitutive receptor dimerization through the formation of *de novo* disulfide bridges. At the extracellular domain, the most common activating mutations are S249C and R248C, whereas transmembrane domain mutations comprise G372C and Y375C (Figure 10)⁹⁵. Of all the alterations, the most frequent one is the S249C and a recent study by our team revealed that this over-representation is due to an

INTRODUCTION

APOBEC (Apolipoprotein B mRNA editing enzyme, catalytic polypeptide-like) deaminase mediated mutagenesis⁹². The oncogenic properties of such mutated FGFR3 forms have been well demonstrated *in vitro*^{35,94,96-98}. Indeed, in a study by our team, overexpression of FGFR3-S249C in NIH3T3 cells led to neoplastic transformation as evidenced by their anchorage-independent cell growth, increased proliferation and capacity to develop tumors in xenografted mice⁹⁶. In the same study, the cell viability of MGHU3, a bladder-cancer derived cell line expressing a mutated, constitutively activated FGFR3 (FGFR3-Y375C); was impacted following the knockdown (siRNA) or inhibition of activity of FGFR3. Tomlinson *et al* further demonstrated that the transforming potential of the 97-7 bladder cancer cell line was altered following the knockdown (shRNA) of FGFR3-S249C. Of note, re-expression of FGFR3-S249C in the shRNA expressing cells led to a re-establishment of the neoplastic phenotype, confirming the oncogenic role of FGFR3 in such cell line⁹⁸. The tumorigenic role of FGFR3 fusion proteins (FGFR3-TACC3, FGFR3-BAIAP2L1) has also been validated *in vitro* and in xenograft models^{97,99}.

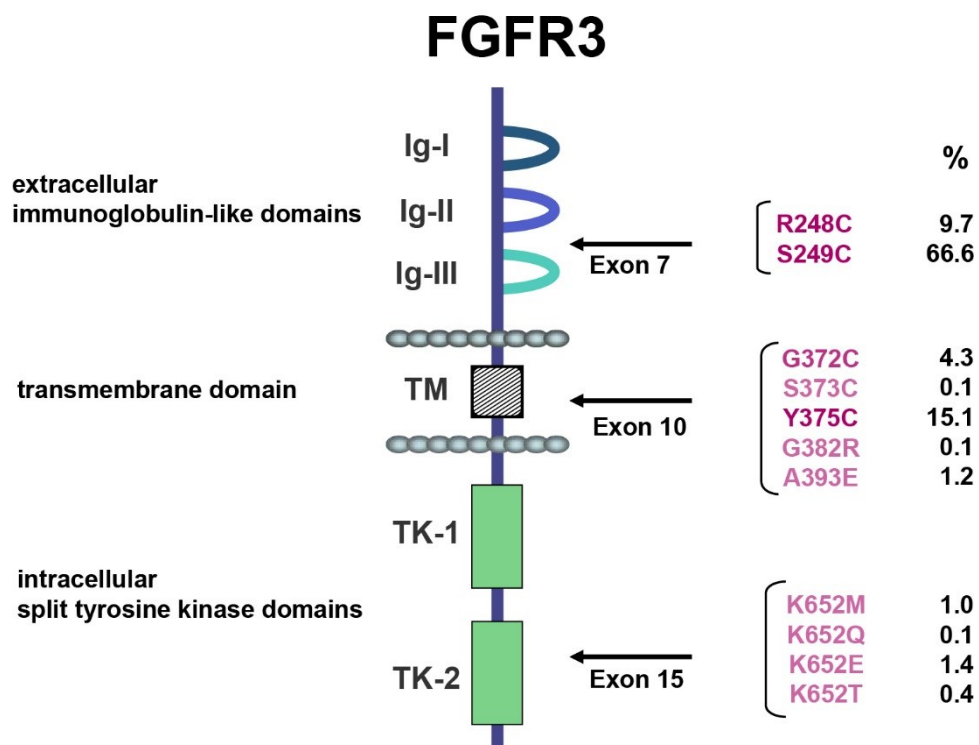


Figure 10. Localization and frequency of FGFR3 point mutations in bladder cancer.

Frequencies are displayed as percentages of all the FGFR3 mutations presently described. Ig- Immunoglobulin-like domain, TK- Tyrosine kinase domain, TM- Transmembrane domain. Adapted from Goebell 2010¹⁰⁰

INTRODUCTION

Until recently, multiple *in vivo* studies had reported that activation of *Fgfr3* alone in genetically engineered mice (GEM) was not sufficient to induce urothelial carcinogenesis. In such studies, tumor formation was observed only when the alteration of *Fgfr3* was coupled to a loss of *Pten*¹⁰¹, a *p53/Rb1* deficiency¹⁰² or to a carcinogen treatment¹⁰³. As part of my thesis project, I characterized a model of GEM overexpressing the human *FGFR3-S249C* in the urothelium. This is the first ever model in which mice overexpressing a *hFGFR3-S249C* develop hyperplastic lesions and low grade papillary urothelial carcinoma, evidencing the tumorigenic role of a mutated FGFR3 *in vivo*.

2.5 FGFR3 as a therapeutic target in bladder cancer

Based on the previous evidence highlighting the role of FGFR3 in bladder tumorigenesis, two main therapeutic strategies have been developed to inhibit its signaling: small-molecule tyrosine kinase inhibitors and monoclonal antibodies.

2.5.1 Small-molecule tyrosine kinase inhibitors

Small-molecule tyrosine kinase inhibitors (TKIs) are molecules mainly targeting the ATP-binding cleft of the kinase domain of multiple receptor tyrosine kinases (RTKs). They exert their inhibitory action by impairing either the catalytic activity of the RTK or the autophosphorylation of its intracellular tyrosine residues. Amongst the TKIs there are non-selective and selective FGFR-TKIs (reviewed in Babina *et al* 2017⁷³).

Non-selective TKIs target multiple RTKs belonging to phylogenetically related families such as vascular endothelial growth factor receptors (VEGFRs) and platelet-derived growth factor receptors (PDGFRs). Non-selective inhibitors are hence less effective at inhibiting the FGFR signaling pathway, and result in more toxic side effects due to their multiple targeting. Examples of these inhibitors include dovitinib (Novartis), ponatinib (ARIAD Pharmaceuticals) and lucitanib (Clovis Oncology). Amongst them, only dovitinib has been tested in a phase II clinical trial in BCG-refractory urothelial carcinoma (NCT01732107). The treatment was not further investigated as long-term treatment resulted in high, frequent toxicity¹⁰⁴.

Selective pan-FGFR TKIs have been developed in order to reduce the multiple TKIs' associated toxicity and increase the FGFR-selective inhibition. Many of them have been evaluated in diverse clinical trials and include: AZD4547, Astra Zeneca; BGJ398, Novartis; Erdafitinib (JNJ42756493), Jansen; Rogaritinib (BAY 1163877), Bayer, and PD173074; Pfizer (only TKI not having been evaluated in clinical trials)^{72,105-108}. Of note, Rogaritinib has been tested in patients selected not on the basis of FGFR3 mutational status, but on high FGFR1-3 expression. Fifty-one patients were evaluated with a disease control rate of 73%, suggesting that tumors may depend on FGFR3 signaling without expressing mutations

INTRODUCTION

affecting the receptor. Of the other inhibitors, erdafitinib is, as previously mentioned, the first FDA approved pan-FGFR inhibitor for the treatment of patients with advanced or metastatic bladder cancer, presenting *FGFR* alterations. Notwithstanding the reduction in toxicity compared to the multi-targeting TKIs, adverse effects are still observed using pan-FGFR inhibitors as they do not only target FGFR3 but also other FGFRs.

2.5.2 Monoclonal antibodies

Monoclonal antibodies targeting the extracellular domain of the FGFR3 have been developed as an alternative to small-molecule tyrosine kinase inhibitors. They act by hampering ligand binding or receptor dimerization, leading to the inhibition of FGFR3 signaling. In contrast to small-molecule tyrosine kinase inhibitors, monoclonal antibodies are less toxic and are highly specific. Furthermore, they may be coupled to immunotoxins or radionucleotides for targeted therapy against cancer cells³⁵.

Studies *in vitro* have demonstrated an inhibitory effect on cell proliferation following the targeting of FGFR3 with monoclonal antibodies in human bladder cancer and multiple myeloma derived cell lines^{109–111}. Subsequently, vofatamab (B-701), an anti-FGFR3 monoclonal antibody is being evaluated in a phase II clinical trial for metastatic urothelial carcinoma (NCT02402542 clinical trial)¹¹².

INTRODUCTION

Despite the preclinical and clinical data evidencing the beneficial outcomes of targeting the FGFR3 signaling in bladder cancer, one of the most important challenges to overcome yet is the development of resistance to treatment. So far, different studies have unveiled the mechanisms of acquired resistance to FGFR-inhibitor including: (i) mutations in the tyrosine kinase domain or ATP-cleft of the receptor or (ii) upregulation of compensatory pathways such as EGFR and ERBB2/3 in bladder cancer (Figure 11)^{113–117}.

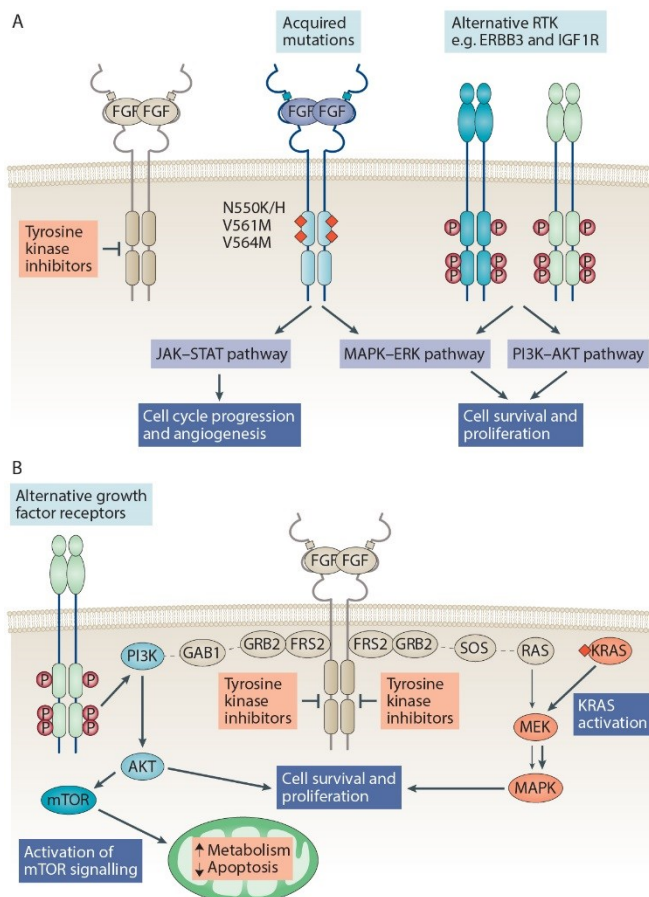


Figure 11. Mechanisms of acquired resistance to fibroblast growth factor receptor inhibition.

Development of resistance to fibroblast growth factor receptor (FGFR) inhibitors has been observed in diverse pre-clinical trials as well as in vitro studies. Resistance may occur through **A** | Emergence of gatekeeper mutations (secondary mutations) affecting the kinase domain of FGFRs hindering correct drug binding. Another possibility involves the bypass of the signaling through the activation/upregulation of alternate receptor tyrosine kinases (RTKs) such as insulin-like growth factor 1 receptor or ERBB family members such as EGFR, HER2 and ERBB3. **B** | Alternate receptors activate signaling pathways such as the PI3K-AKT-mTOR that in turn regulate cell proliferation, metabolism and survival. K-RAS activation as a result of mutations or amplifications can additionally activate the MAPK-ERK signaling pathway in absence of FGFR signaling. FRS2, FGFR substrate 2, GAB1-GRB2-associated binding protein 1, GRB2-growth factor receptor-bound protein 2, JAK-

Janus kinase, SOS-son of sevenless, STAT-signal transducer and activator of transcription. Adapted from Babina 2017⁷³

Whilst the oncogenic properties of an altered FGFR3 have been well established, the signaling network of FGFR3 in bladder cancer remains partially understood. A better understanding of the complex biology of the FGFR3 signaling is needed to accelerate the

INTRODUCTION

identification of predictive markers of response and/or new therapeutic targets, enabling for improvement of combination treatments and prevention of drug resistance.

III. P63

Being one of the genes I identified during my PhD as forming part of the FGFR3 gene regulatory network in bladder cancer, I will give a brief introduction on p63. P63 is a transcription factor belonging to the p53-protein-family and has been widely studied due to its role in epithelial development and differentiation, as well as its double function as an oncogene or tumor suppressor in cancer. In bladder cancer, its overexpression has been widely associated to a more lethal subtype of MIBC.

3.1 Structure and isoforms

The transcription factor p63 (protein encoded by the *TP63* gene) belongs to the p53-family of tumor suppressors: p53/p63/p73. It exhibits strong sequence and structural homology to p53, in particular at the DNA-binding domain, hence sharing targets regulated by p53¹¹⁸. Diverse studies have shown that p53-family members may cooperate to regulate gene transcription, however they also act in an independent way¹¹⁹.

Similar to p53, the p63 protein is composed of three domains: an acidic N-terminal transactivation (TA) domain, a DNA-binding domain (DBD) and a carboxy-oligomerization domain (OD). However, unlike the p53 gene (*TP53*), *TP63* possesses two alternative promoters giving rise to two major classes of isoforms: the full length TAp63 (trans-activating P63) and the N-terminal truncated Δ Np63. Despite presenting a truncated trans-activation domain, the Δ Np63 has been shown to possess a *bona fide* transcriptional activity, acting beyond a dominant-negative protein capable of inhibiting TAp63.

At the C-terminal domain, additional isoforms (α , β , γ , δ and ϵ) are generated as a result of alternative splicing at the 3' mRNA level (Figure 12)¹²⁰. All isoforms share a common DBD and OD and the α -isoforms (TAp63 α and Δ Np63 α), the most abundant of all isoforms; present additional domains at the C-terminal region. These domains include the Sterile alpha motif (SAM) domain and the Transactivation inhibitory domain (TID), involved in the modulation of protein-protein interactions and activity of P63 respectively¹²¹. Of interest, the SAM domain could also be implicated in the regulation of other cellular processes such as apoptosis, focal adhesion, RTK signaling and SUMOylation (reviewed in Westfall *et al* 2004¹¹⁹).

INTRODUCTION

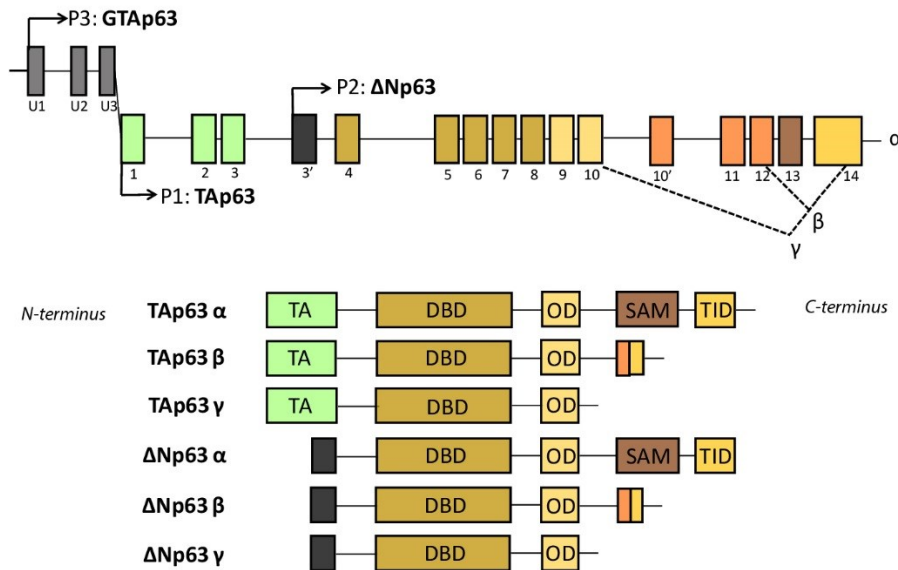


Figure 12. Structure of P63 and its protein isoforms.

Top. Located in chromosome 3q27, the gene encoding for P63 is comprised of 14 exons, spanning 267 kb. Three promoters (P1-P3) encode for three protein isoforms differing at the protein's N-terminus. The two main isoforms are TAp63 and ΔNp63 (N-terminally truncated P63). Despite presenting a truncated N-terminal domain, ΔNp63 has been shown to be transcriptionally active through the presence of a second TA domain.

Bottom. Additional isoforms result from alternative splicing sites (α, β, γ, δ, ε), generating C-terminus variants. Shown are six of the twelve P63 most common isoforms and their functional domains. DBD-DNA Binding Domain, OD-Oligomerization Domain, SAM-Sterile Alpha Motif, TA-Transactivation Domain, TID-Transactivation Inhibitory Domain. Adapted from Gonfloni 2015 ¹²⁰

Many studies have been performed in order to understand the biological and pathological properties of each of the different p63 isoforms, their tissue-specific expression and their capacity to interact with- or antagonize each other. Whilst the main differences between the TAp63 and ΔNp63 have now been unveiled, the functional differences between the minor C-terminal isoforms remain largely unknown.

3.2 Role in development and disease

The TAp63 and Δ Np63 major isoforms display different patterns of expression in cellular compartments and/or tissues, and play distinct (sometimes opposite) roles in diverse biological processes.

The Δ NP63 isoform, and predominantly the Δ Np63 α , is highly expressed in the proliferative compartment of epithelial rich tissues and organs (epidermis, thymus, breast, prostate and urothelium) (reviewed in Bergholz *et al* 2012, Sethi *et al* 2015, Pignon *et al* 2013)^{122–124}. The functional role of Δ Np63 has been investigated in different mouse models where the expression of *p63* or *Δ Np63* has been ablated or increased (overexpressed). *P63*-knockout (KO) and *Δ Np63*KO mice present severe defects in epidermal and epithelial differentiation, limb and craniofacial development and die shortly before birth^{125–127}. In humans, germinal mutations impacting *Δ Np63* have been found in multiple ectodermal dysplastic syndromes (EDS). These syndromes are autosomal dominant hereditary disorders characterized by defective skin, orofacial and limb development¹²⁸. These observations highlight the role of Δ Np63 in epithelial development and maintenance of epithelial stem cell compartment. Of note, the development of bladder urothelium has also been demonstrated to be severely impaired in *P63* null-mice¹²⁹.

Δ Np63 has been shown to control other important processes in epithelia such as cell adhesion and survival. Knockdown of *P63* in a mammary epithelial cell line and in primary keratinocytes led to a downregulation of cell-cell (cadherins, catenins, occludins and desmoplakins) and cell-matrix (particularly integrins β 1, β 4 and α 6) adhesion molecules, resulting in death of the cells by anoikis. Conversely, transfection of cells with a Δ Np63 α copy (but not TAp63 γ) insensitive to shRNA induced knockdown, prevented such cell death (rescue of phenotype)^{130,131}.

On the other hand, TAp63 has been found to be expressed at much lower levels in the epidermal compartment of the skin, having been observed mainly in a subset of dermal stem cells, the skin-derived precursor cells (SKPs). Observations from TAp63KO mice indicated that TAp63 plays an important role in maintaining SKPs in a quiescent state, preventing genomic instability and premature senescence¹³². Further roles that have been identified for TAp63 in other tissues include: preservation of the female germline (protection from DNA-damage as a pro-apoptotic factor), modulator of the cardiac progenitor lineage determination, and regulator of glucose and lipid metabolism^{133–136}.

Even though observations in normal tissue and development have defined that Δ Np63 promotes cell survival and proliferation whereas TAp63 regulates cell senescence and apoptosis, their role in cancer as an oncogene or tumor suppressor are less clear.

3.3 P63 and bladder cancer

Unlike p53, the p63 gene is rarely, if ever, found mutated in human cancers¹³⁷. On the contrary, Δ Np63 overexpression has been observed in numerous tumors of epithelial origin including squamous cell carcinomas (SCC) of the head and neck, esophagus, lung and cervix; and in urothelial, prostate and breast carcinoma (reviewed in Westfall *et al* 2004; Graziano *et al* 2011)^{119,138}. Different studies have shown that Δ Np63 would mainly act as an oncogene through the regulation of cell proliferation, survival and invasion, and the inhibition of apoptosis^{139–141}. Contradictory to this role, Δ Np63 could act as a suppressor of metastasis as its expression in many cancers is correlated to a reduced tumor invasion and metastasis^{121,138,142–145}. On the other hand, TAp63 has been generally observed to act as a tumor and metastasis suppressor^{121,146}.

As mentioned previously, p63 is expressed in the basal and supra-basal cell layers of the urothelium, where it plays an important anti-apoptotic role during bladder development¹⁴⁷. In bladder cancer, the Δ Np63 is the predominantly expressed isoform exhibiting an upregulated expression in early stage tumors that decreases with more advanced TMN grade and stage^{148–152}. In an opposite manner, Δ Np63 overexpression in invasive bladder carcinomas (MIBC), is associated to a poorer prognosis^{129,139,153}. Such contradictory results highlight two important concepts: 1) the complex role and plasticity of p63 in bladder cancer development and progression and 2) the importance of the cellular-context (e.g. functional/transcriptional partners) in defining the clinical outcome of a deregulated p63 signaling.

IV. PRECLINICAL MODELS OF BLADDER CANCER

Although much has been learnt from the clinical and molecular characterization of human bladder tumors, such studies only provide information that is specific to a particular time-point in the development of the disease. Therefore, to study the clinicopathological path of bladder tumor initiation, progression, metastasis and resistance to treatment, the generation of preclinical models is indispensable. Over the years, multiple cellular and murine models of bladder cancer have been developed. Such models have proven valuable for the study of early (pre)malignant stages of the disease, the identification of diagnostic and prognostic biomarkers, and the evaluation of new therapeutic targets.

4.1 Bladder Cancer Derived Cell Lines

There are several bladder cancer derived cell lines representing different bladder cancer subtypes, each exhibiting distinct alterations at the genomic, transcriptomic, proteomic and phenotypic level. For a long time, they have been used to investigate the *in vitro* molecular mechanisms of bladder cancer and response to drug treatments. Moreover, they have been studied *in vivo* in xenografted and syngeneic mouse models^{154–156}. Recent techniques of 3D culture (organoids and spheroids) now also allow to more closely recapitulate an *in vivo* context, whilst presenting the advantages of *in vitro* culturing¹⁵⁷.

In order to identify the best bladder cancer cell line to investigate a specific biological problem, numerous molecular (exome, transcriptome, proteome) and pharmacological (response to drugs or large gene-invalidation screens) characterizations have been carried out^{156,158}. Through such characterizations, cell lines dependent on FGFR3-signaling as a result of activating mutations or chromosomal translocations affecting the receptor, have been identified. The identified cell lines include: MGHU3 (*FGFR3-Y375C*), UMUC14 (*FGFR3-S249C*), RT112 (*FGFR3-TACC3*), RT4 (*FGFR3-TACC3*), SW780 (*FGFR3-BAIAP2L1*) and 97-7 (*FGFR3-S249C*). Additionally, the evaluation of their sensitivity to FGFR-invalidation/inhibition^{94,154,155,158–160} translated into the assessment of FGFR-inhibitors in the clinical trials mentioned in section 2.5 of this introduction.

Irrespective of the many advantages associated to the use of bladder cancer cell lines to study the underlying biology of urothelial carcinoma, there exist many limitations to their use: 1) lack of a real tumor associated microenvironment; 2) induction of genetic changes by serial passaging; and 3) risk of cross-contamination with other commonly used, morphologically similar cell lines. Nonetheless, bladder cancer cell lines will continue to be a crucial model used during the first steps of drug discovery.

4.2 Bladder Cancer Mouse Models

The laboratory mouse has been widely used in bladder cancer research due to their ease of housing and reproduction, as well as their resemblance to their human counterpart. Rodents possess a homologous urinary tract to that of humans, and do not frequently present bladder cancer unless it is induced by a carcinogen or oncogene. Current murine models of bladder cancer can be divided into two categories based on the origin and development of the tumor: 1) non-autochthonous (tumor engraftment) and 2) autochthonous (spontaneous tumor development). (Figure 13)

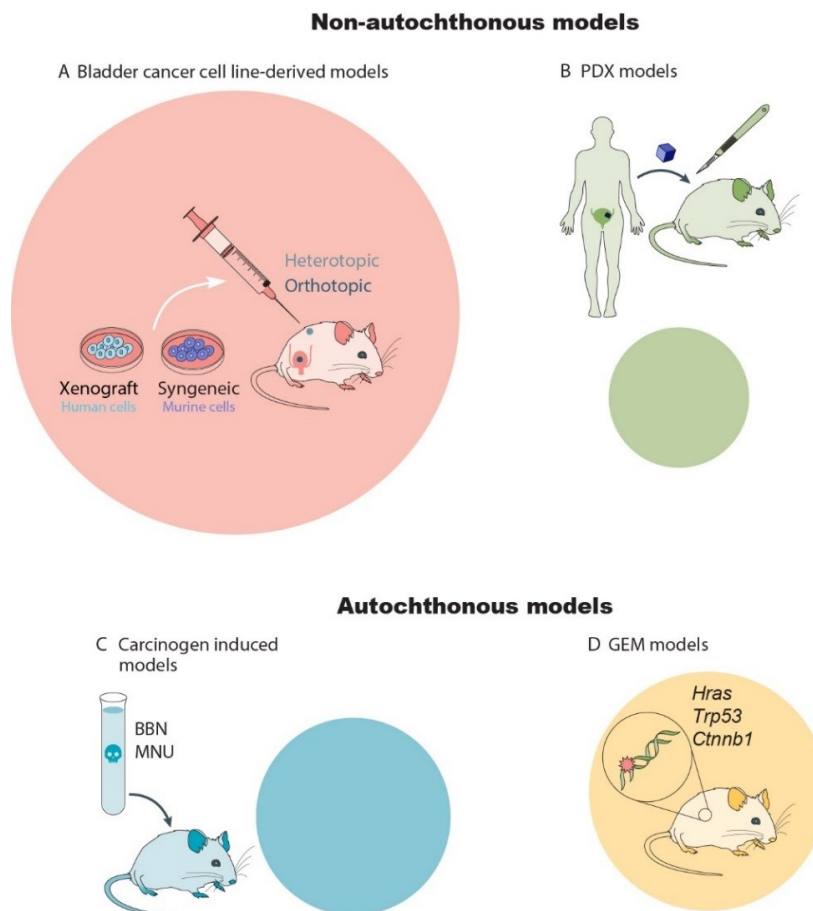


Figure 13. Mouse models of bladder cancer.

Depending on how the tumor was initiated, mouse models of bladder cancer are classified as non-autochthonous (engraftment) or autochthonous (spontaneous).

A. The most widely used model is that of engrafted tumors, derived following the injection of human (xenograft models) or murine (syngeneic models) bladder cancer cell lines. A further classification of these models is made with regard to the site of injection: intravesical (orthotopic) or outside the bladder (heterotopic).

B. Xenograft models may also be derived from the injection of freshly resected human bladder tumors (Patient Derived Xenografts; PDX).

C. Treatment of mice with carcinogens leads to the spontaneous development of bladder tumors.

INTRODUCTION

D. Bladder tumors may additionally arise de novo when mice are genetically engineered (GEM) to carry cloned oncogenes (e.g. Hras) or lack tumor suppressor genes (e.g. Trp53). The size of circles for each model type is a visual approximation of their frequency of use. BBN- N-Butyl-N-(4 hydroxybutyl)nitrosamine), MNU- N-methyl-N-nitrosourea. Adapted from Gengenbacher 2017¹⁶¹; Lorenzatti 2019¹⁶²

4.2.1 Non-Autochthonous Mouse Models

Engraftment or transplantable mouse models are characterized by the implantation of tumoral cells in the host. Depending on the host's immune status, transplantable models may be categorized into syngeneic models (engraftment of murine cancer cells into immunocompetent mice) or xenograft models (inoculation of human bladder cancer cells or patient tumors in immunodeficient mice).

Unlike xenograft models, syngeneic models present the advantage of evaluating tumor progression in immune-competent mice, enabling the study of immune responses to therapy (such as BCG treatment)¹⁶³. On the other hand, xenograft models enable the use of a variety of human primary and tumoral (genetically modified or not) cells permitting a deeper functional analysis of candidate genes. Additionally, they may be established from freshly resected patient tumors (PDX, Patient Derived Xenografts), presenting a potential to model the progression and drug response of an individual patient^{164,165}. In our team, we have used PDX models to study more in depth the FGFR3-signaling *in vivo*⁷⁰.

A further division of the non-autochthonous models is made based on the site of engraftment of tumors: orthotopic engraftment occurs at the lumen of the mouse's bladder, whereas heterotopic engraftment takes place outside the bladder (e.g. subcutaneously in the leg or flank)¹⁶⁶. Orthotopic models present the advantage of permitting the investigation of tumor progression in an organ-specific environment. However, they are difficult to establish and monitor, with a highly variable tumor take rate (from 30-100%) that depends on a multitude of factors. Consequently, subcutaneous heterotopic models have been used in a greater extent, due to the ease of access to the induced tumor. Notwithstanding, the microenvironment present in a heterotopic model differs considerably from the one of the primary tumors.

One last subtype of models is the experimentally induced metastasis model. Host animals are inoculated (via an orthotopic, intracardiac or tail vein injection) with highly metastatic urothelial cell carcinoma variants, and the growth and metastasis of such cells is followed by techniques such as fluorescence. Being one of the main organs of distant metastatic spread, various isogenic models of lung-metastatic bladder cancer cell lines have been established¹⁶⁷⁻¹⁷⁰.

INTRODUCTION

Overall, engraftment models allow for a more or less rapid evaluation of the prognostic and/or therapeutic relevance of a gene or pathway of interest. Yet, tumors in non-autochthonous models do not arise *de novo*, presenting a different disease etiology to the primary tumor.

4.2.2 Autochthonous Mouse Models

Autochthonous mouse models are models in which tumors originate *de novo* as a result of a long-term carcinogen treatment or the activation/inactivation of one or more genes (genetically engineered mice -GEM).

At present, the vast majority of carcinogen induced models are generated following the treatment of mice with BBN, N-Butyl-N-(4-hydroxybutyl)nitrosamine); FANFT, N-[4-(5-nitro-2-furyl)-2-thiazolyl]formamide; and MNU, N-methyl-N-nitrosourea. Incorporation of such carcinogens either in the drinking water, the diet or via intravesical injection (respectively) leads to the development of different phenotypes of urothelial carcinoma^{171,172}. Of note, BBN, the most widely used agent, is a particularly suitable carcinogen as it is similar to a compound present in tobacco smoke¹⁷³. In addition, BBN-induced murine tumors have been demonstrated to recapitulate human MIBC at the histological and molecular level. At the molecular level, they present a high mutational rate with frequent mutations impacting *Trp53*, *Kmt2c* and *Kmt2d*, and overexpress genes associated to a bladder cancer basal phenotype, such as *Egfr*^{50,172,174–177}. Even though they are good models for studying carcinogen induced tumorigenesis, these models present phenotypes that vary greatly depending on the dose and duration of treatment, as well as the genetic background of the mouse used.

Transgenic or genetically engineered mice (GEM) are developed via the cloning or deletion of one or more oncogenes or tumor suppressors, respectively. In this way, they enable the study of the contribution of an individual or a set of genes to bladder tumorigenesis. The most common strategies employed to generate GEM comprise the use of the uroplakin II (UpkII; UpII) promoter to express the gene of interest specifically in the urothelium, and the use of the Cre/loxP system as a method of conditional gene knock-in or knock-out. Primarily using the UpkII system, GEM have shed light on the functional role that genes such as *HRAS*, *P53*, *PTEN*, *RB1*, *FGFR3* and *EGFR* have in the development of bladder cancer^{38,178–183}.

With regard to *FGFR3*, none of the previously reported models of GEM have demonstrated that activation of *Fgfr3/FGFR3* alone is sufficient to act as a driver of urothelial tumorigenesis in mice^{101–103,179}. In one of these studies, Ahmad *et al* introduced *Fgfr3* kinase-domain activating mutations (K66E and K64M) alone or in synergy with mutations affecting *Kras* and beta-catenin (*Ctnnb1*), and did not observe under any circumstances the development of urothelial carcinoma. Nonetheless, an upregulation of the ERK-MAPK

INTRODUCTION

pathway was observed in both *UroIIcre⁺Fgfr3^{+/K644E}* and *UroIIcre⁺Fgfr3^{+/K644M}* mice, compared to wildtype control. Of interest, due to the ectopic expression of the Cre recombinase, skin papillomas and lung tumors did develop in these mice, in synergy with *Kras* and *Ctnnb1* mutations, respectively¹⁷⁹.

Exploring the idea that FGFR3 may drive urothelial carcinogenesis in presence of other cooperating mutations, Foth and Ahmad developed a murine model combining an altered-*Fgfr3* with the deletion of the Pi3k-Akt pathway inhibitor *Pten* (*UroIIcreFgfr3^{+/K644E}Ptenflox/flox* mice). Despite not developing any tumors up to 18 months of monitoring, double *Fgfr3* and *Pten* mutants presented significant histopathological abnormalities in the urothelium¹⁰¹. In the same line of research, Zhou *et al* demonstrated that *Fgfr3b-S243C* mice did not present any malignant phenotype unless combined to the functional invalidation of the p16-Rb and p19-p53-p21 pathways (cross-breed of *Fgfr3b-S243C* mice with UPII-SV40T transgenic mice)¹⁰².

A final study by Foth *et al* evaluated the role of the most frequently observed *FGFR3* alteration (*FGFR3-S249C*) in the progression of BBN-induced tumors. As observed in the previous GEM models, no urothelial carcinomas developed *de novo* in *UroII-hFGFR3IIIbS249C* mice. However, they observed that BBN-treated mice expressing a mutationally active *FGFR3* (*S249C*) presented increased tumor development, more advanced tumors and an altered acute-inflammatory response compared to wild-type controls¹⁰³.

In summary, many challenges are still to be faced regarding the development of a preclinical bladder cancer model that can ultimately be applied to conceive and implement new, more efficient therapeutic approaches. The use of multiple preclinical models, coupled to new analytical strategies, should thus be envisaged to more closely understand the complex pathobiology of bladder cancer.

V. GENE REGULATORY NETWORKS IN BLADDER CANCER

In spite of their informative value, the translatable impact of preclinical models in ameliorating bladder cancer treatment has been small. This can be explained as a result of an often reductionist approach, where the pathogenesis of cancer or its response to a drug was often associated to one or two, isolated pathways. Consequently, the use of systems biology methods to consolidate complex pathway interconnections into large-scale regulatory networks has emerged as an integrative approach to build more solid and accurate models of disease.

A gene regulatory network (GRN) is a collection of genes (and their products) in a cell that interact with each other and with other molecules to control the expression of other genes and their translation into proteins. They represent the complex molecular processes that are activated or inhibited in the cell as a response to different stimuli (Figure 14). When investigating the molecular mechanisms of a disease, GRNs are useful tools as they allow to determine the role of a single gene within a multi-layered network of interacting pathways. This in turn facilitates the identification of network drivers, whose perturbation may have a stronger therapeutic impact than the perturbation of a single component from a linear pathway. As significant redundancy and crosstalk between many signaling pathways exist, inhibition of a single component of one pathway could easily be compensated by activation of another one¹⁸⁴.

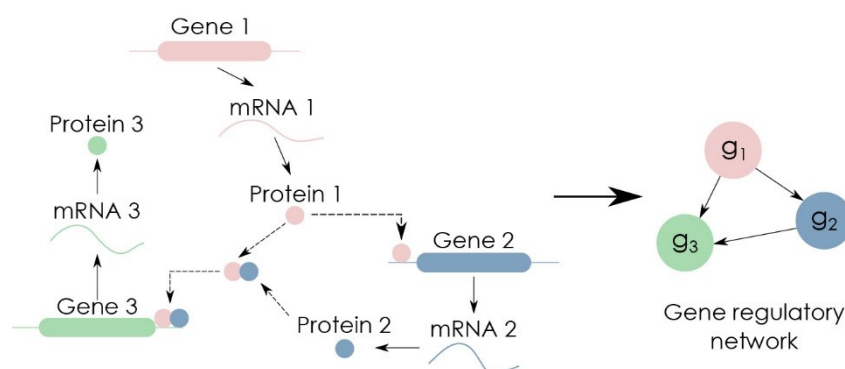


Figure 14. Schematic representation of a gene regulatory network (GRN).

Left. Complex molecular model illustrating the interactions between three genes. Gene 2 is directly regulated by Gene 1, whilst Gene 3 is modulated by both Gene 1 and Gene 2 (cooperativity).

Right. A directed graph (GRN) can represent the previous model through a more abstract structure. Adapted from Huyhn-Tu and Sanguinetti 2018¹⁸⁵

INTRODUCTION

Mathematically, GRNs are directed graphs (directed acyclic graphs; DAGs) comprised of nodes representing genes and edges representing regulatory interactions between them. In such graphs, the directed edge G , from node X to node Y means that X is the cause for Y (Figure 14). Such interaction edges can represent a transcriptional regulation (TF-gene) or a protein-protein interaction (PPI) between the products of those genes. At present, gene regulatory networks are mainly inferred from gene expression data and using a plethora of approaches that employ different algorithms based on statistical (e.g. Linear-regression model, Mutual Information), mathematical (e.g. Boolean and Bayesian Networks, Ordinary Differential Equations) and machine learning (e.g. Neural networks, Fuzzy Logic) methods. (Figure 15)

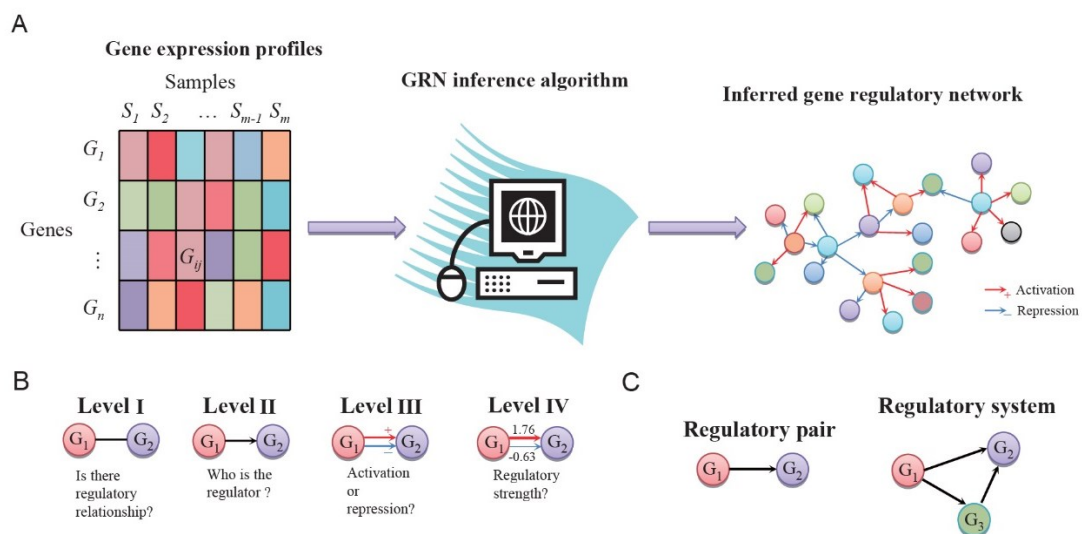


Figure 15. General approach for inferring a gene regulatory network (GRN) from gene expression data.

A. Most GRNs are inferred from transcriptomic data of different types: observational (steady state or time lapse) or experimental (gene perturbation or condition-specific). The GRN will be constructed using the most adapted algorithm to the type of data and biological question to answer. In the case of top-down approaches, prior-knowledge is taken into account, contrary to the de novo constructed GRNs (bottom-up approach).

B. Depending on the algorithm of choice, the regulatory relationships between the nodes (genes) will be established at different levels. When using prior-knowledge, directed (activation/inhibition) relationships are easier to establish.

C. Regulatory pairs are established in this way between two nodes; however, the final gene regulatory system is comprised of more complex relationships which involve the cooperation between genes to indirectly regulate another gene. Adapted from Liu 2015¹⁸⁶

Each GRN reconstruction approach presents different advantages and limitations and each is suited to answer different kinds of questions utilizing distinct data types (e.g. discrete vs continuous) and inference methods^{187,188}. As a detailed description of all the different approaches is beyond the scope of this thesis, only a brief summary of those most commonly

used will be given (based on those that use of observational, steady-state expression data). For more detailed reviews, the reader may refer to (Bansal *et al* 2007¹⁸⁷, Delgado *et al* 2019¹⁸⁹, de Matos-Simoes *et al* 2011¹⁹⁰, Emmert-Streib *et al* 2012¹⁸⁸, Hecker *et al* 2009¹⁹¹, Jong *et al* 2002¹⁹², Karlebach *et al* 2008¹⁹³, Liu *et al* 2019¹⁹⁴, Lee *et al* 2009¹⁹⁵, Linde *et al* 2015¹⁹⁶, Margolin and Califano 2007¹⁹⁷, Maetschke *et al* 2013¹⁹⁸, Sima *et al* 2009¹⁹⁹).

5.1 Main computational methods for GRN inference

Bayesian network

Bayesian approaches infer GRNs by combining probabilistic models with graph theory. In this way, Bayesian networks represent the probabilistic relationships of the genes forming the network through the establishment of a DAG. The probability of expression of a gene is described as the conditional probability of all of its parent genes. Two methods exist to infer a DAG using a Bayesian network approach. The constraint-based method; usually employed for small-sized networks, begins from a fully connected graph and then directed edges between genes are removed when conditional independency is measured. In the score-based approach, the inferred network structure is determined from disconnected graphs and edges are added iteratively based on a scoring function.

Bayesian network inference approaches have been widely used due to the facility to integrate prior interaction data to the network, their flexibility on using discretized or non-discretized data and their intuitive representation of regulatory interactions between genes. Furthermore, due to their stochastic nature, Bayesian network inference methods can take into account noise present in the data of study. Notwithstanding, Bayesian methods present the main problem of needing considerable computational calculation, meaning that the method is restricted to the calculation of smaller sized networks. In addition, as the network is represented as a DAG, it cannot take into account the possibilities of feedback regulatory loops often present in the biological regulation of gene expression (such limitation can be overcome if a dynamic Bayesian approach is used).

Boolean network

Boolean networks are the simplest discrete based models in which the state of a gene can be represented by only two possible levels: active (1) or inactive (0). Two inference approaches are used to define the gene to gene regulatory relationships and they are based either on correlation or machine learning methods. This simple and straightforward method presents the advantage of being fast and efficient. Most importantly, temporal discrete networks can be easily inferred from dynamic datasets such as time series of gene

INTRODUCTION

expression. Two of its main disadvantages however, are that this approach is sensitive to noisy data, and it may not be able to represent more complex details of system behavior.

Ordinary Differential equations (ODE)

Compared to most other methods that use discrete data, the ODE approach employs continuous data and so is used to model dynamic gene regulation. Changes of expression of a gene or protein can be modeled by a mathematical equation taking into account the expression of other genes as well as external factors. Whilst the ODE method allows for the use of steady-state and time-series expression data, such approach is only applicable to small sized networks and oscillatory systems cannot be modeled.

Regression

Regression inference methods define the expression level of a gene as a dependent variable whose value can be explained by a regulator or a group of regulators. Different regression methods exist that will aim at selecting the most relevant subgroups of regulators which best explain the experimentally observed expression of a target gene [Enze Liu 2019].

Regression based approaches are robust, can be computed relatively quickly. However, *a priori* knowledge is needed to define the sets of regulators and depending on the regression model used; the inference may be limited to linear relationships.

Information theory based estimation

Information theory-based approaches (Mutual information, MI), contrary to classic correlation approaches (e.g. Pearson); aim at defining regulatory relationships in a network through estimators that determine the non-linear dependency between two random variables (in this case, genes). One of the first information-theory based methods used to construct a GRN was the relevant networks (RN) method where regulatory edges between pairs of gene nodes were assigned if their associated MI value was greater than a certain threshold¹⁹⁰.

Information theory-based approaches are widely used as they enable the inference of biologically relevant, large scale GRNs at a low computational cost. Amongst the most popular algorithms used that employ information theory-based approaches are ARACNe (Algorithm for the Reverse engineering of Accurate Cellular Network)²⁰⁰, CLR (Context Likelihood of Relatedness)²⁰¹ and MRNET (Minimum Redundancy/Maximum Relevance Networks)²⁰².

Some of the weaknesses of information theory-based methods are that inferred GRNs are static, contain non-directed edges and, most importantly, do not take into account the fact that more than one regulator is often involved in controlling the expression of a target gene.

Neural network

The neural network approach is a machine learning inference method that was inspired by the central nervous system of an animal. Neural network inference approaches are flexible statistical methods that learn to recognize input data and can model any functional relationship between genes (e.g. feedback loops), using any data structure (noise-resistant). The most used models include the recurrent neural network (RNN) and artificial neural network (ANN). Under this inference approach, genes are represented by nodes or neurons whose connections with other nodes represent gene interactions. Whilst these models present many advantages regarding the type of data used and the different nonlinear and dynamic relationships that they are able to infer, the inference of the GRNs requires complex computation and an important training phase of the model.

Overall, there is a vast variety of different computational approaches that exist for the inference of a GRN. Each approach presents different advantages and disadvantages, and is adapted to the use of different data types (static versus dynamic) and distinct representations of relationships (directed, non-directed, temporal, etc.). The choice of inference approach is thus dependent on the biological question that needs to be answered.

Another important aspect to take into account when constructing a GRN is whether external, already published regulatory relationships will be integrated into the algorithm. Depending on the application of the network, a GRN may be inferred using of a predefined network (top-down approach) or inferred *de novo* (bottom-up approach, reverse engineering).

5.2 Top-down GRN inference

Top-down approaches, integrate prior knowledge about the interactions taking place between a set of genes of interest to support the inference of a GRN. Hence, as a first step, a “conceptual” model network is constructed where the regulatory edges between genes are extracted from previously predicted or experimentally observed interactions (e.g. TF-gene or PPI). Such interactions extracted from the literature are more often of a positive nature (a regulatory link exists between both genes) rather than a negative nature (no regulatory link exists) due to the experimental proof of concept that is mostly published (proving that there is no interaction between two genes is difficult to do)^{187,196,203}.

Top-down approaches start from formerly defined interactions which are used to train a machine learning classifier and create a conceptual model. This model is then converted into the computational model of choice (e.g. Boolean method) and, together with experimental

INTRODUCTION

data (usually expression data following the perturbation of a gene), a final, more detailed GRN presenting the dynamics of the initial network is constructed.

An advantage of top-down approaches is that they may be used to model large-scale, GRNs that can be easily validated with further experimental data²⁰⁴. Additionally, as prior knowledge is integrated beforehand, GRNs often have directional relationships (activation or inhibition) that allow to predict the response of the network to a perturbation (e.g. following treatment with a drug of interest)^{205–209}. The main disadvantage however, is that precise context-specific GRNs are hard to derive as they are initially based on published data that is often cell- and organism-unspecific, and that may not occur in the tissue being investigated.

5.3 Bottom-up GRN inference

Bottom-up or reverse-engineering approaches, are based on the *de novo* construction of a GRN from observational (steady-state) or experimental data (following the perturbation of a system. e.g. Gene knock-out / knock-in). Whilst it is difficult to predict precise, directed interactions (in contrast to top-down approaches), the GRNs derived using this approach are specific to the cellular-context under study²¹⁰. In terms of gene regulation, this is very important as even at the signaling pathway level it has often been demonstrated that the activation of one same gene may lead to different signaling cascades that result in distinct phenotypes depending on the cellular background²¹¹. This can be of great importance when considering the translation of inferred driver nodes into therapeutic targets of interest for a particular set of patients (e.g. patients of a bladder cancer subtype that present alterations of *FGFR3*).

To construct GRNs following the bottom-up approach, different statistical, mathematical, machine learning and hybrid methods are used based mainly on the type of initial experimental data (e.g. continuous or discretized) and the distinct manners in which the regulatory relationships between two nodes will be established^{210,212–216}. Most inference methods will identify node regulatory links (gene-gene or TF-gene) by scoring such possible interactions using correlation-based methods such as Pearson or Spearman's coefficient^{217,218}. Yet, more adapted and robust methods have been developed based on mutual information. Amongst them, ARACNe has been one of the most applied algorithms²⁰⁰(many other algorithms from the same laboratory were also developed)^{219,220}. Further methods exist to infer the regulatory relationships between the nodes of the GRN, and are based on different principles. These include probabilistic methods, model-based methods, linear-regression methods, GENIE3 (GEne Network Inference with Ensemble of trees) etc^{196,198}.

INTRODUCTION

Altogether, GRNs have been important in describing the complex relationships between genes and their products and how they regulate a specific phenotype. They enable the identification of driver elements of the network that mediate a disease phenotype, highlighting possible therapeutic targets. Still, without experimental validation, many of the inferred regulatory interactions may simply remain as hypotheses due to many of the assumptions that must be made during GRN modeling (not necessarily representing the biological reality). An iterative interdisciplinary process from computational modeling to experimental validation is therefore indispensable to validate the hypotheses generated through the GRN, allowing for refinement and creation of a new, more realistic GRN (Figure 16).

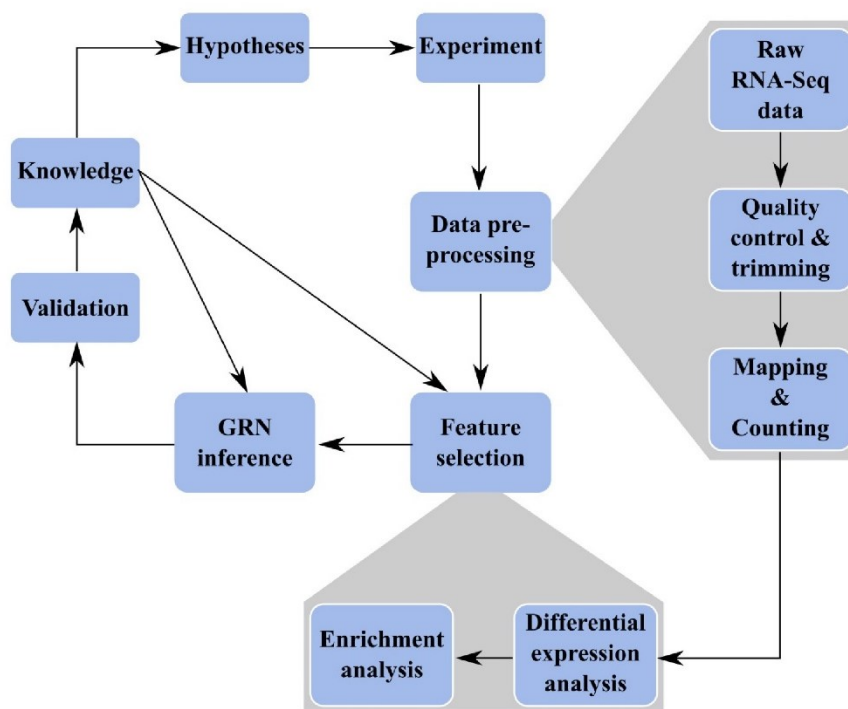


Figure 16. Interdisciplinary workflow of gene regulatory network (GRN) inference.

A gene regulatory network is first inferred from biologically or experimentally derived expression data (e.g. RNA-seq). Once the GRN has been predicted using the most adequate computational approach, functional validation of the inferred regulatory relationships is needed. Different hypotheses will arise from the inferred network, that can next be experimentally validated. This results in the generation of new expression data that can then be used to refine the previously inferred GRN. Adapted from Linde 2015¹⁹⁶

5.4 Choice of algorithm for the characterization of the FGFR3 GRN in bladder cancer

Overall, most GRN inference methods aim at predicting simple regulatory interaction pairs made up of a transcription factor regulating the expression of a target gene²²¹. However, it is known that the transcriptional regulation of a gene in higher eukaryotes is often more complex, involving sets of transcription factors that function together to co-activate or co-repress a target gene^{222,223}. To overcome such problem in this thesis project, we decided to use the H-LICORN (Hybrid-Learning co-operative regulation networks)^{224,225} reverse engineering algorithm to construct a network of cooperative regulators underlying a bladder cancer transcriptome (collaboration with the team of M. Elati from Université de Lille). Supporting our choice of algorithm, a previous study using H-LICORN by our team and that of Elati, uncovered two driver transcription factors forming part of two distinct molecular subtypes of bladder cancer²²⁶

CoRegNet H-LICORN

Forming part of the CoRegNet Bioconductor Package²²⁶, the H-LICORN algorithm couples a data-mining technique with numerical linear regression to infer a list of GRNs from large-scale, transcriptomic data and a list of pre-defined regulators (TFs/coTFs)²²⁴. First, the transcriptomic dataset is discretized into ternary values (-1, 0 and 1) defined against a chosen reference. From the discretized gene expression data, H-LICORN will pre-select the sets of candidate co-activators and co-repressors that regulate the expression of each target gene using a frequent itemset technique. Frequent itemset mining is a data mining technique designed to identify frequently co-occurring elements. For each target gene found in the dataset, k candidate sets of co-regulators will be defined as local subnetworks (GRNs) controlling its expression. In a second step, the algorithm fits a linear regression for each of the identified regulators, with the regulator being the explanatory variable and the target gene the dependent variable. Within the k candidate networks, H-LICORN then selects the GRN that best predicts (smallest prediction error) the expression of that target gene in the different samples, given the state of its regulators (co-activators and co-repressors). The resulting networks are then transformed into a cooperativity network where two regulators will be defined to “cooperatively” interact with each other if they share a sufficient number of target genes. Published regulatory interactions (TF-gene, PPIs) may be further integrated into the constructed network to refine it (Figure 17).

INTRODUCTION

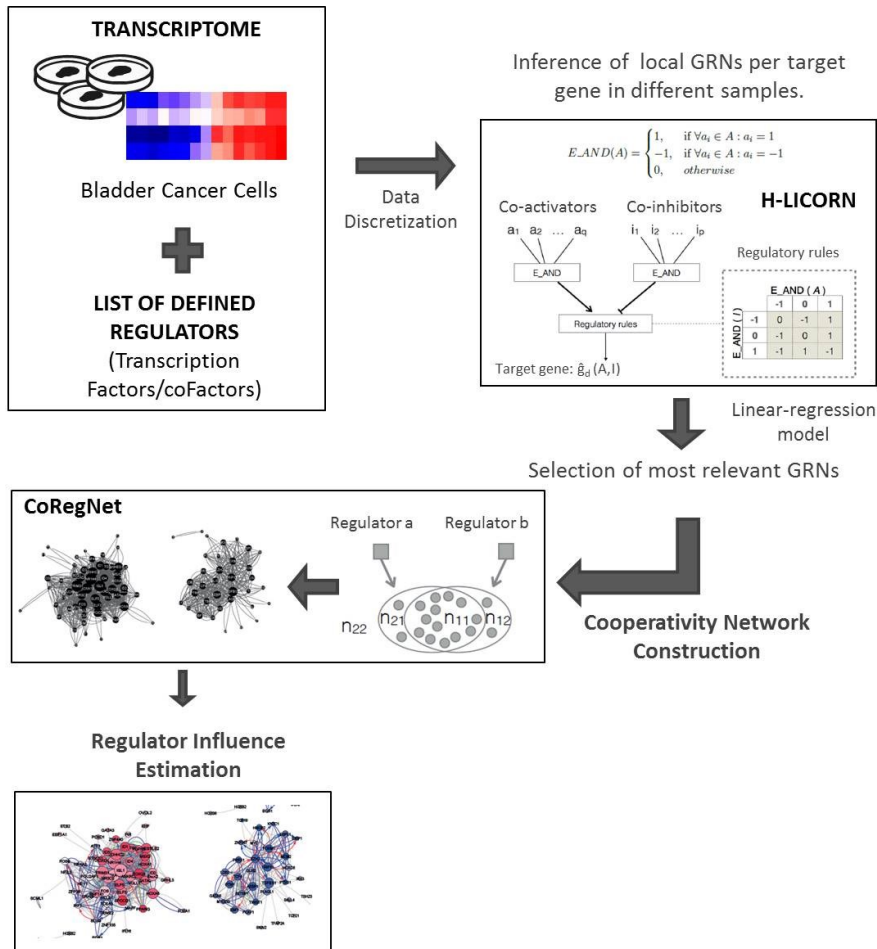


Figure 17. Inference of a context-specific cooperativity network using CoRegNet H-LICORN.

With the aim of assessing the transcriptional programs that are active in a particular dataset or sub-samples of a dataset (e.g. FGFR3 mutated bladder tumors), CoRegNet allows us to estimate the influence that each of the inferred regulators has on its target genes. The influence or activity of a regulator is calculated based on a Welch's t-test comparing the distribution of expression of its activated and repressed target genes. A highly influential regulator in a specific condition would thus result from a significant difference of expression levels between the activated and repressed targets. For example, a regulator is said to be active when the expression of its activated target genes is significantly higher than that of its repressed targets (Figure 17). Through such calculation of regulator activity, CoRegNet not only enables a better, sample-specific biological interpretation, but also leads to an important dimensionality reduction. Instead of providing a large-scale regulatory network describing thousands of gene expression levels, a network of only several hundred co-regulators underlying a sample-specific phenotype is extracted.

OBJECTIVES

OBJECTIVES

OBJECTIVES

Somatic activating mutations or translocations affecting *FGFR3* are amongst the most frequently observed genetic alterations in bladder cancer (mutations- 65% of NMIBC, 15% of MIBC; translocations- 3% of MIBC), making *FGFR3* an appealing therapeutic target. Indeed, several *FGFR*-inhibitors have been recently analyzed in clinical trials and promising response rates have been observed for patients with advanced or metastatic urothelial carcinoma, although the precise durability of such responses is yet unknown. Of serious concern, only 40% of patients present an objective response rate (data from Loriot *et al.*, 2019), and among patients initially responding to *FGFR*-inhibitors around 50 % could become resistant to treatment within 6 months of therapy as observed in preclinical bladder cancer cell line models and other targeted therapies in the clinic (*EGFR*, *BRAF*, *VEGFR*, *KIT*). To date, the signaling network and *in vivo* oncogenic properties of an altered *FGFR3* in bladder cancer remain quite poorly characterized. Consequently, a deeper understanding of the molecular mechanisms underlying an altered *FGFR3* in bladder cancer is needed to improve current targeted therapies and/or propose new therapeutic strategies.

The aim of this project was to identify the gene regulatory network of an altered, constitutively activated *FGFR3* in bladder cancer, and more deeply comprehend its functional role *in vivo*. We hypothesized that the *in vivo* study and characterization of the *FGFR3* gene regulatory network in bladder cancer would allow to: 1) better understand the molecular role of the receptor in the pathogenesis of the disease, and most essentially 2) pinpoint driver genes (master regulators and/or their target genes) of therapeutic interest. Considering the example of combined *MEK* and *RAF* inhibition in melanoma, we can assume that by targeting new driver genes in combination with already existing *FGFR3*-directed therapies, one would either increase the efficacy of the therapy and/or hinder the emergence of resistance to treatment.

OBJECTIVES

As a first objective, we investigated the oncogenic role of a mutated *FGFR3* in bladder cancer *in vivo*. This was achieved through the establishment and characterization of a murine model that overexpressed a frequently mutated form of human *FGFR3* (hFGFR3-S249C) specifically in the urothelium. We searched to understand the *in vivo* consequences of such hFGFR3-S249C overexpression by analyzing and comparing the murine model to human *FGFR3* mutated tumors at the transcriptomic and histopathological level. Moreover, the tumor incidence observed in our murine model led us to explore the male and female incidence ratios in *FGFR3*-mutated human subgroups of MIBC and NMIBCs. Searching for an underlying mechanism, we explored the role of androgen receptor (AR) in *FGFR3* signaling using *in vitro* and *in vivo* models. Relevance of our finding in human tumors was addressed by measuring activity levels of AR in such tumors. We then aimed to examine if AR could be important for the cell viability of *FGFR3*-dependent bladder cancer cell lines. In Chapter 1 of the results section, I discuss these findings and the importance of such preclinical model as well as its potential of use in translational research.

For my second objective, we sought to determine the gene regulatory network (transcription factors and cofactors; TFs/coTFs) driven by *FGFR3* in bladder cancer (FGFR3-GRN). We accomplished this in two main steps that I present in the first part of Chapter 2: Firstly, we inferred a bladder cancer network using a data-mining algorithm (H-LICORN) in collaboration with the team of Mohamed Elati (University of Lille) together with expression data from *FGFR3*-mutated urothelial cancer cell lines and human bladder tumors. As a second step, we evaluated which of the TFs/coTFs of the previously constructed network could be modulated by *FGFR3*. We did so by using transcriptomic data from two preclinical models: 1) *FGFR3*-dependent bladder cancer cell lines in which the gene expression or activity of *FGFR3* was inhibited by means of an siRNA or RTK inhibitor, respectively; and 2) bladder tumors derived from UPII-hFGFR3-S249C mice. This strategy allowed to confirm the network of genes of an altered-*FGFR3* in the context of bladder cancer.

OBJECTIVES

For my third objective; exposed in the second part of Chapter 2, **we searched to identify the key regulators (TFs/coTFs) forming part of the inferred FGFR3-GRN in bladder cancer and mediating FGFR3 oncogenic activities.** To fulfill this objective, we assessed the impact that the knockout or knockdown of a possible driver gene would have on the cell viability of urothelial cancer cell lines expressing an altered-*FGFR3* vs wildtype-*FGFR3*. Amongst the network essential regulators that we identified was the transcription factor p63. This result led us establish my last objective, that I expose in the last part of Chapter 2.

My final objective involved the investigation of the functional role of p63 within the FGFR3-GRN. We aimed to decipher a p63, bladder-cancer specific gene target signature by combining p63-ChIP seq and si*TP63* experiments carried out in *FGFR3*-altered bladder cancer cell lines. Next, in collaboration with the team of Catalina Lodillinsky (Instituto de Oncologia Angel H Roffo, Argentina), we corroborated the biological processes that were predicted to be enriched in our p63 gene signature. More specifically, we studied the role of p63 in the mediation of cell growth, migration and invasion in *FGFR3*-mutated bladder cancer cell lines both *in vitro* (2D and 3D culture) and *in vivo* (xenografts). Finally, to explore the potential consequences of p63 activation in the context of an altered *FGFR3* in bladder tumors, we focused on NMIBC and analyzed the activity of p63 in *FGFR3*-mutated and wt*FGFR3* and their recurrence rates.

RESULTS

RESULTS

Chapter 1. Transgenic hFGFR3-S249C mouse model

1.1 Introduction

Despite its high prevalence, considerable morbidity burden and poor prognosis at advanced stages, bladder cancer has remained under-represented in terms of preclinical *in vivo* models, notably regarding genetically engineered mouse (GEM) models¹⁶¹. GEM models are key for the investigation of the mechanistic pathways mediating tumor formation and progression, and for the identification of potential therapeutic targets.

FGFR3 is a gene of special research interest in bladder cancer as *FGFR3* activating mutations drive an oncogenic dependency that can be therapeutically targeted using FGFR inhibitors. These mutations and overexpression have been strongly associated to low-grade NMIBCs but also to luminal papillary MIBC subtypes^{43,48,51}. Positive responses have been observed in recent clinical trials evaluating FGFR inhibitors in advanced and metastatic urothelial carcinoma patients, leading to the FDA approval of the first FGFR inhibitor (Baleversa; erdafitinib)⁷². Nonetheless, development of resistance to FGFR inhibition is expected to appear as has been observed in preclinical bladder cancer models^{107,113,114,116,117}. The generation of appropriate mouse models that improve our understanding of the role of *FGFR3* in bladder tumor development and progression will be key to better interpret clinical trial results and improve current therapeutic strategies or propose new ones.

At present, three research groups have reported different GEM models to examine the potential of *FGFR3*-activating mutations in driving urothelial carcinoma. Although these studies contributed to the elucidation of the molecular events that may cooperate with *FGFR3* to drive bladder cancer development, none of them demonstrate that the expression of a mutated *Fgfr3/FGFR3* specifically in the urothelium, is able to drive bladder tumorigenesis (up to 12-18months of follow-up of transgenic mice)^{102,103,179}.

During my PhD, I worked together with other PhD students (Mingjun Shi, Jacqueline Fontugne and Xianyu Meng) to characterize a GEM model expressing a human, frequently mutated form of *FGFR3* (S249C) specifically in the urothelium. Compared to previous investigations, we observed that the UplI-driven expression of hFGFR3-S249C led to the development of hyperplastic lesions (6-8 months of age) and non-invasive papillary tumors (from 18 months of age) in transgenic mice versus wild type-control. Moreover, we observed that tumor frequency was dependent on hFGFR3-S249C zygosity. Comparison of histochemical and transcriptomic data confirmed that UplI-hFGFR3-S249C bladder tumors resembled their human counterpart, highlighting the potential use of the model in translational research. Based on the tumor frequency that we observed in male versus female UplI-hFGFR3-S249C mice, we explored human bladder tumor datasets and

RESULTS

confirmed a significantly much stronger male dominance in FGFR3 mutated subgroups of MIBC and NMIBC. Exploring a possible mechanism, we examined AR activation by FGFR3 in *in vitro* and *in vivo* models and we further confirmed that AR activity was higher in FGFR3-mutated NMIBC and MIBC.

RESULTS

1.2 Results

FGFR3 mutations induce bladder cancer formation and favor a male gender bias through the activation of Androgen Receptor

Aura Moreno-Vega^{1,2,*}, Ming-Jun Shi^{1,3,*}, Jacqueline Fontugne^{1,2,*}, Xiang-Yu Meng^{1,2,*}, Florent Dufour^{1,2}, Claire Dunois-Larde^{1,2}, Aurélie Kamoun⁴, Philippe Lamy⁵, Audrey Rapinat⁶, Elodie Chapeaublanc^{1,2}, Olivier Levrel⁷, Thierry Lebret⁸, Anna Almeida⁶, Aurélien De Reynies⁴, Lars Dyrskjøt⁵, Yves Allory^{1,9}, François Radvanyi^{1,2} and Isabelle Bernard-Pierrot^{1,2,#}

¹Institut Curie, PSL Research University, CNRS, UMR144, Equipe Labellisée Ligue contre le Cancer, Paris, France

²Sorbonne Universités, UPMC Université Paris 06, CNRS, UMR144, Paris, France

³Department of Urology, Beijing Friendship Hospital, Capital Medical University, Beijing, China

⁴La ligue contre le cancer, Paris, France

⁵Department of Molecular Medicine, Aarhus University Hospital, Aarhus, Denmark

⁶Institut Curie, Department of translational research, Paris, France

⁷MEDIPATH Les Jalassières, Eguilles, France

⁸Service d'Urologie, Hôpital Foch, Suresnes, France

⁹Institut Curie, Department of Pathology, Saint-Cloud, France

* These authors contributed equally to the work

To whom correspondence should be addressed:

In preparation for submission

Dr Isabelle Bernard-Pierrot

Institut Curie

12 rue Lhomond

75005 Paris

E-mail : isabelle.bernard-pierrot@curie.fr

Tel: +33 1 42 34 63 40, Fax: +33 1 42 34 63 49

Running title: mutated-FGFR3 induces bladder tumors in mice

1.2 Results

Abstract

Somatic mutations of the fibroblast growth factor receptor 3 (FGFR3) are one of the most frequent genetic alterations in bladder carcinomas (~70% of cases). The oncogenic dependency induced by FGFR3 is an Achilles' heel targeted by FGFR3 inhibitors in the clinic for advanced muscle-invasive tumors, yet the tumorigenicity of a mutated-FGFR3 has never been demonstrated in vivo. We report here that the mutated-FGFR3 expression in urothelial cells of transgenic mice induces urothelial hyperplasia and spontaneous genomically unstable low-grade papillary tumors. Gene dosage impacted FGFR3 expression and increased the incidence of tumor formation. This key limitation by expression level could account for the tissue specificity of mutated FGFR3-driven tumors restricted to epithelia presenting high normal expression levels of FGFR3. Transcriptomic analyses of mutated FGFR3-induced mouse tumors show they resemble their human counterparts and highlights an activation of androgen receptor (AR). This regulation of AR activity by FGFR3 was validated in human FGFR3-dependent cell lines and its relevance in human tumors was supported by a higher AR activity in FGFR3-mutated tumors as compared to non-mutated ones. This higher activation of AR induced by FGFR3 could account for the male bias gender observed both in mouse and in FGFR3-mutated human tumors. However, AR activation seems to be critical for tumor formation but not for further tumor growth since its inhibition or knock-down did not impact FGFR3-dependent cell viability.

Significance: Our study represents the first murine model of FGFR3-induced spontaneous bladder carcinomas, demonstrating the tumorigenicity of FGFR3 mutations in vivo. This model of FGFR3-mutated tumors resembles its human counterpart and should allow a better understanding of FGFR3 oncogenic properties. This model sheds light on an AR activation by FGFR3, leading to a male gender bias in FGFR3-mutated tumors. However, once established, FGFR3-dependent tumors do not rely further on AR activity for their growth, excluding single AR inhibition as a therapeutic strategy for these tumors.

RESULTS

Introduction

Bladder cancer (BCa) is the sixth most common cancer in men worldwide, with an even higher incidence in Western Europe and North America (4th most common cancer in men) (1). At first diagnosis, the majority of tumors are non-muscle-invasive urothelial carcinomas (NMIBC) (70%). In spite of their favorable prognosis, NMIBCs have a high recurrence rate (70%) and are able to progress (10-15%) to the more aggressive form of disease, muscle-invasive bladder cancer (MIBC). Different molecular classifications have been established in both NMIBC and MIBC in order to identify different biological processes to support patient stratification and more adapted therapies (2–6).

Fibroblast growth factor receptor 3 (FGFR3) is a tyrosine kinase receptor with frequent genetic alterations in BCa (3,5,7). Point mutations (observed in ~70 % of NMIBC and 15% of MIBC) or chromosomal translocations (affecting ~5% of MIBC) resulting in protein fusions, lead to a constitutively active FGFR3. The oncogenic properties of an altered FGFR3 have been shown in vitro and an FGFR3 oncogenic dependency for tumor growth was demonstrated in vitro as well as in vivo (cell lines or patient derived xenografts) (8–12). Several clinical trials have shown a clinical benefit of FGFR3 inhibition in terms of patient survival (NCT02365597; NCT03473743 and NCT03390504), which has led to the FDA approval of the first FGFR inhibitor Erdafinitib (Balversa), as a treatment for patients with locally advanced or metastatic BCa presenting FGFR alterations. Recently, a phase II study investigating the efficacy of Erdafinitib showed a 40% objective response rate in eligible BCa patients with FGFR alterations (13).

To determine the functional role of mutated-FGFR3 in bladder cancer in vivo, several teams have developed FGFR3-altered genetically engineered mice (GEM). So far, results suggest that although FGFR3 activation alone is not sufficient to induce tumorigenesis (14–16), it can promote tumor formation when associated with other molecular alterations (p53/pRB deficiency (17); PTEN loss (16) or carcinogen treatment (15)).

In this study, we report for the first time a GEM model overexpressing the human FGFR3b-S249C mutant specifically in the urothelium, in which mice developed both hyperplastic lesions and low-grade papillary bladder carcinomas presenting genomic instability. This model resembled human luminal papillary tumors at the histological and transcriptomic level. Gene dosage of FGFR3 impacted the tumor formation rate in this model and the analysis of FGFR3 expression levels in different human normal epithelia allowed us to suggest that expression levels of the receptor determine the tissue specificity of FGFR3-driven tumors. It also highlighted a male gender bias in FGFR3-mutated tumors that could

RESULTS

result from AR activation induced by FGFR3. AR activity nonetheless was not required for viability of FGFR3-dependent cell lines suggesting its key role essentially during tumor initiation rather than tumor growth.

Results

FGFR3-S249C expression in Uroplakin II-expressing cells induces urothelial hyperplasia and non-muscle-invasive low-grade urothelial carcinoma.

To determine the role of a constitutively activated FGFR3 mutant in bladder tumorigenesis, we generated transgenic mice expressing a mutated receptor in the urothelium. We focused on the FGFR3-S249C mutation, the most common FGFR3 mutation in both NMIBC and MIBC (7), and used the uroplakin II gene promoter to target its expression in urothelial cells (Fig.1A). We selected two founders, numbers 569 and 538 that expressed the highest level of the human FGFR3 transgene in the urothelium as evidenced by RT-qPCR (Supplementary Fig 1A). In situ hybridization using a human FGFR3-specific probe showed expression of hFGFR3 mRNA in the supra-basal and intermediate cell layers and in very few basal cells of the urothelium (Supplementary Fig.1B). Moreover, human FGFR3 mRNA expression levels in the urothelium were respectively 4 and 1.5-fold higher than the level of endogenous mouse *Fgfr3* in founders 569 and 538, respectively, as assessed by radioactive PCR (Supplementary Fig 1C). These two founders were viable and fertile and transmitted the transgene to their offspring in a Mendelian fashion.

Following propagation of founder lines, we examined the bladder of transgenic mice aged 1 to 24 months old. Histological analysis showed hyperplastic lesions defined by a thickened urothelium, with an increase in cell layers, lacking cytologic atypia. The penetrance of the phenotype was complete from 6 months of age in both lines. Urothelium from UII-FGFR3-S249C mice exhibited seven to ten cell layers and focally more (ten to twenty) at 18 months (Fig.1B). In contrast, normal mouse urothelium presented only three to four cell layers (Fig.1B). Macroscopically, focal papillary lesions were observed after 15 months with a low penetrance in both lines (~10% and 4% for L569 and L538, respectively). Histological analysis of these lesions revealed they were carcinomas displaying a papillary tumor architecture, characterized by either exophytic or mixed (exophytic and inverted) growth patterns, and low-grade tumor cell cytology, with homogeneous nuclei size (Fig.1B). We focused then on the L569 line presenting a higher penetrance of the phenotype and further characterized these lesions. Hyperplastic lesions were similar to normal urothelium in terms of both proliferation rate and transcriptomic profile, respectively determined by Mki67 expression levels (Fig.1C) and an Affymetrix mouse exon array (Fig.1D). In contrast, tumors presented a significantly higher proliferation rate (Fig.1C) and principal component analysis

RESULTS

highlighted a distinct transcriptomic profile compared to normal and hyperplastic urothelium (Fig. 1D). In good agreement with low-grade tumors, proliferation rate in tumors was low, with <10% of Ki67-labelled cells by immunohistochemistry (Supplementary Fig.2A). Whole exome sequencing analysis of 7 tumors did not reveal any recurrent mutations induced by hFGFR3-249C expression but showed common copy number alterations, the most common being chromosome 16 amplification in 5 out of 7 tumors (Fig.1E). We selected 3 genes (Trat1, Erbb4, Fkbp5) located in 3 amplified regions (chr16, chr1 and chr17, respectively) and verified their frequent amplification by qPCR on genomic DNA, in the tumors previously analyzed by whole exome sequencing and in 4 additional tumors (Supplementary Fig.2B).

Taken together, our results showed that hFGFR3-S249C is oncogenic *in vivo*, inducing genomic instability leading to tumor formation in bladder urothelium.

RESULTS

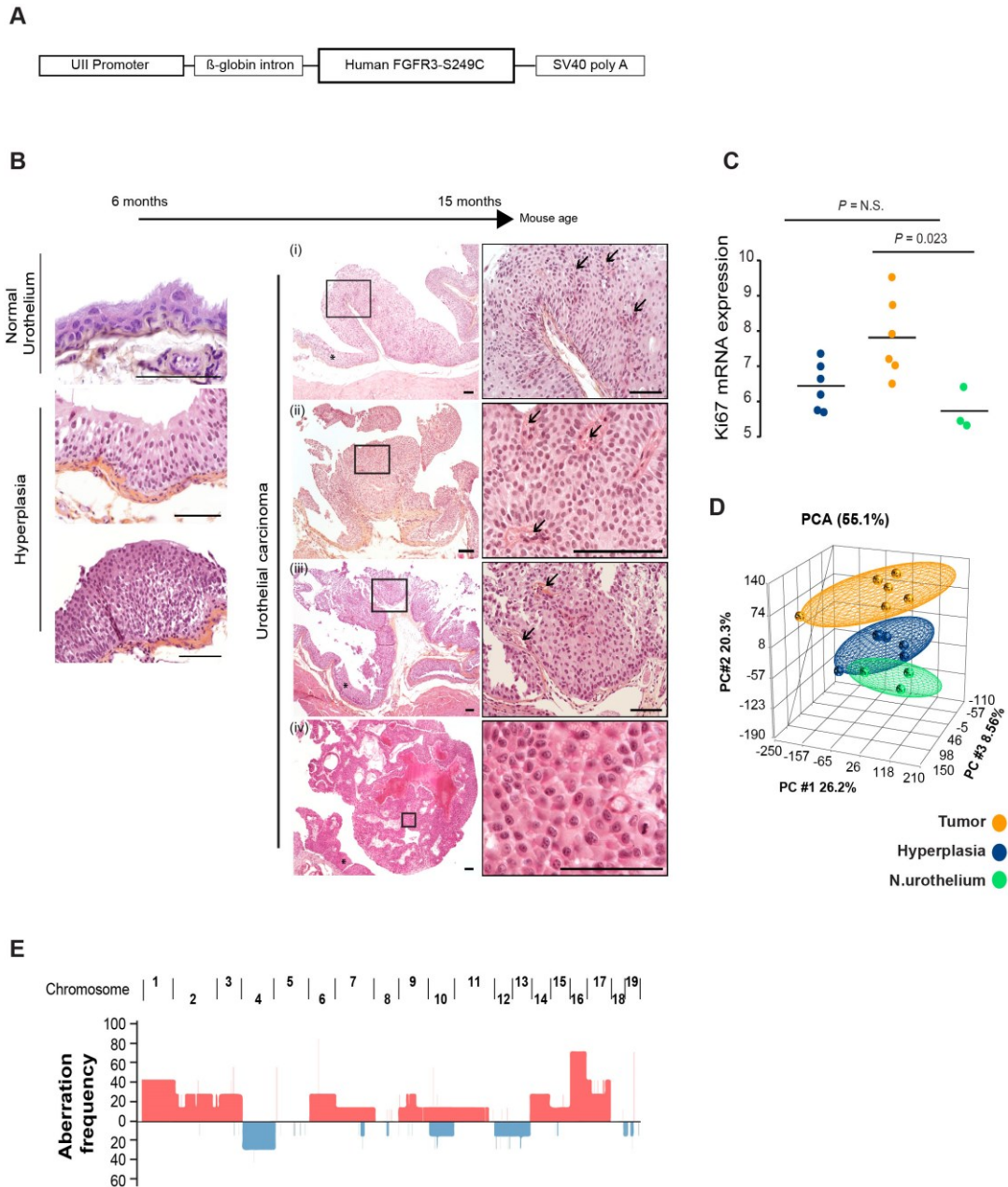


Figure 1. UPII-FGFR3-S249C transgenic mice develop urothelial hyperplasia and non-muscle-invasive low-grade urothelial carcinoma.

- Chimeric construct used to generate transgenic mice, consisting of a 3.6-kb mouse UPII gene promoter and a 2.1-kb human FGFR3b cDNA carrying the mutation S249C.
- Representative H&E histology of urothelial lesions in hFGFR3-S249C mice. Hyperplastic lesions (left panel) or low grade papillary urothelial carcinomas (right panel) developed in hFGFR3 S249C mice from 6 months and 15 months of age, respectively. Stars show tumor-adjacent urothelial hyperplasia. Arrows point to papillae fibrovascular cores. Scale bar: 100 μ m.
- mKi67 mRNA expression levels (Affymetrix Mouse Exon 1.0 ST. Array signal) in tumor and hyperplastic urothelium from UPII-hFGFR3-S249C mice and in normal urothelium from control littermates.
- Principal component analysis of all genes expressed on the Affymetrix Mouse Exon 1.0 ST. Array from tumor and hyperplastic urothelium from UPII- hFGFR3-S249C mice and from normal urothelial samples from control littermate mice (n= 6 tumors, 6 hyperplastic lesions, 3 normal urothelium).

RESULTS

- E. Frequency of chromosomal copy number alterations in tumors from UII-hFGFR3 S249C. (red = gain; blue= loss).

The UII-hFGFR3-S249C model is a luminal papillary model of human BCa.

Given the papillary nature of hFGFR3-S249C-induced tumors, we hypothesized that they recapitulate a luminal-like human bladder cancer molecular phenotype. We and others previously showed that N-Butyl-N(4-hydroxybutyl) (BBN)-induced BCas represent a model of basal-like BCa (18,19). To classify hFGFR3-S249C tumors, we first applied a molecular classifier allowing to distinguish between three classes of NMIBC (5). The six hFGFR3-S249C-induced tumors showed high correlations to centroid of gene expression of NMIBC classes 1 and 3 (both classes being enriched with FGFR3 mutations) (Fig.2A). We also applied the BASE47 classifier to distinguish between luminal and basal BCa subtypes (20). According to this classifier, FGFR3-induced bladder tumors were defined as luminal subtype, whereas our previously obtained BBN-induced tumors (18) were identified as basal subtype (Fig.2B). To further validate our results, we performed a cross-species comparison study by co-clustering the hFGFR3-S249C and BBN mice tumors with human tumors from our CIT cohort (n = 96 MIBCs and 99 NMIBCs) (21) using genes from a recently developed consensus classifier for basal and luminal-papillary human BCas (2) (employing the corresponding orthologues across the species). We found that hFGFR3-S249C and BBN tumors co-clustered with human luminal papillary and basal-like tumors, respectively (Fig.2C). These results are in good agreement with luminal papillary tumors being enriched in FGFR3 mutations.

Former studies have shown that Classes 1 and 3 of NMIBCs are characterized by a lower immune response and infiltrating immune cell activity compared to class 2 tumors (5), and luminal-papillary MIBC similarly display lower immune infiltration signals compared to basal tumors (2). Applying the mouse Microenvironment Cell Populations-counter method (mMCP-counter) (22) to our mice transcriptomic data, we estimated the immune cell infiltration in hFGFR3-S249C and BBN tumors. Consistent with human tumors, we estimated a weak infiltration of hFGFR3-S249C low-grade luminal papillary tumors observed for all type of immune cells, whereas BBN basal tumors presented a higher infiltration by macrophage/monocytes, and cytotoxic lymphocytes (Supplementary Fig.3A). The low immune cell infiltration of hFGFR3-S249C tumors is consistent with FGFR3 mutations synergizing with BBN and suppressing acute inflammation (15). We confirmed that hFGFR3-S249C expression promotes BBN-induced tumor formation (Supplementary Fig.3B) and showed that BBN-hFGFR3-S249C tumors retained features of the basal molecular subtype. Taken together, our data suggest that hFGFR3-S249C mouse tumors recapitulate the human luminal papillary subtype of BCas and could be a useful model to decipher the role of FGFR3 in BCa formation.

RESULTS

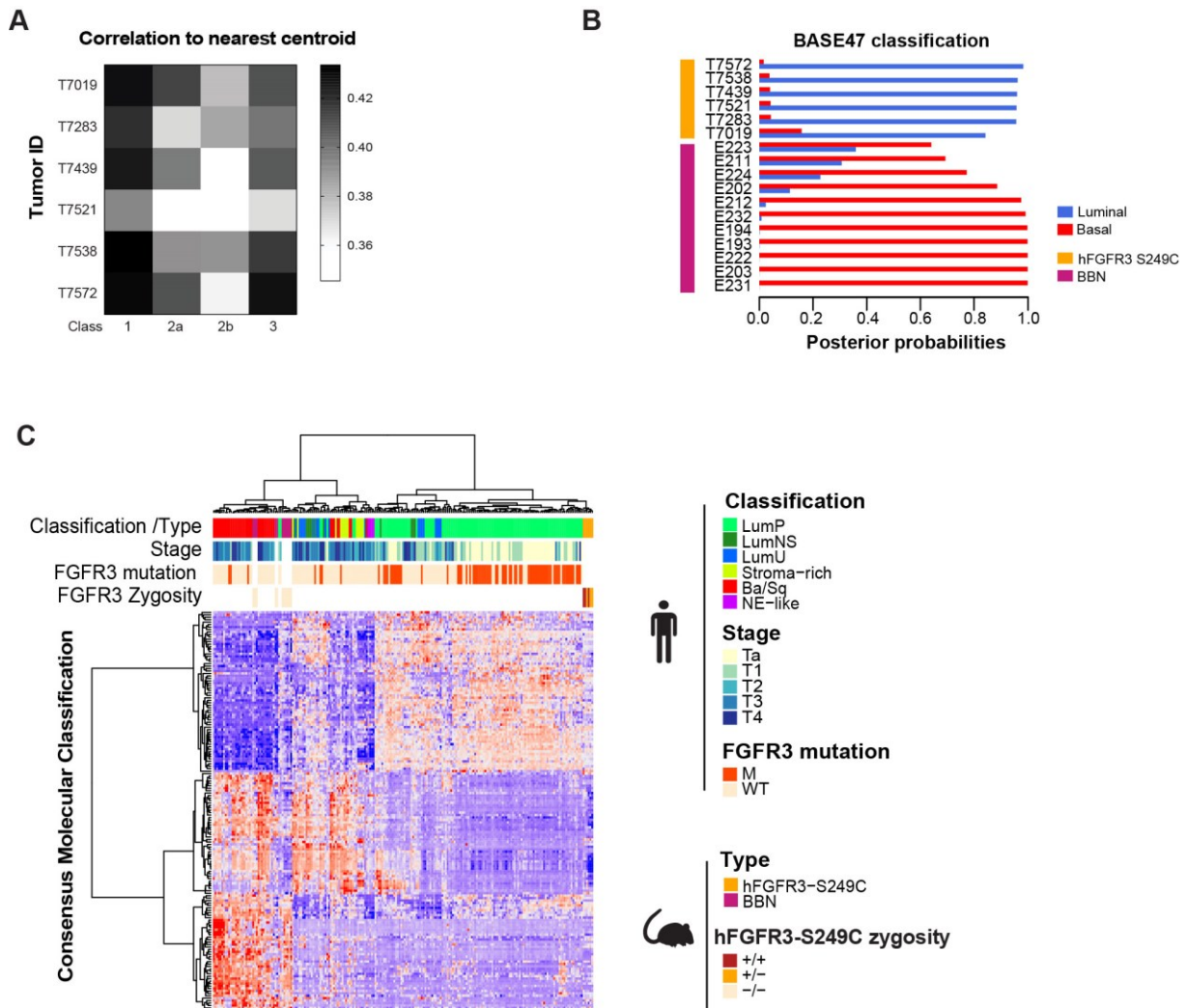


Figure 2. Mouse hFGFR3 S249C bladder tumors resemble human luminal papillary tumors at the transcriptomic level.

- A.** Correlation to the Hedegaard Non-Muscle Invasive Carcinoma classifiers⁽⁵⁾ and B) the BASE47⁽²⁰⁾ classifier for tumors of mice hFGFR3 S249C.
- B.** Muscle-invasive tumors derived from BBN treated mice are used as a control.
- C.** Cross-species, unsupervised hierarchical clustering of mice hFGFR3 S249C tumors (n=6) and human bladder tumors (n= 197 from the CIT series). Clustering done on genes from a consensus classifier for basal and luminal-papillary human BCas⁽²⁾.

RESULTS

FGFR3 expression levels impact tumor formation in UII-hFGFR3-S249C mice and could account for tissue specificity of altered-FGFR3 induced tumors.

We then studied an important series of mice (n = 402) and compared the frequency of tumors in 18-month-old UII-hFGFR3-S249C heterozygous and homozygous mice. The frequency of tumors was significantly higher in homozygous compared to heterozygous mice (~ 40% and 10%, respectively) (Fig.3A). Strikingly, multifocal tumors were specifically identified in homozygous mice, whereas heterozygous mice only developed unifocal tumors, re-enforcing the fact that the urothelium of homozygous mice was more sensitive to spontaneous tumor development than heterozygous mice. We hypothesized that the increased sensitivity to tumor development could be linked to the significantly higher expression level of hFGFR3 in homozygous compared to heterozygous mice, as assessed by RT-qPCR (Fig.3B). Following this hypothesis, we measured FGFR3 expression levels in different normal human epithelia, (including urothelium) obtained after microdissection. Interestingly, epithelia presenting high expression levels of FGFR3 were those in which FGFR3-mutated tumors are described (bladder, skin, exocervix) (Fig.3C) (3,23–25). Our data suggest that FGFR3 mutations require an epithelium with a high expression of FGFR3 to induce tumor formation. Nevertheless, although FGFR3 gene dosage in mice influenced tumor frequency, it did not reduce tumor development latency or induce progression towards muscle-invasive BCa. No histopathological difference was observed between hFGFR3-S249C- induced tumors between heterozygous and homozygous mice.

Mutated-FGFR3 favors a male gender bias in both mouse and human bladder tumors

Interestingly, considering gender of animals that developed tumors, we observed a significant difference between males and females, with males presenting a higher proportion of tumors than females considering tumor zygosity as stratification variable (Fig.3D). In human, it is well known that males are three times more susceptible to BCa than females. However, considering both NMIBC and MIBC FGFR3-mutated tumors, we observed that they were significantly more biased to male gender than wild-type tumors, and this was particularly marked in class 3 of NMIBC and the luminal papillary (LumP) subgroup of MIBC (Fig.3E).

RESULTS

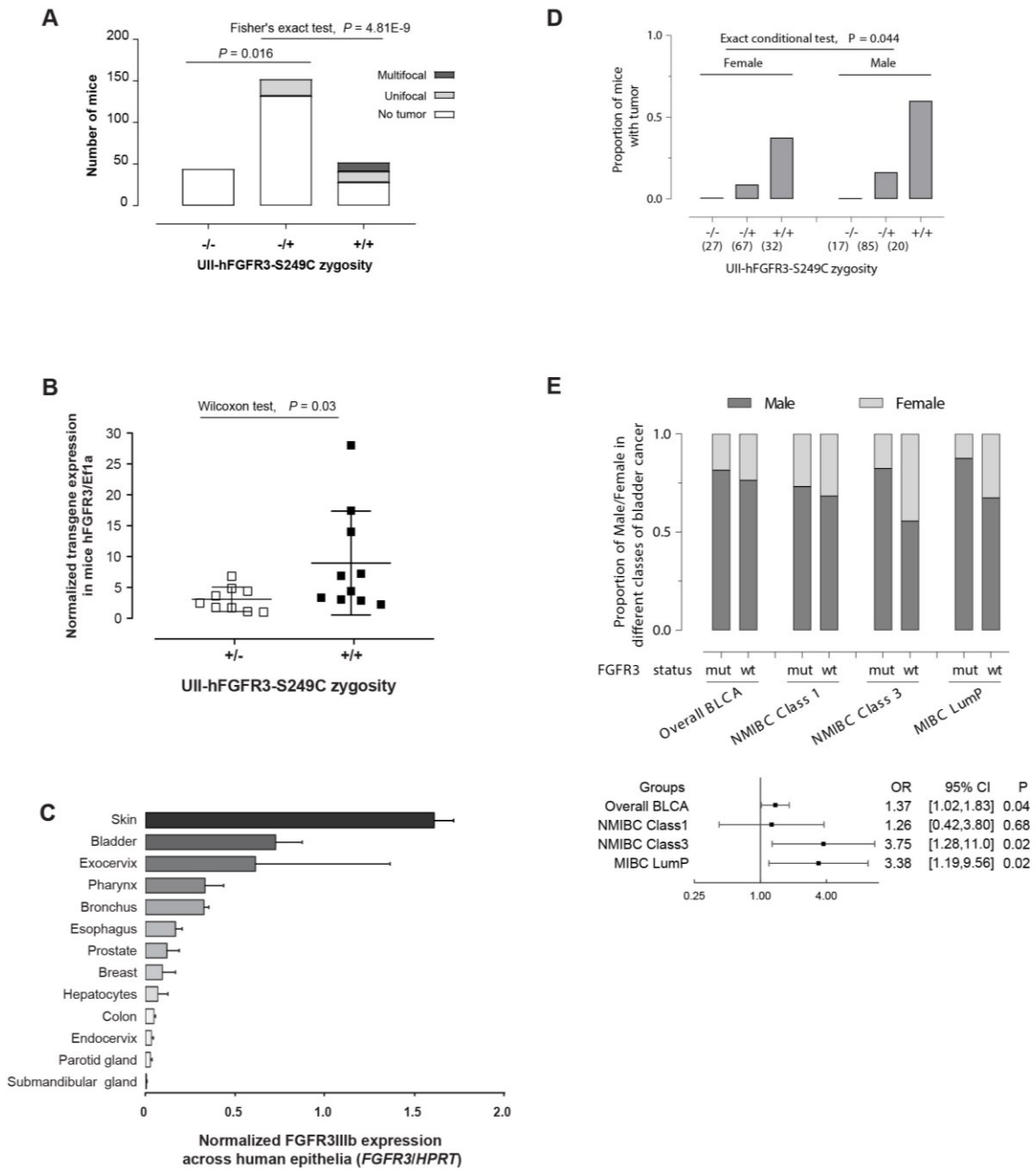


Figure 3. FGFR3-induced tumor development is dependent on FGFR3 expression levels.

- Frequency of unifocal or plurifocal bladder tumor development in hFGFR3-S249C homozygous (+/+) or heterozygous (+/-) mice versus control littermates (-/-).
- Frequency of bladder tumors in male and female Ull-hFGFR3-S249C mice. A-B-Proportions were compared using Fisher exact test.
- hFGFR3 mRNA expression evaluated by RT-qPCR in hFGFR3 S249C homozygous (+/+) or heterozygous (+/-) for mice. Results were normalized using EF1a expression levels. The statistical significance of differences was assessed using Wilcoxon test.
- Gender bias in tumor occurrence, stratified by Ull-hFGFR3-S249C zygosity. A higher proportion of male mice developed a tumor (tumor occurrence rate = 21% vs. 14%, respectively in male and female animals; Zelen's exact conditional test with Ull-hFGFR3-S249C zygosity as stratification, two-sided, $P = 0.044$; common odds ratio estimate = 2.19, 95% confidence interval = [1.02, 4.70])

RESULTS

- E. Comparison of gender distribution between FGFR3-mutated and wild-type human bladder tumors of different subgroups. Molecular classifications for both NMIBC and MIBC as described previously, in which NMIBC Class1 and Class3, and MIBC luminal papillary (MIBC LumP) subtypes are known as to be enriched for FGFR3 mutations (3, 5). NMIBC, non-muscle-invasive bladder cancer; MIBC, muscle-invasive bladder cancer. Odds ratios (ORs), corresponding 95% confidence intervals (95% CIs), and Z-test based P values were calculated (see methods)

Mutated-FGFR3 induces AR activation that could favor tumor development in male.

To unravel the molecular mechanisms that could favor the development of FGFR3-driven tumors in males, we compared transcriptomic data from 6 tumors and 3 normal control urothelia using the LIMMA algorithm. We observed 989 differentially expressed genes (Supplementary Fig.4A) that were enriched in pathways or biological processes related to cell adhesion and migration (Supplementary Fig.4B). However, none of these pathways could explain how a stronger activity of FGFR3 in males could favor tumor formation in such a context. We then focused on studying the transcriptional regulators that could underlie such phenotype. Using the upstream regulator function of the IPA (Ingenuity Pathway Analysis) software, we identified that, among a list of significantly enriched transcription factors (TFs), mutated-FGFR3 expression in mice induced both a significant increase of activity of AR and a decreased activity of estrogen receptor 1 (ESR1) (Fig. 4A, Supplementary Table 1). As control, we also observed that mutated-FGFR3 induced high MYC activity in mouse BCas, in accordance to what we have previously reported in human FGFR3-dependent models *in vitro* and *in vivo* (12). These findings suggest that the modulation of these hormone-receptors by mutated-FGFR3 could induce a gender bias in tumor formation. To further corroborate such results in human, we analyzed transcriptomic data from 3 FGFR3-dependent cell lines (MGH-U3, FGFR3-Y375C mutation; UM-UC-14, FGFR3-S249C mutation; RT112, FGFR3-TACC3 fusion) before and after FGFR3-knockout using the LIMMA algorithm and carried out an IPA analysis on the estimated differentially expressed genes (adjusted *P*-values <0.05; $|\log_2FC|>0.58$). In line with what we observed in murine BCas overexpressing hFGFR3-S249C, depletion of FGFR3 led to a significant decrease of AR and MYC activity. Yet, regarding ESR1, results were contradictory since we also predicted an inhibition of its activity after FGFR3 depletion (Fig.4A). To further validate our transcriptomic based predictions, we used an array to measure the binding of AR, ESR and MYC to their DNA target sequence under FGFR3 inhibited or control conditions in UM-UC-14 cells. We confirmed that the inhibition of FGFR3 in these cells led to a significant decrease of the binding of all three TFs to their DNA-target sequence (Fig.4B). Finally, taking advantage of published AR regulon gene sets (3), we calculated AR regulon activity in both NMIBC and MIBC tumors using gene set variation analysis (GSEA). The relevance of AR activation by mutated-FGFR3 was supported by a significantly higher AR regulon activity in FGFR3-mutated human bladder tumors as compared to tumors without FGFR3 mutations

RESULTS

(Fig.4C, left panel for NMIBC and right for MIBC). Of note, such significance was true in both male and female (Fig.4C) and independent of subtypes of NMIBC/MIBC (Supplementary Fig.5A-B).

Mutated-FGFR3 induced AR activity does not impact cell viability of FGFR3-dependent cells *in vitro*.

Due to the low penetrance and high latency of the phenotype in our UII-hFGFR3-S249C model, we evaluated the role of AR on cell viability in RT112, RT112/84 and UM-UC-14 BCa-derived cell lines expressing an altered FGFR3 and dependent on its activation for their proliferation/survival. We analyzed publicly available data of: (1) gene knock-out using CRISPR-Cas9 in the three aforementioned cell lines (Avena, Broad Institute (26)) (Fig.4D, left panel) and (2) AR-inhibitors treatment of RT112 cells (Drug sensitivity, Broad Institute (26)) (Fig.4D, right panel). None of the FGFR3-dependent cell lines relied on AR activity for cell survival (Fig.4D).

RESULTS

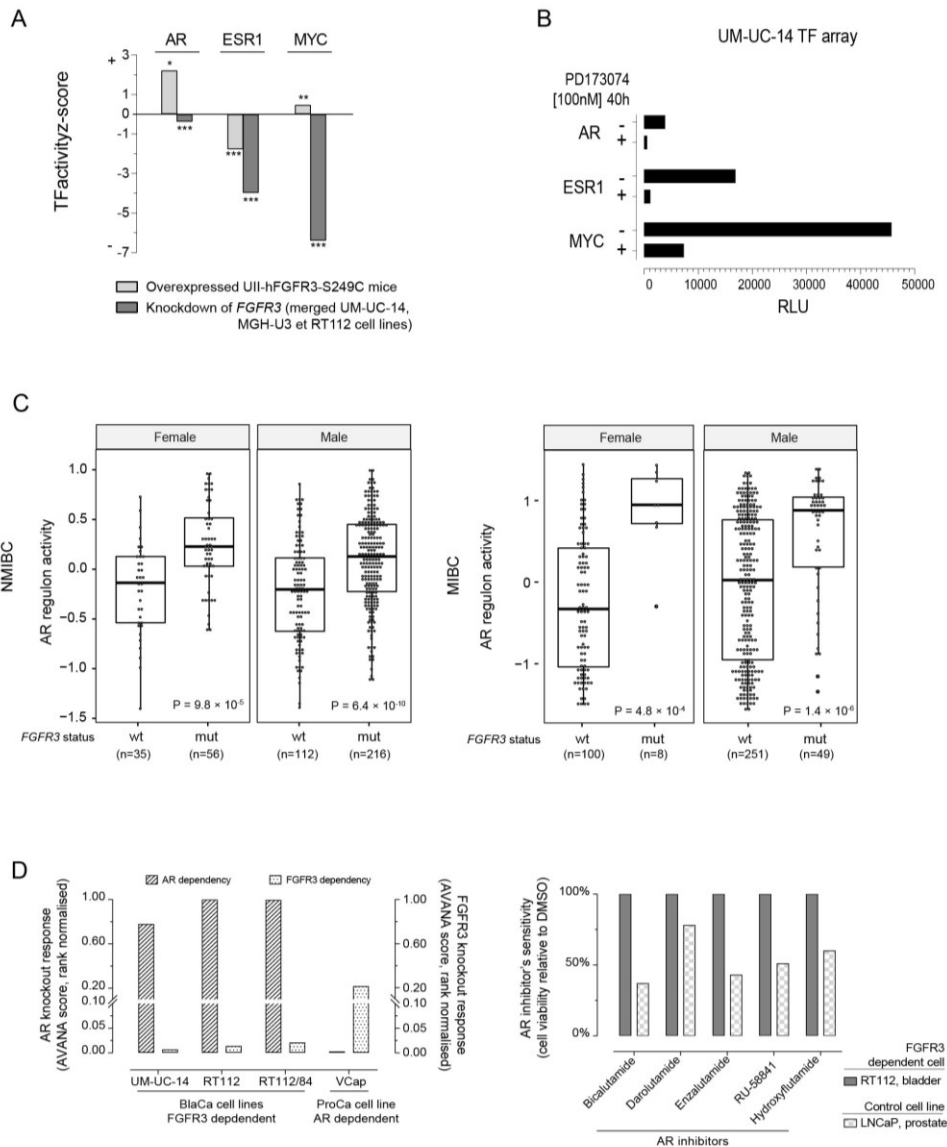


Figure 4.

Figure 4. Androgen receptor is activated by mutated-FGFR3 but does not regulate cell viability of FGFR3-dependent bladder cancer cells.

- A.** Statistically significant activation-states of AR, ESR1 and MYC in FGFR3-induced mouse tumors inferred using the Ingenuity Pathway Analysis (IPA) software. Activation scores were calculated using expression levels of transcription factor target genes in UPII-hFGFR3-S249C mouse bladder tumors. *P*-values of IPA prediction are shown by: * $P < 1E-02$; $P^{**} < 1E-04$; $P^{***} < 1E-07$.
- B.** Activation levels of AR, ER and MYC in UM-UC-14 human bladder cancer cells expressing FGFR3-S249C treated with the pan-FGFR inhibitor PD173074 [100nM,40h]. Activity levels were assayed using a TF Activation Profiling Array (RLU: Relative Luminescence Units).
- C.** Comparison of AR regulon activity between FGFR3-mutated and wild-type NMIBC or MIBC human bladder tumors, shown separately for gender. AR activity score for both NMIBC and MIBC was calculated via GSEA (Gene Set Variation Analysis) analysis, using the AR regulon target gene set previously published for MIBC (Methods). NMIBC, non-muscle-invasive bladder cancer; MIBC, muscle-invasive bladder cancer. *P* values: Wilcoxon test.
- D. Left Panel:** Response to AR knockout and/or inhibition in FGFR3-dependent BCa-derived cell lines (UM-UC-14, RT112 and RT112/84 cells). Prostate cancer cell lines (VCaP and LNCaP cells) were used as AR-responding positive controls whilst response of BCa cells to FGFR3 depletion served as a BCa dependency control. AVANA dependency scores are rank-normalized with 100% representing no-effect of on cell viability. **Right Panel:** Sensitivity to AR inhibition ($n = 5$ different

RESULTS

AR-inhibitors) in RT112 BCa cells as a measure of cell viability transformed from log₂ fold change between inhibitor treatment (n= 5 different AR-inhibitors) and DMSO control.

RESULTS

Discussion

We described here the first transgenic mouse model demonstrating a tumorigenic activity *in vivo* of a mutated-FGFR3. Expression of an hFGFR3-S249C in uroplakin-II expressing cells induces spontaneous low-grade papillary tumor formation and favors BBN carcinogen-induced tumor development. We observed hFGFR3-S249C-induced tumor installation in two different transgenic lines suggesting that the observed effect was likely induced by the expression of the transgene itself rather than to an alteration of an endogenous key gene resulting from the non-specific insertion of the transgene. Surprisingly, mutated-FGFR3 has already been targeted to urothelial cells using the same promoter without any spontaneous tumor formation being observed (14–17). Nonetheless, in some of these studies, expression of the mutated receptor did promote bladder tumor development when induced by exposure to carcinogen (BBN) (15) or in collaboration with *Pten* loss (16) or P53/pRB deficiency (17). This discrepancy between the previously developed GEM models and our GEM model could be linked to the FGFR3 mutation considered (S249C here, K644E in two previous studies (14,16)) or to the use of an inducible model for the expression of FGFR3-S249C in other studies (15,17). We have additionally shown that FGFR3-S249C expression levels impact the frequency of tumor formation, suggesting that a lower expression of the transgene in the former GEM models could also account for the absence of tumor formation in those transgenic mice. We used here the most frequent mutation of FGFR3 in BCa but we have recently shown that the over-representation of this mutation (FGFR3-S249C) was likely due to APOBEC mutagenesis rather than an increased tumorigenicity of such mutation as compared to other recurrent FGFR3 mutations (7). We can therefore suppose that other FGFR3-mutants would induce BCa formation as well.

Recently, the first pan-FGFR inhibitor – Erdafitinib/Balversa – has been approved by the FDA for patients with locally advanced or metastatic BCa presenting FGFR alterations. Considering the increasing interest of targeting FGFR3 for BCa treatment, having a model that resembles human counterparts at histological and transcriptomic levels; such as ours, may have clinical translational value to evaluate drug response and to understand acquired drug resistance mechanisms. In particular, the model we present here is the first immunocompetent model FGFR3-mutated-induced carcinomas. FGFR3 mutated tumors are non-T cell inflamed and have been associated to a poor immune-infiltrated immune-environment being therefore less prone to respond to immunotherapy (3,27,28). To confirm this hypothesis, a phase 1b/2 clinical trial (NCT03123055) comparing the efficacy of an anti-FGFR3 therapy (B-701, specific monoclonal antibody targeting FGFR3) coupled with immunotherapy (pembrolizumab) in advanced BCa patients harboring an altered FGFR3 is ongoing. In line with the literature, our GEM model showed poor infiltration of different immune cell populations. Hence allografts obtained from this model (latency and penetrance

RESULTS

of the phenotype won't allow a direct use of the model), should help a better understanding of immune-escape or immune-suppression mechanisms driven by a mutated/active FGFR3 and allow evaluation of combined therapies using FGFR and check-point inhibitors.

This model of FGFR3-induced tumors should also allow for a better understanding of the signaling pathways activated by FGFR3 during tumor progression. Targeting simultaneously different proteins forming part of the same signaling pathway could increase treatment efficacy and limit resistance as observed with the combination of B-Raf and MEK inhibitors for the treatment of melanoma (29). We recently demonstrated that MYC activation was crucial for FGFR3 oncogenic activities, pointing to a positive feedback loop of potential therapeutic value in BCa (12). Our GEM model confirmed the activation of MYC by FGFR3, which could contribute to an FGFR3-induced tumorigenesis through the promotion of cell hyperproliferation. Our model also highlighted an activation of androgen receptor by mutated-FGFR3 that was further corroborated in human derived preclinical models and supported by a higher activity of AR in FGFR3-mutated tumors compared to wild-type ones. Further analysis of the signaling pathway leading to this ligand-independent but FGFR3-induced activation of AR is worth further investigating. Since we did not observe any transcriptomic or post-transcriptomic regulation of AR expression levels (data not shown), we could assume that as reported for EGFR, FGFR3 could modulate AR activity through its phosphorylation or phosphorylation of a co-regulator. Very likely, the activation of AR could contribute to the obvious biased ratio of FGFR3-induced tumors in males versus females in bladder cancer. Due to the higher proportion of males presenting Bca (three times more males than females presenting with BCa), the interest in understanding the role of AR during bladder tumor development and the interest of AR as a therapeutic target has been a subject of several scientific studies (30,31) and clinical trials. Our results suggest that this interest should be particularly important in an FGFR3-mutated context. However, AR activation would rather favor tumor initiation than tumor growth since AR knock-out or inhibition did not impact cell viability of BCa-derived FGFR3-dependent cell lines *in vitro*. Although Ide and colleagues highlighted the therapeutic value of AR by showing that its inhibition could radiosensitize BCa cells (32), AR does not appear as a single therapeutic strategy for bladder tumors expressing a mutated-FGFR3 according to our search. Nonetheless, the impact of AR inhibition in *in vivo* models and/or on *in vitro* cell migration/invasion is worth evaluating for FGFR3-mutated bladder tumors to have a clear understanding of AR function and its preclinical value for these neoplasms.

RESULTS

Methods

Mouse models

All animals were housed and cared for in accordance with the institutional guidelines of the French National Ethics Committee (Ministère de l'Agriculture et de la Forêt, Direction de la Santé et de la Protection Animale, Paris, France). All experiments were reviewed and approved by the institute curie Animal Care and Use Committee.

Generation of UII-hFGFR3-S249C transgenic mice

The expression of a human FGFR3IIIb carrying the S249C mutation was targeted to the urothelium of mice by using the 5' regulatory region of the mouse uroplakin II promoter. The UII-FGFR3b-S249C construct was obtained by inserting the 3.6 kb murine uroplakin II promoter (UII) (33) excised with Sall and BamHI into the same restriction sites of the vector containing the β -globin intron 2 and the 3' polyadenylation sequences of SV40 (34) followed by the insertion of a human S249C mutated FGFR3 cDNA excised with XbaI and HindIII into the SmaI site of this vector. All PCR-generated segments were verified by sequencing both strands. The pUII-hFGFR3b-S249C constructs excised with KpnI were purified and microinjected into fertilized B6D2 oocytes. Genomic DNA was extracted from mouse tails and screened by PCR for integration of the transgene. Two lines were selected, L569 and L538, and mice were back-crossed five times to a C57BL/6J mice. Mice were of a mixed background and littermates were used as control. Bladder from mice aged 1 to 24 months were examined for macroscopic lesions followed by a histopathological analysis when required. Mice were then intercrossed to obtain hetero- and homozygous mice for the transgene.

Carcinogen treatment

BBN (N-butyl-N-(4-hydroxybutyl)-nitrosamine) was purchased from Tokyo Kasei Kogyo (Tokyo, Japan). Animals were housed in plastic cages in a controlled-environment room maintained at 22°C \pm 1°C with 12h light-12h dark cycles. All animals received food ad libitum. The UII-hFGFR3-S249C mice and control mice were aged 8-10 weeks old at the time of first carcinogen administration. The BBN was diluted at 0.05% in drinking water (ad libitum) for 8 weeks (the BBN solution was freshly prepared every 2-3 days). After withdrawal of BBN administration, drinking water without added chemicals was available ad libitum. Tumor formation and progression was followed weekly by echography. Mice were sacrificed when tumors reached 80% of bladder volume or when weight loss was greater than 20% of body weight.

RESULTS

RT-qPCR analyses

Total RNA from mouse urothelium was obtained using the Rneasy mini kit (Qiagen, Courtaboeuf, France) according to the manufacturer's instructions. One μg of total RNA was reverse transcribed using random hexamers (20 pmol) and 200 units of MMLV reverse transcriptase. The expression levels of the human FGFR3 transgene in urothelium and other tissues of transgenic mice were determined by real time PCR analysis. The mouse Eef1a gene was used as a control gene. Quantitative real time PCR was performed using a SYBR green PCR master Mix according to the manufacturer's instructions (Applied Biosystems, Foster city, CA, USA), on an ABI prism 7900 sequence detection system (Applied Biosystems). FGFR3 expression levels were calculated using the comparative Ct method normalized to Eef1a mRNA expression levels. The sequence of these primers used were as follow:

Gene	Strand	Sequence 5' - 3'
FGFR3	Fwd	AGTCCTGGATCAGTGAGAG
	Reverse	CTGCTCGGGGCCCGTGAACG
Eef1a1	Fwd	CTGGAGCCAAGTGCTAATATGCC
	Reverse	GCCAGGCTTGAGAACACCAGTC

Radioactive PCR

To compare the relative expression of the FGFR3 transgene to that of the endogenous murine Fgfr3 in the transgenic urothelium, transgenic urothelium cDNA was amplified in presence of ^{32}P dCTP using the primers forward 5'-GCAGGCATCCTCAGCTAC-3' and reverse 5'-TGGACTCGACCGGAGCGTA-3' which recognized both human and mouse FGFR3. The 107 bp amplified products were then digested with RsAI and HinP1I. The human amplified product possesses a RsAI restriction site and the mouse amplified product a HinP1I restriction site. After digestion, two fragments of 88 bp and 19 bp were obtained from the amplified human FGFR3 cDNA and two fragments of 59 bp and 48 bp were obtained from the amplified mouse Fgfr3 cDNA. The digested products were subjected to polyacrylamide gel electrophoresis and the intensities of the bands were quantified with a Molecular Dynamics Storm PhosphorImager (Molecular Dynamics/Amersham, Sunnyvale, CA, USA).

Histological analyses

UII-hFGFR3-S249C mutant and control mice bladders were fixed in 10 % formalin, embedded in paraffin and cut at 4- μm thick slides for histological and immunohistochemical

RESULTS

analyses. Histological hematoxylin and eosin-stained (H&E) slides were reviewed by two genito-urinary pathologists.

Whole exome sequencing and identification of copy number alterations

DNA from UII-hFGFR3-S249C mouse normal urothelium, hyperplastic urothelia and urothelial carcinomas was extracted using phenol-chloroform. Whole exome libraries were prepared by Integragen (Evry, France). Raw sequence alignment and variant calling were carried out using Illumina CASAVA 1.8 software (mm10 mouse reference genome). Each variant was annotated according to its presence in the 1000Genome, Exome Variant Server (EVS) or Integragen database, and according to its functional category (synonymous, missense, nonsense, splice variant, frameshift or in-frame indels). Reliable somatic variants were identified as those having a sequencing depth in ≥ 10 reads in tumor and normal urothelium samples, with ≥ 3 variant calls representing $\geq 15\%$ total reads in the tumor, ≤ 1 variant calls representing $< 5\%$ total reads in the normal urothelium, and a QPHRED score ≥ 20 for both SNP detection and genotype calling (≥ 30 for indels).

Copy number alterations (CNAs) were identified using coverage data to calculate the log ratio of the coverage in each tumor sample as compared to a normal urothelium sample. Log-ratio profiles were then smoothed using the circular binary segmentation algorithm as implemented in the Bioconductor package DNACopy. The most frequent smoothed value was considered to be the zero level of each sample. Segments with a smoothed log ratio above zero + 0.15 or below zero - 0.15 were considered to have gains and deletions, respectively. High-level amplification and homozygous deletion thresholds were defined as the mean +7 s.d. of smoothed log ratios in regions with gains and deletions, respectively.

The identified frequent chromosomal gains or deletions were further validated by qPCR using genomic DNA. Primers targeting exonic regions from different genes found in the most frequently altered chromosomes were designed. A Taqman qPCR (Applied Biosystems) was carried out on gDNA to compare expression levels between normal urothelium and tumors from UII-hFGFR3-S249C mice. Normalization was performed using genes present on chromosomes without genomic alteration. The designed primers were the following:

RESULTS

Gene	Exon	Strand	Sequence 5' - 3'
<i>Most frequently altered chromosomes</i>			
<i>ErbB4</i>	26	Fwd	TGCAACGGCTGAGATGTTT
		Reverse	GTGCCACTGGCTTTTCGTAG
<i>Trat1</i>	6	Fwd	GGCCCAGGAAACAGAATACTAA
		Reverse	GAGAAACGTTGGCATCCATT
<i>Fkbp5</i>	9	Fwd	AGGCCGTGATTTCAGTACAGG
		Reverse	TCTGACAGGCCGTATTCCAT
<i>Control chromosomes w/o genomic alteration</i>			
<i>Tgfbr3</i>	13	Fwd	TTGTGTTCAAGTCCGTGTTCA
		Reverse	TTCCTAGAGCACAGCGTCAG
<i>Inpp4b</i>	15	Fwd	GCTACAACCTTCATAGCAACTCA
		Reverse	TCAGGCTGTCTGGAGAACG

Microarray transcriptome profiling

Total RNA (200ng) from UII-hFGFR3-S249C mouse normal urothelium, hyperplastic lesions and urothelial carcinomas was analyzed with the Affymetrix Mouse Exon 1.0 ST. Array gene expression was RMA normalized and annotated to the GRCm38 genome version. The LIMMA algorithm was applied to calculate the genes having a significant change of expression between urothelial carcinomas and normal urothelium or hyperplastic lesions. Genes were considered to be differentially expressed when they presented an absolute log₂FC >0.58 and an adjusted p-value <0.05. P-values were adjusted for multiple comparisons using the Benjamini-Hochberg correction. Upstream regulator analysis based on the differentially expressed genes was performed with IPA software to identify key TFs as well as predict their transcriptional activities. FGFR3 regulated transcriptomes (FGFR3 knockdown versus control) from three BCa-derived cell lines (UM-UC-14, MGH-U3 and RT112) were previously published by host lab (7,12). Since all these cell lines were FGFR3 dependent, we considered them as one group, treated and non-treated, and performed similar analyses as above to double confirm TFs identified from UII-hFGFR3-S249C mouse model.

Pathway and Gene Ontology Biological Processes Enrichment

Genes with an absolute log₂FC of at least 0.58 and an adjusted p-value inferior to 0.05 were used to carry out an enrichment analysis of KEGG Pathways and Gene Ontology Biological Processes. The enrichment analysis was done using David 6.8, mus musculus Affy Exon 1.0 ST background. Significantly enriched pathways were considered when they had an adjusted p-value (Benjamini and Hochberg) inferior to <0.05.

RESULTS

Cross-species hierarchical clustering

Microarray transcriptomic data from UII-hFGFR3-S249C and BBN mice was combined with transcriptomic array data from human bladder tumors (CIT; Affymetrix Exon 1.0 ST; 96 MIBC and 99 NMIBC). Batch effects due to data combination were corrected using the surrogate variable analysis R package. The protocol used for co-clustering of the two species was that of previously described (19). Hierarchical clustering was done using a gene signature derived for the consensus molecular classification of MIBC (2).

Transcriptome classifier

Subtype calls were done on murine hFGFR3 S249C and previously established murine BBN induced tumor transcriptomes. Samples were classified using a 3-classes classifier for NMIBC or the BASE47 classification algorithm and the median centered expression of the murine orthologues found in the BASE47 signature, as previously described (2,19).

Gender bias in tumors with FGFR3 mutations

We established a merged cohort of 1,220 BCa subjects with both FGFR3 mutation and gender information available, based on data from our Carte d'Identité des Tumeurs (CIT) database and public sources (2,3,5,35,36). For MIBC subjects from the TCGA dataset, transcriptome-derived molecular classification was determined as previously described (2). Molecular classification for NMIBC samples included in the UROMOL study was extracted from supplementary data of the associated publication (5). We compared the gender distribution (male vs. female) between bladder cancers harboring or not an FGFR3 mutation in the overall cohort and in the three subgroups enriched in FGFR3 mutations: NMIBC Class1 and Class3, and MIBC luminal papillary subtype. Odds ratios (ORs), corresponding to 95% confidence intervals (95% CIs), and Z-test based *P* values were calculated. An OR > 1 indicates a higher proportion of males in FGFR3 mutated tumors, and a 95% CI not covering 1 or *P* < 0.05 indicates statistically significant difference.

Transcription factor activity analysis

UM-UC-14 cells were seeded in 100mm plates at a density of 3.0x10⁶cells/dish. Cells were plated and left to adhere overnight. Afterwards, cells were treated for 40 hours with the pan-FGFR inhibitor PD173074 [100nM] (Calbiochem, Merck Eurolab, France). Control cells were treated with DMSO vehicle diluted proportionally to the inhibitor. After the 40h of treatment, nuclear fractions were isolated for analysis in the TF Activation Profilin Plate Array I from Signosis (according to the manufacturer's protocol). Cellular fractions were recovered using the Thermo Fisher NE-PER nuclear and cytoplasmic extraction kit (ref 78833), following the manufacturer's instructions).

RESULTS

AR regulon activity

RNA-seq derived transcriptome data (fragments per kilobase of transcript per million, FPKM normalization with log₂ transformation) of the UROMOL NMIBC (n = 476) (5) and TCGA MIBC (n = 408) (3) samples were downloaded from the ArrayExpress (<https://www.ebi.ac.uk/arrayexpress/>, accession number E-MTAB-4321) and UCSC Xena (<https://xenabrowser.net/>) databases, respectively. Computationally predicted AR regulon genes were extracted from supplementary data of TCGA MIBC (3). We calculated for each of the above samples an AR regulon activity score as the difference of the sample-specific enrichment score of positive targets and that of negative targets obtained using the Gene Set Variation Analysis algorithm (37). Comparison of AR regulon activity between FGFR3 mutated and non-mutated tumors was performed in all NMIBC and MIBC samples, as well as in subgroups defined by gender or molecular subtypes.

Response of BCa cell lines to AR inhibition/knockout.

We explored gene dependency to AR knockout and measurements of sensitivity to different AR specific inhibitors (n = 5, including Bicalutamide, Darolutamide, Enzalutamide, RU-58841 and Hydroxyflutamide) in three FGFR3 dependent BCa cell lines (UM-UC-14, RT112 and RT112/84 cells) and from the DepMap data repository. Prostate cancer cell lines (VCaP and LNCaP cells) known as AR-dependent cell lines, were taken as positive control to AR response. The Avana gene dependency of FGFR3 knockout showed a general response to the treatment and was taken as a BCa dependency control. Avana AR/FGFR3 dependency score was rank-normalized, with 100% representing no effect, and cell viability was transformed from log₂ fold change between inhibitor treatment and DMSO control.

Author contributions statement

Conceptualization: M.S, X.M, I.B.P., F.R.; *Methodology:* X.M, P.L., A.K, A.D.R; *Investigation:* A.M.V., M.S, J.F, X.M, F.D, C.D.L, M.L.L, A.R, O.L, I.B.P; *Formal Analysis:* A.M.V., S.M., J.F, X.M., F.D, A.K., E.C, A.A, L.D, Y.A, I.B.P; *Writing –Original Draft:* I.B.P., A.M.V., J.F, S.M.J., X.Y.; *Writing –Review & Editing:* all the authors; *Visualization:* A.M.V., S.M., J.F, X.Y; *Funding Acquisition:* I.B.P and F.R.; *Resources:* T.L, L.D., Y.A.; *Supervision:* I.B.P. and F.R.

RESULTS

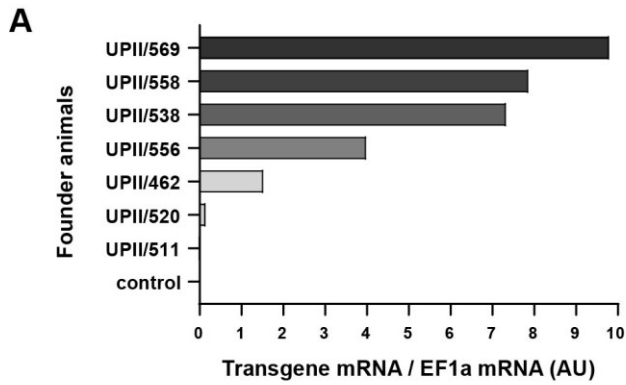
References

1. Bray F, Ferlay J, Soerjomataram I, Siegel RL, Torre LA, Jemal A. Global cancer statistics 2018: GLOBOCAN estimates of incidence and mortality worldwide for 36 cancers in 185 countries. *CA Cancer J Clin.* 2018;68:394–424.
2. Kamoun A, Reyniès A de, Allory Y, Sjö Dahl G, Robertson AG, Seiler R, et al. A Consensus Molecular Classification of Muscle-Invasive Bladder Cancer. *Eur Urol.* 2019;pii: S0302-2838(19)30695-5.
3. Robertson AG, Kim J, Al-Ahmadie H, Bellmunt J, Guo G, Cherniack AD, et al. Comprehensive Molecular Characterization of Muscle-Invasive Bladder Cancer. *Cell.* 2017;171:540-556.e25.
4. Sjö Dahl G, Eriksson P, Liedberg F, Höglund M. Molecular classification of urothelial carcinoma: global mRNA classification versus tumour-cell phenotype classification. *J Pathol.* 2017;242:113–25.
5. Hedegaard J, Lamy P, Nordentoft I, Algaba F, Høyer S, Ulhøi BP, et al. Comprehensive Transcriptional Analysis of Early-Stage Urothelial Carcinoma. *Cancer Cell.* 2016;30:27–42.
6. Kim W-J, Kim E-J, Kim S-K, Kim Y-J, Ha Y-S, Jeong P, et al. Predictive value of progression-related gene classifier in primary non-muscle invasive bladder cancer. *Mol Cancer.* 2010;9:1–9.
7. Shi MJ, Meng XY, Lamy P, Banday AR, Yang J, Moreno-Vega A, et al. APOBEC-mediated Mutagenesis as a Likely Cause of FGFR3 S249C Mutation Over-representation in Bladder Cancer. *Eur Urol.* 2019;76:9–13.
8. Porebska N, Latko M, Kucińska M, Zakrzewska M, Otlewski J, Opaliński Ł. Targeting Cellular Trafficking of Fibroblast Growth Factor Receptors as a Strategy for Selective Cancer Treatment. *J Clin Med.* 2018;8:7.
9. Nakanishi Y, Akiyama N, Tsukaguchi T, Fujii T, Satoh Y, Mizuno H, et al. Mechanism of oncogenic signal activation by the novel fusion kinase FGFR3-BAIAP2L1. *Cancer Res.* 2015;75:123–123.
10. Williams S V., Hurst CD, Knowles MA. Oncogenic FGFR3 gene fusions in bladder cancer. *Hum Mol Genet.* 2013;22:795–803.
11. Bernard-Pierrot I, Brams A, Dunois-Lardé C, Caillault A, Diez de Medina SG, Cappellen D, et al. Oncogenic properties of the mutated forms of fibroblast growth factor receptor 3b. *Carcinogenesis.* 2006;27:740–7.
12. Mahe M, Dufour F, Neyret-Kahn H, Moreno-Vega A, Beraud C, Shi M, et al. An FGFR3/MYC positive feedback loop provides new opportunities for targeted therapies in bladder cancers. *EMBO Mol Med.* 2018;10:pii: e8163.
13. Loriot Y, Necchi A, Park SH, Garcia-Donas J, Huddart R, Burgess E, et al. Erdafitinib in locally advanced or metastatic urothelial carcinoma. *N Engl J Med.* 2019;381:338–48.
14. Ahmad I, Singh LB, Foth M, Morris C-A, Taketo MM, Wu X-R, et al. K-Ras and b-catenin mutations cooperate with Fgfr3 mutations in mice to promote tumorigenesis in the skin and lung, but not in the bladder. *Dis Model Mech.* 2011;4:548–55.
15. Foth M, Ismail NFB, Kung JSC, Tomlinson D, Knowles MA, Eriksson P, et al. FGFR3 mutation increases bladder tumorigenesis by suppressing acute inflammation. *J Pathol.* 2018;246:331–43.
16. Foth M, Ahmad I, Van Rhijn BWG, Van Der Kwast T, Bergman AM, King L, et al. Fibroblast growth factor receptor 3 activation plays a causative role in urothelial cancer pathogenesis in cooperation with Pten loss in mice. *J Pathol.* 2014;233:148–58.
17. Zhou H, He F, Mendelsohn CL, Tang MS, Huang C, Wu XR. FGFR3b extracellular loop mutation lacks tumorigenicity in vivo but collaborates with p53/pRB deficiency to induce high-grade papillary urothelial carcinoma. *Sci Rep.* 2016;6:1–11.
18. Rebouissou S, Bernard-Pierrot I, Reyniès A de, Lepage M-L, Krucker C, Chapeaublanc E, et al. EGFR as a potential therapeutic target for a subset of muscle-invasive bladder cancers presenting a basal-like phenotype. *Sci Transl Med.* 2014;6:244ra91-244ra91.
19. Saito R, Smith CC, Utsumi T, Bixby LM, Kardos J, Wobker SE, et al. Molecular subtype-specific immunocompetent models of high-grade urothelial carcinoma reveal differential neoantigen expression and response to immunotherapy. *Cancer Res.* 2018;78:3954–68.
20. Damrauer JS, Hoadley KA, Chism DD, Fan C, Tiganelli CJ, Wobker SE, et al. Intrinsic subtypes of high-grade bladder cancer reflect the hallmarks of breast cancer biology. *Proc Natl Acad Sci.* 2014;111:3110–5.
21. Biton A, Bernard-Pierrot I, Lou Y, Krucker C, Chapeaublanc E, Rubio-Pérez C, et al. Independent Component Analysis Uncovers the Landscape of the Bladder Tumor Transcriptome and Reveals Insights into Luminal and Basal Subtypes. *Cell Rep.* 2014;9:1235–45.

RESULTS

22. Becht E, Giraldo NA, Lacroix L, Buttard B, Elarouci N, Petitprez F, et al. Estimating the population abundance of tissue-infiltrating immune and stromal cell populations using gene expression. *Genome Biol.* *Genome Biology*; 2016;17:1–20.
23. Logié A, Dunois-Lardé C, Rosty C, Levrel O, Blanche M, Ribeiro A, et al. Activating mutations of the tyrosine kinase receptor FGFR3 are associated with benign skin tumors in mice and humans. *Hum Mol Genet.* 2005;14:1153–60.
24. Hafner C, Van Oers JMM, Vogt T, Landthaler M, Stoehr R, Blaszyk H, et al. Mosaicism of activating FGFR3 mutations in human skin causes epidermal nevi. *J Clin Invest.* 2006;116:2201–7.
25. Rosty C, Aubriot MH, Cappellen D, Bourdin J, Cartier I, Thiery JP, et al. Clinical and biological characteristics of cervical neoplasias with FGFR3 mutation. *Mol Cancer.* 2005;4:2–9.
26. Meyers RM, Bryan JG, McFarland JM, Weir BA, Sizemore AE, Xu H, et al. Computational correction of copy number effect improves specificity of CRISPR-Cas9 essentiality screens in cancer cells. *Nat Genet.* 2017;49:1779–84.
27. Kardos J, Chai S, Mose LE, Selitsky SR, Krishnan B, Saito R, et al. Claudin-low bladder tumors are immune infiltrated and actively immune suppressed. *JCI Insight.* 2016;1:e85902.
28. Sweis RF, Spranger S, Bao R, Paner GP, Stadler WM, Steinberg G, et al. Molecular drivers of the non-T cell-inflamed tumor microenvironment in urothelial bladder cancer. *Cancer Immunol Res.* 2016;4:563–8.
29. Flaherty KT, Infante JR, Daud A, Gonzalez R, Kefford RF, Sosman J, et al. Combined BRAF and MEK Inhibition in Melanoma with BRAF V600 Mutations. *N Engl J Med.* 2012;367:1694–703.
30. Li P, Chen J, Miyamoto H. Androgen receptor signaling in bladder cancer. *Cancers (Basel).* 2017;9:1–14.
31. Hsu JW, Hsu I, Xu D, Miyamoto H, Liang L, Wu XR, et al. Decreased tumorigenesis and mortality from bladder cancer in mice lacking urothelial androgen receptor. *Am J Pathol.* *American Society for Investigative Pathology*; 2013;182:1811–20.
32. Ide H, Inoue S, Mizushima T, Jiang G, Chuang KH, Oya M, et al. Androgen receptor signaling reduces radiosensitivity in bladder cancer. *Mol Cancer Ther.* 2018;17:1566–74.
33. Lin JH, Zhao H, Sun TT. A tissue-specific promoter that can drive a foreign gene to express in the suprabasal urothelial cells of transgenic mice. *PNAS.* 1995;92:679–83.
34. Ramírez A, Bravo A, Jorcano JL, Vidal M. Sequences 5' of the bovine keratin 5 gene direct tissue- and cell-type-specific expression of a lacZ gene in the adult and during development. *Differentiation.* 1994;58:53–64.
35. Guo G, Sun X, Chen C, Wu S, Huang P, Li Z, et al. Whole-genome and whole-exome sequencing of bladder cancer identifies frequent alterations in genes involved in sister chromatid cohesion and segregation. *Nat Genet.* 2013;45:1459–63.
36. Kim PH, Cha EK, Sfakianos JP, Iyer G, Zabor EC, Scott SN, et al. Genomic predictors of survival in patients with high-grade urothelial carcinoma of the bladder. *Eur Urol [Internet]. European Association of Urology*; 2015;67:198–201. Available from: <http://dx.doi.org/10.1016/j.eururo.2014.06.050>
37. Hänzelmann S, Castelo R, Guinney J. GSVA: gene set variation analysis for microarray and RNA-seq data. *BMC Bioinformatics.* 2013;14:1–15.

Supplementary Figures

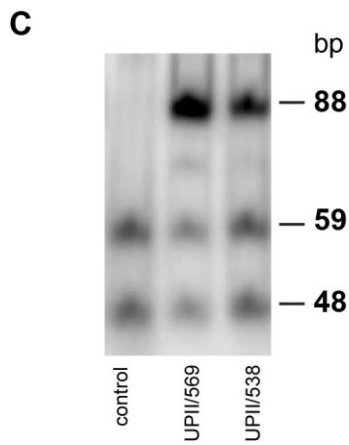
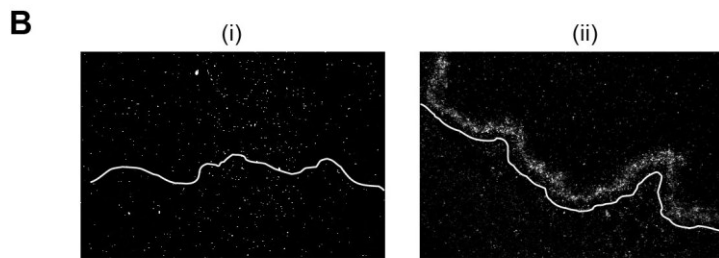


Supplementary Figure 1.

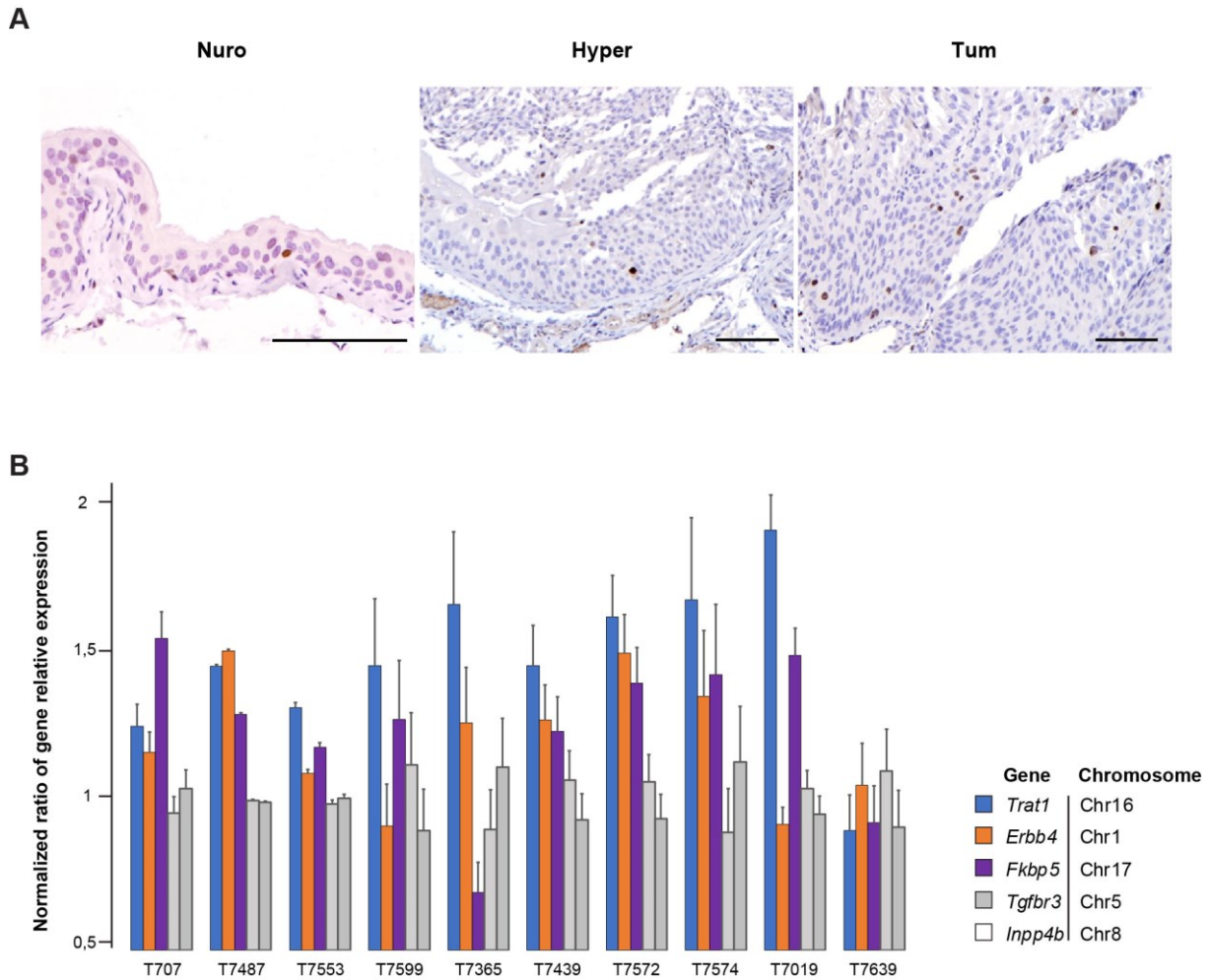
A. Validation of the expression of the relative mRNA expression levels of the human FGFR3 transgene in the urothelium of transgenic UPII-FGFR3-S249C mice.

B. In situ hybridization showing expression of the human FGFR3 transgene at the supra-basal and intermediate cell layers of UPII-FGFR3-S249C mice urothelium (4 months of age). Magnification x100.

C. Radioactive PCR showing the expression of both human and mouse FGFR3 digested amplicons (cDNA) in control and UPII-FGFR3-S249C (line 569 and 538) mice. The bands of 59 and 48 bp correspond to mouse endogenous FGFR3, and the band of 88 bp to the human FGFR3 transgene.



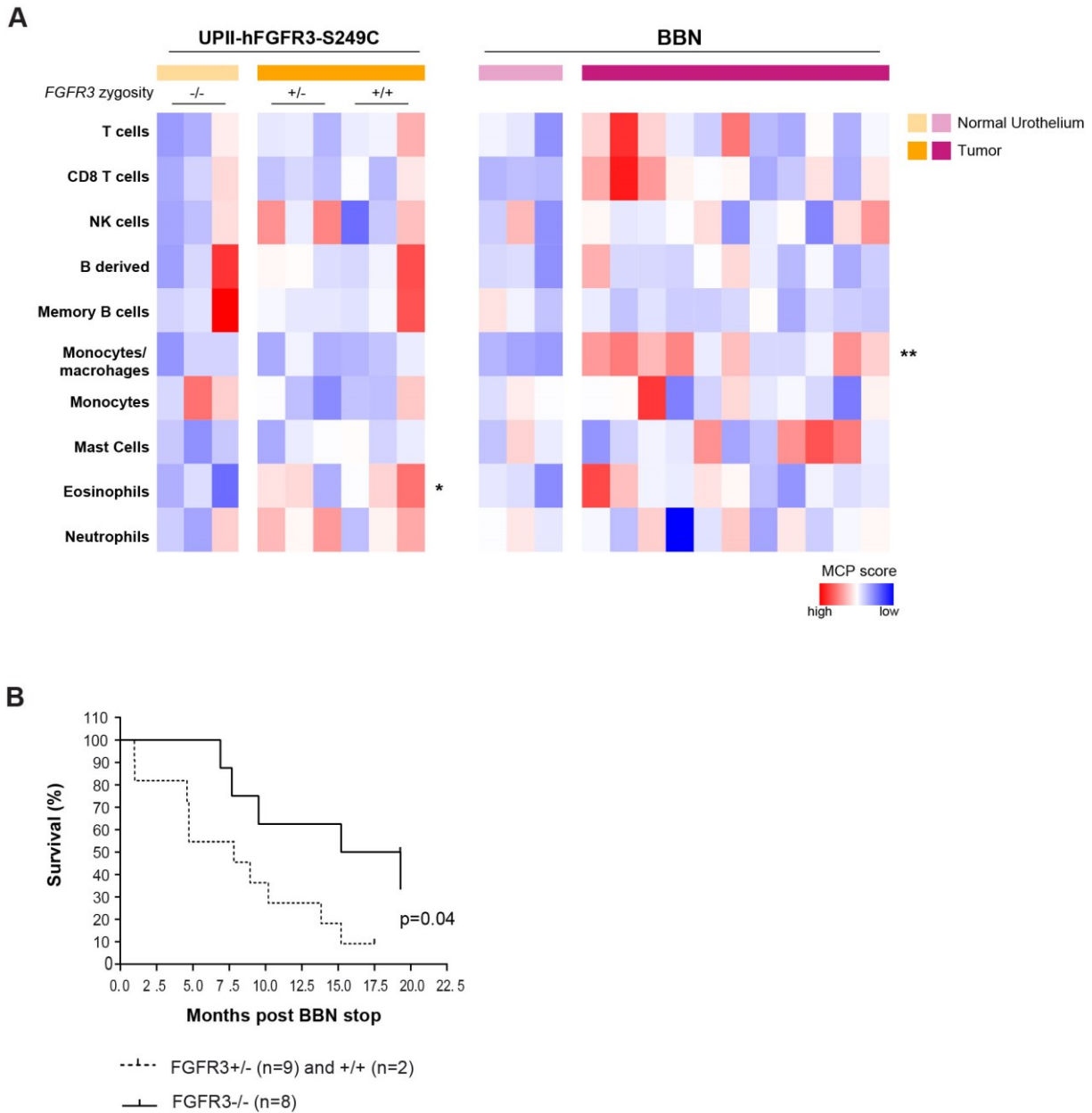
RESULTS



Supplementary Figure 2.

- A.** Representative immunohistochemistry showing Ki67 expression in hyperplastic urothelium (middle panel) and bladder tumor (right panel) of UPII-hFGFR3-S249C mice and in normal urothelia from control littermates (right panel).
- B.** Genomic DNA qPCR validation of genes found in frequently altered regions (chromosomes 1, 16 and 17) of tumors from UPII-hFGFR3-S249C mice. Shown is the ratio of relative expressions of exonic regions of genes found in altered chromosomes (*Trat1*, *ErbB4*, *Fkbp5*) against the genes found in stable chromosomes (*Tgfbr3*, *Inpp4b*). Each relative expression value was calculated using the $2^{-\Delta\Delta Ct}$ method and values were normalized to control urothelia for each sample.

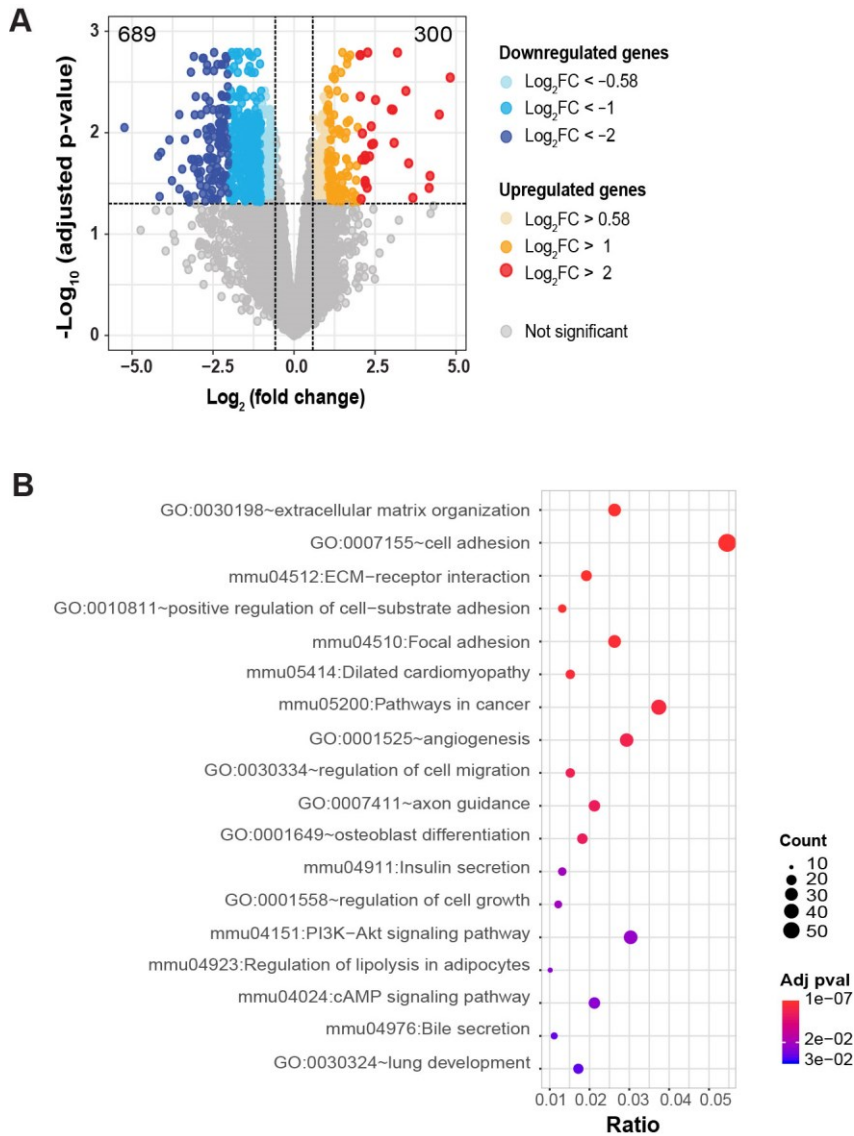
RESULTS



Supplementary Figure 3.

- A.** Heatmap of MCP counter signature for estimation of infiltration of different immune populations based on transcriptomic data from BBN-induced tumors (n=11) and tumors of mice hFGFR3 S249C (n=6) and of. Red indicates high and blue indicates low mRNA expression respectively (normalized mRNA expression levels).
- B.** Survival plot of UPII-hFGFR3-S249C mice (FGFR3 +/- or +/+) versus control mice from littermates (FGFR3 -/-) following treatment with 0.05% BBN in drinking water for 8 weeks.

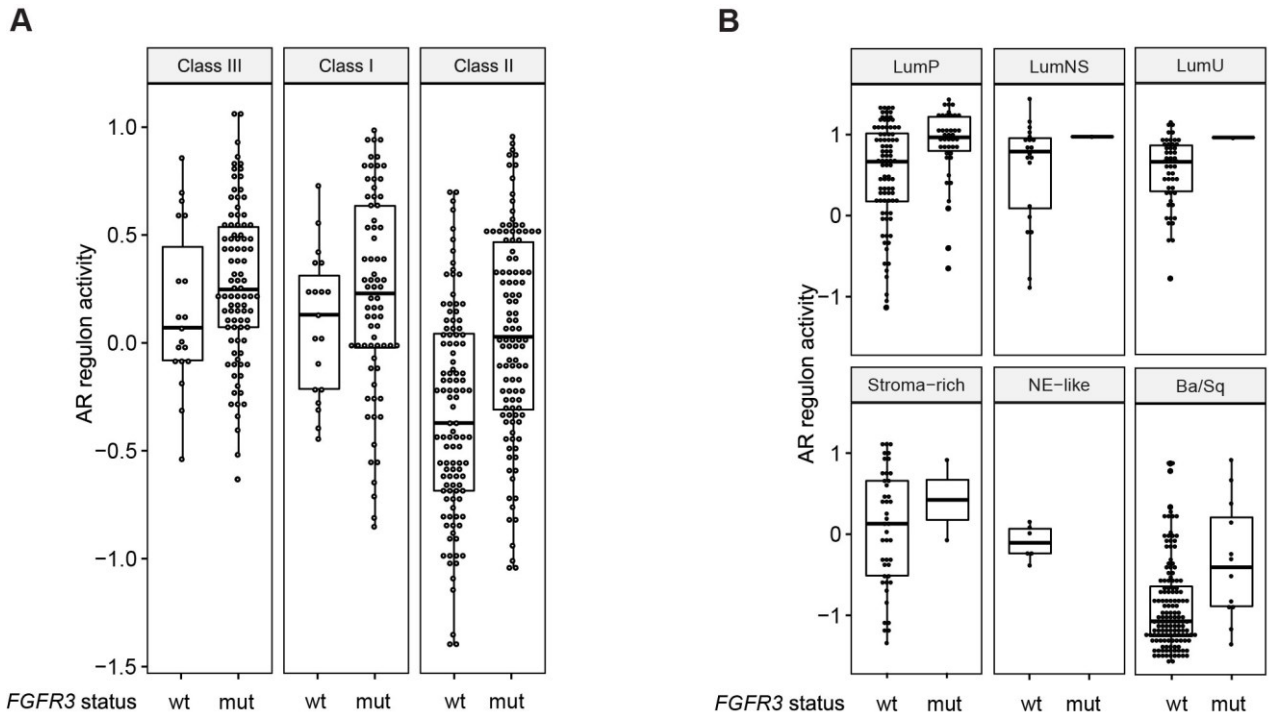
RESULTS



Supplementary Figure 4.

- A.** Volcano plot of the set of differentially expressed genes (DEGs; 989 genes; $|\log_2FC| > 0.58$; $adjpval < 0.05$) by comparing gene expression in hFGFR3 S249C mice tumors compared to normal control urothelium.
- B.** Plot of top 18 Gene Ontology Biological Processes (GO) and murine KEGG (KE) deregulated pathways using a set of 989 differentially expressed genes obtained by comparison of hFGFR3 S249C tumors and normal mouse urothelium ($|\log_2FC| > 0.58$; $adj.p-val < 0.05$). The adjusted p-value of each enriched term, as well as the number of genes assigned to each term (count) and the ratio of assigned genes to total number of genes belonging to a term are displayed.

RESULTS



Supplementary Figure 5.

Comparison of AR regulon activity between FGFR3-mutated and wild-type tumors in different subtypes of NMIBC (A) and MIBC (B). Molecular classifications for both NMIBC and MIBC as described previously.

Supplementary Tables

Supplementary Table 1.

Predicted significantly regulated TFs by overexpression or knockdown of FGFR3

Upstream Regulator	Predicted status	Overexpression of <i>FGFR3</i> (Uii-hFGFR3-S249C Mice)		Knockdown of <i>FGFR3</i> (merged UM-UC-14 MGH-U3 RT112 cells)	
		Activation z-score	Adj. <i>P</i> -value	Activation z-score	Adj. <i>P</i> -value
TP53	Inhibited	-1.855	4.63E-10	6.057	8.48E-31
ESR1	Inhibited	-1.767	4.65E-09	-3.987	6.86E-19
SMARCA4	Inhibited	-1.567	3.19E-10	1.532	4.67E-03
STAT3	Inhibited	-0.115	6.02E-04	-1.797	6.09E-03
MYC	Activated	0.364	1.73E-05	-6.407	3.34E-14
FOXM1	Activated	0.619	9.20E-04	-4.29	1.54E-08
GATA1	Activated	0.707	3.75E-02	4.574	7.60E-07
AR	Activated	2.199	2.59E-03	-0.378	1.70E-08

1.3 Discussion

In our study, we presented the first autochthonous model of FGFR3-induced bladder tumors, evidencing the oncogenic consequences of *FGFR3* activating mutations. Surprisingly, the FGFR3 (S249C) tumorigenic activity observed in our transgenic mice contrasts with the three previously reported GEM models expressing a mutated *Fgfr3/FGFR3*^{102,103,179}. Different reasons explaining such discrepancies may include: 1) the type of FGFR3 mutation that was studied (S249C mutations affecting the extracellular domain of the receptor versus K644E mutations affecting the intracellular kinase domain); 2) the genetic engineering approach (doxocyclin-induced¹⁰² versus stable transgene expression); 3) the expression levels of the *FGFR3* transcript; 4) the delay to examine tumor formation (12 months versus >18 months)¹⁰³, and the genetic background of the mouse model.

Aiming to highlight the potential of use of our autochthonous model in the field of translational research, we confirmed that mouse UPII-hFGFR3-S249C tumors were equivalent to their human counterpart at both the histological and transcriptomic level. In this way, allografts from this model could be used to more deeply evaluate an FGFR3-driven oncogenesis *in vivo*, unveil new therapeutic targets, and, most importantly, test new therapeutic strategies.

By analyzing the course of autochthonous tumor development, we were able to examine disease stages (hyperplastic lesions) that are infrequently found in the clinic, and which can shed light on the molecular mechanisms associated to early bladder tumorigenesis. In addition, the simple observation of tumor frequency in later stages of our model led us to explore frequency data in human bladder tumors and confirm a statistically significant, much stronger male dominance in FGFR3-mutated subtypes of MIBC and NMIBC tumors. We corroborated that a plausible underlying cause could be a higher AR activity induced by a mutated-FGFR3 in both NMIBC and MIBC tumors. Examination of the role and regulation of AR *in vitro* in an altered-FGFR3 context suggested that AR may be important during the initial phases of tumor development. However, AR activity does not seem required for FGFR3-induced cell proliferation/survival, suggesting it may not be involved in tumor progression. Whilst this may at first lead to the conclusion that AR would not necessarily represent a target of therapeutic interest, a recent study by Wu and colleagues²⁴⁶ demonstrated that androgen-suppressive therapy in NMIBC patients resulted in lower tumor recurrence rates. Considering the high recurrence rate in NMIBC patients and its associated co-morbidity on the long-term, such potential therapy could be of great benefit. A deeper

RESULTS

study of AR function within an altered FGFR3 context will be very important to reveal molecular mechanisms of therapeutic interest.

Altogether, we report here the first transgenic mouse model illustrating the *in vivo* tumorigenic activity of a mutated-FGFR3 alone. Use of such immunocompetent, spontaneous bladder tumor GEM model will allow to increase our knowledge of the oncogenic signaling network of FGFR3 *in vivo* and consequently shed light on targetable molecular mechanisms. In addition, observations made from the development of the disease throughout time in our model, may pinpoint towards interesting processes that should be further explored in human bladder tumors.

RESULTS

Chapter 2. FGFR3 Gene regulatory network in bladder cancer

2.1 Introduction

FGFR3 regulates a range of essential cellular processes including proliferation, survival, angiogenesis, migration and differentiation; making it an interesting therapeutic target. Indeed, based on the frequent aberrant activation of this receptor in bladder tumors and the positive outcomes of many clinical trials^{43,48,51,72,92,105–108,247}, the FDA has recently approved the first anti-FGFR therapy for the treatment of advanced stages of the disease⁷². Despite such significant progress, the gene regulatory network of FGFR3 in bladder cancer continues to be little studied. Notably, FGFR3 has been previously reported to present opposite functional roles depending on cellular-context^{84,248–250}. A better understanding of the FGFR3-driven, bladder-cancer-specific regulatory network is thus needed to increase our knowledge of the biology of the disease and understand the specific molecular contexts in which an anti-FGFR therapy would be most efficient.

In the present project, we merged a statistical, reverse-engineering inference method with functional validation to construct a gene regulatory (GRN) network specific to the context of bladder tumors, and that is regulated by an altered-FGFR3. In particular, we were interested on studying the transcription factors and cofactors that co-operatively drive the inferred GRN.

As discussed in the introduction, numerous bioinformatic approaches enable the construction of genome-scale regulatory networks that define the interactions between transcription factors and their target genes. Overall, the methods that most successfully capture biologically relevant relationships have been those that focus on the construction of context-specific networks and that integrate validated regulatory interactions (protein-protein interactions and/or transcriptional regulation) to refine the original network^{188,221}. On this basis, we collaborated with the bioinformatic team of Mohamed Elati (Université de Lille) to employ CoRegNet²²⁶ (Bioconductor), a package adapted for the reverse-engineering inference and analysis of large-scale, context-specific regulatory networks. By implementing the H-LICORN^{224,225} algorithm, CoRegNet allows to infer a cooperativity network of transcription factors and cofactors (TFs/coTFs) that co-regulate the expression of a set of shared target genes. In addition, by calculating a sample-specific activity of the inferred TFs/coTFs, transcriptional programs that are active under diverse cellular contexts can be highlighted. In this way, we inferred a bladder cancer co-regulatory network (BLCA-GRN) from FGFR3-mutated bladder cancer cell lines and bladder tumors transcriptomes. Utilizing experimentally derived data of FGFR3 perturbation *in vitro* and *in vivo*, we identified the

RESULTS

TFs/coTFs that were driven by an altered-FGFR3 and were essential for its tumorigenic activity. The p63 transcription factor emerged as an essential element of the GRN in both non-muscle invasive (NMIBC) and muscle-invasive (MIBC) bladder tumors; whose activity is regulated by FGFR3. We demonstrated that it plays a role in the modulation of tumor growth, cell proliferation, migration and invasion, and that such functional role may explain some of the observed phenotypes in FGFR3-mutated NMIBCs.

2.2 Results

RESULTS

Identification of a key oncogenic role of p63 in altered-FGFR3 tumors through inference of bladder cancer gene regulatory network and functional validations.

Aura Moreno-Vega^{1*}, Macarena Zambrano^{2*}, Julia Puig^{3*}, Florent Dufour¹, Clarice Groeneveld^{1,4}, Mingjun Shi¹, Claire Beraud⁵, Myriam Lasalle⁵, Elodie Chapeaublanc¹, Thierry Lebret⁶, Philippe LLuel⁵, Ana Maria Eijan², Lars Dyrskjot⁷, Mohamed Elati^{3,#}, François Radvanyi^{1,#}, Catalina Lodillinsky^{2,#} and Isabelle Bernard-Pierrot^{1,#,@}

¹ Institut Curie, CNRS, UMR144, Molecular Oncology team, PSL Research University, Paris, France; b Paris-Sud University, Paris-Saclay University, Paris, France;

² Research Area, Institute of Oncology Angel H. Roffo, University of Buenos Aires, Buenos Aires, Argentina

³ Univ. Lille, CNRS, Inserm, CHU Lille, UMR9020 – UMR-1277 - Canther, F-59000 Lille, France

⁴ La ligue contre le cancer, Paris, France

⁵ Urosphere, Toulouse, France

⁶ Service d'Urologie, Hôpital Foch, Suresnes, France

⁷ Department of Molecular Medicine, Aarhus University Hospital, Aarhus, Denmark

In preparation for submission

* These authors contributed equally to the work

These authors co-supervised the study

@ To whom correspondence should be addressed.

Dr Isabelle Bernard-Pierrot

Institut Curie

12 rue Lhomond

75005 Paris

E-mail: isabelle.bernard-pierrot@curie.fr

Tel: +33 1 42 34 63 40, Fax: +33 1 42 34 63 49

RESULTS

Abstract

The alteration of the receptor tyrosine kinase FGFR3 through activating mutations or translocations is one of the most common genetic events in bladder cancer (BLCA). Despite the demonstration of the oncogenic potential of such alterations, the gene regulatory network of an altered-FGFR3 in bladder cancer remains poorly characterized. We combined here a bioinformatic reverse-engineering inference approach together with *in vitro* and *in vivo* FGFR3-perturbation experiments to determine a BLCA regulatory network of transcription factors and co-factors (TFs/coTFs) that are driven by an altered-FGFR3 and critical for its oncogenic activity. Amongst them, we identified p63 in both non-muscle (NMIBC) and muscle invasive bladder cancers (MIBC) and further demonstrated that it mediates tumor growth, cell proliferation and migration of FGFR3-dependent bladder cancer cells. In Ta NMIBC, we observed both higher p63 activity and increased tendency of recurrence in tumors harboring a mutated-FGFR3 as compared to tumors with the wild-type receptor, suggesting that p63 activation by FGFR3 could favor recurrence. Our results elucidate an unexpected oncogenic key role of p63 in luminal papillary tumors bearing FGFR3 mutations and provide a global BLCA specific FGFR3-induced gene regulatory network that should allow a better understanding of FGFR3 induced oncogenic dependency that could have clinical applications.

Introduction

Bladder cancer is the fourth most common cancer in men in industrialized countries and it can be divided into two main groups based on tumor stage. Non-muscle invasive bladder carcinoma is the most frequent subtype at first diagnosis (NMIBC, 75% of patients) and although it is of good prognosis (80% five-year survival rate), an important percentage of patients recur following initial treatment (70% of patients). Furthermore, depending on grade and stage, 5-75% of NMIBC patients will progress into muscle-invasive disease (MIBC)^{1,2}. Contrary to NMIBC, MIBC is a life-threatening disease with a five-year survival of less than 60%, which decreases to less than 6% in presence of metastasis^{3,4}.

The treatment of bladder cancer remains challenging and very expensive due to two different clinical problems: (1) the high recurrence of NMIBC leading to a costly long-term follow-up and (2) the poor survival rate of MIBC, a disease for which there are almost no efficient treatments available. Recently, promising results have been reported in clinical trials targeting FGFR3, a frequently altered receptor tyrosine kinase (RTK) in bladder cancer⁵⁻⁸. Activating mutations affecting *FGFR3* are amongst the most commonly observed genetic alterations in bladder cancer, being present in more than 65% of NMIBCs (enriched in Class 1 and Class 3 subtypes) and 15% of MIBCs (enriched in luminal papillary subtype)^{9,10}. Moreover, translocations leading to active *FGFR3* gene fusions can be observed in 3% of

RESULTS

MIBCs and 30% of MIBCs that present a wild-type *FGFR3*, overexpress the receptor^{11–13}. In 2019, the FDA approved the first pan-inhibitor directed against FGFRs in advanced bladder cancer. However, as previously reported in preclinical bladder cancer models and in other targeted therapies in different cancer types (EGFR, BRAF, KIT; lung cancer, melanoma, gastrointestinal stromal tumors), patients are expected to develop resistance to RTK-targeting treatment^{14–19}. As the *FGFR3* gene regulatory network in bladder cancer remains poorly characterized, a deeper understanding of such network would allow to better comprehend the role of the receptor in the disease and identify new therapeutic targets. Most importantly, the identification of novel targets would improve existing *FGFR3*-targeting therapies and/or prevent the development of resistance to treatment. The identification of MYC; of one key TF activated by *FGFR3*, already allowed us to propose optional therapeutic strategies by inhibiting the *FGFR3*-MYC regulatory loop²⁰. One of the main aims of this study is to provide a global *FGFR3* regulatory network that may be used in the future to discover new driver regulators of therapeutic interest.

There exist many different bioinformatic methods to infer gene regulatory networks (GRNs) from high-throughput data, enabling the discovery of disease-driver genes and or pathways. Up to date, among the approaches that have proved successful are those that allow for the reverse-engineered construction of context-specific networks (e.g. ARACNe, LICORN, GENIE3) and which can be further enriched through the integration of interaction evidences (protein-protein interactions and/or transcriptional regulation)^{21–25}. Here, we use the hybrid-learning co-operative regulation networks (H-LICORN) algorithm that integrates data-mining methods with numerical linear regression to efficiently infer a context-specific GRN^{26,27}. More specifically, we predicted a cooperativity network of transcription factors and cofactors (TFs/coTFs; co-activators and co-repressors) using transcriptomic data from *FGFR3*-mutated bladder cancer cell lines and human bladder tumors. Employing experimentally derived data where the expression or activity of *FGFR3* was altered in *in vitro* and *in vivo* preclinical models, we highlighted the TFs and coTFs from the network that are driven by an altered *FGFR3*. Additionally, we identified the essential regulators of such network through the use of publicly available cell viability data from large CRISPR-Cas9-based screen in *FGFR3*-dependent bladder cancer cell lines²⁸. An important result from our study was the identification of p63 as an essential and active transcription factor forming part of the *FGFR3*-driven regulatory network in bladder cancer. We further showed, that it regulates tumor growth, cell proliferation, migration and invasion through extra-cellular matrix degradation. These functional findings are relevant as they may help to better understand certain phenotypes that are present in *FGFR3*-dependent tumors, such as the one we discuss in this study: a higher tendency of recurrence observed in *FGFR3*-mutated tumors that could be associated with a higher P63 activity.

RESULTS

Results

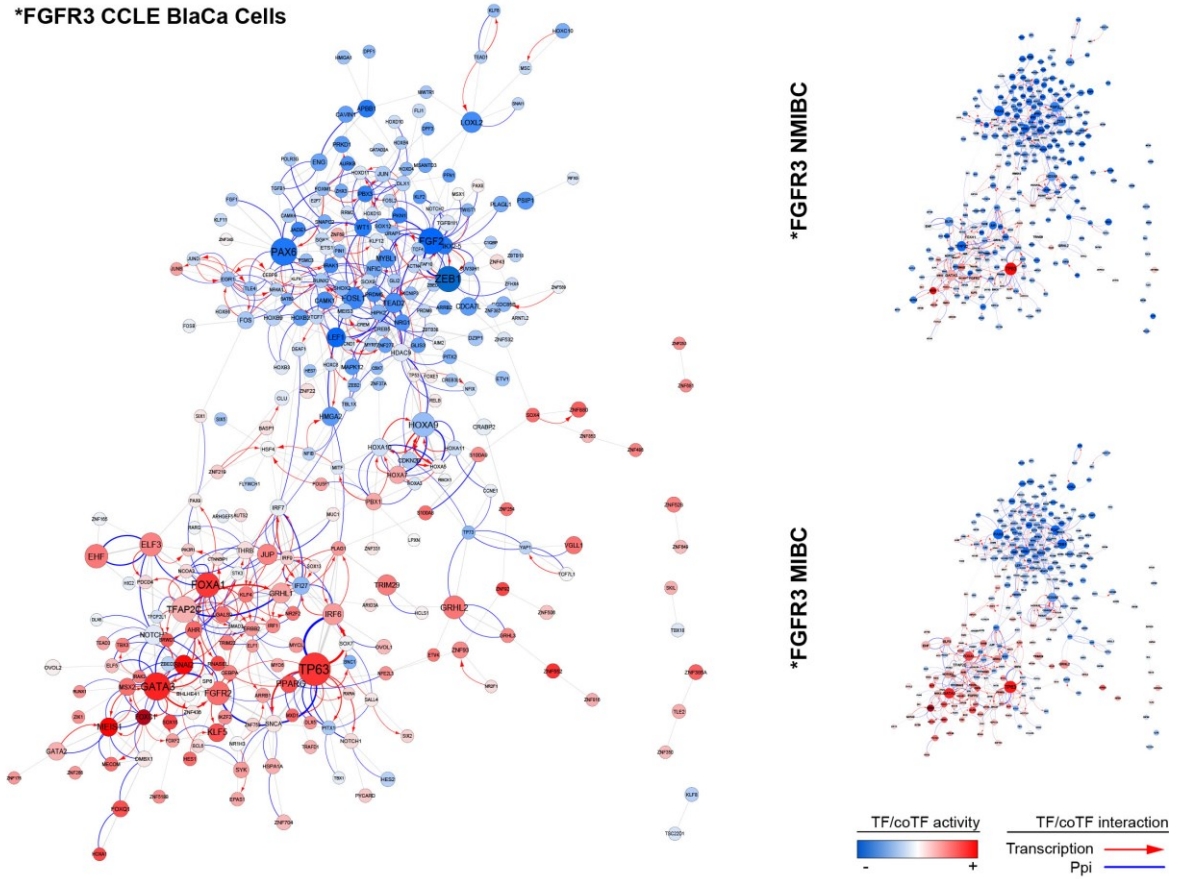
Bladder-cancer gene regulatory network of TFs and coTFs in FGFR3-altered tumors.

Using the CoRegNet package (Bioconductor), we generated a GRN from the transcriptome of the 36 bladder cancer cell lines of the CCLE 2019Q1 and refined it via the integration of protein-protein interactions (ppis) and transcriptional regulatory interactions (transcription factor binding sites; tfbs) (See Methods). To reconstruct the GRN, we chose transcriptomes from bladder tumor-derived epithelial cell lines in order to avoid any bias that would be introduced from using less homogenous transcriptomic data from bladder tumors that contains stromal genes. The resulting GRN was composed of 720 TFs/coTFs, 6 374 target genes and 31 003 regulatory interactions that were significantly enriched for validated ppis (P -value = $6.34e-127$) and tfbs (P -value $< 1e-100$). Based on the shared targets of every pair of TFs/coTFs, the GRN was then transformed into a co-operativity network (co-regulatory BLCA-GRN).

Aiming to highlight the transcriptional program that would be active under an altered-*FGFR3* context, we calculated the activity of each TF/coTF using the CCLE expression data of only previously identified *FGFR3*-dependent bladder cancer cell lines bearing *FGFR3* genomic alterations (translocations leading to fusion proteins or activating point mutations): RT112 (*FGFR3*-*TACC3*), RT112-84 (*FGFR3*-*TACC3*), RT4 (*FGFR3*-*TACC3*), SW-780 (*FGFR3*-*BAIAP2L1*) and UM-UC-14 (*FGFR3*-*S249C*). The computed activity was then projected on the inferred-BLCA-GRN (Figure 1A, left panel). To determine if the resulting network was also representative of human bladder tumors, we re-calculated the activity of the previously inferred TF/coTFs from two expression data sets of *FGFR3*-mutated tumors: 272 NMIBCs⁹ and 52 MIBCs¹⁰ (Figure 1A, right panel). We observed that many of the most active TF/coTFs (4th quartile, $n = 74$) in *FGFR3*-dependent bladder cancer cell lines were also active in both the *FGFR3*-mutated NMIBC and MIBC tumors (Figure 1B). However, we observed stronger similarities in the patterns of TF/coTF activity between the cell lines and the MIBC luminal papillary (LumP) and the NMIBC class 1. This could result from the fact that analyzed cell lines are derived from MIBC, and classified as luminal papillary, and NMIBC class 1 also present a luminal-like differentiation. Corroborating the relevance of our constructed network, we found several previously described bladder-cancer genes within the group of most active TFs/coTFs in these subgroups of luminal papillary tumors such as *GATA3*, *PPARG*, *FOXA1*, *KLF5*, *TRIM29* and *NOTCH3* (Figure 1B, left panel)²⁹⁻³². The difference in the BLCA-GRN among tumors bearing an altered-*FGFR3* suggest that *FGFR3* activity may depend on the molecular subtype, which could have clinical implications. However, 14 TFs/co-TFS are common in all subtypes and may be enriched in key elements of the altered-*FGFR3* pathway (Figure 1B, right panel).

RESULTS

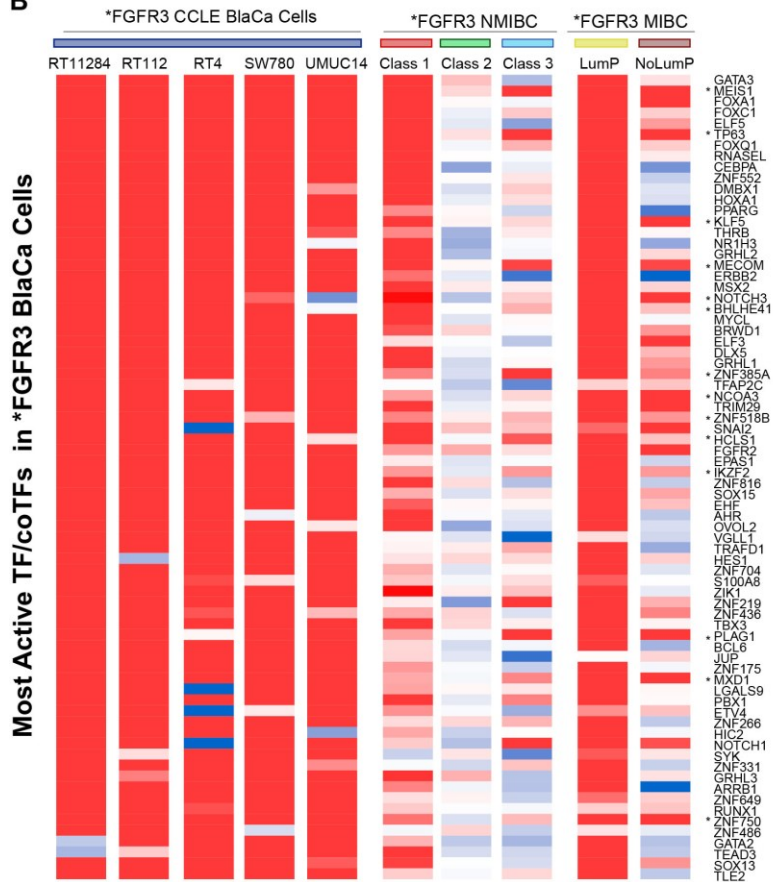
A *FGFR3 CCLE BlaCa Cells



*FGFR3 NMIBC

*FGFR3 MIBC

B



Common Most Active TF/coTFs

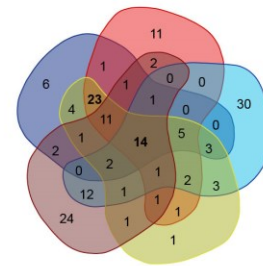


Figure 1.

RESULTS

Figure 1. Transcriptional co-regulatory network of FGFR3-altered bladder cancer cells and tumors.

- A. Left Panel.** Co-operativity network inferred from the transcriptome of 36 bladder cancer derived cell lines (BLCA-GRN) and active only in altered-FGFR3 cells. Nodes represent transcription factors and co-factors (TFs/coTFs). The co-regulatory interactions between nodes are indicated as follows: solely defined by H-LICORN algorithm (gray) and interactions for which there is published evidence such as protein-protein interactions (ppi; blue) and transcriptional regulation (tfbs, red arrows). Node color (red= high; blue = low) represents the mean activity of the corresponding TF/coTF, estimated only from FGFR3-dependent bladder cancer cells (n=5). The size of nodes is proportional to the number of targets of a TF/coTF and the intensity of color to the activation value.
- Right Panel.** Prediction of BLCA-GRN activity employing the transcriptome of human bladder tumors harboring a mutated-*FGFR3* (*FGFR3): Non-muscle invasive bladder carcinoma (NMIBC, n=272; EUROMOL; Upper Panel) and Muscle-invasive bladder carcinoma (MIBC, n=52; TCGA; Lower Panel). The meaning of size and color of nodes, as well as color of edges follows as described above.
- B. Left Panel.** Heatmap display of the most active (4th quartile) TFs/coTFs in FGFR3-dependent bladder cancer cell lines. Each column represents a transcriptomic dataset from which the sample-specific or mean activity of a corresponding TF/coTF (rows) was calculated. The significance of color used to represent TF/coTF activity is the same as described above: red; high activity, blue; low activity.
- Right Panel.** Venn Diagram analysis of each of the most active sets (4th quartile) of TFs/coTFs in five transcriptomic datasets of FGFR3-altered samples: CCLE cell lines, NMIBC of Class 1 and of Class 3, and MIBC of luminal-papillary and non-luminal-papillary subtype. The 14 common most active TFs/coTFs are highlighted on the heatmap by an asterisk.

Essential FGFR3-driven TFs and coTFs in bladder cancer.

To experimentally evaluate part of the inferred co-regulatory BLCA-GRN in tumors bearing an *FGFR3*-alteration, we performed a TF Activation Profiling Plate Array assay on UM-UC-14 cells treated or not with the pan-FGFR inhibitor PD173074 (Figure 2A, right panel). The Array allowed to analyze the activity of 10 out of 74 of the regulators (or family members of the regulators) defined by CoRegNet as being the most active in UM-UC-14 cells (Figure 2A, left panel). Validating part of the predicted co-regulatory network, the inhibition of FGFR3 in UM-UC-14 cells led to a significant decrease in the target DNA sequence binding of all of the 6 TFs/family members of TFs representing in total 9 of the most active regulators in UM-UC-14 cells (Figure 2A, right panel).

Having confirmed at a small scale the reliability of prediction of CoRegNet, we continued to use this tool to compute the activity of the inferred BLCA-GRN regulators using other experimentally derived transcriptomic datasets to identify regulators activated in an altered-FGFR3 context and driven by this receptor. We compared the GRN after inhibition or activation of FGFR3 (Figure 2B). We used publicly available transcriptomic data from MGH-U3 and RT112 cells treated or not with the pan-FGFR3 inhibitor AZD4547 for 2, 6 and 24 hours, and our transcriptomic data from bladder tumors and hyperplasia from mice overexpressing in urothelial cells a human *FGFR3* presenting the S249C mutation, and from littermate control urothelium. We proceeded by first calculating the activity of every TF/coTF in each independent dataset and then focusing on those regulators that presented an opposite activation status between the FGFR3 inhibited bladder cancer cell lines and the

RESULTS

murine bladder tumors overexpressing a constitutively active hFGFR3-S249C (Figure 2B; $n = 25$ TF/coTFs). To determine if such FGFR3-driven regulators were essential elements of the network for FGFR3's oncogenic activity, we evaluated the impact that the knockout of one of such genes would have on the cell viability of FGFR3-dependent bladder cancer cell lines using publicly available data from the high-throughput screening of gene dependencies (Broad Institute, AVANA CRISPR-Cas9 dataset) (Figure 2C). Amongst the few TFs that were identified as being essential for FGFR3-dependent cell lines were TP63 and FOXM1. Strikingly, the knockout of *TP63* (encoding p63) had the strongest impact on cell viability of FGFR3-dependent bladder cancer cells and this impact was greater compared to wt (wild-type) *FGFR3* cells despite a well-established role of p63 in squamous/ basal tumors in general and basal MIBC in particular^{33–35} (Figure 2C).

RESULTS

Figure 2. Identification of FGFR3-regulated TFs and coTFs in bladder cancer: discovery of TP63 as an essential gene.

- A.** Left Panel. TFs/coTFs exhibiting a positive activity calculated from the BLCA-GRN and the transcriptome of the UM-UC-14 cell line. Colored in red are the most active (4th quartile; n=74) regulators. Names of the top 20 most influent regulators are shown. Regulators whose names are further highlighted in red are those that were partially validated using a TF array in 2B. Right Panel. Activation levels of the TFs or TF families present in a TF activation profiling plate array, and representing 10 out of the 74 most active TFs/coTFs in UM-UC-14 cells. UM-UC-14 cells were treated or not with a pan-FGFR inhibitor (PD173074) and TF activity levels were measured as the enrichment of bound TF/probes. Activity profiles that present more than two-fold change between experimental samples are considered significant. RLU: Relative Luminescence Units.
- B.** Left Panel. Venn diagram of the TFs/coTFs of the BLCA-GRN whose estimated activity presents a change following the perturbation of FGFR3 in two transcriptomic datasets: (i) RT112 and MGHU3 treated with FGFR3 inhibitor (AZD4547) and (ii) bladder tumors derived from mice overexpressing a human FGFR3 (S249C) specifically in the urothelium. Focus is made on those regulators presenting an opposite and coherent change of activity following the inhibition or overexpression of FGFR3 in the two preclinical models (n=25). Right Panel. Heatmap display of the 25 commonly deregulated TFs/coTFs and their sample-specific activity (murine tumors; red: high; blue: low), or fold change (FC) of activity with respect to control (cell lines; comparison to untreated cells).
- C.** Impact on cell viability (CERES dependency score) of altered-FGFR3 (red) and non-altered-FGFR3-dependent bladder cancer cell lines upon KO (CRISPR-Cas9 AVANA database, Broad Institute) of one of the 25 common TFs from 2C.

P63 is regulated by FGFR3 and regulates cell proliferation

After examining our BLCA-GRN, we decided to focus the rest of the study on the transcription factor p63 as 1) it was one of the 14 genes found to be activated in both cell lines and FGFR3-altered tumors, independently of the subgroups; 2) it was found to be controlled by altered-FGFR3 and 3) it was essential for FGFR3-dependent bladder cancer cell viability in the AVANA screen.

Firstly, we investigated whether the regulation of p63 activity was due to a modulation of its protein levels by an altered-FGFR3 via the treatment of MGH-U3 (FGFR3-Y375C), UM-UC-14 (FGFR3-S249C) and RT112 (FGFR3-TACC3) bladder cancer cells with the pan-FGFR inhibitor PD173074. Western blot analysis showed a decrease of p63 levels in all three cell lines following the inhibition of FGFR3 (Figure 3A, left panel) without affecting the cellular localization of p63 (Supplementary Figure 1A). Supporting the relevance of these results in human tumors, the levels of p63 were also diminished after the anti-FGFR treatment of a patient derived xenograft (PDX) model harboring an FGFR3-S249C (Figure 3A, right panel). A kinetics of FGFR3 inhibition in RT112 cell lines revealed that the effect of FGFR3 inhibition on p63 levels was observed only at longer treatment times, suggesting that the regulation of p63 may occur at the transcriptomic level, rather than via the stabilization of the protein via the prevention of its degradation by proteasome (Supplementary Figure 1B). Analysis of transcriptomic data obtained after FGFR3 knockdown in MGH-U3 cells identified indeed a significant decrease of TP63 mRNA levels²⁰. Further supporting this transcriptomic regulation of *TP63* by FGFR3, analysis of mRNA levels in human bladder tumors showed

RESULTS

that *TP63* expression was significantly higher in both NMIBCs and MIBCs mutated for *FGFR3* (Figure 3B). Additionally, a significant positive correlation was found between *FGFR3* and *TP63* mRNA levels in both tumor subgroups, independent of *FGFR3* status (NMIBC cor 0.57, pval=6.59e-10; MIBC cor 0.50, pval=1.34e-07; Pearson's correlation). Knowing that there exist many different isoforms of *TP63*, which can have different activities, we verified by RT-qPCR that the Δ NP63 isoform was the dominant isoform expressed in both our human bladder tumors and bladder cancer derived cell lines, whatever the *FGFR3* mutation status (Supplementary Figure 1C-D).

To corroborate the dependency of *FGFR3*-mutated bladder cancer cells on p63 observed in the AVANA CRISPR-Cas9 publicly available data (Figure 2C), we invalidated *TP63* expression using siRNA in MGHU-3 and UM-UC-14 cells. Knockdown of *TP63* by three independent siRNAs led to a significant decrease of cell viability in both *FGFR3*-dependent cell lines (Figure 3C and Supplementary Figure 2A). To evaluate the role of p63 in 3D culture, *in vitro* and *in vivo*, we developed stables clones of inducible-shTP63 (shTP63i) transduced MGH-U3 and UM-UC-14 cells. Doxycycline (Dox) treatment of both shTP63i cells induced a knock-down by ca. 50% of protein expression (Supplementary Figure 2B-D) and significantly impaired cell growth in a 3D culture spheroid model (Figure 3D, Supplementary Figure 2C). Moreover, doxycycline treatment of a xenograft model derived from the shTP63i MGHU-3 cell line led to a significantly stunted tumor growth compared to the untreated control mice (Figure 3E). A reduction in the number of proliferating cell nuclear antigen (PCNA) positive cells was observed in absence of p63, indicating that p63 regulated cell proliferation of *FGFR3*-dependent cells (Figure 3F, Supplementary Figure 2E).

RESULTS

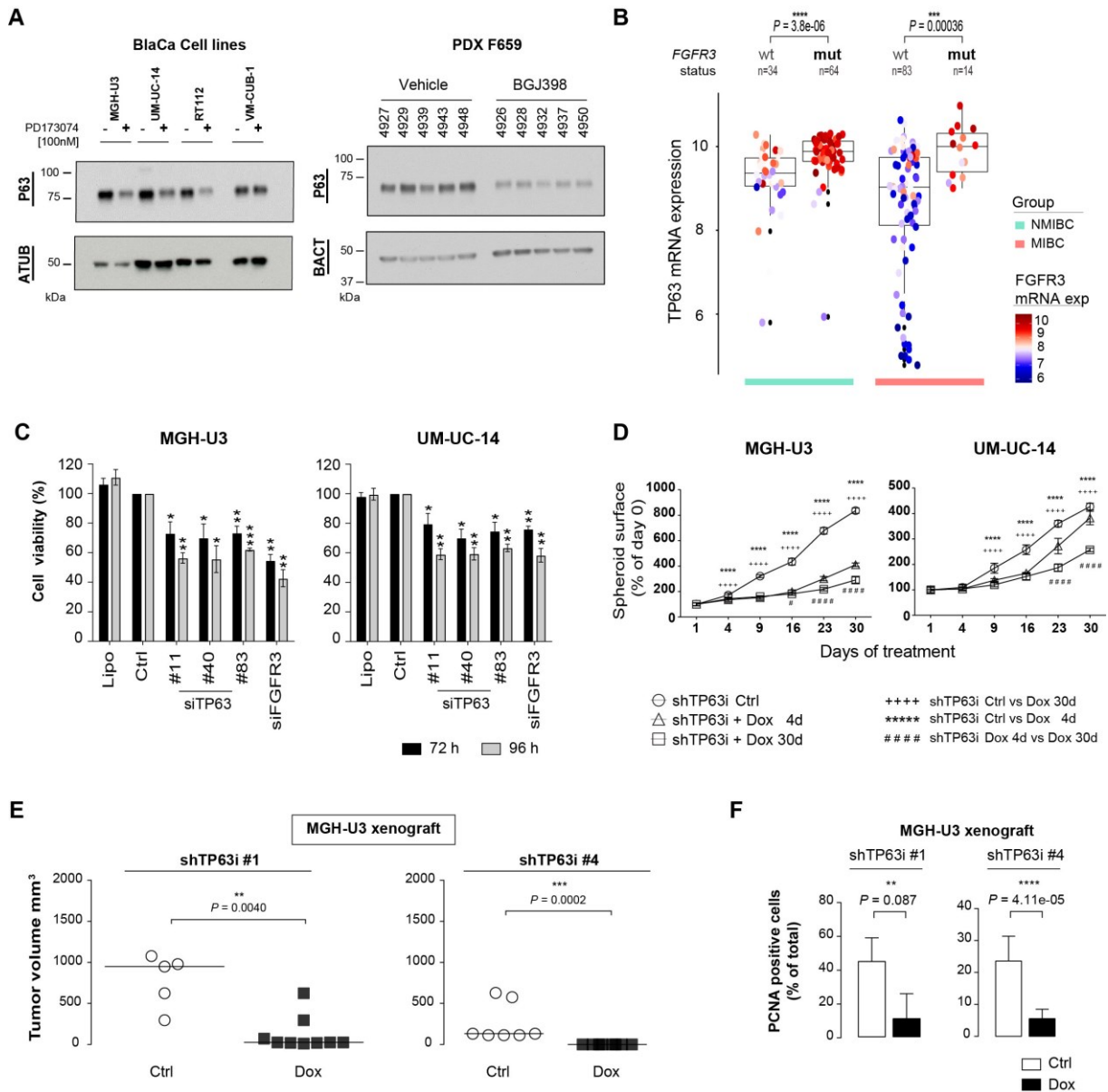


Figure 3. Regulation of *TP63* expression and impact of its knockdown on cell proliferation in an altered-FGFR3 context.

- A.** Western blot of p63 after anti-FGFR3 treatment of MGHU-3 and UM-UC14 cells (PD173074 100nM, 40h) or tumors derived from a mutated-FGFR3 PDX model (BGJ398 30mg/kg/day, 4 days). Actin (BACT) was used as loading control. The blot for MGH-U3 and UM-UC-14 is representative of three independent experiments. VM-CUB1 cells expressing a wtFGFR3 were used as control.
- B.** Comparison of *TP63* mRNA expression levels in the CIT cohort of NMIBC ($n = 98$) and MIBC ($n = 97$) human bladder tumors, subdivided according to *FGFR3* mutational status (wt: wildtype; mut: mutated). Each dot represents an individual sample and the color of the dot is proportional to the centered mRNA expression of *FGFR3* per sample.
- C.** Cell viability assay (Cell Titer-Glo) evaluating the effect of *TP63* knockdown (siRNA) in MGH-U3 and UM-UC-14 cells 72 and 96 hours after transfection.
- D.** Cellular spheroids were established from MGH-U3 and UM-UC-14 cells stably transduced with a Dox-inducible shTP63 (shTP63i). 3D cell growth was analyzed at different stages following the knockdown of *TP63*, induced after doxycycline (Dox) treatment. Spheroids received Dox-treatment either for a long period (30 days) to keep a stable knockdown of *TP63* or for a short period (4 days) to induce a transient knockdown of *TP63* and allow for recovery of expression after. Statistical comparison was done by a 2-way ANOVA.

RESULTS

- E. Murine xenograft tumors were derived from two clones of MGHU-3 bladder cancer cells stably expressing a Dox-inducible shRNA targeting *TP63* (shTP63i#1, shTP63i#4). Xenografted mice received or not doxycycline in the drinking water (Dox;1g/L) for 30 days. Tumor growth was assessed every twice a week. Data is expressed as final tumor volume at the end of treatment. Each dot represents an individual sample. Statistical comparison was done by Wilcoxon's test.
- F. Quantification of proliferating nuclear cell antigen (PCNA) immunostaining in tumors of xenografted mice from 3E (MGH-U3 shTP63i#1: Ctrl $n = 6$, Dox $n = 6$; MGH-U3 shTP63i#4: Ctrl $n = 9$, Dox $n = 9$). Statistical comparison was done by Wilcoxon's test.

p63 favors migration and invasion of FGFR3-dependent bladder cancer cells.

To further assess the functional relevance of p63 within an altered-FGFR3 context in bladder cancer, we generated a p63 target gene signature from MGH-U3 cells. Possible direct transcriptional targets of p63 were investigated by chromatin immunoprecipitation of p63, combined with massive parallel sequencing (ChIP-seq). P63-ChIP-seq of two independent MGH-U3 replicates unveiled 6 000 potential p63-binding sites at a distance +/- 5kb from the transcriptional start site (TSS) of the target gene (Supplementary Figure 3A). We then integrated these results with the RNA-seq expression profiling of siTP63 transfected MGH-U3 cells to define which of the putative target genes were effectively regulated following the knockdown of *TP63* (Supplementary Figure 3B). Gene ontology (GO) enrichment analysis of the p63 direct target genes revealed that p63 positively mediates cellular processes such as cell migration, invasion and proliferation, and represses cellular death (Supplementary Figure 3C).

This transcriptomic analysis corroborated with what we already observed for the role of p63 in regulation on cell proliferation. We then aimed at validated experimentally the role of p63 in mediating cell migration and invasion. Treatment of shTP63i UM-UC-14 cells with doxycycline significantly blunted cell migration as analyzed by a wound healing assay (Figure 4A). Membrane-type I-matrix metalloproteinase (MT1-MMP) plays a central role in pericellular matrix degradation during local invasive programs and metastasis³⁶. An association between p63 and MT1-MMP has already been reported in other models³⁷. Here we observe that silencing of *TP63* led to a significant reduction of gelatin degradation in both shTP63i transduced MGH-U3 and UM-UC-14 cells indicating that MT1-MMP activity is p63 dependent (Figure 4B-C). Underlying this process, the expression of membrane-type I-matrix metalloproteinase (MT1-MMP) was decreased upon *TP63* depletion in MGH-U3 shTP63i cells (Figure 4D). Nonetheless, the exact role of MT1-MMP in such processes in bladder cancer would need to be further studied. Overall, these results demonstrate that p63 mediates both cell migration and invasion through the degradation of extra-cellular matrix in FGFR3-dependent cells.

RESULTS

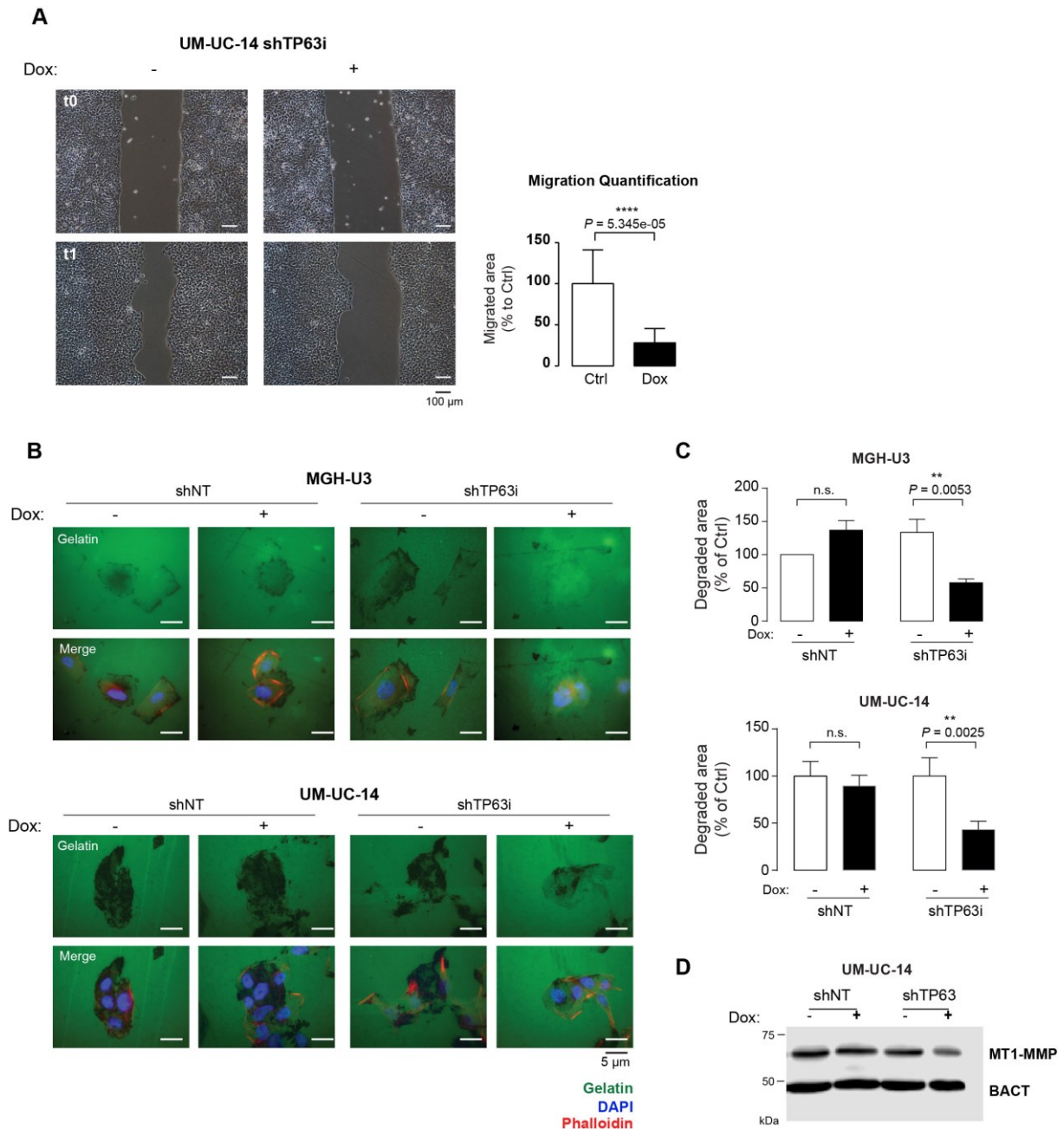


Figure 4. Functional consequences of TP63 gene invalidation in FGFR3-dependent bladder cancer cells: Effect on cell migration and invasion.

- A.** Wound healing assay to measure cell migration of UM-UC-14 shTP63i#4 cells after the doxycycline (Dox)-induced knockdown of *TP63*. Left Panel: representative images depicting the scratch (wound) at time 0 (t0) and 24 hours (t1) post-scratching. Scale bar is equivalent to 100μm. Right panel: Relative wound area was measured at both times to define the percentage of migrated area with respect to Dox-untreated, control cells. Data is expressed as mean ± SD. Statistical differences were defined by a Wilcoxon's test.
- B.** Degradation of Alexa 488 gelatin by MGH-U3 shTP63i#4 and UM-UC-14 shTP63i#4 cells treated or not with Dox to induce *TP63* knockdown. Scale bar is equivalent to 5μm.
- C.** Quantification of degraded gelatin from 3B. Results are expressed as mean ±SD of triplicate samples. The two-way ANOVA test was employed to statistically compare groups. shNT: non-targeting shRNA.
- D.** Western blot of MT1-MMP and β-ACTIN (BACT; loading control) in UM-UC-14 cells transfected with a control (shNT) or *TP63* targeting shRNA, inducible by doxycycline (Dox) treatment.

P63 activation levels are higher in NMIBC bearing FGFR3 alterations and could be associated to the higher tendency of recurrence in these tumors.

RESULTS

Given the key roles of p63 in FGFR3-dependent *in vitro* models, we then further investigated if p63 activity was specifically induced by mutated-FGFR3 and associated with tumor prognosis assuming that its role in migration could favor tumor recurrence. Based on the study by Hernandez *et al*³⁸, we focused on Ta NMIBC tumors that were reported to be enriched in FGFR3 mutations and which presented higher recurrence for certain tumor subgroups. Employing our BLCA-GRN and the UROMOL transcriptomic dataset of NMIBC⁹, we inferred the activity of p63 in the 289 Ta NMIBCs and identified both a significantly higher activity of p63 and a higher tendency of recurrence in mutated-FGFR3 tumors compared to wild-type (Figure 5A-B). These results suggest that p63 may participate in tumor recurrence in a mutated-FGFR3 context.

RESULTS

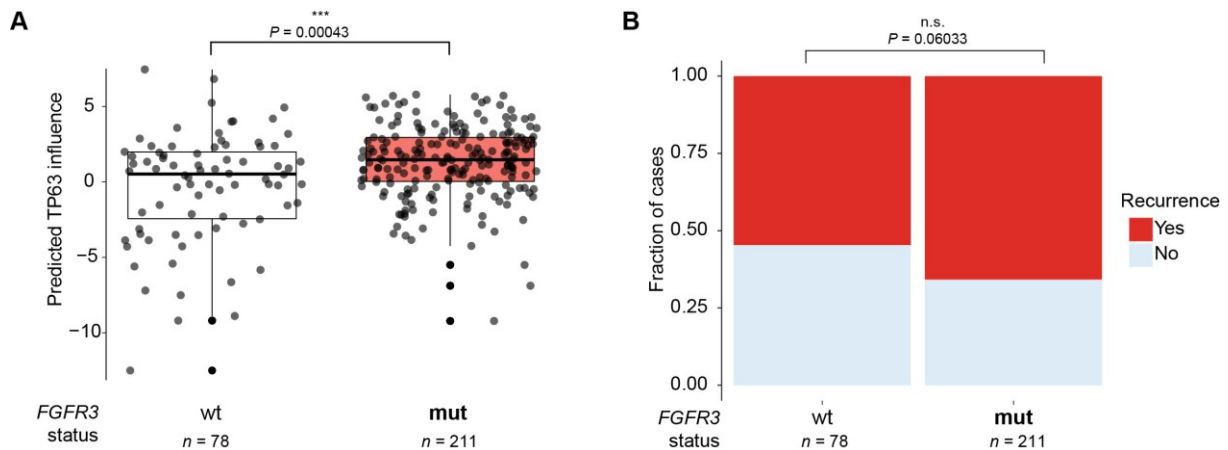


Figure 5. P63 activity levels in FGFR3-mutated NMIBC human tumors.

Activity levels of p63 were predicted from the BLCA-GRN and the UROMOL transcriptomic dataset of human Ta NMIBC tumors. Comparison of activation status was done by grouping samples in different ways:

- A.** Activity levels of p63 in Ta NMIBC (UROMOL) as calculated using the predicted BLCA-GRN. Tumors were separated according to *FGFR3* mutational status (wt: wildtype; $n = 78$, mut: mutated; $n = 211$). Tumors not presenting any information regarding *FGFR3* status were excluded. Each dot represents an individual sample. Wilcoxon's test was used for statistical comparison between groups. Data are expressed as mean \pm SD
- B.** Proportion of recurrence events in wildtype versus mutated-*FGFR3* Ta NMIBCs. Fisher's exact test was carried out to evaluate statistical differences between groups. Number of tumors belonging to each group is indicated under each graph.

Discussion

In summary, through a reverse-engineering method, we have presented here the first bladder-cancer specific gene regulatory network, inferred without any *a priori* knowledge. By using the H-LICORN algorithm and the CoRegNet package, we were able to extract a network of co-operative regulators (TFs/coTFs) whose interactions were refined using regulatory evidences from different data sources. A major reason to focus our study on co-operative TFs/coTFs is that disease phenotypes; including those related to disease progression and response to therapy, have been demonstrated to be maintained by small groups of TFs and coTFs^{39,40}

To produce a more reliable GRN, we inferred our network using a more homogenous transcriptomic dataset from bladder cancer cell lines and subsequently demonstrated that it was also relevant to both NMIBC and MIBC bladder tumors. Notably, many of the regulators forming part of the network were previously associated to bladder cancer and/or urothelial differentiation such as *FOXA1*, *PPARG*, *GATA3*, *TP63*^{10,41,42} emphasizing the biological representativity of the inferred BLCA-GRN. However, when using transcriptomic data from our *FGFR3*-induced mouse model of BLCA and for *FGFR3*-bladder cancer cell lines after *FGFR3* inhibition, we were able to identify some key TFs such as *FOXM1* (Figures 2B and 2C) that were not identified from the human *FGFR3*. We were also not able to validate some previously described key regulators of bladder cancer such as *MYC* involved in a *FGFR3*

RESULTS

regulatory-loop²⁰. This is partly because the algorithm used will infer a GRN only from TFs/coTFs that have a significant variation of expression across the samples in the input data. MYC and FOXM1 do not necessarily vary at the level of mRNA, but are rather controlled at a post-translational level. Such unavoidable limitation, inherent to other GRN reconstruction algorithms²⁵, stresses the importance to use both bioinformatic and experimental approaches to construct GRNs. In this study, by employing transcriptomic data originating from different sources (patient samples and experimental data), we have constructed and validated a GRN characteristic of an altered-FGFR3 context in bladder tumors.

Our analysis showed that the TFs/coTFs activated by FGFR3 were different depending of the molecular tumor subtypes suggesting a context-specific activity of a mutated-FGFR3 which could be involved in the low response rate of FGFR3-altered tumors to anti-FGFR3 therapies (37% partial response and only 3% complete response)⁶.

Among the BLCA-GRN TFs/coTFs being driven by an altered-FGFR3 in all experimental datasets, we surprisingly uncovered the p63 transcription factor. Whereas the role of p63 has been already clearly demonstrated in a bladder cancer in a basal molecular context^{29,33-35}, there exist few reports investigating the role of this transcription factor in the more differentiated, luminal subtype of bladder tumors (enriched for FGFR3 alterations). Of note, whilst this hyperactivation of a p63 regulon was already described in luminal papillary MIBC, no direct link with FGFR3 was made⁴¹. In this study we demonstrated that the expression of p63 is regulated by FGFR3 in bladder cancer cell lines and PDX models. Analysis of its functional role confirmed that p63 is an essential TF mediating cell proliferation, migration and invasion of FGFR3-dependent bladder cancer cell lines.

Considering that p63 is able to drive an invasive program in the more aggressive basal bladder cancer subtypes^{29,35,43,44}, it is striking to observe that it similarly regulates migration/invasion in an altered-FGFR3 context, a context associated to NMIBCs or luminal-like MIBCs. In human bladder tumors, we observed a significantly stronger p63 activation in mutated-FGFR3 NMIBC tumors, associated to a tendency of higher recurrence rate of this mutated-tumors. This led us to hypothesize that p63-induced migration of FGFR3-mutated cells could favor recurrence. The fact that we observed a higher tendency but not a statistical difference of recurrence between mutated-FGFR3 tumors and wild-type tumors suggests that p63 may not be the only player favoring this process. It will be important to further study the functional network of p63 in different subtypes of FGFR3-mutated tumors.

Previous studies have reported that a loss of p63 is associated to a worse outcome (higher recurrence and/or progression) in NMIBC patients^{35,45-49}. This would appear at first as contradictory to our findings revealing a possible association between a higher p63 activity and higher tumor recurrence in certain NMIBC subtypes. A possible explanation of such

RESULTS

discrepancies of results could be linked to the fact that in the former studies, protein expression levels were measured whereas we measured p63 activity through a transcriptomic analysis. Moreover, knowing that p63 may exert opposite functions depending on the cellular background^{50,51}, it is important to more deeply study its context-specific regulation in order to propose therapeutic strategies suited to distinct clinical scenarios.

In this study we have focused on the functional validation of p63, one of the putative essential regulators driven by FGFR3 in bladder tumors. However, our work provides a bladder-cancer-specific GRN that enables the identification of TFs and coTFs that are essential in an altered-FGFR3 context, and that could be studied more in depth to improve current therapeutic options and increase our understanding of bladder cancer biology.

Materials and Methods

Public Data Collection

Human bladder cancer cell transcriptome (RNA-seq) and *FGFR3* mutational status corresponding to 36 bladder cancer cell lines (5 cell lines were mutated for *FGFR3* and were dependent on its signaling) were collected from the Cancer Cell Line Encyclopedia (CCLE DepMap 2019Q1, Broad Cancer Dependency Map Project)⁵².

Bladder tumor transcriptome (RNA-seq) was collected from two large cohorts of NMIBC and MIBC. NMIBC transcriptome and *FGFR3* mutational status were collected from the published dataset by Hedegaard *et al* (ArrayExpress E-MTAB-432)⁹ corresponding to 476 tumors (272 tumors presented a mutated *FGFR3*). The same data (RNA-seq) corresponding to the MIBC cohort was collected from the The Cancer Genome Atlas (TCGA) dataset (cbioPortal)¹⁰ of 408 tumors (52 tumors presented a mutated *FGFR3*).

Gene invalidation (CRISPR-Cas9; CERES dependency score) large screen data to identify essential genes in human cancer cell lines (27 bladder cancer cell lines) was collected from the AVANA genetic dependency dataset (AVANA 2019Q3, Achilles Project, Broad Institute)²⁸.

Transcriptomic data (Human Affymetrix DNA Array U133 Plus 2) of MGH-U3 and RT112 cells treated with AZD459 [100nM] were recovered from the Array Express E-MTAB-4749 dataset⁵³.

RESULTS

Inference of the gene regulatory network (GRN)

As a first step, a bladder-cancer-specific GRN was constructed from the CCLE human bladder cancer cell line transcriptome (n=36 bladder cancer cells) using the Bioconductor CoRegNet package²⁷. The CoRegNet package implements the hybrid learning co-operative regulation networks (H-LICORN) algorithm²⁶ to infer a series of gene regulatory networks (GRN) from transcriptomic data and a list of previously defined regulators. The list of known regulators (transcription factors and co-factors; TFs/coTFs; n=2375) is defined from previously published datasets by Lambert *et al* and Schmeier *et al*^{54,55}. In summary, H-LICORN infers the best GRN that describes the regulatory interactions between regulators and their target genes through four steps: (1) First, the transcriptomic matrix is discretized into -1, 0 and 1 values that fit its per-gene distribution of expression. In addition, genes present in the transcriptome matrix are classified into regulators and target genes and only those presenting a significant variation in expression levels across samples are kept. (2) Second, potential sets of co-activators and co-repressors regulating the expression of a target gene are determined through frequent items search techniques. (3) Third, for each target gene, a list of the candidate co-activators and co-inhibitor sets (GRN) is selected by employing an association rule metric (based on gene regulation). (4) Next, such sets of GRNs are scored following a regression model between the expression of the regulators forming part of the GRN set and the expression of their target genes. For each target gene, the top 10 GRN candidate sets presenting the best R² score are kept. CoRegNet can additionally refine the inferred GRN by integrating published interaction evidences such as protein-protein interactions [HIPPIE⁵⁶, STRING⁵⁷, FANTOM, iRefR HPRD⁵⁸] and transcription factor binding sites (ChEA2⁵⁹; ENCODE CHIP v3, Motif Db Bioconductor; HOCOMOCO⁶⁰, ITFP, ENCODE, Neph2012, TRRUST, Marbach 2016⁶¹, TRED⁶²). Each GRN is given a score that merges the previous R² score and a score representing validated regulatory interactions. The GRN with the maximum final merged score is selected and it is then transformed into a co-regulatory network based on the shared target genes between the inferred regulators.

Estimation of sample-specific TF/coTF activity

Using the CoRegNet package, we further computed a network-based regulatory influence that represents an estimated activity for each TF/coTF having a sufficient number of gene targets, for each transcriptome sample. Briefly, the measure of influence estimates the activity of a TF/coTF based on a Welch t-test comparing the distribution of expression of the set of activated and repressed target genes for each TF/coTF in each individual sample. In addition, an advantage of the CoRegNet package is that one may compute the TF/coTF influence for many different datasets using the regulatory information of one same GRN. In

RESULTS

this study, we constructed a bladder-cancer specific GRN, and then calculated the influence of the inferred TF/coTFs using transcriptomic data from different sources.

Validation of the FGFR3-GRN

Using the inferred bladder-cancer specific GRN, we calculated the influence of the predicted TFs/coTFs using transcriptomic data of preclinical models where the activity or gene expression of FGFR3 was altered. The first dataset used was the E-MTAB-4749 transcriptomic data from MGH-U3 (FGFR3-Y375C) and RT112 (FGFR3-TACC3) bladder cancer cell lines treated with the FGFR pan-inhibitor AZD4547 [100nM, 2,6,24h]⁵³. The second dataset was the human orthologue transcriptomic data of FGFR3-induced murine bladder tumors (murine model of hFGFR3-S249C overexpression in the urothelium) [Moreno-Vega, Shi, Fontugne, Meng 2019 unpublished]. The most influent TFs/coTFs additionally presenting an opposite and coherent activity between the FGFR3-inhibited and FGFR3-overexpressed preclinical models were taken as FGFR3-driven regulators.

Visualization of the GRNs

Visualization of the constructed networks and overlay of the computed influence and regulatory interactions was done using Cytoscape⁶³.

Cell culture

Human bladder cancer derived cell lines were obtained from different repositories: RT112, UM-UC-14 and VM-CUB-1 were obtained from DSMZ (Heidelberg, Germany); SW-780 cells were obtained from ATCC (Virginia, United States); UM-UC-5 were obtained from the ECACC collection (Porton Dow, England) and MGH-U3 and RT4 were kindly supplied by Dr. Francisco X. Real. The MGH-U3 and UM-UC-14 harbor the Y375C and S249C FGFR3 mutation respectively. RT112 and RT4 express the FGFR3-TACC3 translocation, whereas the SW780 present the FGFR3-BAIAP2L1 translocation. UM-UC-5 and VM-CUB-1 express a wildtype *FGFR3*. MGH-U3, UM-UC-14, UM-UC-5 and SW-780 were cultured in DMEM whilst RT112 and RT4 were cultured in RPMI. All culture media were supplemented with 10% fetal bovine serum. Cell culture was carried out at 37°C under a 5% CO₂ atmosphere.

FGFR3 inhibition in vitro

MGH-U3, RT112, RT4, SW-780, UM-UC-14, UM-UC-5 and VM-CUB-1 cell lines were seeded in 100mm plates at the following respective total densities: 5.0x10⁶, 4.0x10⁶, 4.5x10⁶, 1.8x10⁶, 3.0x10⁶, 5.0x10⁶, 1.8x10⁶ and 0.8x10⁶ cells/100mm dish. Cells were plated and left to adhere overnight. Thereafter, cells were treated for 40 hours with the pan-FGFR inhibitor PD173074 [100nM] (Calbiochem, Merck Eurolab, France). Control cells were treated with

RESULTS

DMSO vehicle diluted in the same way as the inhibitor. At the end of treatment, whole cell lysates or nuclear and cytosolic cell fractions were recovered for immunoblotting. Cellular fractions were obtained using the Thermo Fisher NE-PER nuclear and cytoplasmic extraction kit (ref 78833), according to the manufacturer's protocol.

Transcription Factor Activity Array

The activity of 48 families of transcription factors was analyzed from the isolated nuclear extracts obtained from UM-UC-14 cells treated or not for 40 hours with 100nM PD173074 using the TF Activation Profiling Plate Array I kit from Signosis (following the manufacturer's instructions).

Gene knockdown and cell viability assays

MGH-U3 and UM-UC-14 cells were transfected for 48, 72 and 96 hours with 5nM siRNA together with Lipofectamine RNAi Max reagent (Invitrogen) as indicated in the manufacturer's protocol. For protein or RNA analyzes, cells were plated in six-well plates at a seeding density of 300 000 cells/well for MGH-U3 cells and 150 000 cells/well for UM-UC-14 cells and cells were lysed at 48h after transfection with appropriate lysis buffer. For cell viability assays, cells were plated in ninety-six well plates at a seeding density of 10 000 cells/well for MGH-U3 cells and 5 000 cells/well for UM-UC-14 cells and cell viability was measured (Cell Titer Glo, Promega) at 72 and 96 hours.

Three different TP63 siRNA (TP63 siRNA #11, #40, #83; Ambion Silencer select, ThermoFisher Scientific) were used and a siRNA targeting FGFR3 was used as a positive control (Qiagen). As negative controls, we used an siRNA directed against luciferase (Qiagen SI03650353) and the non-targeting negative control Silencer Select (Thermo Fisher Scientific

4390846). The sequences of siRNAs employed are as follows:

	Strand	Sequence 5'-3'
<i>TP63</i> <i>ref</i> <i>s16411</i>	#11 (4392420)	sense GGAUGAAGAUAGCAUCAGA
	anti-sense UCUGAUGCUAUCUUCAUCC	
<i>TP63</i> <i>ref</i> <i>s229400</i>	#40 (4392420)	sense GAACCGCCGUCCAAUUUU
	anti-sense UAAAAUUGGACGGCGGUU	

RESULTS

<i>TP63</i>	#83	sense	UGAUGAACUGUUAUACUU
<i>ref (4392420 s531583)</i>		anti-sense	UAAGUAUAACAGUUCAUCA
<i>FGFR3</i>	#4	sense	CCUGCGUCGUGGAGAACAATT
<i>ref (4392420 s5168)</i>		anti-sense	UUGUUCUCCACGACGCAGGTG

Real-time reverse transcription quantitative PCR

RNA from bladder cancer cell lines was extracted with Qiagen's RNA easy minikit, in accordance to the manufacturer's protocol. RNA from our human bladder tumor cohort was extracted through cesium chloride density centrifugation as mentioned further on.

Reverse transcription was performed with 1µg of total RNA employing the High-Capacity cDNA reverse transcription kit (Applied Biosystems). cDNAs were subsequently amplified by PCR in a Roche real-time thermal cycler with the Roche *Taqman* master mix and the following master probe primers:

Gene	Strand	Sequence 5' - 3'	Roche probe	<i>Taqman</i>
Δ Np63	sense	GGTTGGCAAATCCTGGAG	No. 56	
	antisense	GGTTCGTGTACTGTGGCTCA		
18s rRNA	sense	GGAGAGGGAGCCTGAGAAAC	No. 8	
	antisense	TCGGGAGTGGGTAATTTGC		

Immunoblotting

Protein extraction of MGH-U3, RT112, RT4, SW-780, UM-UC-14, UM-UC-5 and VM-CUB-1 cell lines was done through cell lysis in Laemmli buffer (50 mM pH 6.8 Tris-HCl, 2.5 mM EDTA, 2.5 mM EGTA, 2 mM DTT, 5% glycerol, 2% SDS) supplemented with protease inhibitors and phosphatase inhibitors (Roche). Following clarification of cell lysates by centrifugation, protein levels were quantified with the BCA protein assay (Thermo Fisher Scientific). Ten micrograms of whole cell lysate and five micrograms of cell fractionation lysate were resolved by SDS-PAGE in 7.5% or 15% polyacrylamide gels depending on the molecular weight of the proteins to be analyzed. Gels were electrotransferred into nitrocellulose membranes (BioRad) and protein transfer was verified by Amido Black staining before immunoblotting. Proteins were detected with antibodies against p63 (Abcam ab5309, 1/4000 dilution), MYC (Cell Signaling Technology 9402, diluted 1/1,000), and FGFR3 (Abcam ab133644, diluted 1/5,000). Alpha-tubulin and beta-actin (Sigma Aldrich references T6199 and A2228, respectively; both diluted at 1/20,000) were used as loading controls. The

RESULTS

secondary antibodies used were HRP-linked anti-mouse IgG and anti-rabbit IgG (Cell Signaling Technology references 7076 and 7074, respectively, both diluted at 1/3,000).

For shTP63i cells, cells were plated in 60mm plates and treated with or without dox for 72 hours. Protein was then extracted using RIPA-EDTA and protease cocktail inhibitor. Protein concentration was measured using the Bradford method (MERK1103060500). Proteins (50-80uG) were resolved in polyacrylamide gels and then transferred to PVDF membranes and incubated with antibodies against p63 (ab53039) b-Actin (sigma A5441) MT1-MMP (sc-30074) and revealed using Li-cor C-Digit Blot scanner. Images were analyzed by Gel Pro Analyzer software.

Human samples

We used RNA extracted from 163 bladder tumors of our Carte d'Identites cohort (CIT; 79 NMIBCs and 80 MIBCs). Tumor samples were flash-frozen and stored at -80°C immediately after transurethral resection or cystectomy. Immunohistochemical analysis by hematoxylin and eosin (H&E) staining confirmed that all tumor samples contained more than 80% of tumor cells (staining of sections adjacent to the samples used for transcriptome analyses). All patients provided informed consent, and the study was approved by the institutional review boards of the Foch, Institut Gustave Roussy and Henri Mondor Hospitals. Extraction of RNA, DNA and protein from the surgical samples was done by cesium chloride density centrifugation as previously described⁶⁴. FGFR3 mutations were determined through the SNaPshot technique.

Transcriptomic data was further obtained from 98 NMIBC and 97 MIBC tumors using the Affymetrix Human Exon 1.0 ST array. Differential gene expression analysis was done with the LIMMA R package, and *P*-values were adjusted for multiple testing through the Benjamini-Hochberg (FDR) method.

RNA-seq

For a whole genome profiling experiment, MGH-U3 cells were transfected for 48 hours with TP63 siRNA #11 (as described above)

Triplicate RNA isolates from siTP63 transfected and control (lipofectamine RNA iMax, Invitrogen) were prepared using the Qiagen RNA easy minikit supplemented with DNase treatment, and RNA sample quality was controlled with the Agilent 2100 Bioanalyzer system. RNA sequencing was carried out on stranded mRNA (1 µg) with an Illumina NovaSeq S1 sequencing system at a sequencing depth of 30 million reads per sample. Quality control and filtering of data was carried out using FastQC (Babraham Bioinformatics Institute, Cambridge). Filtered reads were mapped to the hg19 human genome and

RESULTS

annotated using the STAR aligner. Statistically significant differences in gene expression were determined by performing a LIMMA-VOOM using eBayes statistics. The P-values were adjusted for multiple testing through the Benjamini-Hochberg (FDR) method.

P63-ChIP-seq

MGH-U3 cells were cross-linked in 1% formaldehyde for 10min at room temperature. The reaction was stopped with glycine (final concentration 125mM, 5min incubation at room temperature). Fixed cells were then washed twice with PBS and harvested with a cell scraper. Following centrifugation (11500rpm 5min); the cell pellet was resuspended in extraction buffer (250mM sucrose, 10mL Tris-HCl pH8, 10mM MgCl₂, 1% Triton and 5mM β-mercaptoethanol) supplemented with protease inhibitors (Roche). Cells were centrifuged at 3,000g for 10min and recovered samples were analyzed using the ChIP-IT High Sensitivity kit (Active Motif, 53040). ChIP was carried out using a p63 antibody (Cell Signaling Technology, D2K8X XP, 13109). Sequencing and analysis of results was carried out in collaboration with the sequencing platform of the IGBMC Strasbourg. Sequences were aligned to the human hg19 genome using Bowtie⁶⁵ and peaks were called using the SPP v1.14 R package from the Kundaje Lab Tools⁶⁶. ChIP-seq data was processed following the ENCODE-DCC ChIP-seq pipeline 2 (Anshul Kundaje, <https://github.com/ENCODE-DCC/chip-seq-pipeline2>). ChIP-seq results represent two independent experiments.

P63 Gene targets in MGH-U3

Genes being directly regulated by p63 in MGH-U3 cells were determined as those genes that had a statistically significant change of expression following the knockdown of *TP63* ($|\logFC| > 1$; adjusted *P*-value ≤ 0.05) and additionally presented a strong peak at +/- 5kb from their TSS (P63-ChIP-seq). Amongst these genes, those having a statistically significant $\logFC \leq 1$ would be considered as p63 activated targets, whereas those having a $\logFC \geq 1$ would be considered as p63 repressed targets.

Gene ontology enrichment

The DAVID Functional Annotation Tool v6.8 was used to identify biological processes (GO-BPs) that were enriched in the set of p63 target genes (n=330 activated targets, n=391 repressed targets). Significantly enriched GO-BPs were considered as those having an adjusted *P*-value (Benjamini-Hochberg) ≤ 0.05 .

Spheroid growth

3D cell cultures were generated by the hanging drop seeding method 3x10³ cells in 20ul of complete medium, during 72hs (MGHU3) or 96hs (UM-UC-14) and then plated on agar

RESULTS

coated-96 wells plates. Cultured medium with or without DOX was completely replaced twice a week and images were taken weekly. Diameter was measured using Image J software and then surface was calculated. After 30 days, spheroids were fixed in methacarn and embedded in paraffin to be sliced and immunostained using a standard immunofluorescence method. p63 was stained with primary antibody CM163B (Biocare medical) and secondary antibody Alexa 488 (ab150113). Nuclei were stained using DAPI (Cas28718-90-3, Sigma-Aldrich).

Gelatin degradation assay

FITC-labeled gelatin was obtained from Invitrogen. Coverslips coated with fluorescent gelatin were prepared as described by Artym et al. 2006. In brief, coverslips (18-mm diameter) were coated with polylysin 0.5 $\mu\text{g/ml}$ for 20 min at room temperature, washed with PBS, and fixed with 0.5% glutaraldehyde (Sigma-Aldrich) for 15 min. After three washes, the coverslips were inverted on an 80- μl drop of 0.2% fluorescently labeled gelatin and incubated for 10 min at room temperature. After washing with PBS, coverslips were incubated in 5 mg/ml sodium borohydride for 3 min, washed three times in PBS, and finally incubated in 2 ml of complete medium for a minimum of 2 h before adding the cells. Cells were treated with or without DOX (100 ng/ml) for 72 hours before the assay and plated on coated coverslips in DMEMF12 containing 10% FCS. Then, cells were incubated at 37°C for 5 hours (MGHU3) or overnight (UM-UC-14). Cells were fixed with PFA 4% for 20 min. Cells were immunostained for F-actin (AA22283, Life technologies) and nuclei with DAPI (Cas28718-90-3, Sigma-Aldrich) and imaged with 40 \times objective in at least 15 fields per experiment. For quantification of degradation, the total area of degraded matrix in one field (black pixels) measured using the Image J was divided by the total number of phalloidin-labeled cells in the field to define a degradation index.

Wound healing assay

Cells were seeded in 6 wells plates and treated with or without DOX during 72h. Two wounds were performed in each well and then a PBS wash was performed to eliminate the released cells. Culture medium was replaced for 2% FBS medium. Pictures were taken immediately (t_0) and 24 hours later (t_1). Wound area was measured in both situations using Image J and migrated area was calculated using the formula: $(A_{t1} \times 100) / A_{t0}$ and then relativized to control.

RESULTS

***In vivo* models**

i. Mice UPII-hFGFR3-S249C transcriptome

We used the transcriptome from tumor samples of a previously established FGFR3-induced murine model of bladder tumors [Moreno-Vega, Shi, Fontugne, Meng 2019 unpublished]. In brief, the expression of the human FGFR3IIIb carrying the S249C mutation was specifically targeted to the urothelium of mice through the use of the murine uroplakin II promoter. Mice developed hyperplastic lesions and low-grade papillary tumors from 6 and 18 months of age respectively. Genes exhibiting a change of expression between UPII-hFGFR3 mice tumors and control urothelium were defined via the analysis of extracted mRNA using the Affymetrix Mouse Exon 1.0 ST array, followed by the use of the LIMMA algorithm to define statistically significant changes of expression. The *P*-values were adjusted for multiple testing through the Benjamini-Hochberg (FDR) method [Moreno-Vega, Shi, Fontugne, Meng 2019 unpublished].

ii. FGFR3 inhibition in vivo (PDX model)

Protein lysates (20µg) derived from previously established patient-derived bladder cancer xenografts (PDX) of mice treated or not with the pan-FGFR inhibitor BGJ398 (30mg/kg/day; 4 days) were used for immunoblotting²⁰.

iii. Nude mice tumor growth

Nude male mice were obtained from: CNEA (Comisión Nacional de Energía Atómica). All the procedures were approved by the CICUAL (Comité Institucional para el Uso y Cuidado de Animales de Laboratorio) Instituto de Oncología A.H. Roffo (Protocol number 2017/03) Human bladder cancer TP63 silenced cells were injected subcutaneously in the right flank of 20 mice (2x10⁶ cells in 100ul of PBS). When the tumors were palpable (1mmx1mm) 10 mice received 1g/L of DOX in the drinking water (DOX group) and 10 mice only water (Ctrl group). Tumors were measured using caliper twice a week and volume was calculated with the formula: $\frac{3}{4}\pi \times (\text{largest diameter}) \times (\text{shorter diameter})^2$. At the end of the experiment mice were sacrificed and tumors removed, fixed in methacarn and latter paraffin embedded to be sliced and immunostained. p63 was labeled with the primary antibody CM163B (Biocare medical) and secondary antibody Alexa 546(A110003). PCNA with primary antibody (2586, Cell Signalling) and secondary Alexa 488 (ab150113). Nuclei were stained using DAPI (Cas28718-90-3, Sigma-Aldrich).

RESULTS

Statistical analysis

All experiments were independently carried out two or three times, with each experiment presenting triplicates. Data are presented as means \pm SD. Wilcoxon's unpaired tests were used for multiple comparisons. For microarray data analysis, the linear models for microarray data (LIMMA)⁶⁷ R package was used and *P*-values were adjusted via the Benjamini-Hochberg method.

Author contributions statement

Conceptualization, M.E., F.R, C.L., I.B.P.; *Methodology*, A.M.V., J.P., M.Z., C.G.; *Investigation*, A.M.V., M.Z. J.P, F.D, F.D., M.S, C.B, M.L; *Formal Analysis*, A.M.V., M.Z, F.D, C.G, M.S, L.D.; *Writing –Original Draft*, A.M.V., C.L, I.B.P.; *Writing –Review & Editing*, all the authors; *Visualization*, A.M.V., M.Z, M.S; *Funding Acquisition*, M.E, C.L, I.B.P. and F.R; *Resources*, T.L, Y.A, P.L, A.M.E, L.D.; *Data curation*, E.C.; *Supervision*, C.L, I.B.P. and F.R.;

References

1. Babjuk, M. *et al.* European Association of Urology Guidelines on Non-muscle-invasive Bladder Cancer (TaT1 and Carcinoma In Situ) - 2019 Update. *European Urology* **76**, 639–657 (2019).
2. Gierrh, M. & Burger, M. Bladder cancer: Progress in defining progression in NMIBC. *Nat. Rev. Urol.* **10**, 684–685 (2013).
3. Funt, S. A. & Rosenberg, J. E. Cancer and Future Horizons. **14**, 221–234 (2018).
4. Park, J. C., Citrin, D. E., Agarwal, P. K. & Apolo, A. B. Multimodal management of muscle-invasive bladder cancer. *Curr. Probl. Cancer* **38**, 80–108 (2014).
5. Collin, M.-P. *et al.* Discovery of Rogaratinib (BAY 1163877): a pan-FGFR Inhibitor. *ChemMedChem* **13**, 437–445 (2018).
6. Loriot, Y. *et al.* Erdafitinib in Locally Advanced or Metastatic Urothelial Carcinoma. *N. Engl. J. Med.* **381**, 338–348 (2019).
7. Pal, S. K. *et al.* Efficacy of BGJ398, a Fibroblast Growth Factor Receptor 1–3 Inhibitor, in Patients with Previously Treated Advanced Urothelial Carcinoma with *FGFR3* Alterations. *Cancer Discov.* **8**, 812–821 (2018).
8. Siefker-Radtke, A. O. A phase 2 study of JNJ-42756493, a pan-FGFR tyrosine kinase inhibitor, in patients (pts) with metastatic or unresectable urothelial cancer (UC) harboring FGFR gene alterations. *J. Clin. Oncol.* (2016).
9. Hedegaard, J. *et al.* Comprehensive Transcriptional Analysis of Early-Stage Urothelial Carcinoma. *Cancer Cell* **30**, 27–42 (2016).
10. Robertson, A. G. *et al.* Comprehensive Molecular Characterization of Muscle-Invasive Bladder Cancer. *Cell* **171**, 540-556.e25 (2017).
11. Robertson, A. G. *et al.* Comprehensive Molecular Characterization of Muscle-Invasive Bladder Cancer. *Cell* **171**, 540-556.e25 (2017).
12. Shi, M. J. *et al.* APOBEC-mediated Mutagenesis as a Likely Cause of FGFR3 S249C Mutation Over-representation in Bladder Cancer. *Eur. Urol.* **76**, 9–13 (2019).
13. Tomlinson, D., Baldo, O., Harnden, P. & Knowles, M. FGFR3 protein expression and its relationship to mutation status and prognostic variables in bladder cancer. *J. Pathol.* **213**, 91–98 (2007).
14. Chell, V. *et al.* Tumour cell responses to new fibroblast growth factor receptor tyrosine kinase inhibitors and identification of a gatekeeper mutation in FGFR3 as a mechanism of acquired resistance. *Oncogene* **32**, 3059–3070 (2013).
15. Flaherty, K. T. *et al.* Combined BRAF and MEK Inhibition in Melanoma with BRAF V600 Mutations. *N. Engl. J. Med.* **367**, 1694–1703 (2012).
16. Pearson, A. *et al.* Parallel RNA Interference Screens Identify EGFR Activation as an Escape Mechanism in FGFR3-Mutant Cancer. *Cancer Discov.* **3**, 1058–1071 (2013).
17. Niederst, M. J. & Engelman, J. A. Bypass mechanisms of resistance to receptor tyrosine kinase

RESULTS

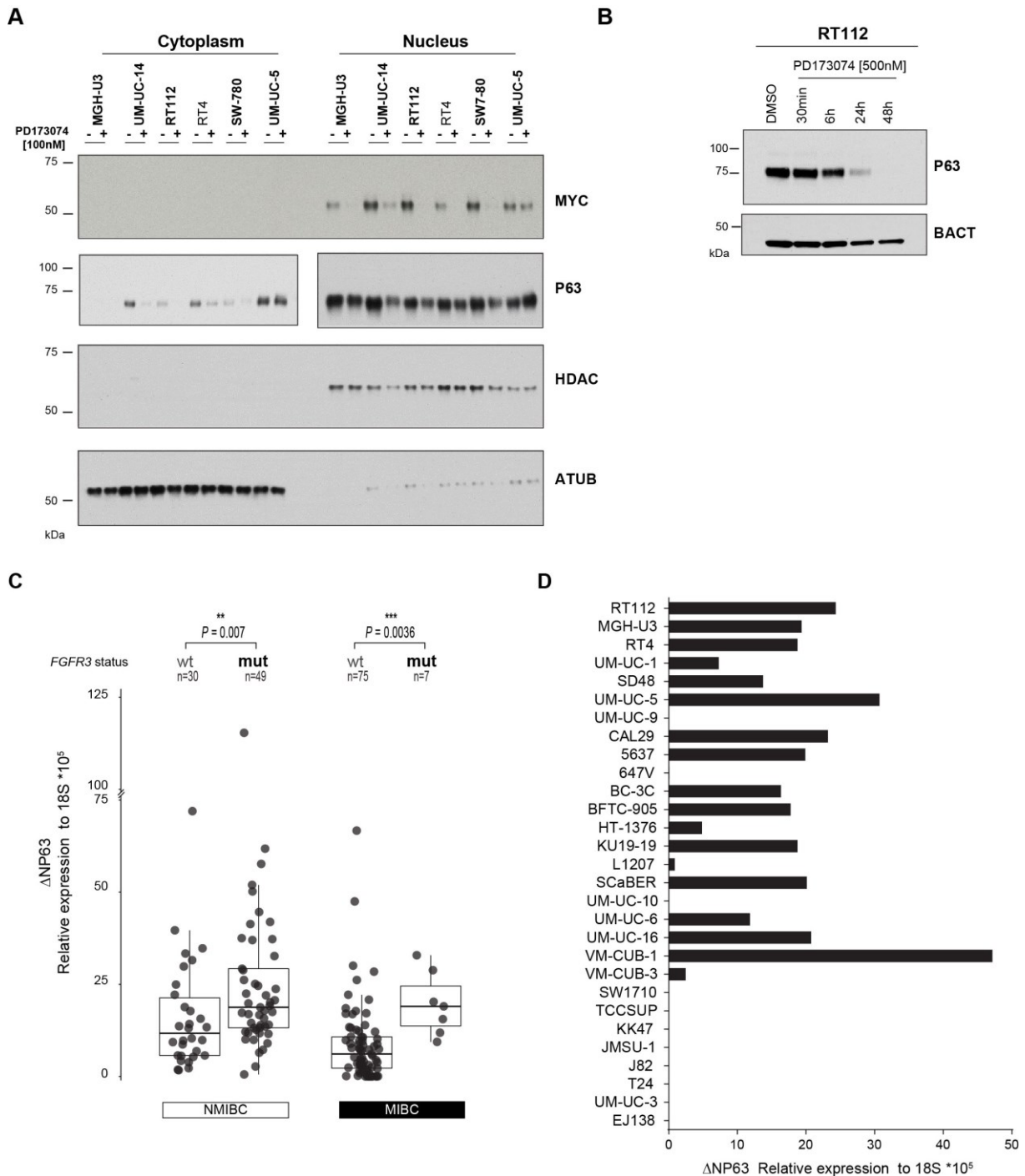
- inhibition in lung cancer. *Science Signaling* **6**, (2013).
18. Wang, J. *et al.* Ligand-associated ERBB2/3 activation confers acquired resistance to FGFR inhibition in FGFR3-dependent cancer cells. *Oncogene* **34**, 2167–2177 (2015).
 19. Wang, L. *et al.* A Functional Genetic Screen Identifies the Phosphoinositide 3-kinase Pathway as a Determinant of Resistance to Fibroblast Growth Factor Receptor Inhibitors in FGFR Mutant Urothelial Cell Carcinoma [Figure presented]. *Eur. Urol.* **71**, 858–862 (2017).
 20. Mahe, M. *et al.* An FGFR3/MYC positive feedback loop provides new opportunities for targeted therapies in bladder cancers. *EMBO Mol. Med.* e8163 (2018). doi:10.15252/emmm.201708163
 21. Linde, J., Schulze, S., Henkel, S. G. & Guthke, R. Data- and knowledge-based modeling of gene regulatory networks: An update. *EXCLI J.* **14**, 346–378 (2015).
 22. Elati, M. *et al.* LICORN: Learning cooperative regulation networks from gene expression data. *Bioinformatics* **23**, 2407–2414 (2007).
 23. Emmert-Streib, F., Glazko, G. V., Altay, G. & Simoes, R. de M. Statistical inference and reverse engineering of gene regulatory networks from observational expression data. *Frontiers in Genetics* **3**, (2012).
 24. Huynh-Thu, V. A., Irrthum, A., Wehenkel, L. & Geurts, P. Inferring regulatory networks from expression data using tree-based methods. *PLoS One* **5**, (2010).
 25. Margolin, A. A. *et al.* ARACNE: An algorithm for the reconstruction of gene regulatory networks in a mammalian cellular context. *BMC Bioinformatics* **7**, (2006).
 26. Chebil, I., Nicolle, R., Santini, G., Rouveirol, C. & Elati, M. Hybrid method inference for the construction of cooperative regulatory network in human. *IEEE Trans. Nanobioscience* **13**, 97–103 (2014).
 27. Nicolle, R., Radvanyi, F. & Elati, M. CoRegNet: Reconstruction and integrated analysis of co-regulatory networks. *Bioinformatics* **31**, 3066–3068 (2014).
 28. Meyers, R. M. *et al.* Computational correction of copy number effect improves specificity of CRISPR-Cas9 essentiality screens in cancer cells. *Nat. Genet.* **49**, 1779–1784 (2017).
 29. Palmboos, P. L. *et al.* ATDC/TRIM29 drives invasive bladder cancer formation through miRNA-mediated and epigenetic mechanisms. *Cancer Res.* **75**, 5155–5166 (2015).
 30. Trabelsi, N., Setti Boubaker, N., Said, R. & Ouerhani, S. Notch Pathway: Bioinformatic Analysis of Related Transcription Factors within Bladder Cancer Types and Subtypes. *IRBM* **39**, 261–267 (2018).
 31. Warrick, J. I. *et al.* FOXA1, GATA3 and PPAR γ Cooperate to drive luminal subtype in bladder cancer: A molecular analysis of established human cell lines. *Sci. Rep.* **6**, (2016).
 32. Zhang, X. *et al.* Somatic Superenhancer Duplications and Hotspot Mutations Lead to Oncogenic Activation of the KLF5 Transcription Factor. *Cancer Discov.* **8**, 108–125 (2018).
 33. Choi, W. *et al.* Identification of distinct basal and luminal subtypes of muscle-invasive bladder cancer with different sensitivities to frontline chemotherapy. *Cancer Cell* **25**, 152–65 (2014).
 34. Guo, C. C. *et al.* Dysregulation of EMT Drives the Progression to Clinically Aggressive Sarcomatoid Bladder Cancer. *Cell Rep.* **27**, 1781-1793.e4 (2019).
 35. Karni-Schmidt, O. *et al.* Distinct expression profiles of p63 variants during urothelial development and bladder cancer progression. *Am. J. Pathol.* **178**, 1350–1360 (2011).
 36. Castro-Castro, A. *et al.* Cellular and Molecular Mechanisms of MT1-MMP-Dependent Cancer Cell Invasion. *Annu. Rev. Cell Dev. Biol.* **32**, 555–576 (2016).
 37. Lodillinsky, C. *et al.* p63/MT1-MMP axis is required for in situ to invasive transition in basal-like breast cancer. *Oncogene* **35**, 344–357 (2016).
 38. Hernández, S. *et al.* Prospective study of FGFR3 mutations as a prognostic factor in nonmuscle invasive urothelial bladder carcinomas. *J. Clin. Oncol.* **24**, 3664–3671 (2006).
 39. Bradner, J. E., Hnisz, D. & Young, R. A. Transcriptional Addiction in Cancer. *Cell* **168**, 629–643 (2017).
 40. Lee, T. I. & Young, R. A. Transcriptional regulation and its misregulation in disease. *Cell* **152**, 1237–1251 (2013).
 41. Kamoun, A. *et al.* A Consensus Molecular Classification of Muscle-invasive Bladder Cancer. *Eur. Urol.* (2019). doi:10.1016/j.eururo.2019.09.006
 42. Rebouissou, S. *et al.* EGFR as a potential therapeutic target for a subset of muscle-invasive bladder cancers presenting a basal-like phenotype. *Sci. Transl. Med.* **6**, 244ra91 (2014).
 43. Choi, W. *et al.* p63 expression defines a lethal subset of muscle-invasive bladder cancers. *PLoS One* **7**, (2012).
 44. He, Y. *et al.* Impaired delta Np63 expression is associated with poor tumor development in transitional cell carcinoma of the bladder. *J. Korean Med. Sci.* **23**, 825–832 (2008).
 45. Gaya, J. M. *et al.* Δ np63 expression is a protective factor of progression in clinical high grade

RESULTS

- T1 bladder cancer. *J. Urol.* **193**, 1144–1150 (2015).
46. Koga, F. *et al.* Impaired Δ Np63 expression associates with reduced β -catenin and aggressive phenotypes of urothelial neoplasms. *Br. J. Cancer* **88**, 740–747 (2003).
 47. Fukushima, H. *et al.* Loss of Δ Np63 α promotes invasion of urothelial carcinomas via N-cadherin/Src homology and collagen/extracellular signal-regulated kinase pathway. *Cancer Res.* **69**, 9263–9270 (2009).
 48. Papadimitriou, M. A. *et al.* Δ Np63 transcript loss in bladder cancer constitutes an independent molecular predictor of TaT1 patients post-treatment relapse and progression. *J. Cancer Res. Clin. Oncol.* **145**, 3075–3087 (2019).
 49. Park, B. J. *et al.* Frequent alteration of p63 expression in human primary bladder carcinomas. *Cancer Res.* **60**, 3370–4 (2000).
 50. Chen, Y. *et al.* A double dealing tale of p63: an oncogene or a tumor suppressor. *Cellular and Molecular Life Sciences* **75**, 965–973 (2018).
 51. Tran, M. N. *et al.* The p63 protein isoform Δ Np63 α inhibits epithelial-mesenchymal transition in human bladder cancer cells: Role of miR-205. *J. Biol. Chem.* **288**, 3275–3288 (2013).
 52. Barretina, J. *et al.* The Cancer Cell Line Encyclopedia enables predictive modelling of anticancer drug sensitivity. *Nature* **483**, 603–607 (2012).
 53. Delpuech, O. *et al.* Identification of pharmacodynamic transcript biomarkers in response to FGFR inhibition by AZD4547. *Mol. Cancer Ther.* **15**, 2802–2813 (2016).
 54. Lambert, S. A. *et al.* The Human Transcription Factors. *Cell* **172**, 650–665 (2018).
 55. Schmeier, S., Alam, T., Essack, M. & Bajic, V. B. TcoF-DB v2: Update of the database of human and mouse transcription co-factors and transcription factor interactions. *Nucleic Acids Res.* **45**, D145–D150 (2017).
 56. Schaefer, M. H. *et al.* Hippie: Integrating protein interaction networks with experiment based quality scores. *PLoS One* **7**, (2012).
 57. Franceschini, A. *et al.* STRING v9.1: Protein-protein interaction networks, with increased coverage and integration. *Nucleic Acids Res.* **41**, (2013).
 58. Keshava Prasad, T. S. *et al.* Human Protein Reference Database - 2009 update. *Nucleic Acids Res.* **37**, (2009).
 59. Kou, Y. *et al.* ChEA2: Gene-set libraries from ChIP-X experiments to decode the transcription regulome. in *Lecture Notes in Computer Science (including subseries Lecture Notes in Artificial Intelligence and Lecture Notes in Bioinformatics)* **8127 LNCS**, 416–430 (2013).
 60. Kulakovskiy, I. V. *et al.* HOCOMOCO: Expansion and enhancement of the collection of transcription factor binding sites models. *Nucleic Acids Res.* **44**, D116–D125 (2016).
 61. Marbach, D. *et al.* Tissue-specific regulatory circuits reveal variable modular perturbations across complex diseases. *Nat. Methods* **13**, 366–370 (2016).
 62. Jiang, C., Xuan, Z., Zhao, F. & Zhang, M. Q. TRED: A transcriptional regulatory element database, new entries and other development. *Nucleic Acids Res.* **35**, (2007).
 63. Shannon, P. *et al.* Cytoscape: A software Environment for integrated models of biomolecular interaction networks. *Genome Res.* **13**, 2498–2504 (2003).
 64. Calderaro, J. *et al.* PI3K/AKT pathway activation in bladder carcinogenesis. *Int. J. Cancer* **134**, 1776–1784 (2014).
 65. Langmead, B. Aligning short sequencing reads with Bowtie. *Curr. Protoc. Bioinforma.* (2010). doi:10.1002/0471250953.bi1107s32
 66. Landt, S. G. *et al.* ChIP-seq guidelines and practices of the ENCODE and modENCODE consortia. *Genome Research* **22**, 1813–1831 (2012).
 67. Ritchie, M. E. *et al.* Limma powers differential expression analyses for RNA-sequencing and microarray studies. *Nucleic Acids Res.* **43**, e47 (2015).

RESULTS

Supplementary Figures



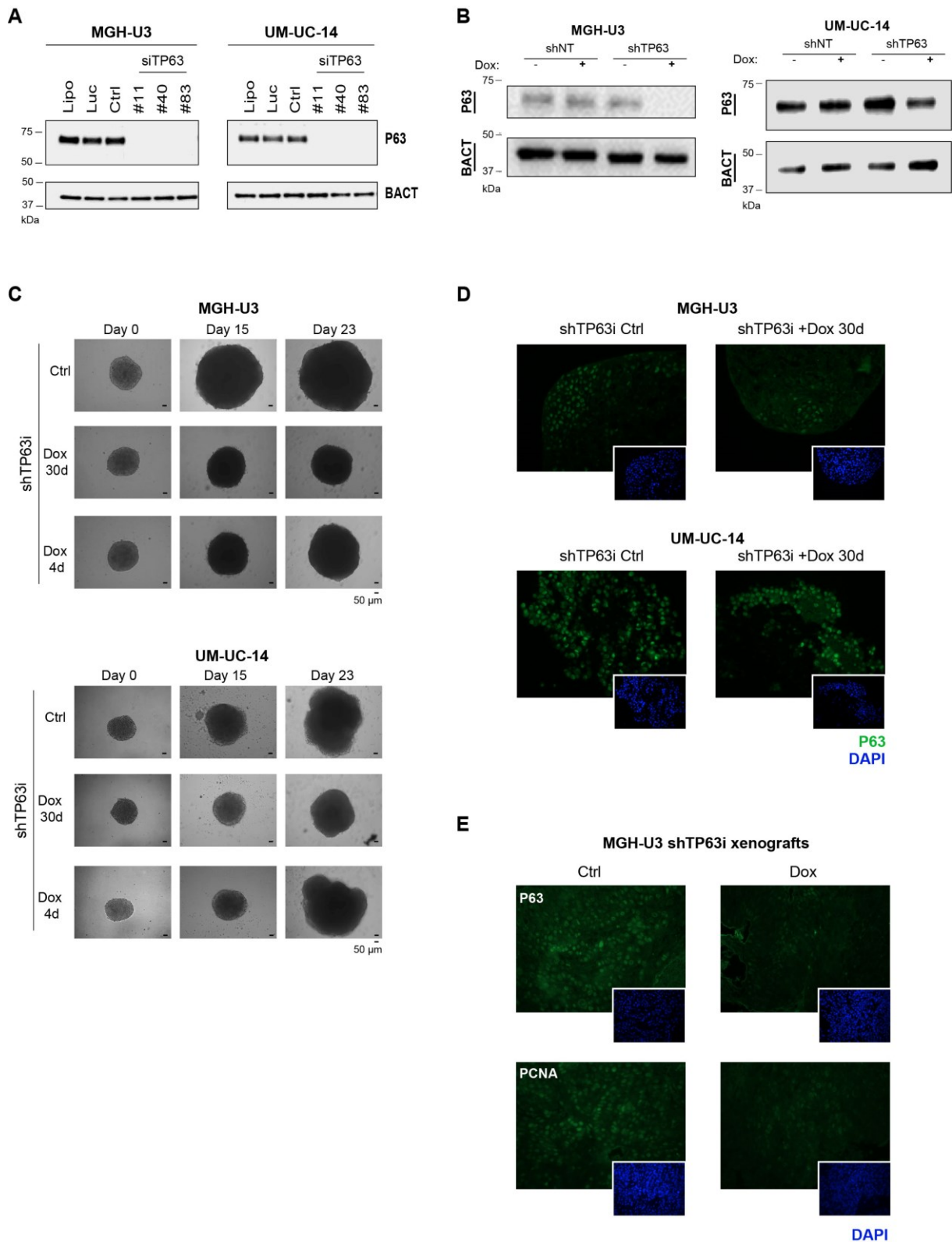
Supp Figure 1. TP63 expression in bladder cancer cell lines and human bladder tumors harboring an altered-FGFR3.

A. Western blot assay comparing p63 expression levels at the cytoplasmic and nuclear compartments of FGFR3-dependent cells (MGH-U3, UM-UC-14, RT112, RT4, SW780) treated or not with a pan-FGFR inhibitor (PD173074, 100nM, 40h). UM-UC-5 cells expressing a wtFGFR3 were used as control. MYC protein levels were used as a technical control based on the previously reported FGFR3-MYC regulatory-loop²⁰. Proteins used as loading control and control of cell fraction purity were: HDAC and ATUB.

RESULTS

- B.** RT112 cells were treated with DMSO (48hours) or the pan-FGFR inhibitor PD173074 [500nM] for 30min, 6h, 24, and 48h. Cell lysates were recovered at each time point and analyzed by immunoblotting using antibodies against p63. Actin was used as a loading control.
- C.** Relative expression of the Δ Np63 isoform with respect to the 18S ribosomal subunit in human bladder tumors from the CIT cohort (NMIBC; $n = 79$, MIBC $n = 82$).
- D.** Relative expression of the Δ Np63 isoform with respect to the 18S ribosomal subunit in bladder cancer derived cell lines.

RESULTS



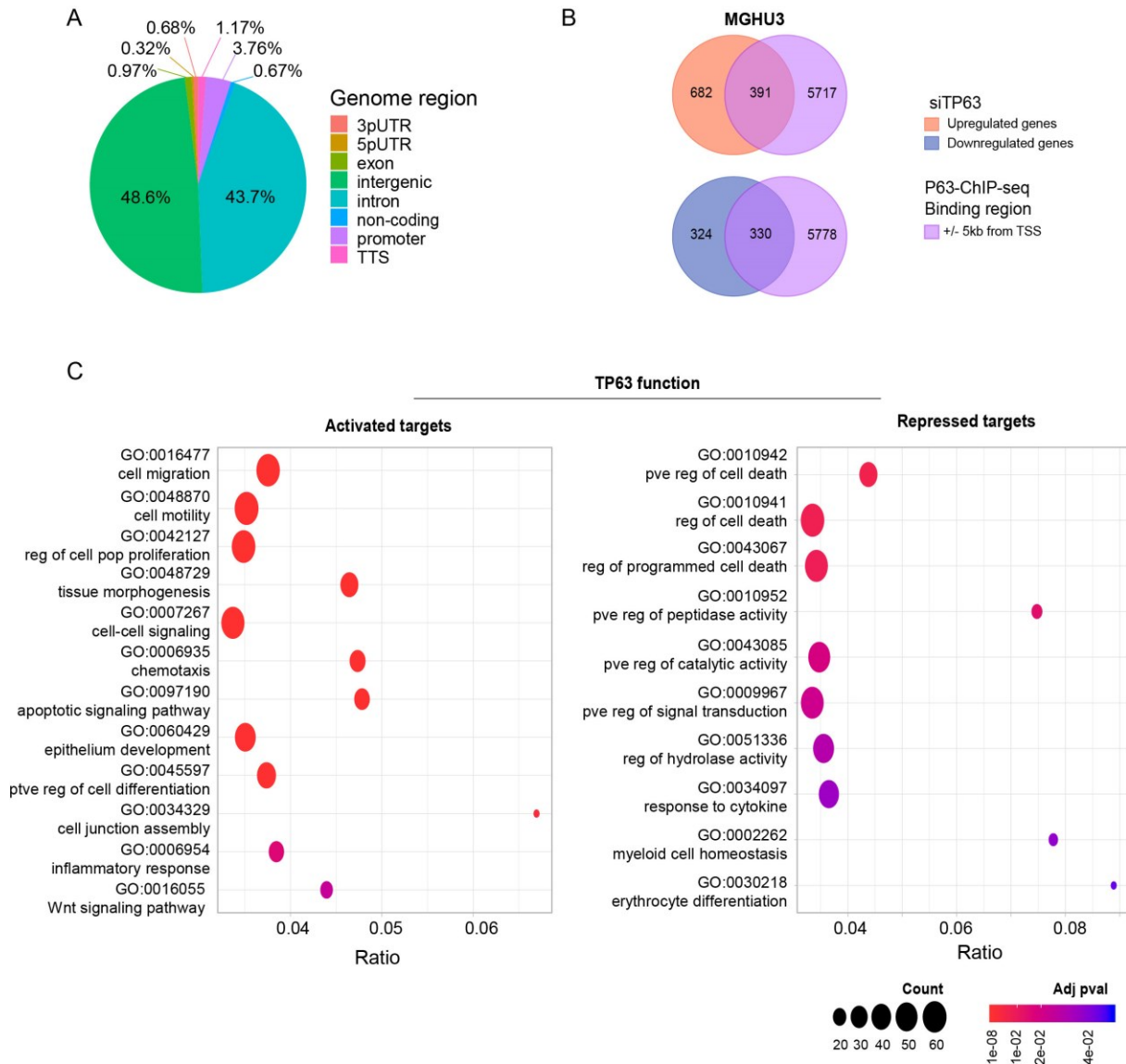
Supp Figure 2. Transient and stable knockdown of *TP63* in FGFR3-mutated bladder cancer cell lines.

A. MGH-U3 and UM-UC-14 were transfected with three different siRNAs targeting *TP63* (siTP63 #11, #40, #83). Forty-eight hours after transfection, cell lysates were recovered and analyzed by immunoblotting with antibodies against p63. Actin (BACT) was used as a loading control.

RESULTS

- B.** MGH-U3 and UM-UC-14 cells stably expressing a doxycycline (Dox)-inducible shRNA directed against *TP63* (shTP63i) were treated or not with Dox and efficiency of knockdown was corroborated by western blotting of p63. Actin (BACT) was used as a loading control.
- C.** Representative microscopy images of MGH-U3 shTP63i#4 and UM-UC-14 shTP63i#4 treated or not with Dox for a long (30 days; 30d) or short (4 days; 4d) time period. Scale bar represents 50 μ m.
- D-E.** Representative immunofluorescence images of p63 staining-cells in: D. MGH-U3 shTP63i#4 and UM-UC-14 shTP63i#4 cultures treated or not with Dox and E. Tumors from xenografted mice generated with MGH-U3 shTP63i#4 cells, and treated or not with Dox for 30 days.

RESULTS



Supp Figure 3. P63 target genes in an altered-FGFR3 bladder cancer context.

- Genome binding profile of p63 from P63-ChIPseq of MGH-U3 cells.
- Selection of possible p63 targets in MGH-U 3 cells through a Venn Diagram analysis of significant P63ChIPseq peaks (+/- 5kb from the transcription start site; TSS) and genes whose expression was significantly changed upon knockdown of *TP63* in MGH-U3. Results represent two independent experiments.
- Significantly enriched Gene Ontology Biological Processes (GO/BPs) of the p63 targets determined in Supp Figure 3B. Only GO/BPs presenting an adjusted p-value <0.05 with at least 10 genes contributing to their enrichment were considered. P-values were adjusted by the Benjamini-Hochberg method.

2.3 Discussion

In the afore presented paper draft, we applied a strategy merging computational inference and functional validation to reveal a gene regulatory network composed of co-operative transcription factors and cofactors, and representative of a bladder cancer state. Investigation of the transcriptionally active program possibly governed by an altered-FGFR3 unexpectedly unveiled p63. Former studies have corroborated an important role of p63 in bladder cancer progression, where a high $\Delta Np63$ expression has been associated to poor prognosis and clinical outcome in basal-like MIBC^{129,139,153}. Remarkably, we confirmed in this work that cell proliferation, migration and invasion are likewise regulated by p63 in luminal like FGFR3-dependent bladder cancer cells (associated to a more differentiated state).

As mentioned in the results section, the choice of the bioinformatic algorithm was made based on the advantages that it presented: construction of a large, context-specific co-regulatory network without any prior knowledge, and ability to measure a sample-unique transcriptional activity for the inferred regulators. Nonetheless; as for many other network inference methods, the algorithm we chose presents certain limitations, which were confirmed when we were not able to validate the previously published FGFR3-MYC loop⁷⁰. Using a combination of various inference methods followed by functional validation with distinct types of data (as we have tried to do in this study) is thus important to complete the inferred GRN, and produce biologically relevant networks.

In our case, we presented here the CoRegNet strategy, however we had formerly utilized the knowledge-based Ingenuity Pathway Analysis (IPA) software to identify upstream regulators activated or repressed by an altered-FGFR3⁷⁰. Since the IPA software infers a regulator based on the expression levels of its target genes and independently of its own expression levels, other transcription factors may be unveiled (i.e. MYC) (Figure 6A). IPA investigation of the transcription factors regulating the set of genes that had a statistically significant change of expression upon FGFR3 knockdown in MGH-U3 (FGFR3-Y375C), UM-UC-14 (FGFR3-S249C) and RT112 bladder cancer cells confirmed some of regulators predicted by CoRegNet such as AHR, BCL6, FOS, IRF7, TP53 and TP63 as well as regulators of the same TF family such as CREB1, TRIM24, GATA1, CEBPB, RARA, TBX2, TRIM24 and ZNF217. Additionally, IPA similarly identified AHR, FOS, T53 and TP63 in bladder tumors of our hFGFR3-S249C murine model (Figure 6A).

RESULTS

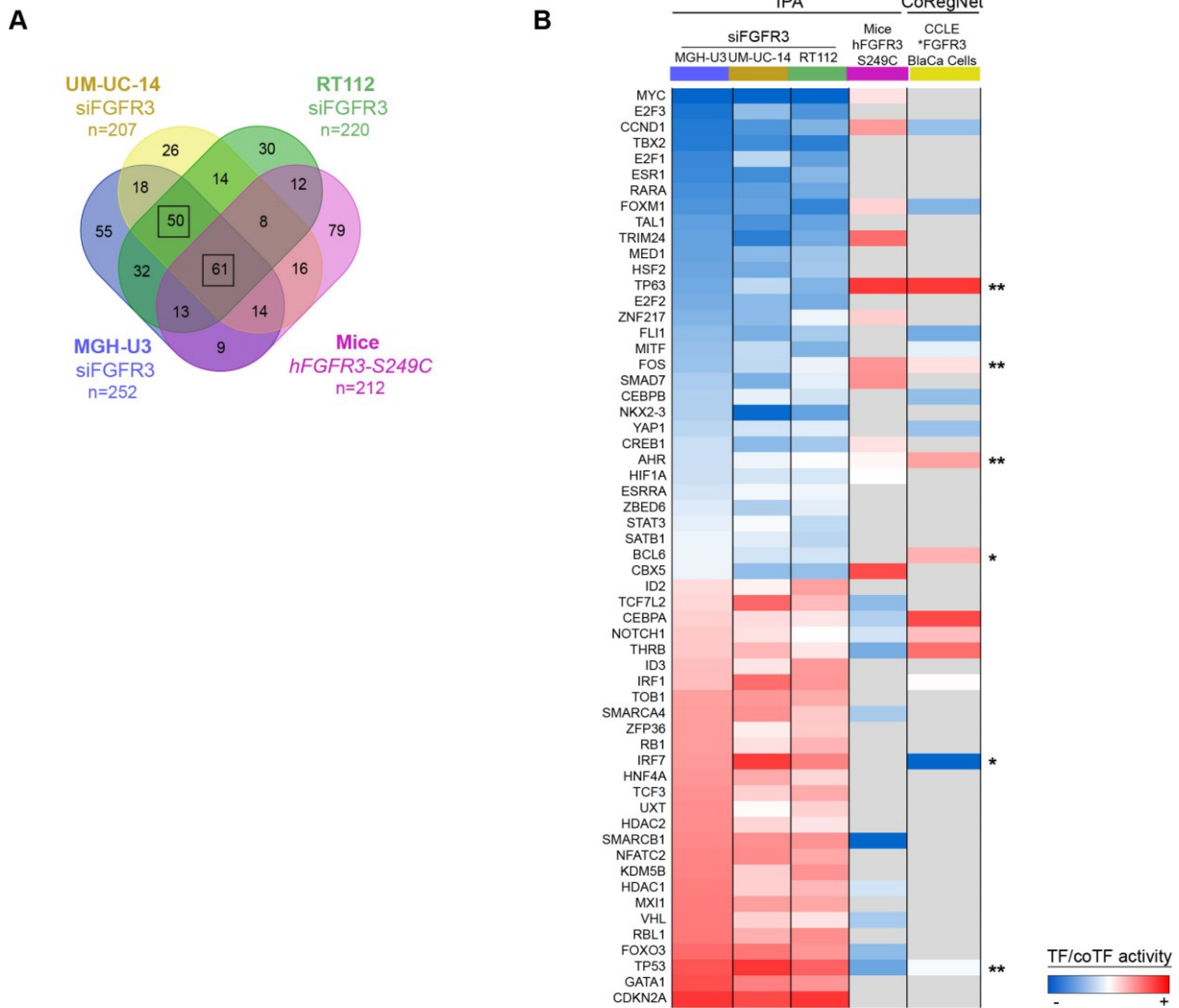


Figure 6| Transcriptional program downstream of FGFR3: Ingenuity Pathway Analysis (IPA) inference.

A. Venn diagram of significantly predicted transcription factors and cofactors (TFs/coTFs) predicted to regulate genes whose expression was significantly altered following: (i) the knockdown of FGFR3 in three different bladder cancer cell lines (MGH-U3, UM-U-C14 and RT112) or (ii) the overexpression of hFGFR3-S249C in mouse urothelium. The total number of regulators found per individual group is indicated.

B. Heatmap of activation status of commonly predicted TFs/coTFs from presenting a coherent and opposite activation state (IPA inferred activation z-score) between the three different siFGFR3 transfected bladder cancer cell lines (MGHU3, UMUC14 and RT112). and the hFGFR3-S249C murine tumors (n = 58/111) coherent regulators). Activation status for CoRegNet commonly inferred regulators is shown (activity in *FGFR3 CCLE bladder cancer cells; regulators highlighted with asterisks). Red squares represent an active TF/coTF, whereas blue squares represent an inactive or repressed TF/coTF. Gray represents a regulator that was not predicted in the corresponding dataset

Being confident about the biological representativity of our FGFR3 perturbation datasets (bladder cancer cells and murine model), we then chose to use them to further examine the CoRegNet inferred BLCA-GRN. Unfortunately, for the bladder cancer cell line data we came across unforeseen results: whilst we had individually validated multiple regulators, the overall transcriptional program that we observed to be active in control, vehicle (lipofectamine; Lipo)

RESULTS

treated cells, corresponded to the one observed in basal-like MIBCs and was opposite to the one seen in treatment-naïve cells (*FGFR3 CCLE BLCA cells) (Figure 7A). As we observed this in our three independent datasets (Lipo vs siFGFR3; MGH-U3, UM-UC-14, RT112), we first hypothesized that this could somehow be an undesired, unknown effect of the lipofectamine treatment. We thus searched for published datasets of FGFR3 perturbation where other techniques such as shRNA (lipofectamine not used) or small molecule inhibitors were used. The calculation of the active TFs/coTFs under these experimental contexts confusingly revealed that for the shRNA dataset (shFGFR3 RT112 cells), we had the same results as before, with control cells presenting a basal-like transcriptional program (Figure 7A). In contrast, the control cells (DMSO) from the anti-FGFR treated RT112 and MGH-U3 dataset (E-MTAB-4749)²⁶⁷ presented network activity phenotypes similar to the ones we observed in our BLCA-GRN (Figure 1A, results section page 81). These findings suggested that the lipofectamine treatment was not causing a shift in the transcriptional program underlying these cells, so we proposed a new hypothesis where the initial seeding concentration of the cells could impact their proliferative state (and hence their transcriptional program). As cells are usually seeded at very low initial concentrations for both siRNA and shRNA invalidation experiments, control siRNA/shRNA cells could be in a longer proliferative state in contrast to control cells used in an FGFR-inhibition setting where a higher cell density from the beginning would lead cells to fall into a quiescent state more quickly. In an effort to corroborate such hypothesis, we examined the set of TFs/coTFs that was active in proliferating normal human urothelium (NHU) cells (at 6 and 24 hours of culture). We effectively observed a transcriptional program that was similarly active between proliferating NHU and our lipofectamine-treated cells and control shFGFR3 RT112 (Figure 7). Further supporting our hypothesis, we saw this same pattern when analyzing MIBC tumors of the neuroendocrine-like (NE-like) subtype, which is associated to high cell cycle activity⁴⁸. This evidence provides a first possible explanation to our contradictory findings, yet more would need to be done to better understand and experimentally validate such shift in network phenotype. Lastly, we still corroborated in all the four knockdown datasets that p63 was active in the control cells (Lipo MGH-U3, UM-UC-14, RT112; Control shFGFR3 RT112) and that it was inhibited following the perturbation of FGFR3 (Figure 7B; same results as IPA Figure 6). Having previously confirmed that p63 mediates cell proliferation, this could come as extra evidence supporting p63's functional role in an altered-FGFR3 context.

RESULTS



Figure 7 | Transcriptionally active BLCA-GRN subnetworks: validation in distinct biological contexts.

- A.** Heatmap display of the most (4th quartile) and least (1st quartile) active transcription factors and cofactors (TFs/coTFs) in FGFR3-dependent bladder cancer cell lines (MGH-U3, RT112, RT112/84, RT4, SW-780, UM-UC-14), as calculated from the BLCA-GRN. Each column represents a transcriptomic dataset from which the sample-specific or mean activity of a corresponding TF/coTF (rows) was calculated. Color of rows represents TF/coTF activity: red; high activity, blue; low activity. The names of the top 20 most and top 20 least active regulators are shown.
- B.** Zoom of heatmap in 1A depicting inferred p63 activity levels calculated from the different transcriptomic datasets shown. Ba/sq: Basal squamous, BlaCa: Bladder cancer, Lipo: lipofectamine, LumP: Luminal papillary, MIBC: Muscle-invasive bladder carcinoma, NE-like: Neuroendocrine-like, NHU: Normal human urothelium, Prolif: proliferating.

Overall, we have presented an approach to construct an FGFR3-driven GRN specific of bladder tumors and which can lead to the identification of key regulators such as p63. Whilst we focused mainly on the validation of p63, the presented BLCA-GRN may be used in the future to better understand the role of FGFR3 in the etiology and progression of bladder cancer; as well as unveil new therapeutic targets. Importantly, the second key element identified in the FGFR3-GRN network, FOXM1, would remain to be further studied as a high

RESULTS

expression of this transcription factor has been related to a poor prognosis in bladder cancer^{282,283}.

Finally, whilst we did not exploit the co-operativity information given by the BLCA-GRN, it will be crucial to investigate if simultaneous targeting of pairs of key elements of the network would result in more efficient cell death that could be translated in improved therapeutic strategies in the clinic.

CONCLUSIONS AND PERSPECTIVES

CONCLUSIONS AND PERSPECTIVES

During this thesis project, two strategies were pursued with the aim of increasing our knowledge about the role and molecular mechanisms of an altered-FGFR3 in bladder tumorigenesis and progression.

The first strategy sought to assess the *in vivo* functional impact of altered-FGFR3 expression in the urothelium of mice. The results found show that the expression of a human mutated-FGFR3 (S249C) alone can lead to abnormal urothelial differentiation, giving rise to hyperplastic lesions and spontaneous neoplastic transformation in transgenic mice. This provided the first *in vivo* evidence of the oncogenic potential of a mutated-FGFR3 alone, and shed light onto some unexpected molecular mechanisms underlying FGFR3 induced tumorigenesis: AR activation. Whilst the role of androgens in bladder tumorigenesis has already been studied before²⁸⁴, this is the first time that FGFR3 is demonstrated to favor tumor development through regulation of sex hormone receptors (activation of AR and inhibition of ESR1). It would thus be of strong interest to evaluate the impact of a combined anti-FGFR and androgen-repressive therapy in FGFR3-altered bladder cancer preclinical models.

Despite being equivalent to its human counterpart at the histopathological and molecular level, our GEM model presented the main limitation of high latency (15-18 months to develop a tumor) and low penetrance, limiting its use for translational research protocols. To overcome such problem, we suggest that allografts from this model be generated for further investigation of FGFR3 *in vivo* molecular mechanisms or *in vivo* drug testing. As an example, by presenting a low tumor immune infiltrate (in accordance to the literature), our immunocompetent GEM could be used to increase our understanding of FGFR3-driven immune-escape and/or immune-suppression mechanisms, and permit the evaluation of combined anti-FGFR and immune check-point inhibitors.

The construction of a GRN using transcriptomic samples from our murine transgenic model would have enabled a deeper understanding of the *in vivo* functional role of FGFR3 in bladder tumorigenesis. However, we were limited by the small number of samples obtained (n= 6 tumors, 6 hyperplastic lesions and 3 normal urothelial), meaning that we had to adapt our analysis with the most adequate approaches such as IPA inference of transcriptional regulators and enrichment of biological processes/pathways. Interestingly, the inference of significantly enriched transcription factors in UII-hFGFR3-S49C murine tumors, enabled us not only to detect AR, but also p63, a transcription factor that we would be unveiling via a different approach (CoRegNet H-LICORN; context-specific cooperativity network). Finally, we searched to combine our *in vivo* strategy to our approach of GRN inference method by using the UII-hFGFR3-S249C transcriptome to validate the transcriptionally active programs from the inferred network of cooperative TFs/coTFs in bladder cancer.

CONCLUSIONS AND PERSPECTIVES

The second strategy aimed to infer the network of co-activators and co-repressors (TFs/coTFs) mediated by an altered-FGFR3 in bladder cancer and was based on the integration of computational tools (CoRegNet H-LICORN) and experimental validation (gene invalidation). Taking advantage of the transcription factor influence function of CoRegNet, we were able to validate the TFs/coTFs whose activity was driven by an altered FGFR3. For this, we used both observational (FGFR3-altered human bladder tumors and bladder cancer cell lines) and experimental data (preclinical models of FGFR3 perturbation: UII-hFGFR3-S249C mice; bladder cancer cell lines invalidated or inhibited for FGFR3). In this manner, we elucidated an essential role of p63 in luminal-like FGFR3-dependent bladder cancer cells and explored the functional consequences of its high activity in NMIBC bladder tumors. Concluding that p63 played a similar, yet slightly different role in both altered-FGFR3 tumors (associated to a luminal-like phenotype) and basal-like MIBCs, we hypothesized that a fine tuning of p63's activity may occur at the level of its co-regulatory partners. A way of corroborating this hypothesis could involve the use of proteomic data that could reveal interacting partners in bladder cancer cell lines representative of the different tumor subgroups. Most importantly, as no drugs have been reported to target p63, by studying its context-specific transcriptional network in more depth, druggable interacting partners or target genes may be identified.

As mentioned in the introduction, no perfect GRN inference method exists, meaning that whilst we were able to produce a context-specific, biologically relevant network using CoRegNet H-LICORN, certain expected TFs/coTFs were not predicted. For example; the well-established FGFR3-MYC regulatory loop (see annex I) was not identified, nor was the AR receptor (both identified in our UII-hFGFR3-S249C model using IPA). As H-LICORN will take into account only TFs/coTFs whose expression varies significantly across samples (defined during the data discretization process), MYC and AR were probably not identified. As is often the case for many TFs, they are regulated at the post-translational level rather than at the transcriptional level. Altogether, these limitations highlight the necessity to constantly combine different inference methods with experimental validation to produce more accurate GRNs (as was done in this project). Having context-specific, biologically relevant GRNs will consequently allow to better stratify patients that present the adequate molecular context to best respond to a targeted therapy.

As a whole, this study provides two strategies that contribute both independently and together to the deeper understanding of the role of an altered-FGFR3 in bladder tumorigenesis and bladder cancer progression; and allow to reveal new therapeutic targets that would improve current therapies. Whereas we have focused on corroborating only certain elements of the altered-FGFR3 BLCA-GRN (i.e. p63 and AR), it will be interesting to investigate the role of other transcription factors that were identified such as FOXM1

CONCLUSIONS AND PERSPECTIVES

(Chapter 2, Figure 2), a transcription factor which, similar to p63, has been described important in the basal subtype of bladder tumors (more aggressive and not dependent on FGFR3)⁴⁸.

Lastly, an analysis of the presented network with other high-through put data such as proteomics, genomics, epigenetic modifications or metabolomics would be important to increase the strength of the biological prediction of the model.

BIBLIOGRAPHY

Bibliography

1. Khandelwal, P., Abraham, S. N. & Apodaca, G. Cell biology and physiology of the uroepithelium. *American Journal of Physiology - Renal Physiology* **297**, (2009).
2. Kobayashi, T., Owczarek, T. B., McKiernan, J. M. & Abate-Shen, C. Modelling bladder cancer in mice: opportunities and challenges. *Nat. Rev. Cancer* **15**, 42–54 (2015).
3. Jost, S. P. Cell cycle of normal bladder urothelium in developing and adult mice. *Virchows Arch. B. Cell Pathol. Incl. Mol. Pathol.* **57**, 27–36 (1989).
4. Kreft, M. E., Sterle, M., Veranic, P. & Jezernik, K. Urothelial injuries and the early wound healing response: tight junctions and urothelial cytodifferentiation. *Histochem. Cell Biol.* **123**, 529–39 (2005).
5. Lavelle, J. *et al.* Bladder permeability barrier: recovery from selective injury of surface epithelial cells. *Am. J. Physiol. Physiol.* **283**, F242–F253 (2002).
6. Varley, C. L., Stahlschmidt, J., Smith, B., Stower, M. & Southgate, J. Activation of Peroxisome Proliferator-Activated Receptor- γ Reverses Squamous Metaplasia and Induces Transitional Differentiation in Normal Human Urothelial Cells. *Am. J. Pathol.* (2004). doi:10.1016/S0002-9440(10)63737-6
7. Ferlay, J. *et al.* Estimating the global cancer incidence and mortality in 2018: GLOBOCAN sources and methods. *International Journal of Cancer* **144**, 1941–1953 (2019).
8. International Agency for Research on Cancer. World Health Organization. Cancer Today. Available at: <https://gco.iarc.fr/today/home>. (Accessed: 19th January 2020)
9. Freedman, N. D., Silverman, D. T., Hollenbeck, A. R., Schatzkin, A. & Abnet, C. C. Association between smoking and risk of bladder cancer among men and women. *JAMA - J. Am. Med. Assoc.* **306**, 737–745 (2011).
10. Sanli, O. *et al.* Bladder cancer. *Nat. Rev. Dis. Prim.* **3**, 1–19 (2017).
11. Burch, J. D. *et al.* Risk of bladder cancer by source and type of tobacco exposure: A case-control study. *Int. J. Cancer* **44**, 622–628 (1989).
12. Samanic, C. *et al.* Smoking and bladder cancer in Spain: Effects of tobacco type, timing, environmental tobacco smoke, and gender. *Cancer Epidemiol. Biomarkers Prev.* **15**, 1348–1354 (2006).
13. Burger, M. *et al.* Epidemiology and risk factors of urothelial bladder cancer. *European Urology* **63**, 234–241 (2013).
14. Latifovic, L. *et al.* Bladder cancer and occupational exposure to diesel and gasoline engine emissions among Canadian men. *Cancer Med.* **4**, 1948–1962 (2015).
15. Purdue, M. P., Hutchings, S. J., Rushton, L. & Silverman, D. T. The proportion of cancer attributable to occupational exposures. *Ann. Epidemiol.* **25**, 188–92 (2015).
16. Barakat, R. M. R. Epidemiology of Schistosomiasis in Egypt: Travel through Time: Review. *Journal of Advanced Research* **4**, 425–432 (2013).
17. Guey, L. T. *et al.* Genetic susceptibility to distinct bladder cancer subphenotypes. *Eur. Urol.* **57**, 283–92 (2010).
18. Taioli, E. & Raimondi, S. Genetic susceptibility to bladder cancer. *Lancet* **366**, 610–612 (2005).
19. Comp erat, E. M. *et al.* Grading of Urothelial Carcinoma and The New ‘World Health Organisation Classification of Tumours of the Urinary System and Male Genital Organs 2016’. (2018). doi:10.1016/j
20. Kamat, A. M. *et al.* Bladder cancer. *The Lancet* **388**, 2796–2810 (2016).
21. Dinney, C. P. N. *et al.* Focus on bladder cancer. *Cancer Cell* **6**, 111–6 (2004).
22. McConkey, D. J. *et al.* Molecular genetics of bladder cancer: Emerging mechanisms of tumor initiation and progression. *Urologic Oncology: Seminars and Original Investigations* **28**, 429–440 (2010).
23. Cairns, P., Shaw, M. E. & Knowles, M. A. Initiation of bladder cancer may involve deletion of a tumour-suppressor gene on chromosome 9. *Oncogene* **8**, 1083–1085 (1993).
24. Miyao, N. *et al.* Role of chromosome 9 in human bladder cancer. *Cancer Res.* **53**, 4066–70 (1993).
25. Obermann, E. C. *et al.* Frequent genetic alterations in flat urothelial hyperplasias and concomitant papillary bladder cancer as detected by CGH, LOH, and FISH analyses. *J. Pathol.* **199**, 50–57 (2003).
26. Rebouissou, S. *et al.* CDKN2A homozygous deletion is associated with muscle invasion in FGFR3-mutated urothelial bladder carcinoma. *J. Pathol.* **227**, 315–324 (2012).
27. Billerey, C. *et al.* Frequent FGFR3 mutations in papillary non-invasive bladder (pTa) tumors. *Am. J. Pathol.* **158**, 1955–9 (2001).

BIBLIOGRAPHY

28. Cappellen, D. *et al.* Frequent activating mutations of FGFR3 in human bladder and cervix carcinomas. *Nat. Genet.* **23**, 18–20 (1999).
29. Zieger, K. *et al.* Role of activating fibroblast growth factor receptor 3 mutations in the development of bladder tumors. *Clin. Cancer Res.* **11**, 7709–19 (2005).
30. López-Knowles, E. *et al.* PIK3CA mutations are an early genetic alteration associated with FGFR3 mutations in superficial papillary bladder tumors. *Cancer Res.* **66**, 7401–7404 (2006).
31. Platt, F. M. *et al.* Spectrum of phosphatidylinositol 3-kinase pathway gene alterations in bladder cancer. *Clin. Cancer Res.* **15**, 6008–6017 (2009).
32. Balbás-Martínez, C. *et al.* Recurrent inactivation of STAG2 in bladder cancer is not associated with aneuploidy. *Nat. Genet.* **45**, 1464–1469 (2013).
33. Solomon, D. A. *et al.* Frequent truncating mutations of STAG2 in bladder cancer. *Nat. Genet.* **45**, 1428–1430 (2013).
34. Taylor, C. F., Platt, F. M., Hurst, C. D., Thygesen, H. H. & Knowles, M. A. Frequent inactivating mutations of STAG2 in bladder cancer are associated with low tumour grade and stage and inversely related to chromosomal copy number changes. *Hum. Mol. Genet.* **23**, 1964–1974 (2014).
35. di Martino, E., L'Hôte, C. G., Kennedy, W., Tomlinson, D. C. & Knowles, M. A. Mutant fibroblast growth factor receptor 3 induces intracellular signaling and cellular transformation in a cell type- and mutation-specific manner. *Oncogene* **28**, 4306–16 (2009).
36. Downes, M. R. *et al.* Analysis of papillary urothelial carcinomas of the bladder with grade heterogeneity: supportive evidence for an early role of CDKN2A deletions in the FGFR3 pathway. *Histopathology* **70**, 281–289 (2017).
37. Wu, X. R. Urothelial tumorigenesis: A tale of divergent pathways. *Nature Reviews Cancer* **5**, 713–725 (2005).
38. Puzio-Kuter, A. M. *et al.* Inactivation of p53 and Pten promotes invasive bladder cancer. *Genes Dev.* **23**, 675–680 (2009).
39. Inamura, K. Bladder Cancer: New Insights into Its Molecular Pathology. *Cancers (Basel)*. **10**, (2018).
40. Jung, S. *et al.* The role of immunohistochemistry in the diagnosis of flat urothelial lesions: a study using CK20, CK5/6, P53, Cd138, and Her2/Neu. *Ann. Diagn. Pathol.* **18**, 27–32 (2014).
41. Sfakianos, J. P. *et al.* The role of PTEN tumor suppressor pathway staining in carcinoma in situ of the bladder. *Urol. Oncol.* **32**, 657–62 (2014).
42. Knowles, M. A. & Hurst, C. D. Molecular biology of bladder cancer: new insights into pathogenesis and clinical diversity. *Nat. Publ. Gr.* **15**, 25–41 (2015).
43. Hedegaard, J. *et al.* Comprehensive Transcriptional Analysis of Early-Stage Urothelial Carcinoma. *Cancer Cell* **30**, 27–42 (2016).
44. Hurst, C. D. *et al.* Genomic Subtypes of Non-invasive Bladder Cancer with Distinct Metabolic Profile and Female Gender Bias in KDM6A Mutation Frequency. *Cancer Cell* **32**, 701-715.e7 (2017).
45. Sjö Dahl, G. *et al.* A molecular taxonomy for urothelial carcinoma. *Clin. Cancer Res.* **18**, 3377–3386 (2012).
46. Choi, W. *et al.* Identification of distinct basal and luminal subtypes of muscle-invasive bladder cancer with different sensitivities to frontline chemotherapy. *Cancer Cell* **25**, 152–65 (2014).
47. Damrauer, J. S. *et al.* Intrinsic subtypes of high-grade bladder cancer reflect the hallmarks of breast cancer biology. *Proc. Natl. Acad. Sci. U. S. A.* **111**, 3110–5 (2014).
48. Kamoun, A. *et al.* A Consensus Molecular Classification of Muscle-invasive Bladder Cancer. *Eur. Urol.* (2019). doi:10.1016/j.eururo.2019.09.006
49. Mo, Q. *et al.* Prognostic Power of a Tumor Differentiation Gene Signature for Bladder Urothelial Carcinomas. *J. Natl. Cancer Inst.* **110**, 448–459 (2018).
50. Rebouissou, S. *et al.* EGFR as a potential therapeutic target for a subset of muscle-invasive bladder cancers presenting a basal-like phenotype. *Sci. Transl. Med.* **6**, 244ra91 (2014).
51. Robertson, A. G. *et al.* Comprehensive Molecular Characterization of Muscle-Invasive Bladder Cancer. *Cell* **171**, 540-556.e25 (2017).
52. Sjö Dahl, G., Eriksson, P., Liedberg, F. & Höglund, M. Molecular classification of urothelial carcinoma: global mRNA classification versus tumour-cell phenotype classification. *J. Pathol.* **242**, 113–125 (2017).
53. Marzouka, N. A. D. *et al.* A validation and extended description of the Lund taxonomy for urothelial carcinoma using the TCGA cohort. *Sci. Rep.* **8**, (2018).
54. Babjuk, M. *et al.* European Association of Urology Guidelines on Non-muscle-invasive Bladder Cancer (TaT1 and Carcinoma In Situ) - 2019 Update. *European Urology* **76**, 639–657 (2019).

BIBLIOGRAPHY

55. Brausi, M. *et al.* Variability in the recurrence rate at first follow-up cystoscopy after TUR in stage Ta T1 transitional cell carcinoma of the bladder: a combined analysis of seven EORTC studies. *Eur. Urol.* **41**, 523–31 (2002).
56. DeGeorge, K. C., Holt, H. R. & Hodges, S. C. Bladder Cancer: Diagnosis and Treatment. *American family physician* **96**, 507–514 (2017).
57. Park, J. C., Citrin, D. E., Agarwal, P. K. & Apolo, A. B. Multimodal management of muscle-invasive bladder cancer. *Curr. Probl. Cancer* **38**, 80–108 (2014).
58. Souhami, L., Rene, N. & Cury, F. B. Conservative Treatment of Invasive Bladder Cancer. *Curr. Oncol.* **16**, (2009).
59. Bellmunt, J., Mottet, N. & De Santis, M. Urothelial carcinoma management in elderly or unfit patients. *Eur. J. Cancer, Suppl.* **14**, 1–20 (2016).
60. De Santis, M. *et al.* Randomized phase II/III trial assessing gemcitabine/carboplatin and methotrexate/carboplatin/vinblastine in patients with advanced urothelial cancer who are unfit for cisplatin-based chemotherapy: EORTC study 30986. *J. Clin. Oncol.* **30**, 191–199 (2012).
61. Gierth, M. & Burger, M. Bladder cancer: Progress in defining progression in NMIBC. *Nat. Rev. Urol.* **10**, 684–685 (2013).
62. Mar, N. & Dayyani, F. Management of Urothelial Bladder Cancer in Clinical Practice: Real-World Answers to Difficult Questions. *J. Oncol. Pract.* **15**, 421–428 (2019).
63. Funt, S. A. & Rosenberg, J. E. Cancer and Future Horizons. **14**, 221–234 (2018).
64. Berdik, C. & Ashour, M. Unlocking bladder cancer. *Nature* **551**, S34–S35 (2017).
65. Hindy, J.-R., Souaid, T., Kourie, H. R. & Kattan, J. Targeted therapies in urothelial bladder cancer: a disappointing past preceding a bright future? *Future Oncol.* **15**, 1505–1524 (2019).
66. Bellmunt, J., Powles, T. & Vogelzang, N. J. A review on the evolution of PD-1/PD-L1 immunotherapy for bladder cancer: The future is now. *Cancer Treatment Reviews* **54**, 58–67 (2017).
67. Darling, H. S. & Bellmunt, J. Immunotherapy in non-metastatic urothelial cancer: back to the 'future'. *Expert Opinion on Biological Therapy* **19**, 685–695 (2019).
68. Rouanne, M. *et al.* Development of immunotherapy in bladder cancer: Present and future on targeting PD(L)1 and CTLA-4 pathways. *World J. Urol.* **36**, 1727–1740 (2018).
69. Dufour, F. *et al.* TYRO3 as a molecular target for growth inhibition and apoptosis induction in bladder cancer. *Br. J. Cancer* **120**, 555–564 (2019).
70. Mahe, M. *et al.* An FGFR3/MYC positive feedback loop provides new opportunities for targeted therapies in bladder cancers. *EMBO Mol. Med.* e8163 (2018). doi:10.15252/emmm.201708163
71. Rochel, N. *et al.* Recurrent activating mutations of PPAR γ associated with luminal bladder tumors. *Nat. Commun.* **10**, (2019).
72. Lorient, Y. *et al.* Erdafitinib in Locally Advanced or Metastatic Urothelial Carcinoma. *N. Engl. J. Med.* **381**, 338–348 (2019).
73. Babina, I. S. & Turner, N. C. Advances and challenges in targeting FGFR signalling in cancer. *Nat. Rev. Cancer* **17**, 318–332 (2017).
74. Gez, E. *et al.* Efficacy of BGJ398, a Fibroblast Growth Factor Receptor 1–3 Inhibitor, in Patients with Previously Treated Advanced Urothelial Carcinoma with FGFR3 Alterations. *Cancer Discov.* **8**, 812–821 (2018).
75. Turner, N. & Grose, R. Fibroblast growth factor signalling: From development to cancer. *Nature Reviews Cancer* **10**, 116–129 (2010).
76. Holzmann, K. *et al.* Alternative splicing of fibroblast growth factor receptor IgIII loops in cancer. *Journal of Nucleic Acids* **2012**, (2012).
77. Pandith, A. A., Shah, Z. A. & Siddiqi, M. A. Oncogenic role of fibroblast growth factor receptor 3 in tumorigenesis of urinary bladder cancer. *Urol. Oncol.* **31**, 398–406 (2013).
78. Iyer, G. & Milowsky, M. I. Fibroblast growth factor receptor-3 in urothelial tumorigenesis. *Urologic Oncology: Seminars and Original Investigations* **31**, 303–311 (2013).
79. Ahmad, I., Iwata, T. & Leung, H. Y. Mechanisms of FGFR-mediated carcinogenesis. *Biochim. Biophys. Acta - Mol. Cell Res.* **1823**, 850–860 (2012).
80. Bryant, D. M. & Stow, J. L. Nuclear translocation of cell-surface receptors: Lessons from fibroblast growth factor. *Traffic* **6**, 947–954 (2005).
81. Latko, M. *et al.* Cross-Talk between Fibroblast Growth Factor Receptors and Other Cell Surface Proteins. *Cells* **8**, 455 (2019).
82. Tiong, K. H., Mah, L. Y. & Leong, C.-O. Functional roles of fibroblast growth factor receptors (FGFRs) signaling in human cancers. *Apoptosis* **18**, 1447–68 (2013).
83. Chen, L. A Ser365-Cys mutation of fibroblast growth factor receptor 3 in mouse downregulates Ihh/PTHrP signals and causes severe achondroplasia. *Hum. Mol. Genet.* **10**, 457–465 (2001).

BIBLIOGRAPHY

84. Colvin, J. S., Bohne, B. A., Harding, G. W., McEwen, D. G. & Ornitz, D. M. Skeletal overgrowth and deafness in mice lacking fibroblast growth factor receptor 3. *Nat. Genet.* **12**, 390–397 (1996).
85. Foldynova-Trantirkova, S., Wilcox, W. R. & Krejci, P. Sixteen years and counting: The current understanding of fibroblast growth factor receptor 3 (FGFR3) signaling in skeletal dysplasias. *Human Mutation* **33**, 29–41 (2012).
86. Chesi, M. *et al.* Frequent translocation t(4;14)(p16.3;q32.3) in multiple myeloma is associated with increased expression and activating mutations of fibroblast growth factor receptor 3. *Nat. Genet.* **16**, 260–264 (1997).
87. Chesi, M. *et al.* Activated fibroblast growth factor receptor 3 is an oncogene that contributes to tumor progression in multiple myeloma. *Blood* **97**, 729–36 (2001).
88. Hafner, C. *et al.* Oncogenic PIK3CA mutations occur in epidermal nevi and seborrhic keratoses with a characteristic mutation pattern. *Proc. Natl. Acad. Sci. U. S. A.* **104**, 13450–13454 (2007).
89. Logié, A. *et al.* Activating mutations of the tyrosine kinase receptor FGFR3 are associated with benign skin tumors in mice and humans. *Hum. Mol. Genet.* **14**, 1153–1160 (2005).
90. van Rhijn, B. W. G. *et al.* Novel fibroblast growth factor receptor 3 (FGFR3) mutations in bladder cancer previously identified in non-lethal skeletal disorders. *Eur. J. Hum. Genet.* **10**, 819–24 (2002).
91. Neuzillet, Y. *et al.* A meta-analysis of the relationship between FGFR3 and TP53 mutations in bladder cancer. *PLoS One* **7**, e48993 (2012).
92. Shi, M. J. *et al.* APOBEC-mediated Mutagenesis as a Likely Cause of FGFR3 S249C Mutation Over-representation in Bladder Cancer. *Eur. Urol.* **76**, 9–13 (2019).
93. Tomlinson, D., Baldo, O., Harnden, P. & Knowles, M. FGFR3 protein expression and its relationship to mutation status and prognostic variables in bladder cancer. *J. Pathol.* **213**, 91–98 (2007).
94. Williams, S. V., Hurst, C. D. & Knowles, M. A. Oncogenic FGFR3 gene fusions in bladder cancer. *Hum. Mol. Genet.* **22**, 795–803 (2013).
95. Knowles, M. A. Role of FGFR3 in urothelial cell carcinoma: Biomarker and potential therapeutic target. *World Journal of Urology* **25**, 581–593 (2007).
96. Bernard-Pierrot, I. *et al.* Oncogenic properties of the mutated forms of fibroblast growth factor receptor 3b. *Carcinogenesis* **27**, 740–747 (2006).
97. Nakanishi, Y. *et al.* Mechanism of Oncogenic Signal Activation by the Novel Fusion Kinase FGFR3-BAIAP2L1. *Mol. Cancer Ther.* **14**, 704–712 (2015).
98. Tomlinson, D. C., Hurst, C. D. & Knowles, M. A. Knockdown by shRNA identifies S249C mutant FGFR3 as a potential therapeutic target in bladder cancer. *Oncogene* **26**, 5889–99 (2007).
99. Wu, Y.-M. *et al.* Identification of targetable FGFR gene fusions in diverse cancers. *Cancer Discov.* **3**, 636–47 (2013).
100. Goebell, P. J. & Knowles, M. A. Bladder cancer or bladder cancers? Genetically distinct malignant conditions of the urothelium. *Urol. Oncol.* **28**, 409–28
101. Foth, M. *et al.* Fibroblast growth factor receptor 3 activation plays a causative role in urothelial cancer pathogenesis in cooperation with Pten loss in mice. *J. Pathol.* **233**, 148–58 (2014).
102. Zhou, H. *et al.* FGFR3b extracellular loop mutation lacks tumorigenicity in vivo but collaborates with p53/pRB deficiency to induce high-grade papillary urothelial carcinoma. *Sci. Rep.* **6**, (2016).
103. Foth, M. *et al.* FGFR3 mutation increases bladder tumourigenesis by suppressing acute inflammation. *J. Pathol.* **246**, 331–343 (2018).
104. Hahn, N. M. *et al.* A Phase II Trial of Dovitinib in BCG-Unresponsive Urothelial Carcinoma with FGFR3 Mutations or Overexpression: Hoosier Cancer Research Network Trial HCRN 12-157. *Clin. Cancer Res.* **23**, 3003–3011 (2017).
105. Collin, M.-P. *et al.* Discovery of Rogaratinib (BAY 1163877): a pan-FGFR Inhibitor. *ChemMedChem* **13**, 437–445 (2018).
106. Nogova, L. *et al.* Evaluation of BGJ398, a Fibroblast growth factor receptor 1-3 kinase inhibitor, in patients with advanced solid tumors harboring genetic alterations in fibroblast growth factor receptors: Results of a global phase I, dose-escalation and dose-expansion study. *J. Clin. Oncol.* **35**, 157–165 (2017).
107. Pal, S. K. *et al.* Efficacy of BGJ398, a Fibroblast Growth Factor Receptor 1–3 Inhibitor, in Patients with Previously Treated Advanced Urothelial Carcinoma with FGFR3 Alterations. *Cancer Discov.* **8**, 812–821 (2018).

BIBLIOGRAPHY

108. Siefker-Radtke, A. O. A phase 2 study of JNJ-42756493, a pan-FGFR tyrosine kinase inhibitor, in patients (pts) with metastatic or unresectable urothelial cancer (UC) harboring FGFR gene alterations. *J. Clin. Oncol.* (2016).
109. Martínez-Torrecuadrada, J. *et al.* Targeting the extracellular domain of fibroblast growth factor receptor 3 with human single-chain Fv antibodies inhibits bladder carcinoma cell line proliferation. *Clin. Cancer Res.* **11**, 6280–90 (2005).
110. Qing, J. *et al.* Antibody-based targeting of FGFR3 in bladder carcinoma and t(4;14)-positive multiple myeloma in mice. *J. Clin. Invest.* **119**, 1216–1229 (2009).
111. Trudel, S. *et al.* The inhibitory anti-FGFR3 antibody, PRO-001, is cytotoxic to t(4;14) multiple myeloma cells. *Blood* **107**, 4039–46 (2006).
112. Necchi, A. *et al.* Fierce-21: Phase II study of vofatmab (B-701), a selective inhibitor of FGFR3, as salvage therapy in metastatic urothelial carcinoma (mUC). *J. Clin. Oncol.* **37**, 409–409 (2019).
113. Chell, V. *et al.* Tumour cell responses to new fibroblast growth factor receptor tyrosine kinase inhibitors and identification of a gatekeeper mutation in FGFR3 as a mechanism of acquired resistance. *Oncogene* **32**, 3059–3070 (2013).
114. Herrera-Abreu, M. T. *et al.* Parallel RNA interference screens identify EGFR activation as an escape mechanism in FGFR3-mutant cancer. *Cancer Discov.* **3**, 1058–1071 (2013).
115. Touat, M., Ileana, E., Postel-Vinay, S., André, F. & Soria, J. C. Targeting FGFR signaling in cancer. *Clin. Cancer Res.* **21**, (2015).
116. Wang, J. *et al.* Ligand-associated ERBB2/3 activation confers acquired resistance to FGFR inhibition in FGFR3-dependent cancer cells. *Oncogene* **34**, 2167–2177 (2015).
117. Wang, L. *et al.* A Functional Genetic Screen Identifies the Phosphoinositide 3-kinase Pathway as a Determinant of Resistance to Fibroblast Growth Factor Receptor Inhibitors in FGFR Mutant Urothelial Cell Carcinoma [Figure presented]. *Eur. Urol.* **71**, 858–862 (2017).
118. Marcel, V. *et al.* Biological functions of p53 isoforms through evolution: Lessons from animal and cellular models. *Cell Death and Differentiation* **18**, 1815–1824 (2011).
119. Westfall, M. D. & Pietsenpol, J. A. p63: Molecular complexity in development and cancer. *Carcinogenesis* **25**, 857–64 (2004).
120. Gonfloni, S., Caputo, V. & Iannizzotto, V. P63 in health and cancer. *Int. J. Dev. Biol.* **59**, 87–93 (2015).
121. Chen, Y. *et al.* A double dealing tale of p63: an oncogene or a tumor suppressor. *Cellular and Molecular Life Sciences* **75**, 965–973 (2018).
122. Bergholz, J. & Xiao, Z. X. Role of p63 in development, tumorigenesis and cancer progression. *Cancer Microenviron.* **5**, 311–322 (2012).
123. Sethi, I. *et al.* A global analysis of the complex landscape of isoforms and regulatory networks of p63 in human cells and tissues. *BMC Genomics* **16**, (2015).
124. Pignon, J. C. *et al.* P63-expressing cells are the stem cells of developing prostate, bladder, and colorectal epithelia. *Proc. Natl. Acad. Sci. U. S. A.* **110**, 8105–8110 (2013).
125. Mills, A. A. *et al.* p63 is a p53 homologue required for limb and epidermal morphogenesis. *Nature* **398**, 708–13 (1999).
126. Romano, R. A. *et al.* ΔNp63 knockout mice reveal its indispensable role as a master regulator of epithelial development and differentiation. *Development* **139**, 772–782 (2012).
127. Yang, A. *et al.* p63 is essential for regenerative proliferation in limb, craniofacial and epithelial development. *Nature* **398**, 714–8 (1999).
128. Browne, G. *et al.* Differential altered stability and transcriptional activity of ΔNp63 mutants in distinct ectodermal dysplasias. *J. Cell Sci.* **124**, 2200–2207 (2011).
129. Karni-Schmidt, O. *et al.* Distinct expression profiles of p63 variants during urothelial development and bladder cancer progression. *Am. J. Pathol.* **178**, 1350–1360 (2011).
130. Carroll, D. K. *et al.* p63 regulates an adhesion programme and cell survival in epithelial cells. *Nat. Cell Biol.* **8**, 551–61 (2006).
131. Carroll, D. K., Brugge, J. S. & Attardi, L. D. p63, cell adhesion and survival. *Cell Cycle* **6**, 255–61 (2007).
132. Su, X. *et al.* TAp63 Prevents Premature Aging by Promoting Adult Stem Cell Maintenance. *Cell Stem Cell* **5**, 64–75 (2009).
133. Deutsch, G. B. *et al.* DNA damage in oocytes induces a switch of the quality control factor TAp63α from dimer to tetramer. *Cell* **144**, 566–576 (2011).
134. Rouleau, M. *et al.* TAp63 is important for cardiac differentiation of embryonic stem cells and heart development. *Stem Cells* **29**, 1672–1683 (2011).
135. Suh, E. K. *et al.* p63 protects the female germ line during meiotic arrest. *Nature* **444**, 624–628

BIBLIOGRAPHY

- (2006).
136. Su, X. *et al.* TAp63 is a master transcriptional regulator of lipid and glucose metabolism. *Cell Metab.* **16**, 511–525 (2012).
 137. Hagiwara, K., McMenemy, M., Miura, K. & Harris, C. Mutational analysis of the p63/p73L/p51/p40/CUSP/KET gene in human cancer cell lines using intronic primers. - PubMed - NCBI. *Cancer Res.* 4165–4169 (1999).
 138. Graziano, V. & De Laurenzi, V. Role of p63 in cancer development. *Biochimica et Biophysica Acta - Reviews on Cancer* **1816**, 57–66 (2011).
 139. He, Y. *et al.* Impaired delta Np63 expression is associated with poor tumor development in transitional cell carcinoma of the bladder. *J. Korean Med. Sci.* **23**, 825–832 (2008).
 140. Li, C. *et al.* Pin1 modulates p63 α protein stability in regulation of cell survival, proliferation and tumor formation. *Cell Death Dis.* **4**, (2013).
 141. Sen, T. *et al.* Δ Np63 α confers tumor cell resistance to cisplatin through the AKT1 transcriptional regulation. *Cancer Res.* **71**, 1167–1176 (2011).
 142. Hu, L. *et al.* Δ Np63 α is a common inhibitory target in oncogenic PI3K/Ras/Her2-induced cell motility and tumor metastasis. *Proc. Natl. Acad. Sci. U. S. A.* **114**, E3964–E3973 (2017).
 143. Tran, M. N. *et al.* The p63 protein isoform Δ Np63 α inhibits epithelial-mesenchymal transition in human bladder cancer cells: Role of miR-205. *J. Biol. Chem.* **288**, 3275–3288 (2013).
 144. Wu, J. *et al.* Δ Np63 α activates CD82 metastasis suppressor to inhibit cancer cell invasion. *Cell Death Dis.* **5**, (2014).
 145. Yoshida, T. *et al.* Dynamic Change in p63 Protein Expression during Implantation of Urothelial Cancer Clusters. *Neoplasia* **17**, 574–585 (2015).
 146. Caron de Fromental, C., Aberdam, E. & Aberdam, D. [The two faces of p63, Janus of the p53 gene family]. *Med. Sci. (Paris)*. **28**, 381–7 (2012).
 147. Cheng, W. *et al.* Δ Np63 plays an anti-apoptotic role in ventral bladder development. *Development* **133**, 4783–4792 (2006).
 148. Compérat, E. *et al.* Immunohistochemical expression of p63, p53 and MIB-1 in urinary bladder carcinoma. A tissue microarray study of 158 cases. *Virchows Arch.* **448**, 319–24 (2006).
 149. Fukushima, H. *et al.* Loss of Δ Np63 α promotes invasion of urothelial carcinomas via N-cadherin/Src homology and collagen/extracellular signal-regulated kinase pathway. *Cancer Res.* **69**, 9263–9270 (2009).
 150. Koga, F. *et al.* Impaired Δ Np63 expression associates with reduced β -catenin and aggressive phenotypes of urothelial neoplasms. *Br. J. Cancer* **88**, 740–747 (2003).
 151. Koga, F. *et al.* Impaired p63 expression associates with poor prognosis and uroplakin III expression in invasive urothelial carcinoma of the bladder. *Clin. Cancer Res.* **9**, 5501–7 (2003).
 152. Papadimitriou, M. A. *et al.* Δ Np63 transcript loss in bladder cancer constitutes an independent molecular predictor of TaT1 patients post-treatment relapse and progression. *J. Cancer Res. Clin. Oncol.* **145**, 3075–3087 (2019).
 153. Choi, W. *et al.* p63 expression defines a lethal subset of muscle-invasive bladder cancers. *PLoS One* **7**, (2012).
 154. Earl, J. *et al.* The UBC-40 Urothelial Bladder Cancer cell line index: a genomic resource for functional studies. *BMC Genomics* **16**, 403 (2015).
 155. Nickerson, M. L. *et al.* Molecular analysis of urothelial cancer cell lines for modeling tumor biology and drug response. *Oncogene* **36**, 35–46 (2017).
 156. Zuiverloon, T. C. M., De Jong, F. C., Costello, J. C. & Theodorescu, D. Systematic Review: Characteristics and Preclinical Uses of Bladder Cancer Cell Lines. *Bladder Cancer* **4**, 169–183 (2018).
 157. Mullenders, J. *et al.* Mouse and human urothelial cancer organoids: A tool for bladder cancer research. *Proc. Natl. Acad. Sci. U. S. A.* **116**, 4567–4574 (2019).
 158. Meyers, R. M. *et al.* Computational correction of copy number effect improves specificity of CRISPR-Cas9 essentiality screens in cancer cells. *Nat. Genet.* **49**, 1779–1784 (2017).
 159. Lamont, F. R. *et al.* Small molecule FGF receptor inhibitors block FGFR-dependent urothelial carcinoma growth in vitro and in vivo. *Br. J. Cancer* **104**, 75–82 (2011).
 160. McDonald, E. R. *et al.* Project DRIVE: A Compendium of Cancer Dependencies and Synthetic Lethal Relationships Uncovered by Large-Scale, Deep RNAi Screening. *Cell* **170**, 577–592.e10 (2017).
 161. Gengenbacher, N., Singhal, M. & Augustin, H. G. Preclinical mouse solid tumour models: Status quo, challenges and perspectives. *Nature Reviews Cancer* **17**, 751–765 (2017).
 162. Lorenzatti Hiles, G. *et al.* A surgical orthotopic approach for studying the invasive progression of human bladder cancer. *Nat. Protoc.* **14**, 738–755 (2019).

BIBLIOGRAPHY

163. Zhang, Z. *et al.* The therapeutic potential of SA-sCD40L in the orthotopic model of superficial bladder cancer. *Acta Oncol. (Madr)*. **50**, 1111–1118 (2011).
164. Cirone, P., Andresen, C. J., Eswaraka, J. R., Lappin, P. B. & Bagi, C. M. Patient-derived xenografts reveal limits to PI3K/mTOR- and MEK-mediated inhibition of bladder cancer. *Cancer Chemother. Pharmacol.* **73**, 525–38 (2014).
165. Inoue, T., Terada, N., Kobayashi, T. & Ogawa, O. Patient-derived xenografts as in vivo models for research in urological malignancies. *Nat. Rev. Urol.* **14**, 267–283 (2017).
166. John, B. A. & Said, N. Insights from animal models of bladder cancer: Recent advances, challenges, and opportunities. *Oncotarget* **8**, 57766–57781 (2017).
167. Kovnat, A. *et al.* Malignant properties of sublines selected from a human bladder cancer cell line that contains an activated c-Ha-ras oncogene. *Cancer Res.* **48**, 4993–5000 (1988).
168. Liu, Y.-R., Lee, Y.-F., Yin, P.-N. & Messing, E. MP65-18 BLADDER CANCER EXTRACELLULAR VESICLES FACILITATE METASTASIS. *J. Urol.* **199**, (2018).
169. Nicholson, B. E. *et al.* Profiling the evolution of human metastatic bladder cancer. *Cancer Res.* **64**, 7813–7821 (2004).
170. Said, N., Smith, S., Sanchez-Carbayo, M. & Theodorescu, D. Tumor endothelin-1 enhances metastatic colonization of the lung in mouse xenograft models of bladder cancer. *J. Clin. Invest.* **121**, 132–147 (2011).
171. Cohen, S. M. Promotion in urinary bladder carcinogenesis. *Environ. Health Perspect.* **50**, 51–59 (1983).
172. Fantini, D. *et al.* A Carcinogen-induced mouse model recapitulates the molecular alterations of human muscle invasive bladder cancer. *Oncogene* **37**, 1911–1925 (2018).
173. Vasconcelos-Nóbrega, C., Colaço, A., Lopes, C. & Oliveira, P. A. BBN as an urothelial carcinogen. *In Vivo* **26**, 727–739 (2012).
174. Dunois-Lardé, C., Levrel, O., Brams, A., Thiery, J. P. & Radvanyi, F. Absence of FGFR3 mutations in urinary bladder tumours of rats and mice treated with N-butyl-N-(4-hydroxybutyl)nitrosamine. *Mol. Carcinog.* **42**, 142–149 (2005).
175. Marjou, A. E. Involvement of epidermal growth factor receptor in chemically induced mouse bladder tumour progression. *Carcinogenesis* **21**, 2211–2218 (2000).
176. Saito, R. *et al.* Molecular Subtype-Specific Immunocompetent Models of High-Grade Urothelial Carcinoma Reveal Differential Neoantigen Expression and Response to Immunotherapy. *Cancer Res.* **78**, 3954–3968 (2018).
177. Williams, P. D., Lee, J. K. & Theodorescu, D. Molecular credentialing of rodent bladder carcinogenesis models. *Neoplasia* **10**, 838–846 (2008).
178. Ahmad, I. *et al.* Ras mutation cooperates with β -catenin activation to drive bladder tumorigenesis. *Cell Death Dis.* **2**, (2011).
179. Ahmad, I. *et al.* K-Ras and β -catenin mutations cooperate with Fgfr3 mutations in mice to promote tumorigenesis in the skin and lung, but not in the bladder. *DMM Dis. Model. Mech.* **4**, 548–555 (2011).
180. Ahmad, I. *et al.* β -Catenin activation synergizes with PTEN loss to cause bladder cancer formation. *Oncogene* **30**, 178–89 (2011).
181. Cheng, J. *et al.* Overexpression of epidermal growth factor receptor in urothelium elicits urothelial hyperplasia and promotes bladder tumor growth. *Cancer Res.* **62**, 4157–63 (2002).
182. F., H. *et al.* Deficiency of pRb family proteins and p53 in invasive urothelial tumorigenesis. *Cancer Res.* **69**, 9413–9421 (2009).
183. Zhang, Z. T. *et al.* Role of Ha-ras activation in superficial papillary pathway of urothelial tumor formation. *Oncogene* **20**, 1973–1980 (2001).
184. Prahallad, A. & Bernards, R. Opportunities and challenges provided by crosstalk between signalling pathways in cancer. *Oncogene* **35**, 1073–1079 (2016).
185. Huynh-Thu, V. A., Irrthum, A., Wehenkel, L. & Geurts, P. Inferring regulatory networks from expression data using tree-based methods. *PLoS One* **5**, (2010).
186. Liu, Z.-P. Reverse Engineering of Genome-wide Gene Regulatory Networks from Gene Expression Data. *Curr. Genomics* **16**, 3–22 (2015).
187. Bansal, M., Belcastro, V., Ambesi-Impiombato, A. & Di Bernardo, D. How to infer gene networks from expression profiles. *Mol. Syst. Biol.* **3**, (2007).
188. Emmert-Streib, F., Glazko, G. V., Altay, G. & Simoes, R. de M. Statistical inference and reverse engineering of gene regulatory networks from observational expression data. *Frontiers in Genetics* **3**, (2012).
189. Delgado, F. M. & Gómez-Vela, F. Computational methods for Gene Regulatory Networks reconstruction and analysis: A review. *Artificial Intelligence in Medicine* **95**, 133–145 (2019).

BIBLIOGRAPHY

190. de Matos Simoes, R. & Emmert-Streib, F. Influence of statistical estimators of mutual information and data heterogeneity on the inference of gene regulatory networks. *PLoS One* **6**, e29279 (2011).
191. Hecker, M., Lambeck, S., Toepfer, S., van Someren, E. & Guthke, R. Gene regulatory network inference: Data integration in dynamic models-A review. *BioSystems* **96**, 86–103 (2009).
192. De Jong, H. Modeling and simulation of genetic regulatory systems: A literature review. *J. Comput. Biol.* **9**, 67–103 (2002).
193. Karlebach, G. & Shamir, R. Modelling and analysis of gene regulatory networks. (2008). doi:10.1038/nrm2503
194. Liu, E., Li, L. & Cheng, L. Gene Regulatory Network Review. in *Encyclopedia of Bioinformatics and Computational Biology* 155–164 (Elsevier, 2019). doi:10.1016/b978-0-12-809633-8.20218-5
195. Lee, W. P. & Tzou, W. S. Computational methods for discovering gene networks from expression data. *Briefings in Bioinformatics* **10**, 408–423 (2009).
196. Linde, J., Schulze, S., Henkel, S. G. & Guthke, R. Data- and knowledge-based modeling of gene regulatory networks: An update. *EXCLI J.* **14**, 346–378 (2015).
197. Margolin, A. A. & Califano, A. Theory and limitations of genetic network inference from microarray data. in *Annals of the New York Academy of Sciences* **1115**, 51–72 (Blackwell Publishing Inc., 2007).
198. Maetschke, S. R., Madhamshettiwar, P. B., Davis, M. J. & Ragan, M. A. Supervised, semi-supervised and unsupervised inference of gene regulatory networks. *Brief. Bioinform.* **15**, 195–211 (2014).
199. Sima, C., Hua, J. & Jung, S. Inference of Gene Regulatory Networks Using Time-Series Data: A Survey. *Curr. Genomics* **10**, 416–429 (2009).
200. Margolin, A. A. *et al.* ARACNE: An algorithm for the reconstruction of gene regulatory networks in a mammalian cellular context. *BMC Bioinformatics* **7**, (2006).
201. Madar, A., Greenfield, A., Vanden-Eijnden, E. & Bonneau, R. DREAM3: Network inference using dynamic context likelihood of relatedness and the inferelator. *PLoS One* **5**, e9803 (2010).
202. Meyer, P. E., Kontos, K., Lafitte, F. & Bontempi, G. Information-theoretic inference of large transcriptional regulatory networks. *Eurasip J. Bioinforma. Syst. Biol.* **2007**, (2007).
203. Kulasiri, D. & He, Y. *Computational Systems Biology of Synaptic Plasticity. BSI Graduate School* **10**, (WORLD SCIENTIFIC (EUROPE), 2017).
204. Li, F., Long, T., Lu, Y., Ouyang, Q. & Tang, C. The yeast cell-cycle network is robustly designed. *Proc. Natl. Acad. Sci. U. S. A.* **101**, 4781–4786 (2004).
205. Alonso, A. M., Corvi, M. M. & Diambra, L. Gene target discovery with network analysis in *Toxoplasma gondii*. *Sci. Rep.* **9**, (2019).
206. De Magalhães, J. P. & Toussaint, O. How bioinformatics can help reverse engineer human aging. *Ageing Research Reviews* **3**, 125–141 (2004).
207. Iadevaia, S., Lu, Y., Morales, F. C., Mills, G. B. & Ram, P. T. Identification of optimal drug combinations targeting cellular networks: Integrating phospho-proteomics and computational network analysis. *Cancer Res.* **70**, 6704–6714 (2010).
208. Saez-Rodriguez, J. *et al.* Comparing signaling networks between normal and transformed hepatocytes using discrete logical models. *Cancer Res.* **71**, 5400–11 (2011).
209. Yeang, C.-H. & Vingron, M. A joint model of regulatory and metabolic networks. *BMC Bioinformatics* **7**, 332 (2006).
210. Wagner, J. P. *et al.* Receptor tyrosine kinases fall into distinct classes based on their inferred signaling networks. *Sci. Signal.* **6**, (2013).
211. Osmanbeyoglu, H. U., Toska, E., Chan, C., Baselga, J. & Leslie, C. S. Pancancer modelling predicts the context-specific impact of somatic mutations on transcriptional programs. *Nat. Commun.* **8**, 14249 (2017).
212. Fletcher, M. N. C. *et al.* Master regulators of FGFR2 signalling and breast cancer risk. *Nat. Commun.* **4**, 2464 (2013).
213. Galatro, T. F. *et al.* Transcriptomic analysis of purified human cortical microglia reveals age-associated changes. *Nat. Neurosci.* **20**, 1162–1171 (2017).
214. Lefebvre, C. *et al.* A human B-cell interactome identifies MYB and FOXM1 as master regulators of proliferation in germinal centers. *Mol. Syst. Biol.* **6**, (2010).
215. Nasser, S., Cunliffe, H. E., Black, M. A. & Kim, S. Context-specific gene regulatory networks subdivide intrinsic subtypes of breast cancer. *BMC Bioinformatics* **12**, S3 (2011).
216. Trébulle, P., Nicaud, J. M., Leplat, C. & Elati, M. Inference and interrogation of a coregulatory network in the context of lipid accumulation in *Yarrowia lipolytica*. *npj Syst. Biol. Appl.* **3**,

BIBLIOGRAPHY

- (2017).
217. Carter, S. L., Brechbühler, C. M., Griffin, M. & Bond, A. T. Gene co-expression network topology provides a framework for molecular characterization of cellular state. *Bioinformatics* **20**, 2242–50 (2004).
 218. Langfelder, P. & Horvath, S. WGCNA: An R package for weighted correlation network analysis. *BMC Bioinformatics* **9**, (2008).
 219. Giorgi, F. M. *et al.* Inferring Protein Modulation from Gene Expression Data Using Conditional Mutual Information. *PLoS One* **9**, e109569 (2014).
 220. Wang, K. *et al.* Genome-wide identification of post-translational modulators of transcription factor activity in human B cells. *Nat. Biotechnol.* **27**, 829–837 (2009).
 221. Marbach, D. *et al.* Wisdom of crowds for robust gene network inference. *Nat. Methods* **9**, 796–804 (2012).
 222. Reiter, F., Wienerroither, S. & Stark, A. Combinatorial function of transcription factors and cofactors. *Current Opinion in Genetics and Development* **43**, 73–81 (2017).
 223. Wilkinson, A. C., Nakauchi, H. & Göttgens, B. Mammalian Transcription Factor Networks: Recent Advances in Interrogating Biological Complexity. *Cell Systems* **5**, 319–331 (2017).
 224. Chebil, I., Nicolle, R., Santini, G., Rouveirol, C. & Elati, M. Hybrid method inference for the construction of cooperative regulatory network in human. *IEEE Trans. Nanobioscience* **13**, 97–103 (2014).
 225. Elati, M. *et al.* LICORN: Learning cooperative regulation networks from gene expression data. *Bioinformatics* **23**, 2407–2414 (2007).
 226. Nicolle, R., Radvanyi, F. & Elati, M. CoRegNet: Reconstruction and integrated analysis of co-regulatory networks. *Bioinformatics* **31**, 3066–3068 (2014).
 227. Damrauer, J. S. *et al.* Intrinsic subtypes of high-grade bladder cancer reflect the hallmarks of breast cancer biology. *Proc. Natl. Acad. Sci.* **111**, 3110–3115 (2014).
 228. Biton, A. *et al.* Independent Component Analysis Uncovers the Landscape of the Bladder Tumor Transcriptome and Reveals Insights into Luminal and Basal Subtypes. *Cell Rep.* **9**, 1235–1245 (2014).
 229. Becht, E. *et al.* Estimating the population abundance of tissue-infiltrating immune and stromal cell populations using gene expression. *Genome Biol.* **17**, 1–20 (2016).
 230. Robertson, A. G. *et al.* Comprehensive Molecular Characterization of Muscle-Invasive Bladder Cancer. *Cell* **171**, 540-556.e25 (2017).
 231. Hafner, C. *et al.* Mosaicism of activating FGFR3 mutations in human skin causes epidermal nevi. *J. Clin. Invest.* **116**, 2201–2207 (2006).
 232. Rosty, C. *et al.* Clinical and biological characteristics of cervical neoplasias with FGFR3 mutation. *Mol. Cancer* **4**, 2–9 (2005).
 233. Mahe, M. *et al.* An FGFR3/MYC positive feedback loop provides new opportunities for targeted therapies in bladder cancers. *EMBO Mol. Med.* **10**, pii: e8163 (2018).
 234. Singh, L. B. *et al.* K-Ras and -catenin mutations cooperate with Fgfr3 mutations in mice to promote tumorigenesis in the skin and lung, but not in the bladder. *Dis. Model. Mech.* **4**, 548–555 (2011).
 235. Kardos, J. *et al.* Claudin-low bladder tumors are immune infiltrated and actively immune suppressed. *JCI Insight* **1**, e85902 (2016).
 236. Sweis, R. F. *et al.* Molecular drivers of the non-T cell-inflamed tumor microenvironment in urothelial bladder cancer. *Cancer Immunol. Res.* **4**, 563–8 (2016).
 237. Flaherty, K. T. *et al.* Combined BRAF and MEK Inhibition in Melanoma with BRAF V600 Mutations. *N. Engl. J. Med.* **367**, 1694–1703 (2012).
 238. Hsu, J. W. *et al.* Decreased tumorigenesis and mortality from bladder cancer in mice lacking urothelial androgen receptor. *Am. J. Pathol.* **182**, 1811–1820 (2013).
 239. Li, P., Chen, J. & Miyamoto, H. Androgen receptor signaling in bladder cancer. *Cancers (Basel)* **9**, 1–14 (2017).
 240. Ide, H. *et al.* Androgen receptor signaling reduces radiosensitivity in bladder cancer. *Mol. Cancer Ther.* **17**, 1566–1574 (2018).
 241. Lin, J. H., Zhao, H. & Sun, T. T. A tissue-specific promoter that can drive a foreign gene to express in the suprabasal urothelial cells of transgenic mice. *PNAS* **92**, 679–683 (1995).
 242. Ramírez, A., Bravo, A., Jorcano, J. L. & Vidal, M. Sequences 5' of the bovine keratin 5 gene direct tissue- and cell-type-specific expression of a lacZ gene in the adult and during development. *Differentiation* **58**, 53–64 (1994).
 243. Guo, G. *et al.* Whole-genome and whole-exome sequencing of bladder cancer identifies frequent alterations in genes involved in sister chromatid cohesion and segregation. *Nat.*

BIBLIOGRAPHY

- Genet.* **45**, 1459–1463 (2013).
244. Kim, P. H. *et al.* Genomic predictors of survival in patients with high-grade urothelial carcinoma of the bladder. *Eur. Urol.* **67**, 198–201 (2015).
 245. Hänzelmann, S., Castelo, R. & Guinney, J. GSVA: gene set variation analysis for microarray and RNA-seq data. *BMC Bioinformatics* **14**, 1–15 (2013).
 246. Wu, S. C. *et al.* Androgen Suppression Therapy Is Associated with Lower Recurrence of Non-muscle-invasive Bladder Cancer. *Eur. Urol. Focus* (2019). doi:10.1016/j.euf.2019.04.021
 247. Joerger, M. *et al.* Rogaratinib treatment of patients with advanced urothelial carcinomas prescreened for tumor FGFR mRNA expression. *J. Clin. Oncol.* **36**, 494–494 (2018).
 248. Cappellen, D. *et al.* Frequent activating mutations of FGFR3 in human bladder and cervix carcinomas. *Nat. Genet.* **23**, 18–20 (1999).
 249. Lafitte, M. *et al.* FGFR3 has tumor suppressor properties in cells with epithelial phenotype. *Mol. Cancer* **12**, (2013).
 250. Naski, M. C., Wang, Q., Xu, J. & Ornitz, D. M. Graded activation of fibroblast growth factor receptor 3 by mutations causing achondroplasia and thanatophoric dysplasia. *Nat. Genet.* **13**, 233–237 (1996).
 251. Pearson, A. *et al.* Parallel RNA Interference Screens Identify EGFR Activation as an Escape Mechanism in FGFR3-Mutant Cancer. *Cancer Discov.* **3**, 1058–1071 (2013).
 252. Niederst, M. J. & Engelman, J. A. Bypass mechanisms of resistance to receptor tyrosine kinase inhibition in lung cancer. *Science Signaling* **6**, (2013).
 253. Meyers, R. M. *et al.* Computational correction of copy number effect improves specificity of CRISPR-Cas9 essentiality screens in cancer cells. *Nat. Genet.* **49**, 1779–1784 (2017).
 254. Palmbo, P. L. *et al.* ATDC/TRIM29 drives invasive bladder cancer formation through miRNA-mediated and epigenetic mechanisms. *Cancer Res.* **75**, 5155–5166 (2015).
 255. Trabelsi, N., Setti Boubaker, N., Said, R. & Ouerhani, S. Notch Pathway: Bioinformatic Analysis of Related Transcription Factors within Bladder Cancer Types and Subtypes. *IRBM* **39**, 261–267 (2018).
 256. Warrick, J. I. *et al.* FOXA1, GATA3 and PPAR γ Cooperate to drive luminal subtype in bladder cancer: A molecular analysis of established human cell lines. *Sci. Rep.* **6**, (2016).
 257. Zhang, X. *et al.* Somatic Superenhancer Duplications and Hotspot Mutations Lead to Oncogenic Activation of the KLF5 Transcription Factor. *Cancer Discov.* **8**, 108–125 (2018).
 258. Guo, C. C. *et al.* Dysregulation of EMT Drives the Progression to Clinically Aggressive Sarcomatoid Bladder Cancer. *Cell Rep.* **27**, 1781–1793.e4 (2019).
 259. Castro-Castro, A. *et al.* Cellular and Molecular Mechanisms of MT1-MMP-Dependent Cancer Cell Invasion. *Annu. Rev. Cell Dev. Biol.* **32**, 555–576 (2016).
 260. Lodillinsky, C. *et al.* p63/MT1-MMP axis is required for in situ to invasive transition in basal-like breast cancer. *Oncogene* **35**, 344–357 (2016).
 261. Hernández, S. *et al.* Prospective study of FGFR3 mutations as a prognostic factor in nonmuscle invasive urothelial bladder carcinomas. *J. Clin. Oncol.* **24**, 3664–3671 (2006).
 262. Bradner, J. E., Hnisz, D. & Young, R. A. Transcriptional Addiction in Cancer. *Cell* **168**, 629–643 (2017).
 263. Lee, T. I. & Young, R. A. Transcriptional regulation and its misregulation in disease. *Cell* **152**, 1237–1251 (2013).
 264. Gaya, J. M. *et al.* Δ p63 expression is a protective factor of progression in clinical high grade T1 bladder cancer. *J. Urol.* **193**, 1144–1150 (2015).
 265. Park, B. J. *et al.* Frequent alteration of p63 expression in human primary bladder carcinomas. *Cancer Res.* **60**, 3370–4 (2000).
 266. Barretina, J. *et al.* The Cancer Cell Line Encyclopedia enables predictive modelling of anticancer drug sensitivity. *Nature* **483**, 603–607 (2012).
 267. Delpuech, O. *et al.* Identification of pharmacodynamic transcript biomarkers in response to FGFR inhibition by AZD4547. *Mol. Cancer Ther.* **15**, 2802–2813 (2016).
 268. Lambert, S. A. *et al.* The Human Transcription Factors. *Cell* **172**, 650–665 (2018).
 269. Schmeier, S., Alam, T., Essack, M. & Bajic, V. B. TcoF-DB v2: Update of the database of human and mouse transcription co-factors and transcription factor interactions. *Nucleic Acids Res.* **45**, D145–D150 (2017).
 270. Schaefer, M. H. *et al.* Hippie: Integrating protein interaction networks with experiment based quality scores. *PLoS One* **7**, (2012).
 271. Franceschini, A. *et al.* STRING v9.1: Protein-protein interaction networks, with increased coverage and integration. *Nucleic Acids Res.* **41**, (2013).
 272. Keshava Prasad, T. S. *et al.* Human Protein Reference Database - 2009 update. *Nucleic Acids*

BIBLIOGRAPHY

- Res.* **37**, (2009).
273. Kou, Y. *et al.* ChEA2: Gene-set libraries from ChIP-X experiments to decode the transcription regulome. in *Lecture Notes in Computer Science (including subseries Lecture Notes in Artificial Intelligence and Lecture Notes in Bioinformatics)* **8127 LNCS**, 416–430 (2013).
 274. Kulakovskiy, I. V. *et al.* HOCOMOCO: Expansion and enhancement of the collection of transcription factor binding sites models. *Nucleic Acids Res.* **44**, D116–D125 (2016).
 275. Marbach, D. *et al.* Tissue-specific regulatory circuits reveal variable modular perturbations across complex diseases. *Nat. Methods* **13**, 366–370 (2016).
 276. Jiang, C., Xuan, Z., Zhao, F. & Zhang, M. Q. TRED: A transcriptional regulatory element database, new entries and other development. *Nucleic Acids Res.* **35**, (2007).
 277. Shannon, P. *et al.* Cytoscape: A software Environment for integrated models of biomolecular interaction networks. *Genome Res.* **13**, 2498–2504 (2003).
 278. Calderaro, J. *et al.* PI3K/AKT pathway activation in bladder carcinogenesis. *Int. J. Cancer* **134**, 1776–1784 (2014).
 279. Langmead, B. Aligning short sequencing reads with Bowtie. *Curr. Protoc. Bioinforma.* (2010). doi:10.1002/0471250953.bi1107s32
 280. Landt, S. G. *et al.* ChIP-seq guidelines and practices of the ENCODE and modENCODE consortia. *Genome Research* **22**, 1813–1831 (2012).
 281. Ritchie, M. E. *et al.* Limma powers differential expression analyses for RNA-sequencing and microarray studies. *Nucleic Acids Res.* **43**, e47 (2015).
 282. Rinaldetti, S. *et al.* FOXM1 predicts overall and disease specific survival in muscleinvasive urothelial carcinoma and presents a differential expression between bladder cancer subtypes. *Oncotarget* **8**, 47595–47606 (2017).
 283. Rinaldetti, S. *et al.* FOXM1 predicts disease progression in non-muscle invasive bladder cancer. *J. Cancer Res. Clin. Oncol.* **144**, 1701–1709 (2018).
 284. Okajima, E., Hiramatsu, T., Iriya, K., Ijuin, M. & Matsushima, S. Effects of sex hormones on development of urinary bladder tumours in rats induced by N-butyl-N-(4-hydroxybutyl) nitrosamine. *Urol. Res.* **3**, 73–9 (1975).

APPENDIX

An FGFR3/MYC positive feedback loop provides new opportunities for targeted therapies in bladder cancers

Mélanie Mahe^{1,2,†}, Florent Dufour^{1,2,†}, Hélène Neyret-Kahn^{1,2}, **Aura Moreno-Vega**^{1,2}, Claire Beraud³, Mingjun Shi^{1,2}, Imene Hamaidi⁴, Virginia Sanchez-Quiles^{1,2}, Clementine Krucker^{1,2}, Marion Dorland-Galliot^{1,2}, Elodie Chapeaublanc^{1,2}, Remy Nicolle^{1,2}, Hervé Lang⁴, Celio Pouponnot^{5,6,7}, Thierry Massfelder⁸, François Radvanyi^{1,2} & Isabelle Bernard-Pierrot^{1,2,*}

¹ Institut Curie, CNRS, UMR144, Equipe Labellisée Ligue contre le Cancer, PSL Research University, Paris, France

² CNRS, UMR144, Sorbonne Universités, UPMC Université Paris 06, Paris, France

³ UROLEAD SAS, School of Medicine, Strasbourg, France

⁴ Department of Urology, Nouvel Hôpital Civil, Hôpitaux Universitaires de Strasbourg, Strasbourg, France

⁵ Institut Curie, Orsay, France

⁶ CNRS UMR3347, Centre Universitaire, Orsay, France

⁷ INSERM U1021, Centre Universitaire, Orsay, France

⁸ INSERM UMR_S1113, Section of Cell Signalization and Communication in Kidney and Prostate Cancer, School of Medicine, Fédération de Médecine Translationnelle de Strasbourg (FMTS), INSERM and University of Strasbourg, Strasbourg, France

*Corresponding author.

Tel: +33 1 42 34 63 40; Fax: +33 1 42 34 63 49

E-mail: isabelle.bernard-pierrot@curie.fr

†These authors contributed equally to this work



An FGFR3/MYC positive feedback loop provides new opportunities for targeted therapies in bladder cancers

Mélanie Mahe^{1,2,†}, Florent Dufour^{1,2,†}, Hélène Neyret-Kahn^{1,2}, Aura Moreno-Vega^{1,2}, Claire Beraud³, Mingjun Shi^{1,2}, Imene Hamaidi⁴, Virginia Sanchez-Quiles^{1,2}, Clementine Krucker^{1,2}, Marion Dorland-Galliot^{1,2}, Elodie Chapeaublanc^{1,2}, Remy Nicolle^{1,2}, Hervé Lang⁴, Celio Pouponnot^{5,6,7}, Thierry Massfelder⁸, François Radvanyi^{1,2} & Isabelle Bernard-Pierrot^{1,2,*} 

Abstract

FGFR3 alterations (mutations or translocation) are among the most frequent genetic events in bladder carcinoma. They lead to an aberrant activation of FGFR3 signaling, conferring an oncogenic dependence, which we studied here. We discovered a positive feedback loop, in which the activation of p38 and AKT downstream from the altered FGFR3 upregulates MYC mRNA levels and stabilizes MYC protein, respectively, leading to the accumulation of MYC, which directly upregulates FGFR3 expression by binding to active enhancers upstream from FGFR3. Disruption of this FGFR3/MYC loop in bladder cancer cell lines by treatment with FGFR3, p38, AKT, or BET bromodomain inhibitors (JQ1) preventing MYC transcription decreased cell viability *in vitro* and tumor growth *in vivo*. A relevance of this loop to human bladder tumors was supported by the positive correlation between FGFR3 and MYC levels in tumors bearing FGFR3 mutations, and the decrease in FGFR3 and MYC levels following anti-FGFR treatment in a PDX model bearing an FGFR3 mutation. These findings open up new possibilities for the treatment of bladder tumors displaying aberrant FGFR3 activation.

Keywords BET inhibitors; bladder cancer; FGFR3; MYC; p38

Subject Categories Cancer; Urogenital System

DOI 10.15252/emmm.201708163 | Received 15 June 2017 | Revised 19 January 2018 | Accepted 23 January 2018 | Published online 20 February 2018

EMBO Mol Med (2018) 10: e8163

Introduction

Bladder cancer is the ninth most common cancer worldwide, with approximately 430,000 new cases diagnosed in 2012 and 165,000 deaths annually (Antoni *et al*, 2017). Non-muscle-invasive carcinomas (NMIBCs) account for 70% of cases at first diagnosis. These tumors often have a favorable prognosis following transurethral resection with or without intravesical chemotherapy or immunotherapy with Bacillus Calmette-Guérin (BCG). NMIBC often recurs (50–60% of cases) and sometimes progresses to a muscle-invasive tumor (5–40% progression, depending on clinical and pathological features). This high recurrence rate and the need for monitoring contribute to the economic burden of bladder cancer treatment. Muscle-invasive bladder carcinoma (MIBC) is a major clinical issue, because, even with radical cystectomy as the standard treatment, overall survival at 5 years is only about 50%, and the combination of this treatment with neoadjuvant and/or adjuvant chemotherapy increases overall survival only moderately. No major improvement in survival has been achieved over the last 20 years (Witjes *et al*, 2013). A clinical response to immune checkpoint inhibitors has recently been reported, but only a subset of patients respond to such treatment, and it remains unclear how to identify these patients (Powles *et al*, 2014; Bajorin *et al*, 2015; Bellmunt *et al*, 2017a,b; Davarpanah *et al*, 2017). Some targeted therapies have also yielded promising efficacy results. This is the case, for example, for mTOR inhibitors for patients with TSC1 mutations, anti-HER2 treatments for HER2-amplified MIBC, and anti-FGFR therapies for MIBC with activating FGFR mutations or translocations (Abbosh *et al*, 2015; Rouanne *et al*, 2016). The definition of

1 Institut Curie, CNRS, UMR144, Equipe Labellisée Ligue contre le Cancer, PSL Research University, Paris, France

2 CNRS, UMR144, Sorbonne Universités, UPMC Université Paris 06, Paris, France

3 UROLEAD SAS, School of Medicine, Strasbourg, France

4 Department of Urology, Nouvel Hôpital Civil, Hôpitaux Universitaires de Strasbourg, Strasbourg, France

5 Institut Curie, Orsay, France

6 CNRS UMR3347, Centre Universitaire, Orsay, France

7 INSERM U1021, Centre Universitaire, Orsay, France

8 INSERM UMR_S1113, Section of Cell Signaling and Communication in Kidney and Prostate Cancer, School of Medicine, Fédération de Médecine Translationnelle de Strasbourg (FMTS), INSERM and University of Strasbourg, Strasbourg, France

*Corresponding author. Tel: +33 1 42 34 63 40; Fax: +33 1 42 34 63 49; E-mail: isabelle.bernard-pierrot@curie.fr

†These authors contributed equally to this work

therapeutic strategies to improve treatment outcomes remains of the utmost importance.

FGFR3 (fibroblast growth factor receptor) belongs to a family of structurally related tyrosine kinase receptors (FGFR1-4). These receptors regulate various physiological processes, including proliferation, differentiation, migration, and apoptosis. There has been considerable interest in the FGFR family (FGFR1-4), as these receptors are frequently involved, through various mechanisms, in genetic disorders and cancer, leading to their identification as possible targets for treatment (Haugsten *et al*, 2010). *FGFR3* is frequently altered through activating mutations and translocations generating *FGFR3*-gene fusions (Billerey *et al*, 2001; Tcga, 2014). Mutations are, by far, the most frequent alterations of *FGFR3*, occurring in almost 50% of bladder tumors (70% of NMIBCs and 15–20% of MIBCs). The two most frequent mutations are the S249C and Y375C mutations, which affect the extracellular domain of the receptor. *FGFR3* translocations leading to the production of *FGFR3-TACC3* and *FGFR3-BAIAP2L1* fusion proteins were recently identified in 3% of MIBCs (Tcga, 2014). These alterations are thought to be “oncogenic drivers”, because the expression of an altered *FGFR3* induces cell transformation (Bernard-Pierrot *et al*, 2006; Williams *et al*, 2013; Wu *et al*, 2013; Nakanishi *et al*, 2015). Furthermore, several preclinical studies in cell lines and xenograft models of bladder cancer have shown that *FGFR3* alterations confer sensitivity to *FGFR* inhibitors, which have anti-proliferative and pro-apoptotic effects (Bernard-Pierrot *et al*, 2006; Wu *et al*, 2013; Nakanishi *et al*, 2015). Together, these findings highlight the critical role of *FGFR3* in bladder tumor carcinogenesis, raising the possibility of developing anti-*FGFR3* therapies for both NMIBC and MIBC (Chae *et al*, 2017). Promising results were recently reported for four out of the five patients with *FGFR3*-mutated bladder cancers enrolled in a phase I clinical trial of the pan-*FGFR* kinase inhibitor BGJ398 (Nogova *et al*, 2017). However, based on observations for other targeted therapies (EGFR, BRAF, KIT) for various cancers, including colon and lung cancers, melanoma, and gastrointestinal tumors, *FGFR3*-targeted therapies will probably turn out to be limited by multiple mechanisms of intrinsic and acquired resistance, such as ERBB2/3 or EGFR activation (Flaherty *et al*, 2012; Herrera-Abreu *et al*, 2013; Niederst & Engelman, 2013; Wang *et al*, 2015). The signaling pathway activated by mutated *FGFR3* and *FGFR3*-fusion proteins is not well characterized, particularly for bladder cancer. Improvements in our understanding of the molecular mechanisms underlying the oncogenic activity of activated *FGFR3* in bladder tumors may facilitate the identification of new drug targets that could be acted on together with *FGFR3*, to increase the efficacy of anti-*FGFR3* therapies and/or to prevent potential drug resistance. Such strategies, based on the simultaneous inhibition of two or more targets in a single pathway, have already been explored for many specific pairs of agents, in both clinical and preclinical studies (Flaherty *et al*, 2012; Li *et al*, 2014; Ran *et al*, 2015). In this study, we aimed to characterize the aberrantly activated *FGFR3* signaling pathways involved in bladder cancer cell growth/transformation. We studied genes regulated by constitutively activated *FGFR3* in two bladder tumor-derived cell lines, MGH-U3 and RT112, harboring an *FGFR3* mutation (Y375C) and a fusion gene (*FGFR3-TACC3*), respectively. We identified *MYC* as a key transcription factor that is overexpressed and activated in response to *FGFR3* activity, and critical for *FGFR3*-induced cell proliferation. We showed here that

FGFR3 is a direct target gene of *MYC*, which binds to active enhancers located upstream from *FGFR3*, establishing an *FGFR3/MYC* positive feedback loop. This loop may be relevant in human tumors, because *MYC* and *FGFR3* expression levels were found to be positively correlated in tumors bearing *FGFR3* mutations in two independent transcriptomic datasets ($n = 63$ and $n = 271$), and because *FGFR3* inhibition in a patient-derived tumor xenograft (PDX) model harboring an *FGFR3-S249C* mutation decreased the levels of both *MYC* and *FGFR3*. We found that *MYC* mRNA levels and protein stability were dependent on p38 and AKT activation, respectively, downstream from *FGFR3* activation. Finally, we showed, in xenograft models, that *FGFR3* activation conferred sensitivity to *FGFR3* and p38 inhibitors and to a BET bromodomain inhibitor (JQ1) preventing *MYC* transcription. These findings therefore suggest new treatment options for bladder cancers in which *FGFR3* is aberrantly activated.

Results

MYC is a key master regulator of proliferation in the aberrantly activated *FGFR3* pathway

We investigated the molecular mechanisms underlying the oncogenic activity of aberrantly activated *FGFR3* in bladder carcinomas, by studying the MGH-U3 and RT112 cell lines. These cell lines were derived from human bladder tumors, and they endogenously express a mutated activated form of *FGFR3* (*FGFR3-Y375C*, the second most frequent mutation in bladder tumors) and the *FGFR3-TACC3* fusion protein (the most frequent *FGFR3* fusion protein in bladder tumors), respectively. The growth and transformation of these cell lines are dependent on *FGFR3* activity (Bernard-Pierrot *et al*, 2006; Williams *et al*, 2013; Wu *et al*, 2013). We conducted a gene expression analysis with Affymetrix DNA arrays, in these cell lines, with and without *FGFR3* siRNA treatment. We identified 741 and 3,124 genes displaying significant differential expression after *FGFR3* depletion in MGH-U3 and RT112 cells, respectively (adjusted P -values < 0.05 , $|\log_2(\text{FC})| > 0.5$; Dataset EV1). An analysis of these two lists of *FGFR3*-regulated genes using the upstream regulator function of Ingenuity Pathway Analysis (IPA) software identified upstream regulators activated and inhibited by *FGFR3* (Fig 1A, left panel). The top 10 transcriptional regulators with activity modulated by *FGFR3* were common to the two cell lines and are listed in the right panel in Fig 1A. The transcription factor predicted to be the most strongly inhibited here after *FGFR3* depletion, in both cell lines, was the proto-oncogene *MYC*, for which mRNA levels were downregulated. This downregulation of *MYC* mRNA levels after *FGFR3* knockdown with siRNA was further confirmed by reverse transcription-quantitative polymerase chain reaction (RT-qPCR) (30–70% decrease, depending on the cell line used; Fig 1B). Consistent with these results suggesting that *MYC* mRNA levels are modulated by constitutively activated *FGFR3*, an analysis of previously described transcriptomic data for our CIT-series (“*Carte d’Identité des Tumeurs*”; tumor identity card) of bladder tumors revealed a significant upregulation of *MYC* mRNA levels in tumors harboring an *FGFR3* mutation ($n = 63$) relative to normal urothelium samples ($n = 4$), whereas no such overexpression was observed for tumors expressing wild-type *FGFR3* ($n = 122$; Fig 1C). Moreover, *MYC*

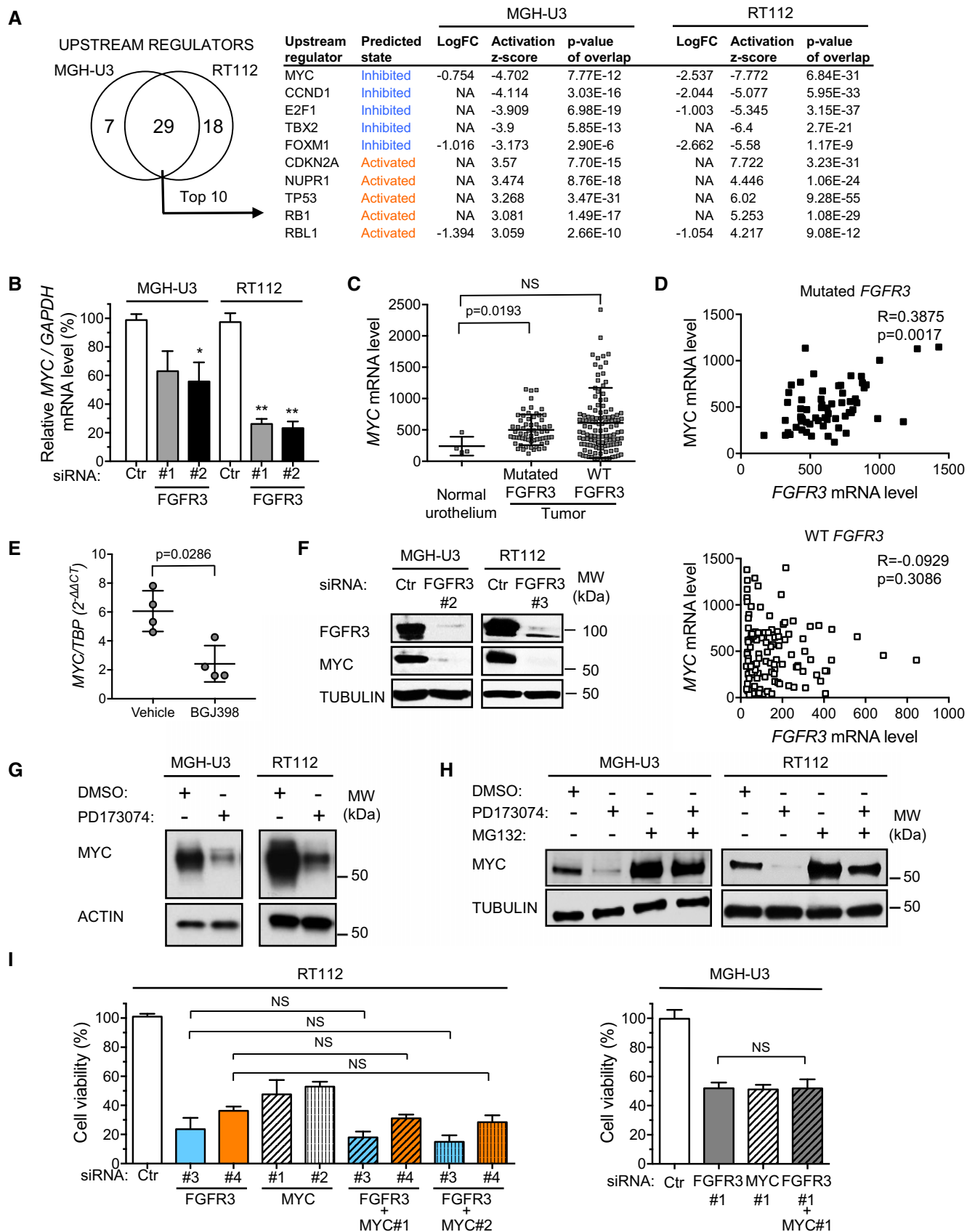


Figure 1.

Figure 1. MYC is a key upstream regulator activated by FGFR3 that is required for FGFR3-induced bladder cancer cell growth.

- A Venn diagram showing the number of upstream regulators (transcription factors) significantly predicted by Ingenuity Pathway Analysis to be involved in the regulation of gene expression observed after *FGFR3* knockdown in RT112 and MGH-U3 cells (left panel). List of the top 10 upstream regulators modulated by *FGFR3* expression in both cell lines. The Log_2FC of the transcription factor itself is also indicated. NA indicates that the FC was beyond the threshold defining genes as differentially expressed after *FGFR3* depletion (see Materials and Methods).
- B Relative *MYC* mRNA levels in MGH-U3 and RT112 cells transfected for 72 h with siRNAs targeting *FGFR3* or a control siRNA (Ctr). The results presented are the means of two independent experiments carried out in triplicate; the standard errors are indicated. The significance of differences was assessed in unpaired Student's *t*-tests, * $P < 0.05$; ** $0.001 < P < 0.005$.
- C *MYC* mRNA levels in normal human urothelium ($n = 4$) and in the CIT cohort of human bladder tumors bearing *FGFR3* mutations ($n = 63$) or wild-type *FGFR3* ($n = 122$). The significance of differences was assessed in Mann–Whitney tests, and means and standard errors are represented.
- D *MYC* and *FGFR3* mRNA levels in human bladder tumors harboring either mutated *FGFR3* (upper panel) or wild-type *FGFR3* (lower panel). Spearman's coefficient and *P*-values are indicated for the correlations between *MYC* and *FGFR3* mRNA levels in each group.
- E *MYC* mRNA levels in a PDX model bearing a *FGFR3*-S249C mutation and treated daily, for 4 days, with 30 mg/kg BGJ398, a pan-FGFR inhibitor, or with vehicle ($n = 4$ mice per group). Means and standard errors are represented. The significance of differences was assessed in Mann–Whitney tests.
- F Western blot (72 h after transfection) comparing *FGFR3* and *MYC* levels in MGH-U3 and RT112 cells transfected with a control siRNA (Ctr) or with siRNAs targeting *FGFR3*.
- G Western blot comparing *MYC* levels in MGH-U3 and RT112 cells, treated for 2 h with DMSO or the pan-FGFR inhibitor, PD173074 (500 nM).
- H Western blot comparing *MYC* levels in MGH-U3 and RT112 cells treated for 3 h with FGFR inhibitor (0.5 μM PD173074) or proteasome inhibitor (10 μM MG132), alone or in combination.
- I Cell viability assay comparing the impact of *MYC* and/or *FGFR3* downregulation on RT112 (left panel, CellTiter-Glo) and MGH-U3 (right panel, MTT assay) cell viability (72 h post-transfection). The results presented are the means of three independent experiments carried out in triplicate, error bars represent standard deviations. Tukey's multiple comparisons tests were performed to evaluate the significance of differences. The results of the statistical analysis are summarized in Dataset EV2.
- Source data are available online for this figure.

expression was positively correlated with *FGFR3* expression in bladder tumors harboring a mutated *FGFR3* (Fig 1D, upper panel), whereas no such correlation was observed in tumors bearing wild-type *FGFR3* ($n = 122$; Fig 1D, lower panel). Similar results were also observed for another publicly available transcriptomic dataset for 416 bladder tumors (271 with *FGFR3* mutations) and eight normal samples (Hedegaard *et al*, 2016; Appendix Fig S1A and B), suggesting that mutated *FGFR3* may also regulate *MYC* expression in human bladder carcinomas. Support for this hypothesis was provided by the significant decrease in *MYC* mRNA levels induced by 4 days of anti-FGFR treatment in tumors from a PDX model (F659) bearing an *FGFR3*-S249C mutation (Fig 1E). As in cell lines, *FGFR3*-S249C expression conferred *FGFR3* dependence on the PDX model, in which anti-FGFR treatment with BGJ398 decreased tumor growth by 60% after 29 days of administration (Appendix Fig S2).

MYC is a key regulator of proliferation and its deregulation can promote oncogenesis in various types of cancer (Dang, 2012). We therefore investigated the role of *MYC* as a master regulator of proliferation in bladder cell lines expressing aberrantly activated *FGFR3*. Western blot analysis further showed that *FGFR3* depletion resulted in the almost total loss of *MYC* from both MGH-U3 and RT112 cells (Fig 1F). The discrepancy between the decreases in *MYC* mRNA (Fig 1B) and protein levels (Fig 1F) suggested that the aberrant activation of *FGFR3* regulated *MYC* not only at mRNA level, but also through stabilization of the protein. This hypothesis was also supported by the time course of *MYC* expression on Western blots after the inhibition of *FGFR3* with PD173074. Indeed, *MYC* levels decreased rapidly, after 30 min of treatment, in MGH-U3 cells (Appendix Fig S3A), and expression was totally lost after 2 h of treatment, in both MGH-U3 and RT112 cells (Fig 1G and Appendix Fig S3A). *MYC* protein stability is, thus, tightly controlled by the proteasome. We therefore investigated the possible role of *FGFR3* in this process, by treating MGH-U3 and RT112 cells with a pan-FGFR inhibitor (PD173074), either alone or in combination with a proteasome inhibitor (MG132; Fig 1H). Western blot analysis showed that the downregulation of *MYC* induced by the

inhibition of *FGFR3* was abolished by MG132, in both cell lines. Overall, our results indicate that the inhibition of aberrantly activated *FGFR3* decreases *MYC* mRNA levels and favors proteolysis of the *MYC* protein by the proteasome, thereby decreasing its transcriptional activity. We then investigated the possible contribution of *MYC* to the oncogenic activity of aberrantly activated *FGFR3*. We compared the effects on viability of depleting *FGFR3* and *MYC* alone or together, with siRNA, in RT112 and MGH-U3 cells (Fig 1I). *FGFR3* and *MYC* siRNAs efficiently knocked down the levels of the targeted proteins (Appendix Fig S3B). The depletion of either *MYC* or *FGFR3* resulted in significantly lower cell viability than for cells treated with the control siRNA (Fig 1I, right and left panels and Dataset EV2 for the *P*-values). No significant additive effect relative to *FGFR3* depletion alone was observed in RT112 and MGH-U3 cells with a simultaneous knockdown of *FGFR3* and *MYC* expression, suggesting that *MYC* is a key downstream effector of the aberrantly activated *FGFR3* pathway mediating cell proliferation.

FGFR3 and MYC are involved in a positive feedback loop in which FGFR3 is a direct transcriptional target of MYC in bladder cancer cell lines with constitutively activated FGFR3

Surprisingly, we observed that the treatment of MGH-U3 and RT112 cells with a *MYC* siRNA strongly decreased *FGFR3* levels (Fig 2A). RT-qPCR showed that this loss of *FGFR3* expression was due to a decrease in *FGFR3* mRNA levels after *MYC* knockdown (Fig 2B). We investigated whether *FGFR3* was a direct transcriptional target of *MYC*, by analyzing *MYC* occupancy of the *FGFR3* locus by chromatin immunoprecipitation and quantitative PCR (ChIP-qPCR). Using the publicly available ENCODE data for three different cancer cell lines, we designed primers binding to two potential enhancers, the promoter and an intragenic region of *FGFR3* (Appendix Fig S4A). According to ENCODE data, the enrichment of *MYC* and activation marks (H3K27ac) in the E1 and E2 enhancers is correlated with the level of *FGFR3* transcription (Appendix Fig S4A). We

checked, by ChIP-qPCR, that the selected FGFR3 promoter and enhancers did harbor the expected histone activation marks (H3K27ac and H3K4me3) in RT112 cells (Appendix Fig S4B). Finally, we showed that the two *FGFR3* enhancer regions tested were enriched in *MYC*, consistent with the direct regulation of *FGFR3* expression by *MYC*, at the transcriptional level (Fig 2C). This regulation of *FGFR3* by *MYC* seemed to be quite specific to bladder cancer, because *MYC* binding to the *FGFR3* enhancers or promoter was rarely observed in a publicly available dataset encompassing 118 *MYC* chromatin immunoprecipitation and sequencing (ChIP-Seq) in different tissues (Appendix Fig S5A). Binding was observed in two known FGFR3-dependent cell lines, MCF7 and HepG2 (Qiu et al, 2005; Tomlinson et al, 2012), in some blood-derived cell lines and in one lung cancer-derived cell line. *MYC* activation did not seem to be sufficient to induce FGFR3 regulation. Indeed, *MYC* ChIP-Seq data acquired for two inducible models of *MYC* overexpression/activation (LNCaP and U2OS cells; Walz et al, 2014; Barfeld et al, 2017) showed no *MYC* enrichment on the *FGFR3* enhancers or promoter after *MYC* activation (Appendix Fig S5B and C). Our data therefore identify *MYC* as a master regulator of proliferation activated downstream from FGFR3 (Fig 1) and as a positive regulator of FGFR3 expression in bladder cancer lines (Fig 2A–C). Consistent with this FGFR3/*MYC* positive feedback loop, we also observed that the treatment of RT112 and MGH-U3 cells with a pan-FGFR kinase inhibitor abolished both *MYC* and FGFR3 expression (Fig 2D). This result was confirmed in two other cell lines expressing constitutively activated FGFR3: UM-UC-14 (FGFR3-S249C) and RT4 (FGFR3-TACC3 breakpoint exon 18 FGFR3–exon 4 TACC3, whereas FGFR3-TACC3 breakpoint exon 18 FGFR3–exon 11 TACC3 is expressed in RT112; Williams et al, 2013; Earl et al, 2015; Fig 2D). These four cell lines express low levels of *FGFR1*, *FGFR2*, and *FGFR4*, as assessed with an Affymetrix U133plus2 array, suggesting that the observed effect was mostly due to FGFR3 inhibition (data not shown). However, treatment had no effect on *MYC* and FGFR3 expression in UM-UC-5 cells, which express wild-type FGFR3 (Fig 2D). These results suggest that the FGFR3/*MYC* positive feedback loop is a general mechanism, regardless of the type of FGFR3 alteration, but that it is dependent on activated FGFR3. Using RT112 and MGH-U3 xenograft models treated for 9 days with a pan-FGFR inhibitor, PD173074, which delayed tumor growth (Appendix Fig S6A), we also showed *in vivo* that FGFR3 and *MYC* were involved in a positive feedback circuit inducing bladder tumor growth. Indeed, immunoblot analysis revealed that FGFR3 inhibition resulted in lower levels of both *MYC* and FGFR3 in the xenografts (Fig 2E). Finally, we made use of our PDX model (F659) harboring an FGFR3-S249C mutation to demonstrate that this FGFR3/*MYC* loop was relevant to human tumors. Indeed, the treatment of tumor-bearing mice for 4 days with another pan-FGFR inhibitor, BGJ398, which inhibited PDX tumor growth (Appendix Fig S6B), decreased both *MYC* and FGFR3 levels in the tumors (Fig 2F).

MYC accumulation induced by aberrantly activated FGFR3 in bladder tumors depends on p38 and AKT activation

Given the importance of the FGFR3/*MYC* loop in all our tested models, including the PDX model, we characterized the underlying mechanisms. We investigated the signals downstream from FGFR3

responsible for the observed higher levels of *MYC* mRNA and greater *MYC* protein stability in bladder cancer cells harboring FGFR3 mutations (Fig 1).

We first used transformed NIH-3T3 cells expressing FGFR3-S249C established in a previous study (Bernard-Pierrot et al, 2006) to confirm that mutated FGFR3 expression induced an upregulation of *MYC* mRNA levels (Appendix Fig S7A). We investigated the activation of three pathways known to be activated by tyrosine kinase receptors and, in particular, FGFRs (p38, AKT, ERK1/2; Powers et al, 2000; Appendix Fig S7B), and evaluated their role in the cell transformation induced by mutated FGFR3 (Appendix Fig S7C). We found that the activation of p38 and AKT mediated cell transformation downstream from the mutated FGFR3 whereas ERK1/2 activation was less crucial for FGFR3 activity. It has been established that p38 can induce the stabilization of *MYC* mRNA or the upregulation of *MYC* protein levels through an increase in transcription (Chen et al, 2005) whereas AKT can induce the stabilization of *MYC* protein (Tsai et al, 2012). We thus investigated the involvement of these two pathways in our urothelial models, MGH-U3 and RT112 cells. We showed that p38 and AKT were constitutively activated in both cell lines. This activation was dependent on FGFR3 expression, because it was abolished by *FGFR3* knockdown (Fig 3A). We then explored the role of p38 in the FGFR3-induced upregulation of *MYC* mRNA levels, using a p38 siRNA targeting *MAPK14* (p38 α), the predominant isoform in MGH-U3 and RT112 cells, as shown by Affymetrix U133 plus 2.0 DNA chip analyses (data not shown). Immunoblot analysis showed that the efficient depletion of p38 resulted in the loss of about 50% of *MYC* in both MGH-U3 and RT112 cells, whereas *MYC* loss was total following *FGFR3* depletion (Fig 3B). This decrease in *MYC* levels is consistent with the decrease in *MYC* mRNA levels observed on RT-qPCR 72 h after p38 depletion (Fig 3C), suggesting that p38 plays a key role in *MYC* mRNA regulation but that another pathway downstream from FGFR3 is probably responsible for regulating the stability of the protein (Fig 1).

MYC degradation by the proteasome is regulated by glycogen synthase kinase 3 (GSK3). The activity of GSK3 is regulated by phosphorylation, including that of the Ser9 residue of GSK3 β and the Ser21 residue of GSK3 α , by AKT, in particular (Gregory et al, 2003). In accordance with this mechanism, we demonstrated, in RT112 and MGH-U3 cells, that FGFR3 inhibition with a pan-FGFR inhibitor (PD173074) decreased the phosphorylation of AKT at Ser473 and that of GSK3 β at Ser9 (Fig 3D). We found that PI3-kinase inhibition by LY294002 inhibited AKT phosphorylation and decreased both the phosphorylation of the Ser9 residue of GSK3 β and *MYC* protein levels (Fig 3E). Thus, FGFR3 induces AKT phosphorylation, leading to the inhibition of GSK3 β through Ser9 phosphorylation, thereby preventing the proteasome-mediated proteolysis of *MYC*. Our results thus demonstrate that, downstream from the aberrantly activated FGFR3, both p38 and AKT are involved in the induction of *MYC* accumulation, which, in turn, drives cell proliferation. Consistent with these results for p38, reverse-phase protein array (RPPA) analysis of a panel of 129 tumors showed that p38 was significantly more phosphorylated in tumors expressing a mutated FGFR3 than in tumors expressing wild-type FGFR3 (Fig 3F, left panel). AKT was not differentially phosphorylated in tumors with and without *FGFR3* mutations, suggesting that, in bladder cancer, AKT can be activated by several mechanisms including the aberrant activation of FGFR3,

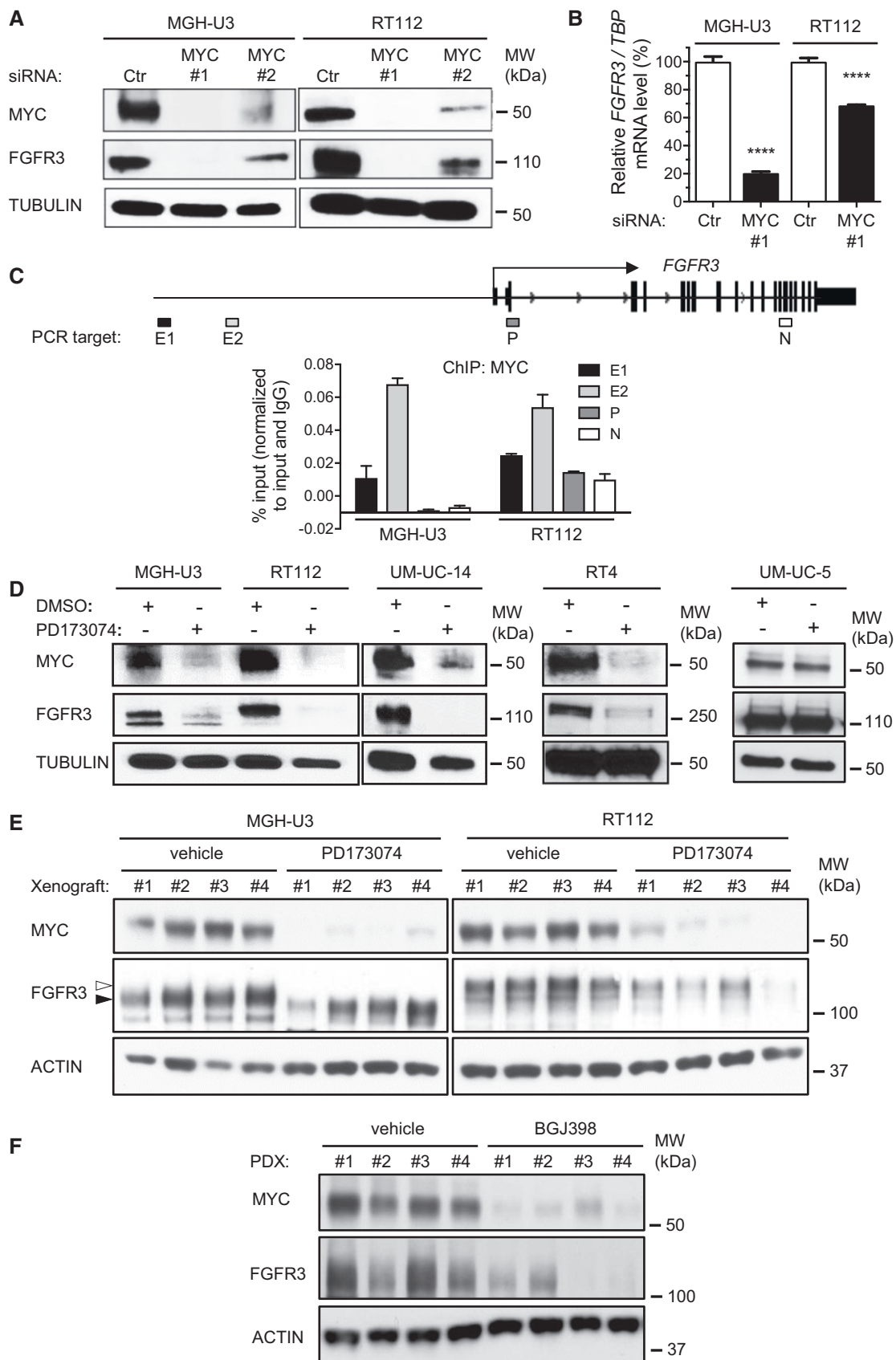


Figure 2.

Figure 2. MYC and FGFR3 are involved in a positive feedback loop in bladder cancer cell lines expressing an activated form of FGFR3.

- A The expression of MYC and FGFR3 was analyzed by Western blotting in lysates from MGH-U3 and RT112 cells transfected for 72 h with MYC siRNAs. Tubulin was used as a loading control.
- B Relative *FGFR3* mRNA levels in MGH-U3 and RT112 cells transfected for 72 h with siRNAs targeting MYC or a control siRNA (Ctr). The results presented are the means of two independent experiments carried out in triplicate; the standard errors are indicated. Unpaired Student's *t*-tests were used for comparison with the control, *****P* < 0.0001.
- C ChIP-qPCR for MYC at the *FGFR3* locus in MGH-U3 and RT112 cells (lower panel). The qPCR target loci of *FGFR3* are schematized (upper panel). Data presented are representative of two replicate experiments. Error bars show standard deviation of three replicate qPCR reactions.
- D RT112, MGH-U3, UM-UC-14, RT4, and UM-UC-5 cells were treated for 48 h with a pan-FGFR inhibitor (500 nM PD173074). Lysates were obtained, and levels of FGFR3 and MYC were analyzed by Western blotting with appropriate antibodies. An anti-tubulin antibody was used as a loading control.
- E MGH-U3 and RT112-derived xenograft tumors from mice treated for 9 days with vehicle or PD173074 (25 mg/kg/day) were lysed and immunoblotted with anti-FGFR3 and anti-MYC antibodies. Actin was used as a loading control. Black and white arrowheads indicate WT FGFR3 and FGFR3-TACC3 bands, respectively.
- F PDX tumors bearing the FGFR3-S249C mutation from mice treated for 4 days with vehicle or BGJ398 (30 mg/kg/day) were lysed and immunoblotted with anti-FGFR3 and anti-MYC antibodies. Actin was used as a loading control.

Source data are available online for this figure.

such as EGFR activation in basal tumors (Rebouissou *et al*, 2014; Fig 3F, right panel). The FGFR3/MYC positive feedback loop involving p38 and AKT activation by FGFR3 identified in bladder cancer cell lines may, therefore, also occur in human bladder tumors with genetic alterations of FGFR3. The disruption of this loop with inhibitors of AKT and p38 may, therefore, constitute an effective way of treating these tumors.

Targeting FGFR3, p38, or AKT is an effective strategy for inhibiting the growth and transformation of bladder cancer cells expressing aberrantly activated FGFR3

We evaluated the effects of p38 and PI3K inhibitors (SB203580 and LY294002, respectively) on the viability of RT112 and MGH-U3 cells (Fig 4A) and on MGH-U3 cell transformation (Fig 4B). The inhibition of these two pathways decreased the viability of MGH-U3 and RT112 cells and the anchorage-independent growth of MGH-U3 cells as efficiently as FGFR3 inhibition with a pan-FGFR inhibitor, PD173074. Using a *MAPK14* siRNA, we confirmed that p38 α depletion decreased the viability of RT112 and MGH-U3 cells and the anchorage-independent growth of MGH-U3 cells (Fig 4C and D). We also validated *in vivo* the critical role of p38 in mutated FGFR3-induced tumor growth, by showing that p38 inhibition with SB203580 significantly slowed the tumor growth of MGH-U3 and RT112 xenografts in athymic nude mice (Fig 4E). An AKT inhibitor has already been shown to decrease MGH-U3 xenograft growth slightly in athymic nude mice (Davies *et al*, 2015).

MYC acts as a key master regulator of proliferation in the FGFR3 pathway, rendering FGFR3-dependent cells sensitive to a BET bromodomain inhibitor (JQ1)

We looked for other ways to disrupt the FGFR3/MYC loop in bladder tumors bearing *FGFR3* mutations. Recent studies have shown that the indirect inhibition of MYC through the targeting of proteins involved in the regulation of its transcription is an effective strategy for treating MYC-dependent tumors (Posternak & Cole, 2016). In particular, several studies have highlighted the use of bromodomain inhibitors as an effective strategy for blocking MYC transcription (Delmore *et al*, 2011; Mertz *et al*, 2011). We therefore focused on JQ1, a potent and well-characterized BET bromodomain inhibitor that inhibits the binding of bromodomain-containing protein 4 (BRD4) to acetylated lysine residues on histones, thereby preventing

transcription. It is particularly active against MYC, the transcription of which seems to be dependent on the binding of BRD4 to its enhancers or “super-enhancers” (Lovén *et al*, 2013). We first analyzed the BRD4 occupancy of the MYC locus by ChIP-qPCR in the RT112 and MGH-U3 bladder cell lines (Fig 5A). Using publicly available data for histone marks, we designed primers binding to one potential enhancer, one control negative region and the promoter (Appendix Fig S8A) and checked that the selected regions harbored the expected histone marks in the RT112 bladder cell line (Appendix Fig S8B). The MYC enhancer was slightly enriched in BRD4, and the MYC promoter was strongly enriched in BRD4. In both cases, this enrichment was prevented by JQ1 treatment (Fig 5A). We then checked, by Western blotting, that JQ1 treatment inhibited MYC and FGFR3 expression, in both cell lines (Fig 5B). The observed inhibition was of similar strength to the FGFR3 inhibition observed with 1 μ M PD173074 (Fig 5B). By contrast, treatment with (–)-JQ1, the inactive enantiomer of (+)-JQ1, had little impact on MYC and FGFR3 levels (Fig 5B). Consistent with this inhibition of MYC and FGFR3 expression following JQ1 treatment, we also showed that JQ1 treatment significantly decreased the viability of RT112 and MGH-U3 cells *in vitro* (Fig 5C). Finally, we showed *in vivo* that JQ1 treatment significantly slowed the growth of MGH-U3 and RT112 xenografts in nude mice (Fig 5D). However, on the one hand, the inhibition of tumor growth by JQ1 treatment was relatively modest. In the other hand, although they slowed tumor growth, FGFR inhibitors did not trigger a regression of tumor size (Appendix Fig S6A). We therefore hypothesized that a combinatorial treatment might improve the response. We tested this hypothesis *in vitro*, on MGH-U3 and RT112 cell viability that made it possible to use ranges of doses for both molecules (Appendix Fig S9A). We found that simultaneous use of the two drugs increased treatment efficacy over that achieved with the two drugs used separately, as highlighted in Fig 5E. A mathematical analysis of our results by the Loewe additivity method (Fouquier & Guedj, 2015) showed that the two drugs had an additive effect in most cases, and possibly even a synergistic effect at some concentrations (Appendix Fig S9B).

Discussion

Alterations of FGFR3 (mutations or translocation) are among the most frequent genetic events in bladder carcinoma, occurring in

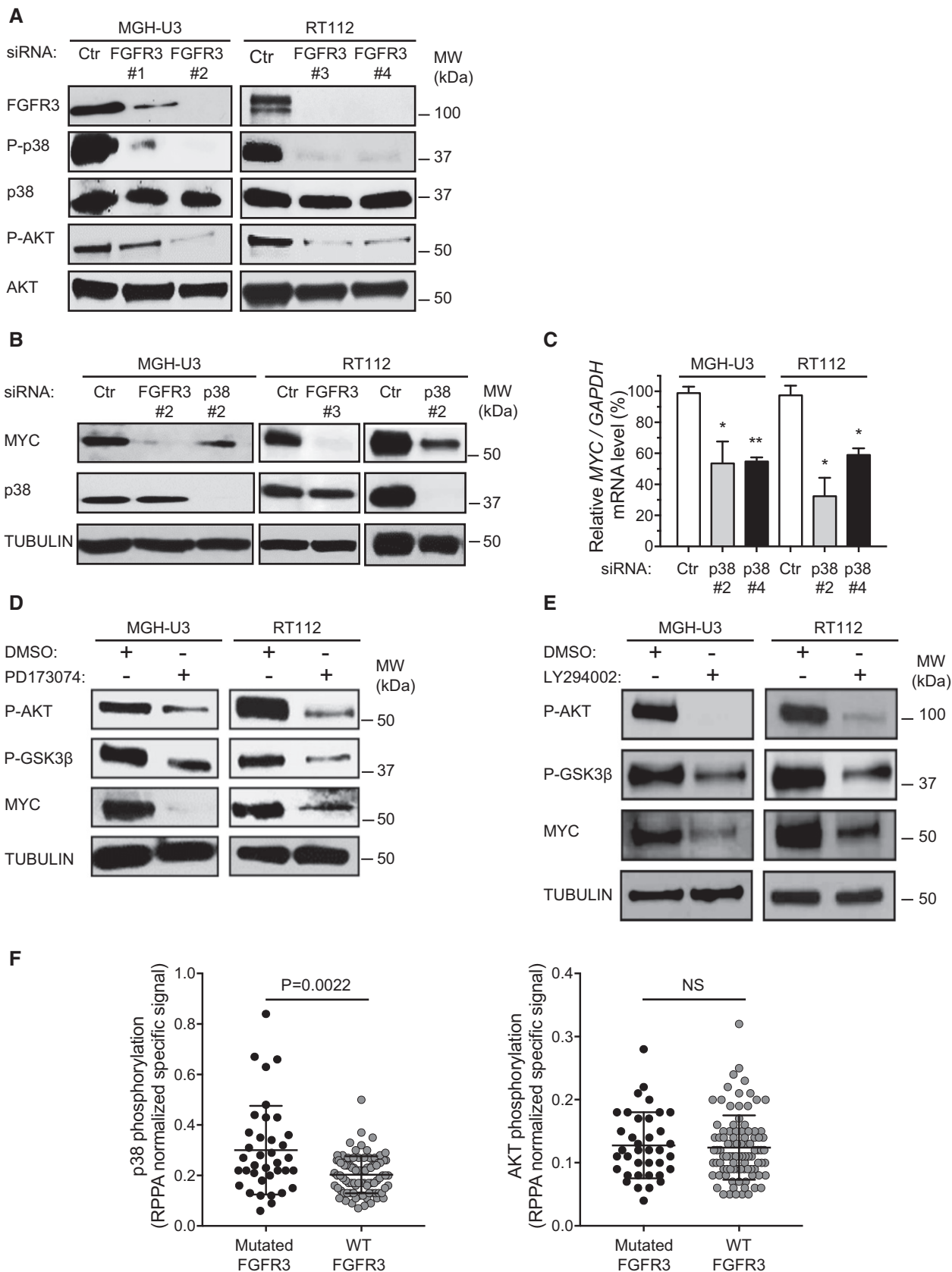


Figure 3.

Figure 3. The MYC accumulation induced by activated FGFR3 is dependent on the activation of p38 and AKT.

- A MGH-U3 and RT112 human bladder tumor cells were transfected with control siRNA (Ctr) or with siRNAs targeting *FGFR3*. Lysates were obtained and the levels of p38, phospho-p38 [P-p38 Thr180/Tyr182], AKT, phospho-AKT (P-AKT Ser473), and *FGFR3* were assessed by Western blotting. Different siRNAs were used in the two cell lines (see Materials and Methods).
- B MGH-U3 and RT112 cells were transfected for 72 h with a siRNA targeting either *FGFR3* or *MAPK14* (p38 α). Lysates were obtained and MYC and p38 protein levels were analyzed by Western blotting.
- C MGH-U3 and RT112 cells were transfected with *MAPK14* (p38 α) siRNA for 72 h. The level of MYC mRNA level was determined by RT-qPCR (left panel). The results presented are the means and standard errors of two independent experiments carried out in triplicate. Unpaired Student's *t*-tests were used for comparison with appropriate siRNA control (Ctr), **P* < 0.05; ***P* < 0.005.
- D MGH-U3 and RT112 cells were treated for 2 h with DMSO or a FGFR inhibitor (0.5 μ M PD173074). Lysates were obtained and analyzed by Western blotting with antibodies against MYC, phospho-AKT (Ser473) and phospho-GSK3 β (Ser9). Tubulin was used as a loading control.
- E Western blot comparing MYC, phospho-AKT (Ser473) and phospho-GSK3 β (Ser9) levels in MGH-U3 and RT112 cells treated for 3 h with a PI3 kinase inhibitor (20 μ M LY294002) or control DMSO. Tubulin was used as a loading control.
- F The level of phosphorylation of p38 (left panel) and AKT (right panel) was assessed by reverse-phase protein array (RPPA) in 129 human bladder tumors, as described in the Materials and Methods. *FGFR3* mutations were present in 38 tumors. No tumor harbored an *FGFR3*-TACC3 or *FGFR3*-BAIAP2L1 fusion gene. Mann-Whitney test was used for comparisons between mutated and non-mutated tumors. Means and standard errors are represented.

about 70% of NMIBCs and 20% of MIBCs. These alterations induce the constitutive activation of FGFR3 and lead to an oncogene dependence to FGFR3. In this study, we characterized further the mechanisms involved in the activity of aberrantly activated FGFR3, highlighting new possibilities for the treatment of bladder tumors with activating alterations of FGFR3. We found that MYC played a crucial role in the aberrantly activated FGFR3 pathway. This transcription factor regulated by FGFR3 was involved in FGFR3-driven cell proliferation in two bladder cancer-derived cell lines expressing FGFR3 (FGFR3-Y375C) or the fusion protein FGFR3-TACC3. We also showed that MYC upregulated FGFR3 expression directly, by binding to enhancers upstream from FGFR3, as part of a FGFR3/MYC positive feedback loop operating both *in vitro* and *in vivo* in bladder cancer-derived cell lines xenografts and in a PDX model bearing an FGFR3 mutation. The FGFR3-driven accumulation of MYC was due to both an increase in MYC mRNA levels and stabilization of the MYC protein. FGFR3 increases MYC mRNA levels by activating the p38 α MAP kinase. FGFR3 also induces stabilization of the MYC protein, by activating AKT, which, in turn, phosphorylates the Ser9 residue of GSK3 β , thereby preventing its interaction with MYC and the degradation of this protein by the proteasome. Finally, our results provide *in vitro* and *in vivo* proof of concept in xenografts that the inhibition of MYC expression, and, in turn, of FGFR3 expression, by an inhibitor of AKT or p38 or a BET bromodomain inhibitor (JQ1) is a potentially effective strategy for the treatment of FGFR3-dependent bladder tumors. The results obtained with FGFR3 inhibitors in one PDX model and in two cell lines xenografts were similar, increasing our confidence in the relevance of our results to human tumors. Based on the results presented here, we devised a model for this newly identified FGFR3/MYC positive feedback loop involved in bladder tumor cell proliferation (Graphical abstract). Interestingly, studies of MYC mRNA levels and of the phosphorylation of p38 and AKT in human bladder tumor samples harboring *FGFR3* mutations suggested that this loop might also operate in tumors. The relevance to human tumors was further supported by the decrease in FGFR3 and MYC levels following anti-FGFR treatment in a PDX model bearing an *FGFR3* mutation. The insight into the aberrantly activated FGFR3 pathway provided by this study could make it possible to identify tumors presenting alterations to this pathway, such as MYC overexpression or p38 activation, in the absence of FGFR-activating genetic alterations. These tumors might also benefit from the alternative therapeutic strategies

proposed in this study for bladder tumors displaying aberrant FGFR3 activation.

We found that FGFR3 activation increased MYC expression and that *FGFR3* was a direct transcriptional target of MYC. This FGFR3/MYC positive feedback loop probably contributes to the higher levels of FGFR3 expression previously observed in human bladder tumors with *FGFR3* mutations (Bernard-Pierrot *et al*, 2006). It has been suggested that this overexpression is also mediated by a loss of microRNAs99/100 targeting *FGFR3* in bladder tumors (Catto *et al*, 2009; Blick *et al*, 2013).

In this study, we searched for transcriptional regulators involved in the regulation of gene expression induced by two types of aberrantly activated FGFR3: a mutated form of the receptor (Y375C) and a fusion protein (FGFR3-TACC3). Specific signaling pathways—PLC γ activation (Williams *et al*, 2013) and localization to the kinetochore (Singh *et al*, 2012)—have been associated with these two forms, but we observed a large overlap between the transcriptional regulators driven by these two types of receptors. Furthermore, both types of receptor acted via the same molecular mechanism, the activation of p38 and AKT, leading to MYC accumulation, resulting in the induction of hyperproliferation. Most of the upstream regulators activated by both types of receptor in this study have also been shown to be regulated by FGFR3-BAIAP2L1, another form of aberrantly activated FGFR3, in RAT2 cells (Nakanishi *et al*, 2015). In both this and a previous study, we found that FGFR3 activation inhibited tumor suppressor pathways involving RB1/RBL1, TP53, or P16 (*CDKN2A*) and activated pro-proliferative pathways involving E2F, CCND1, or TBX2. However, the MYC activation described here was not observed in RAT2 cells. This discrepancy may reflect differences in the technical approach used (inhibition versus overexpression), the species and tissues studied (human epithelium versus rat fibroblast) or the thresholds used to identify genes regulated by FGFR3, and the upstream regulators involved in their regulation.

In a study using a very different approach published during the preparation of this manuscript, MYC was also implicated in pathways involving activated FGFRs in several different types of cancer (Liu *et al*, 2016). This study showed that the altered FGFRs were associated with an increase in MYC protein stability. In one cell line displaying FGFR1 amplification, the authors showed, as suggested by our data for FGFR3 revealing a lack of synergy between MYC and *FGFR3* knockdown, that MYC was the main effector of FGFR1

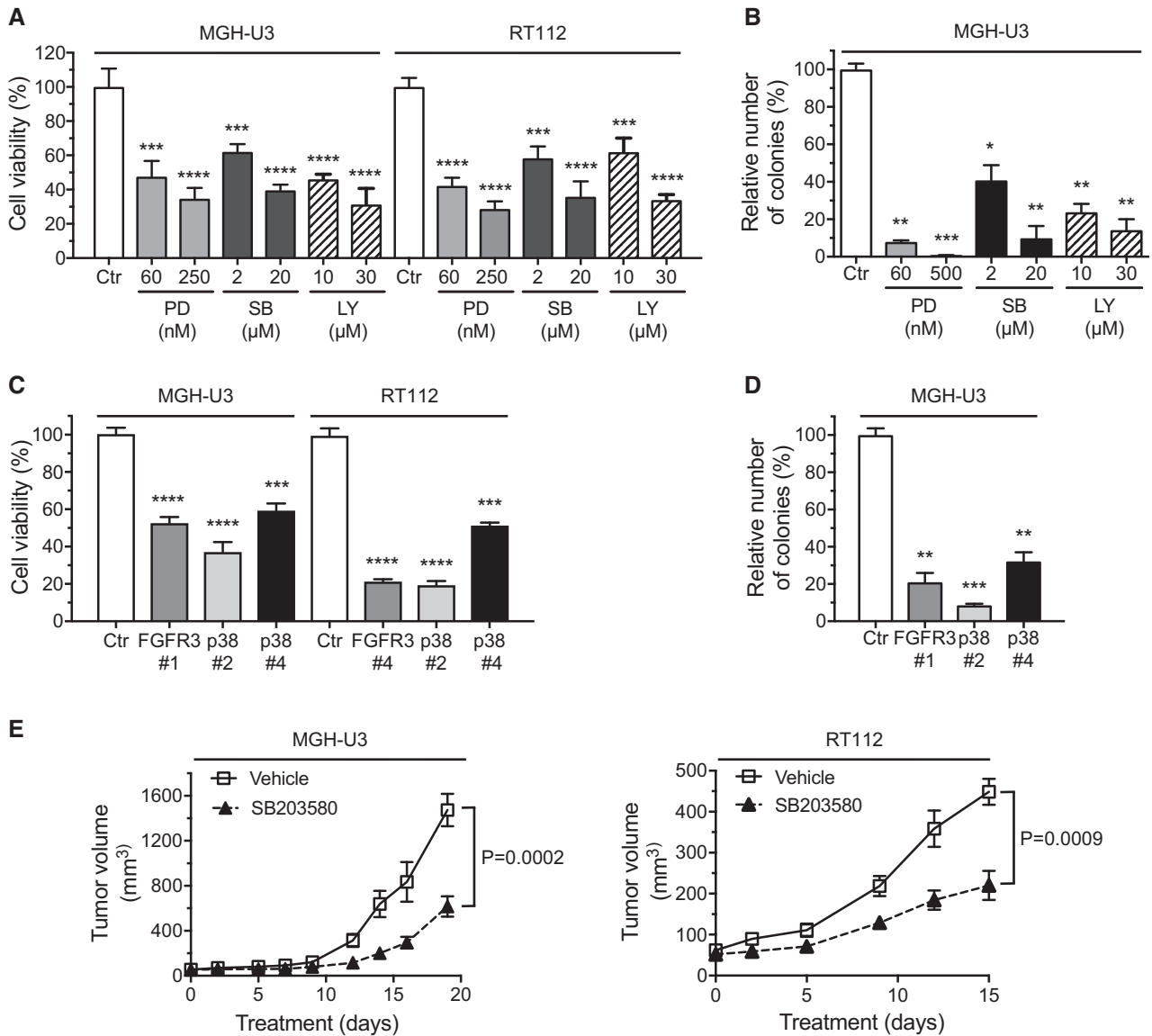


Figure 4. The inhibition of p38 or AKT reduces the growth and transformation of bladder cancer cells expressing aberrantly activated FGFR3.

A MGH-U3 and RT112 cells were treated with control DMSO, PD [PD173074 (FGFR inhibitor)], SB [SB203580 (p38 inhibitor)] or LY [LY294002 (PI3 kinase inhibitor)] for 72 h and cell viability was then assessed by measuring MTT incorporation.

B Impact of PD (PD173074), SB (SB203580), or LY (LY294002) treatment on the cell anchorage-independent growth of MGH-U3 cells. Colonies in soft agar with diameters greater than 50 μm were counted 14 days after seeding in the presence of inhibitors.

C Comparison of the effects of *MAPK14* (p38α isoform) and *FGFR3* knockdown on the viability of MGH-U3 and RT112 cells, as measured by MTT incorporation.

D Soft agar colony formation assay for MGH-U3 cells transfected with siRNA against *FGFR3* or *MAPK14* (p38α isoform). Cells were grown for 14 days before counting.

E MGH-U3 bladder cancer cells were injected into nude mice ($n = 5$ animals/group), two xenografts per animal (one in each flank). Nine days later, the mice received an injection of vehicle or SB203580 (100 μl of 20 μM SB203580) into the tumor, once daily, 6 days per week. Tumor size was measured at the indicated time point, and tumor volume was calculated.

Data information: (A–D) The results presented are the means of two independent experiments carried out in triplicate; the standard errors are indicated. Unpaired Student's *t*-tests were used to assess the significance of differences, * $P < 0.05$; ** $0.001 < P < 0.005$; *** $0.0001 < P < 0.001$; **** $P < 0.0001$. (E) Data are presented as means ± SEM. Results were compared in Mann–Whitney test.

activity, because the effect of FGFR inhibitors was abolished by an undegradable MYC mutant. They suggested that MYC protein stabilization was due to the activation of ERK1/2, rather than AKT as described here. Our results clearly highlighted the crucial role of AKT in sustaining MYC stability through the phosphorylation of

GSK3β. However, we did not study the impact of ERK1/2 inactivation in our FGFR3-dependent bladder tumor models and we cannot, therefore, rule out the possible involvement of this pathway in cooperation with the AKT pathway, as shown for RAS (Sears *et al*, 2000; Yeh *et al*, 2004). Furthermore, we also highlighted the role of

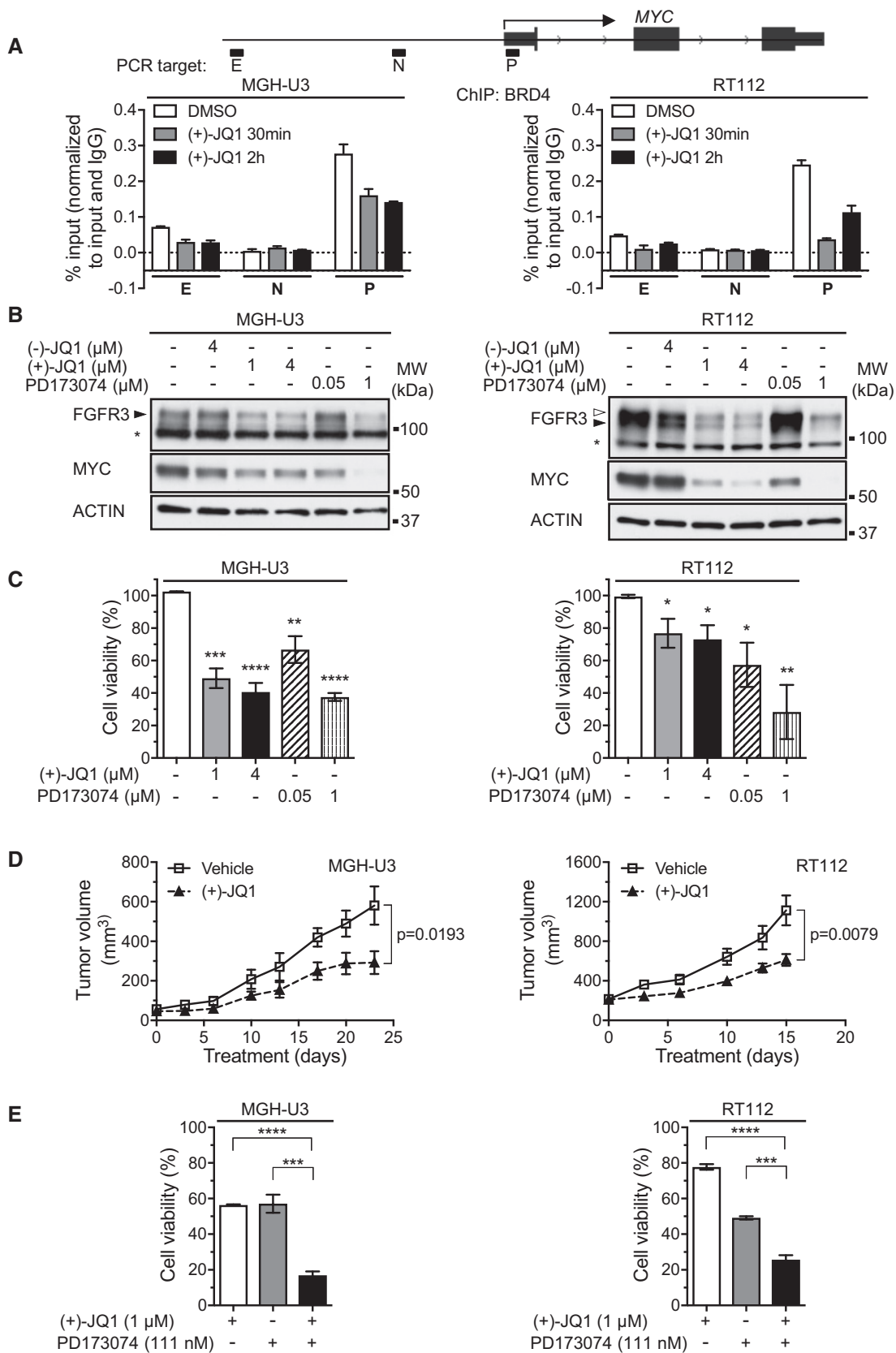


Figure 5.

Figure 5. The MYC accumulation induced by activated FGFR3 confers sensitivity to BET bromodomain inhibitors in FGFR3-dependent bladder cancer cells *in vitro* and *in vivo*.

- A The qPCR target loci for MYC are shown (upper panel). ChIP–qPCR of BRD4 for the MYC locus in MGH-U3 and RT112 cells treated with DMSO or 1 μ M (+)-JQ1 for 30 or 120 min (lower panels). Data presented are representative of two replicate experiments. Error bars show standard deviation of three replicate qPCR reactions.
- B Western blot analysis of MYC and FGFR3 expression in lysates from MGH-U3 and RT112 cells treated with (+)-JQ1 (1 or 4 μ M) for 48 h. Anti-actin antibody was used as a loading control. Pan-FGFR inhibitor, PD173074 (50 nM and 1 μ M), and inactive enantiomer (–)-JQ1 (4 μ M) were used as controls. Black and white arrowheads indicate WT FGFR3 and FGFR3-TACC3 bands, respectively. Asterisk indicates non-specific band.
- C MGH-U3 and RT112 cells were treated for 72 h with DMSO, (+)-JQ1 (1 or 4 μ M) or PD133074 (50 nM or 1 μ M). Cell viability was measured with CellTiter-Glo. Results were compared with those for a DMSO control in unpaired Student's *t*-tests, * $P < 0.05$; ** $0.001 < P < 0.005$; *** $0.0001 < P < 0.001$; **** $P < 0.0001$. Means and standard errors are represented. Three replicates were performed.
- D MGH-U3 and RT112 bladder cancer cells were injected into nude mice ($n = 6$ animals/group), two xenografts per animal (one in each flank). Nine and seven days later, the mice received an injection of vehicle or (+)-JQ1 (IP injection, 50 mg/kg, once daily, 6 days per week), respectively. Tumor growth was assessed twice weekly, by measuring tumor size. Data are presented as means \pm SEM. Results were compared in Wilcoxon's test.
- E MGH-U3 and RT112 cells were treated for 72 h with (+)-JQ1 and PD133074 alone or in combination. Cell viability was measured with CellTiter-Glo. Data are presented as means \pm SD of three experiments carried out in triplicate. Results for the drug combination were compared with those for each individual drug separately, in unpaired Student's *t*-tests, *** $0.0001 < P < 0.001$; **** $P < 0.0001$.

Source data are available online for this figure.

mutated FGFR3, dependent on p38 activation, in the upregulation of MYC mRNA levels both in cell lines and in a PDX model. MYC overexpression which often leads to MYC oncogene addiction has been associated with aggressive phenotype in many tumor types (Dang, 2012; Stine *et al*, 2015). This is not the case in bladder cancer since the majority of FGFR3-mutated tumors are low-stage, low-grade tumors. Furthermore, among FGFR3-mutated tumors, no difference in MYC expression could be observed in MIBC and NMIBC (data not shown). This could be related to a specific FGFR3-induced MYC transcriptomic program in bladder tumors (Kress *et al*, 2015). Consistent with its key role in FGFR signaling, MYC was also recently identified as a potential marker of the anti-FGFR response, because cells expressing both MYC and FGFRs have been shown to be more sensitive to anti-FGFR therapies (Malchers *et al*, 2014; Liu *et al*, 2016). In light of its key role downstream from FGFR, MYC inhibition appears to be a valuable therapeutic strategy for bladder tumors with FGFR3 alterations. MYC has emerged as a clear therapeutic target in other cancers, and many strategies for inhibiting MYC activity through direct or indirect means have been described (Posternak & Cole, 2016). We evaluated the therapeutic potential of BET bromodomain inhibitors, a class of epigenetic modulators that emerged in a clinical setting. We demonstrated that JQ1 prevented BRD4 binding to the MYC promoter and enhancer, thereby inhibiting MYC expression and, consequently, the growth of bladder tumor cells expressing activated forms of FGFR3 both *in vitro* and *in vivo* in xenograft. These preclinical results suggest that bladder tumors with FGFR3 alterations could potentially be treated with BET bromodomain inhibitors. Resistance to monotherapy with BET bromodomain inhibitors has been observed and linked to kinome reprogramming in ovarian cancer (Kurimchak Alison *et al*, 2016) or to a decrease in PP2A activity in triple-negative breast cancer (Shu *et al*, 2016). Resistance to anti-FGFR therapies has also been observed in FGFR3-dependent cells and linked to the activation of ERBB2/3 or EGFR (Herrera-Abreu *et al*, 2013; Wang *et al*, 2015). These observed resistances could be overcome by combination strategies, involving PI3K inhibitors, for example (Wang *et al*, 2017). The use of a combination of a pan-FGFR inhibitor and a BET bromodomain inhibitor induced a stronger growth inhibition as compared to each individual drug *in vitro*. *In vivo* tests for these treatments are currently underway for our PDX model.

We also demonstrated that the activation of both p38 and AKT was critical for the induction of bladder cancer cell proliferation and transformation by FGFR3. This critical role was linked to the ability of these two pathways to induce MYC accumulation, by increasing MYC mRNA levels and by stabilizing the MYC protein, respectively. The role of AKT in cancer progression has been clearly demonstrated for various tumors (Vivanco & Sawyers, 2002), including bladder cancer (Calderaro *et al*, 2014). The role of p38 in cancer is dual, p38 playing both a tumor suppressor role by inducing cell apoptosis and protumorigenic functions depending on the cancer types (Koul *et al*, 2013; Igea & Nebreda, 2015). The opposite functions could be related to cell specificity, nature of the stimuli, the isoform activated since p38 exist as four isoforms or the component downstream p38. p38 can be activated by tyrosine kinase receptors (PDGF receptor, VEGF receptor, EGF receptor, FGFR1) to function as a positive regulator of tumor progression, mediating motility and invasion, suppressing apoptosis, stimulating the epithelial-to-mesenchymal transition in various cell types (Bates & Mercurio, 2003; Frey *et al*, 2004; Nishihara *et al*, 2004). Our results demonstrating that p38 α promotes proliferation, by upregulating MYC mRNA levels are in line with the protumorigenic functions of p38 and with recent studies in breast, head and neck cancers and nasopharyngeal carcinoma (Leelahavanichkul *et al*, 2014; Li *et al*, 2017; Wada *et al*, 2017). The activation of p38 by activated-FGFR3 in bladder tumors contributes to malignant behavior and the inhibition of this activation may be of therapeutic value, as reported for an increasing number of cancers (Koul *et al*, 2013; Igea & Nebreda, 2015).

Our results thus suggest alternative strategies targeting different aspects of FGFR3 signaling that might be beneficial for the treatment of bladder tumors expressing aberrantly activated FGFR3. Targeting two parts of the signaling pathway simultaneously may increase treatment efficacy or delay the development of tumor resistance, as observed clinically in melanomas harboring RAF mutations managed with treatments targeting RAF and MEK (Flaherty *et al*, 2012). It has already been reported that of the simultaneous inhibition of FGFR3 and AKT in MGH-U3 xenograft models increases treatment efficacy over than achieved with either of the two drugs used separately (Davies *et al*, 2015). Such strategies are widely tested in different tumor types and in

particular using pan-FGFR inhibitors. A multi-drug phase II clinical trial including pan-FGFR inhibitor (BGJ398) together with a MEK inhibitor (MEK162) and a RAF inhibitor (LGX818) is currently ongoing in advanced BRAF melanoma (NCT02159066). A phase Ib trial of BGJ398 in combination with BYL719 (PI3K inhibitor) on solid tumors showed encouraging results as eight patients over 24 showed a partial response, among them, one patient with a urothelial carcinoma bearing FGFR3-TACC3 had a complete tumor shrinkage for 4 months (NCT01928459). FGFR3-TACC3 fusion protein expression has been reported in several other cancers, including glioblastoma (Singh *et al*, 2012) and lung adenocarcinoma (Capelletti *et al*, 2014). It would be interesting to determine whether this FGFR3/MYC feedback loop, mediated by AKT and p38, also operates in other types of human cancers expressing FGFR3-TACC3. If so, these treatments could be extended to other cancer types.

Materials and Methods

Cell culture and transfection

The human bladder-derived cell lines RT112, RT4, UM-UC-14, and UM-UC-5 were obtained from DSMZ (Heidelberg, Germany). MGH-U3 cells were kindly provided by Dr. Paco Real (CNIO, Madrid). We mostly used RT112 and MGH-U3 cells. RT112 cells were derived from a transitional cell carcinoma (TCC; histological grade G2) excised from a woman with untreated primary urinary bladder carcinoma. The MGH-U3 cell line was established with cells from a 76-year-old patient with a history of recurrent non-invasive bladder carcinomas (papillary TCC, histological grade G1; Lin *et al*, 1985). MGH-U3 cells harbor a homozygous FGFR3-Y375C mutation and RT112 cells have a FGFR3-TACC3 translocation. A comprehensive genomic characterization of these cells has been reported (Earl *et al*, 2015). MGH-U3, UM-UC-5, and UM-UC-14 cells were cultured in DMEM, whereas RT112 and RT4 cells were cultured in RPMI. Media were supplemented with 10% fetal calf serum (FCS). Cells were incubated at 37°C, under an atmosphere containing 5% CO₂. The identity of the cell lines used was checked by analyzing genomic alterations with comparative genomic hybridization arrays (CGH array), and the *FGFR3* and *TP53* mutations were checked with the SNaPshot technique (for *FGFR3*) or by classical sequencing (for *TP53*), the results obtained being compared with the initial description of the cells. We routinely checked for mycoplasma contamination.

Transfected NIH-3T3 cells expressing the mutated human FGFR3b-S249C receptor (clones S249C1.1, S249C 1.2) or transfected with the control pcDNA1-Neo plasmid (clones Neo1.5, Neo 2.1) were established during a previous study (Bernard-Pierrot *et al*, 2006). They were cultured in DMEM supplemented with 10% newborn calf serum (NCS), 2 mM glutamine, 100 U/ml penicillin, 100 µg/ml streptomycin, and 400 µg/ml G418.

For siRNA transfection, MGH-U3 and RT112 cells were used to seed six-well or 24-well plates at a density of 250,000 cells/well for MGH-U3 cells and 200,000 cells/well for RT112 cells. Cells were transfected with 5 (*FGFR3* siRNA #3 and #4) or 20 nM siRNA in the presence of Lipofectamine RNAi Max reagent (Invitrogen), in accordance with the manufacturer's protocol. siRNAs were purchased

from Ambion and Qiagen. For the control siRNA, we used a Qiagen control targeting luciferase (SI03650353).

The sequences of the siRNAs were as follows:

FGFR3 #1	5'-GCUUUACCUUUUAUGCAA-3' (sense strand)
	5'-UUGCAUAAAAGGUAAGGC-3' (antisense strand)
FGFR3 #2	5'-GGGAAGCCGUGAAUUCAGU-3' (sense strand)
	5'-ACUGAAUUCACGGUCC-3' (antisense strand)
FGFR3 #3	5'-CCGUAGCCGUGAAGAUC-3' (sense strand)
	5'-AGCAUCUUCACGGCUACGG-3' (antisense strand)
FGFR3 #4	5'-CCUGCGUCGUGGAGAACA-3' (sense strand)
	5'-UUGUUCUCCACGACGAG-3' (antisense strand)

FGFR3 siRNA#1 and siRNA#2 targeted exon 19 of *FGFR3* (NM_001163213). They therefore knocked down the expression of wild-type and mutated *FGFR3*, but not of the *FGFR3*-fusion gene containing the first 18 exons of *FGFR3* (Wu *et al*, 2013). Conversely, siRNA#3 and siRNA#4 targeted exons 12 and 6 of *FGFR3* (NM_001163213), respectively, knocking down both wild-type and *FGFR3*-TACC3 expression in RT112 cells.

p38α #2	5'-GGUCUCUGGAGAAUCAA-3' (sense strand)
	5'-UUGAAUUCUCCGAGACC-3' (antisense strand)
p38α #4	5'-CUGCGGUUACUAAACAUA-3' (sense strand)
	5'-UAUGUUUAGUAACCGCAG-3' (antisense strand)
p38α refers to <i>MAPK14</i>	
MYC #1	5'-UCCCGGAGUUGGAAACAATT-3' (sense strand)
	5'-UUGUUUCCAUCUCCGGGATC-3' (antisense strand)
MYC #2	5'-CGGUGCAGCCGUUUUCUATT-3' (sense strand)
	5'-UAGAAUACGGCUGCACCAG-3' (antisense strand)

Cell viability was assessed with the MTT assay (0.5 mg/ml) in 24-well plates, or the CellTiter-Glo assay (Promega) in 96-well plates, 72 h after transfection. Cell lysates were also prepared 72 h after transfection, in six-well plates, for subsequent immunoblotting analysis.

Kinase and protein inhibitors

The inhibitors LY294002, PD98059, SB203580, SU5402, and PD173074 were purchased from Calbiochem (Merck Eurolab, Fontenay Sous Bois, France). MG132 was obtained from Selleckchem (Euromedex, Souffelweyersheim, France). BGJ398 was purchased from LC Laboratories (USA).

The inhibitors (+)-JQ1, (−)-JQ1 and PD173074 (for *in vivo* studies) were purchased from MedChem Express (MedChemtronica, Stockholm, Sweden).

Immunoblotting

NIH-3T3, MGH-U3, RT112, RT4, UM-UC-14, and UM-UC-5 cells were resuspended in Laemmli lysis buffer [50 mM Tris-HCl (pH 6.8), 2 mM DTT, 2.5 mM EDTA, 2.5 mM EGTA, 2% SDS, 5% glycerol with protease inhibitors and phosphatase inhibitors

(Roche)], and the resulting lysates were clarified by centrifugation. The protein concentration of the supernatants was determined with the BCA protein assay (Thermo Scientific, France). Proteins (10–50 µg) were resolved by SDS–PAGE in 10% polyacrylamide gels, electrotransferred onto Bio-Rad nitrocellulose membranes, and analyzed with antibodies against p38 and the phosphorylated form of p38 (Thr180/Tyr182; Cell Signaling Technology # 9212 and # 4511, used at 1/5,000), AKT and the phosphorylated form of AKT (Ser473; Cell Signaling Technologies # 2920 and # 4060, used at 1/5,000), GSK3β (Ser9; Cell Signaling Technology # 5558, used at 1/1,000), MYC (Cell Signaling Technology # 9402, used at 1/1,000), α-tubulin and β-actin (Sigma Aldrich #T6199, used at 1/15,000 and #A2228, used at 1/25,000), or the extracellular domain of FGFR3 (Abcam, # ab133644, 1/5,000). Anti-mouse IgG, HRP-linked, and anti-rabbit IgG, HRP-linked antibody (Cell Signaling Technology # 7076 and # 7074, used at 1/3,000) were used as secondary antibodies. Protein loading was checked by Amido Black staining of the membrane after electrotransfer.

ChIP–qPCR

RT112 and MGH-U3 cells were cross-linked directly by adding 1% formaldehyde to the medium and incubating for 10 min at room temperature. The reaction was stopped by adding glycine to a final concentration of 0.125 M and incubating for 5 min at room temperature. The cells were then harvested. The fixed cells were rinsed twice with PBS, resuspended in extraction buffer [0.25 M sucrose, 10 mM Tris–HCl pH 8, 10 mM MgCl₂, 1% Triton, 5 mM β–mercaptoethanol, protease inhibitors (Roche)] and centrifuged at 3,000 × g for 10 min. We then used the ChIP–IT[®] High Sensitivity kit (Active motif), treating the samples according to the manufacturer's instructions. ChIP was performed with the following antibodies: mouse anti-BRD4 (Bethyl Laboratories A301-985A50), rabbit polyclonal anti-c-MYC (Santa Cruz sc-764), anti-H3K4me3 (Abcam ab8580-25), and anti-H3K27ac (Abcam ab4729) antibodies and the rabbit IgG polyclonal isotype control antibody (Abcam ab37415).

For ChIP–qPCR experiments, quantitative PCR was performed with the SYBR Green PCR kit from Applied Biosystems. Enrichment in ChIPed DNA was calculated as a percentage of the input minus IgG ChIP signal. The sequences of the primers used were as follows:

FGFR3 locus		
E1	AAGATGAGCAAGGCACCTG (forward)	CTCCAGGTCAGAACCAAAGC (reverse)
E2	ACACGCAGGCACACACAG (forward)	AGGGCTTGTGCTTCTCTG (reverse)
P	GCAGGTAAGAAGGGACCCAC (forward)	CGGAATCCGGGCTCTAACC (reverse)
N	ACTCCTTCGACACCTGCAAG (forward)	GTCCTGAAGGTGAGCTGCT (reverse)
MYC locus		
E	TCTTGCCAGACCTAATGCTG (forward)	CCTTGCCACATTGCTTATC (reverse)
N	CAGCTAAATGGCACATAGGC (forward)	ATATTGCCCGGCTAATCTC (reverse)
P	TTCGGGTAGTGGAAAACCAG (forward)	GTGCAATAGCGCAGGAATG (reverse)

Soft agar assay

MGH-U3 cells (20,000), untransfected or transfected with siRNA, were used to seed 12-well plates containing DMEM supplemented with 10% FCS and 1% agar, in triplicate. Cells were cultured in the presence or absence of inhibitors in the agar and culture medium, as appropriate. The medium was changed weekly. The plates were incubated for 14 days, and colonies larger than 50 µm in diameter, as measured with a phase-contrast microscope equipped with a measuring grid, were counted.

RNA extraction from cell lines

RNA was isolated from cell lines with RNeasy Mini kits (Qiagen, Courtaboeuf, France).

Real-time reverse transcription-quantitative PCR

Reverse transcription was performed with 1 µg of total RNA, with the High-Capacity cDNA reverse transcription kit (Applied Biosystems), and *MYC* and *GAPDH* and *TATA-box binding Protein (TBP)* were amplified by PCR in a Roche real-time thermal cycler, with the Roche *Taqman* master mix (Roche) with the Hs00153408_m1, Hs02758991_g1 and 4326322E assays on demand (encompassing primers and *Taqman* probes) purchased from Applied Life Technologies.

DNA array

For the identification of genes displaying changes in expression after the depletion of *FGFR3* in MGH-U3 cells, we transfected the cells for 72 h with *FGFR3* siRNA#1, *FGFR3* siRNA#2 or SMARTpool: ON-TARGETplus *FGFR3* siRNA (Dharmacon, L-0031333-00-0005). For the identification of genes displaying a change in expression after *FGFR3* depletion in RT112 cells, we transfected the cells for 40 h with *FGFR3* siRNA#3 or *FGFR3* siRNA#4. mRNA was extracted and purified with RNeasy Mini kits (Qiagen). Total RNA (200 ng) from control and siRNA-treated MGH-U3 and RT112 cells was analyzed with the Affymetrix human exon 1.0 ST DNA array and the Affymetrix U133 plus 2 DNA array, respectively, as previously described for PPARG-regulated genes (Biton *et al*, 2014). The microarray data described here are available from GEO (<https://www.ncbi.nlm.nih.gov/geo/>) under accession number GSE84733. The LIMMA algorithm was used to identify genes differentially expressed between *FGFR3* siRNA-treated (two and three different siRNAs were used for RT112 and MGH-U3 cells, respectively) and Lipofectamine-treated cells (three replicates; Ritchie *et al*, 2015). The *P*-values were adjusted for multiple testing by Benjamini–Hochberg FDR methods. Genes with a log₂ fold-change of at least 0.58, in a positive or negative direction, with a FDR below 5%, were considered to be differentially expressed.

Human bladder samples

We used protein extracted from 129 human bladder tumors (57 non-muscle-invasive and 72 muscle-invasive tumors) for RPPA analysis (Calderaro *et al*, 2014). The flash-frozen tumor samples were stored at –80°C immediately after transurethral resection or

cystectomy. All tumor samples contained more than 80% tumor cells, as assessed by the hematoxylin and eosin (H&E) staining of histological sections adjacent to the samples used for transcriptome analyses. All subjects provided informed consent, and the study was approved by the institutional review boards of the Henri Mondor, Foch and Institut Gustave Roussy Hospitals. RNA, DNA, and protein were extracted from the surgical samples by cesium chloride density centrifugation, as previously described (Calderaro *et al*, 2014). *FGFR3* mutations were studied with the SNaPshot technique. The expression of *FGFR3-TACC3* and *FGFR3-BAIAP2L1* was analyzed by PCR, as previously described (Wu *et al*, 2013).

Lyophilized proteins were solubilized in Laemmli sample buffer and boiled for 10 min. Protein concentrations were determined with the Bio-Rad Bradford Protein Assay Kit (Bio-Rad, France).

Reverse-phase protein array (RPPA)

Reverse-phase protein array with specific anti-phospho-AKT (S473; Cell Signaling Technology # 4058, used at 1/1,000) and anti-phospho-p38 (T180/Y182; BD Biosciences #612288, used at 1/500) antibodies was performed and analyzed as previously described (Calderaro *et al*, 2014). The specificity of the antibodies used for RPPA for the protein of interest was checked by Western blotting with 18 tumor lysates, before the study. We obtained a Pearson coefficient for the correlation between RPPA and Western blotting of 0.84 for P-AKT (66) and 0.88 for P-p38 (data not shown).

In vivo models

Mouse experiments reported herein were approved by Animal Housing and Experiment Board of the French government.

Xenograft models

Six-week-old female Swiss *nu/nu* mice (Charles River Laboratories) were raised in the animal facilities of Institut Curie, in specific pathogen-free conditions. They were housed and cared for in accordance with the institutional guidelines of the French National Ethics Committee (*Ministère de l'Agriculture et de la Forêt, Direction de la Santé et de la Protection Animale*, Paris, France), under the supervision of authorized investigators. Mice received a subcutaneous injection, into each flank (dorsal region), of 5×10^6 RT112 or MGH-U3 bladder cancer cells in 100 μ l PBS. For each study, with each of the cell lines, mice were randomly separated into two groups when tumors reached a volume of 100 mm³ (± 20). For *FGFR3* inhibition studies, the mice were treated daily for 9 days, by oral gavage with PD173074 (25 mg/kg; $n = 4$) in one group and with vehicle (0.05 M acetate buffer) in the other ($n = 4$). The tumors were then removed. Part of the tumor was flash-frozen in liquid nitrogen for protein extraction in Laemmli buffer. For p38 inhibition studies, one group received daily injections of SB203580 (100 μ l, 20 μ M) into the tumor ($n = 5$), whereas the other group received daily injections of vehicle (PBS; $n = 5$). For JQ1 treatment, mice received a daily intraperitoneal injection of 50 mg/kg JQ1 ($n = 6$) or vehicle (10% DMSO, 90% 10% 2-hydroxypropyl β -cyclodextrin; $n = 6$). For each treatment, the tumor was measured twice weekly with calipers, and its volume in mm³ was calculated with the formula: $\pi/6 \times (\text{largest diameter}) \times (\text{shortest diameter})^2$.

Patient-derived Tumor Xenograft (PDX) model (F659)

A patient-derived bladder cancer xenograft model (F659) was established as follow. A fresh specimen was collected from a patient diagnosed with a muscle-invasive bladder carcinoma with two positive perivesical lymph nodes (pT3bN2Mx), in accordance with French regulations concerning patient information and consent and then xenografted subcutaneously in the interscapular space of 5-week-old male Swiss *nu/nu* mice (Charles River Laboratories) and serially passaged into male Swiss *nu/nu* mice (Charles River Laboratories). DNA was isolated from snap-frozen tumor from the patient and from the PDX tumor (at passage 3 in mice), with a classical phenol-chloroform-isoamyl alcohol extraction protocol. *FGFR3* mutations were studied by the SNaPshot method, as previously described (van Oers *et al*, 2005), and a *FGFR3-S249C* heterozygous mutation was detected in both samples.

For treatment with the pan-FGFR inhibitor, BGJ398, PDX (F659) tumor tissue at passage 4 in mice was cut into small pieces (5 mm³) and subcutaneously xenografted into multiple mice in the interscapular region. When tumor sizes reached 100–200 mm³, mice were randomly divided into two groups and treated by daily oral gavage with BGJ398 (30 mg/kg, LC Laboratories) or vehicle (0.05 M acetate buffer). Tumor growth was measured twice weekly with an electronic caliper, and tumor volume was calculated and expressed relative to the initial size of the tumor. Two experiments were conducted as follows: one for a long-term treatment (29 days; $n = 5$ animal per group) in which tumors were monitored for two additional weeks after the end of treatment, and one for a short-term treatment over a period of 4 days ($n = 4$ animal per group). The mice were sacrificed at the end of the experiments. Their tumors were harvested and flash-frozen. RNA was isolated with Trizol, and proteins were recovered by lysis in Laemmli buffer for subsequent RT-qPCR and Western blot analyses, respectively.

Statistical analysis

Linear models for microarray data (LIMMA) was used to analyze DNA array experiments involving simultaneous comparisons between large numbers of RNA targets (Ritchie *et al*, 2015). All functional experiments were carried out twice or three times, in triplicate. Data are expressed as means \pm SD. Tukey's tests were used for multiple comparisons, and unpaired Student's *t*-tests (two-tailed) or Mann-Whitney *U*-tests were used for other statistical analyses. The control siRNA group, the IgG group, or the vehicle group was used as the reference group, depending on the experiment. The RPPA signals of tumors with and without *FGFR3* mutations were compared in Wilcoxon's rank sum tests. Non-parametric Spearman' rank correlation tests were carried out to evaluate the correlation between levels of *MYC* and *FGFR3* mRNA in human bladder tumors.

Data availability

Transcriptomic data obtained with Affymetrix U133plus2.0 DNA arrays for our CIT-cohorts of bladder tumors, encompassing 82 NMIBCs and 85 MIBCs, were previously deposited on the publicly available ArrayExpress databases E-MTAB-1803 and E-MTAB-1940, respectively (El Behi *et al*, 2013; Biton *et al*, 2014; Rebouissou *et al*, 2014). RNA-Seq data for an independent cohort of 416 tumors were available from ArrayExpress E-MTAB-4321 (Hedegaard *et al*, 2016).

The paper explained

Problem

Bladder cancer is the ninth most common cancer worldwide. FGFR3 alterations (mutations or translocations) are among the most frequent genetic events in bladder carcinoma. They lead to constitutive activation of the receptor and to oncogene addiction to FGFR3. Anti-FGFR therapies have recently yielded promising results, but the efficacy of such targeted therapies is currently limited by the emergence of resistance. In this study, we investigated the molecular mechanisms underlying the oncogenic activity of activated FGFR3 in bladder tumors, with a view to identifying new drug targets to improve treatment efficacy and/or limit resistance.

Results

We identified MYC as a key master regulator of proliferation activated by aberrantly activated FGFR3 in bladder cancer-derived cell lines. We showed that *FGFR3* is a direct target gene of MYC establishing an FGFR3/MYC positive feedback loop. Consistently, we found that human bladder tumors bearing *FGFR3* mutations had levels of *FGFR3* and *MYC* expression that were positively correlated. Further evidence of relevance to human tumors was provided by the use of a PDX model carrying an *FGFR3* mutation, in which FGFR3 inhibition induced a decrease in the expression of both MYC and FGFR3. We demonstrated that this loop was dependent on the activation of p38 and AKT by FGFR3, regulating *MYC* mRNA levels and protein stability, respectively. We showed that p38 and AKT activity were required for FGFR3-induced cell proliferation. Finally, we demonstrated that JQ1, a BET bromodomain inhibitor, was able to prevent *MYC* and *FGFR3* expression. JQ1 treatment significantly decreased cell viability *in vitro* and tumor outgrowth in a xenograft model.

Impact

We have identified a novel FGFR3-MYC positive feedback loop in bladder tumor cell lines harboring aberrantly activated FGFR3, which may be of clinical relevance, because it was also found in a PDX model harboring an *FGFR3* mutation. We also provide the first proof of concept that disrupting this loop with various inhibitors of FGFR3, p38, or AKT or with BET bromodomain inhibitors (JQ1) is of potential therapeutic value. These findings open up new possibilities for the treatment of bladder tumors displaying aberrant FGFR3 activation. The simultaneous inhibition of two targets from the same pathway may increase efficacy and prevent the development of resistance, as reported for the use of BRAF and MEK inhibitors for the treatment of melanoma with *BRAF* mutations.

FGFR3 mutational status and data for eight normal samples were kindly provided by Dr. Ellen Zwarthoff (Erasmus MC Cancer Institute, the Netherlands) and Dr. Lars Dyrskjøl (Aarhus University Hospital, Denmark). The microarray for MGH-U3 and RT112 cells treated with *FGFR3* siRNA are available from GEO (<https://www.ncbi.nlm.nih.gov/geo/>) under accession number GSE84733.

Expanded View for this article is available online.

Acknowledgements

We thank David Gentien and Leanne De Koning from the genomics and RPPA platforms, respectively, of Institut Curie. We thank Ellen Zwarthoff (Erasmus MC Cancer Institute, the Netherlands) and Dr. Lars Dyrskjøl (Aarhus University Hospital, Denmark) for providing *FGFR3* mutations for their cohort of tumors for which transcriptomic data were publicly available and transcriptomic data for eight normal samples, respectively. This work was supported by a grant from *Ligue Nationale Contre le Cancer* (IBP, FR, MM, HNK, RN, CK, MDG) as an

associated team (*Equipe labellisée*), the “*Carte d'Identité des Tumeurs*” program initiated, developed, and funded by *Ligue Nationale Contre le Cancer*, the “LIONS” project funded by INSERM/ITMO Cancer and the “Tumult” project funded by INCa. HNK and VSQ were supported by a fellowship from *Ligue Nationale Contre le Cancer*.

Author contributions

MM, FD, HN-K, CP, FR, and IB-P designed the study. MM, FD, HN-K, AM-V, CB, MS, IH VS-Q, CK, MD-G, and IB-P performed experiments and analyzed data. FD, EC, and RN carried out bioinformatics analyses. CB, HL, and TM established the PDX model. IB-P supervised the study. MM, FD, HN-K, FR, and IB-P wrote the manuscript. All authors made comments on the manuscript.

Conflict of interest

The authors declare that they have no conflict of interest.

References

- Abbosh PH, McConkey DJ, Plimack ER (2015) Targeting signaling transduction pathways in bladder cancer. *Curr Oncol Rep* 17: 58
- Antoni S, Ferlay J, Soerjomataram I, Znaor A, Jemal A, Bray F (2017) Bladder cancer incidence and mortality: a global overview and recent trends. *Eur Urol* 71: 96–108
- Bajorin D, Plimack ER, Seifker-radtke A, Choueiri TK, Wit RD, Sonpavde G, Gipson A, Brown H, Mai Y, Pang L *et al* (2015) Keynote-052: Phase 2 study of pembrolizumab (MK-3475) as first-line therapy for patients with unresectable or metastatic urothelial cancer ineligible for cisplatin-based therapy. *J Clin Oncol* 33: 3475
- Barfeld SJ, Urbanucci A, Itkonen HM, Fazli L, Hicks JL, Thiede B, Rennie PS, Yegnasubramanian S, DeMarzo AM, Mills IG (2017) c-Myc antagonises the transcriptional activity of the androgen receptor in prostate cancer affecting key gene networks. *EBioMedicine* 18: 83–93
- Bates RC, Mercurio AM (2003) Tumor necrosis factor- α stimulates the epithelial-to-mesenchymal transition of human colonic organoids. *Mol Biol Cell* 14: 1790–1800
- Bellmunt J, de Wit R, Vaughn DJ, Fradet Y, Lee JL, Fong L, Vogelzang NJ, Climent MA, Petrylak DP, Choueiri TK *et al* (2017a) Pembrolizumab as second-line therapy for advanced urothelial carcinoma. *N Engl J Med* 376: 1015–1026
- Bellmunt J, Powles T, Vogelzang NJ (2017b) A review on the evolution of PD-1/PD-L1 immunotherapy for bladder cancer: the future is now. *Cancer Treat Rev* 54: 58–67
- Bernard-Pierrot I, Brams A, Dunois-Lardé C, Caillaud A, Diez de Medina SG, Cappellen D, Graff G, Thiery JP, Chopin D, Ricol D *et al* (2006) Oncogenic properties of the mutated forms of fibroblast growth factor receptor 3b. *Carcinogenesis* 27: 740–747
- Billerey C, Chopin D, Bralet M-P, Lahaye J-B, Abbou CC, Bonaventure J, Zafrani S, Kwast TVD, Thiery JP, Radvanyi F (2001) Frequent *FGFR3* mutations in papillary non-invasive bladder (pTa) tumors. *Am J Pathol* 158: 1955–1959
- Biton A, Bernard-Pierrot I, Lou Y, Krucker C, Chapeaublanc E, Rubio-Pérez C, López-Bigas N, Kamoun A, Neuzillet Y, Gestraud P *et al* (2014) Independent component analysis uncovers the landscape of the bladder tumor transcriptome and reveals insights into luminal and basal subtypes. *Cell Rep* 9: 1235–1245
- Blick C, Ramachandran A, Wigfield S, McCormick R, Jubb A, Buffa FM, Turley H, Knowles MA, Cranston D, Catto J *et al* (2013) Hypoxia regulates *FGFR3*

- expression via HIF-1 α and miR-100 and contributes to cell survival in non-muscle invasive bladder cancer. *Br J Cancer* 109: 50–59
- Calderaro J, Rebouissou S, de Koning L, Masmoudi A, Héroult A, Dubois T, Maille P, Soyeux P, Sibony M, de la Taille A et al (2014) PI3K/AKT pathway activation in bladder carcinogenesis. *Int J Cancer* 134: 1776–1784
- Capelletti M, Dodge ME, Ercan D, Hammerman PS, Park SI, Kim J, Sasaki H, Jablons DM, Lipson D, Young L et al (2014) Identification of recurrent FGFR3-TACC3 fusion oncogenes from lung adenocarcinoma. *Clin Cancer Res* 20: 6551–6558
- Catto JWF, Miah S, Owen HC, Bryant H, Myers K, Larré S, Milo M, Rehman I, Rosario DJ, Di E et al (2009) Distinct microRNA alterations characterize high and low grade bladder cancer. *Can Res* 69: 8472–8481
- Chae YK, Ranganath K, Hammerman PS, Vaklavas C, Mohindra N, Kalyan A, Matsangou M, Costa R, Carneiro B, Villaflor VM et al (2017) Inhibition of the fibroblast growth factor receptor (FGFR) pathway: the current landscape and barriers to clinical application. *Oncotarget* 8: 16052–16074
- Chen S, Qiong Y, Gardner D (2005) A role for p38 mitogen-activated protein kinase and c-myc in endothelin-dependent rat aortic smooth muscle cell proliferation. *Hypertension* 47: 252–258
- Dang CV (2012) MYC on the path to cancer. *Cell* 149: 22–35
- Davarpanah NN, Yuno A, Trepel JB, Apolo AB (2017) Immunotherapy: a new treatment paradigm in bladder cancer. *Curr Opin Oncol* 29: 184
- Davies BR, Guan N, Logie A, Crafter C, Hanson L, Jacobs V, James N, Dudley P, Jacques K, Ladd B et al (2015) Tumors with AKT1E17K mutations are rational targets for single agent or combination therapy with AKT inhibitors. *Mol Cancer Ther* 14: 2441–2451
- Delmore JE, Issa GC, Lemieux ME, Rahl PB, Shi J, Jacobs HM, Kastiris E, Gilpatrick T, Paranal RM, Qi J et al (2011) BET bromodomain inhibition as a therapeutic strategy to target c-Myc. *Cell* 146: 904–917
- Earl J, Rico D, Carrillo-de-Santa-Pau E, Rodríguez-Santiago B, Méndez-Pertuz M, Auer H, Gómez G, Grossman HBHB, Pisano DGDG, Schulz WAWA et al (2015) The UBC-40 Urothelial Bladder Cancer cell line index: a genomic resource for functional studies. *BMC Genom* 16: 403
- El Behi M, Krumeich S, Lodillinsky C, Kamoun A, Tibaldi L, Sugano G, De Reynies A, Chapeaublanc E, Laplanche A, Lebret T et al (2013) An essential role for decorin in bladder cancer invasiveness. *EMBO Mol Med* 5: 1835–1851
- Flaherty KT, Infante JR, Daud A, Gonzalez R, Kefford RF, Sosman J, Hamid O, Schuchter L, Cebon J, Ibrahim N et al (2012) Combined BRAF and MEK inhibition in melanoma with BRAF V600 mutations. *N Engl J Med* 367: 1694–1703
- Fouquier J, Guedj M (2015) Analysis of drug combinations: current methodological landscape. *Pharmacol Res Perspect* 3: e00149
- Frey MR, Golovin A, Polk DB (2004) Epidermal growth factor-stimulated intestinal epithelial cell migration requires Src family kinase-dependent p38 MAPK signaling. *J Biol Chem* 279: 44513–44521
- Gregory MA, Qi Y, Hann SR (2003) Phosphorylation by glycogen synthase kinase-3 controls c-myc proteolysis and subnuclear localization. *J Biol Chem* 278: 51606–51612
- Haugsten EM, Wiedlocha A, Olsnes S, Wesche J (2010) Roles of fibroblast growth factor receptors in carcinogenesis. *Mol Cancer Res* 8: 1439–1452
- Hedegaard J, Lamy P, Nordentoft I, Algaba F, Hoyer S, Ulhøi BP, Vang S, Reinert T, Hermann GG, Mogensen K et al (2016) Comprehensive transcriptional analysis of early-stage urothelial carcinoma. *Cancer Cell* 30: 27–42
- Herrera-Abreu MT, Pearson A, Campbell J, Shnyder SD, Knowles MA, Ashworth A, Turner NC (2013) Parallel RNA interference screens identify EGFR activation as an escape mechanism in FGFR3-mutant cancer. *Cancer Discov* 3: 1058–1071
- Igea A, Nebreda AR (2015) The stress kinase p38 α as a target for cancer therapy. *Cancer Res* 75: 3997–4002
- Koul HK, Pal M, Koul S (2013) Role of p38 MAP kinase signal transduction in solid tumors. *Genes Cancer* 4: 342–359
- Kress TR, Sabo A, Amati B (2015) MYC: connecting selective transcriptional control to global RNA production. *Nat Rev Cancer* 15: 593–607
- Kurimchak AM, Shelton C, Duncan KE, Johnson KJ, Brown J, O'Brien S, Gabbasov R, Fink LS, Li Y, Lounsbury N, et al (2016) Resistance to BET bromodomain inhibitors is mediated by kinome reprogramming in ovarian cancer. *Cell Rep* 16: 1273–1286
- Leelahavanichkul K, Amornphimoltham P, Molinolo AA, Basile JR, Koontongkaew S, Gutkind JS (2014) A role for p38 MAPK in head and neck cancer cell growth and tumor-induced angiogenesis and lymphangiogenesis. *Mol Oncol* 8: 105–118
- Li F, Zhao C, Wang L (2014) Molecular-targeted agents combination therapy for cancer: developments and potentials. *Int J Cancer* 134: 1257–1269
- Li A, Shi D, Xu B, Wang J, Tang YL, Xiao W, Shen G, Deng W, Zhao C (2017) S100A6 promotes cell proliferation in human nasopharyngeal carcinoma via the p38/MAPK signaling pathway. *Mol Carcinog* 56: 972–984
- Lin CW, Lin JC, Prout GR (1985) Establishment and characterization of four human bladder tumor cell lines and sublines with different degrees of malignancy. *Cancer Res* 45: 5070–5079
- Liu H, Ai J, Shen A, Chen Y, Wang X, Peng X, Chen H, Shen Y, Huang M, Ding J et al (2016) c-Myc alteration determines the therapeutic response to FGFR inhibitors. *Clin Cancer Res* 23: 974–984
- Lovén J, Hoke HA, Lin CY, Lau A, David A, Vakoc CR, Bradner JE, Lee TI, Richard A (2013) Selective inhibition of tumor oncogenes by disruption of super-enhancers. *Cell* 153: 320–334
- Malchers F, Dietlein F, Schöttle J, Lu X, Nogova L, Albus K, Fernandez-Cuesta L, Heuckmann JM, Gautschi O, Diebold J et al (2014) Cell-autonomous and non-cell-autonomous mechanisms of transformation by amplified FGFR1 in lung cancer. *Cancer Discov* 4: 246–257
- Mertz JA, Conery AR, Bryant BM, Sandy P, Balasubramanian S, Mele DA, Bergeron L, Sims RJ III (2011) Targeting MYC dependence in cancer by inhibiting BET bromodomains. *Proc Natl Acad Sci USA* 108: 16669–16674
- Nakanishi Y, Akiyama N, Tsukaguchi T, Fuji T, Satoh Y, Ishii N, Aoki M (2015) Mechanism of oncogenic signal by the novel fusion kinase FGFR3-BAIAP2L1. *Mol Cancer Ther* 14: 704–712
- Niederst MJ, Engelman JA (2013) Bypass mechanisms of resistance to receptor tyrosine kinase inhibition in lung cancer. *Sci Signal* 6: re6
- Nishihara H, Hwang M, Kizaka-Kondoh S, Eckmann L, Insel PA (2004) Cyclic AMP promotes cAMP-responsive element-binding protein-dependent induction of cellular inhibitor of apoptosis protein-2 and suppresses apoptosis of colon cancer cells through ERK1/2 and p38 MAPK. *J Biol Chem* 279: 26176–26183
- Nogova L, Sequist LV, Perez Garcia JM, Andre F, Delord JP, Hidalgo M, Schellens JH, Cassier PA, Camidge DR, Schuler M et al (2017) Evaluation of BGJ398, a fibroblast growth factor receptor 1-3 kinase inhibitor, in patients with advanced solid tumors harboring genetic alterations in fibroblast growth factor receptors: results of a global phase I, dose-escalation and dose-expansion study. *J Clin Oncol* 35: 157–165
- van Oers JM, Lurkin I, van Exsel AJ, Nijssen Y, van Rhijn BW, van der Aa MN, Zwarthoff EC (2005) A simple and fast method for the simultaneous detection of nine fibroblast growth factor receptor 3 mutations in bladder cancer and voided urine. *Clin Cancer Res* 11: 7743–7748

- Posternak V, Cole MD (2016) Strategically targeting MYC in cancer. *F1000Res* 5: 408
- Powers CJ, McLeskey SW, Wellstein A (2000) Fibroblast growth factors, their receptors and signaling. *Endocr Relat Cancer* 7: 165–197
- Powles T, Eder JP, Fine GD, Braithel FS, Loriot Y, Cruz C, Bellmunt J, Burris HA, Petrylak DP, Teng S-L et al (2014) MPDL3280A (anti-PD-L1) treatment leads to clinical activity in metastatic bladder cancer. *Nature* 515: 558–562
- Qiu WH, Zhou BS, Chu PG, Chen WG, Chung C, Shih J, Hwu P, Yeh C, Lopez R, Yen Y (2005) Over-expression of fibroblast growth factor receptor 3 in human hepatocellular carcinoma. *World J Gastroenterol* 11: 5266–5272
- Ran L, Sirota I, Cao Z, Murphy D, Chen Y, Shukla S, Xie Y, Kaufmann MC, Gao D, Zhu S et al (2015) Combined inhibition of MAP Kinase and KIT signaling synergistically destabilizes ETV1 and suppresses GIST tumor growth. *Cancer Discov* 5: 304–315
- Rebouissou S, Bernard-Pierrot I, de Reyniès A, Lepage M-L, Krucker C, Chapeaublanc E, Héroult A, Kamoun A, Caillault A, Letouzé E et al (2014) EGFR as a potential therapeutic target for a subset of muscle-invasive bladder cancers presenting a basal-like phenotype. *Sci Transl Med* 6: 244ra291
- Ritchie ME, Phipson B, Wu D, Hu Y, Law CW, Shi W, Smyth GK (2015) limma powers differential expression analyses for RNA-sequencing and microarray studies. *Nucleic Acids Res* 43: e47
- Rouanne M, Loriot Y, Lebret T, Soria JC (2016) Novel therapeutic targets in advanced urothelial carcinoma. *Crit Rev Oncol Hematol* 98: 106–115
- Sears R, Nuckolls F, Haura E, Taya Y, Tamai K, Nevins JR (2000) Multiple Ras-dependent phosphorylation pathways regulate Myc protein stability. *Genes Dev* 14: 2501–2514
- Shu S, Lin CY, He HH, Witwicki RM, Tabassum DP, Roberts JM, Janiszewska M, Hun JS, Yi L, Ryan J et al (2016) Response and resistance to BET bromodomain inhibitors in triple negative breast cancer. *Nature* 67: 413–417
- Singh D, Chan JM, Zoppoli P, Niola F, Castano A, Liu EM, Reichel J, Porrati P, Qiu K, Gao Z et al (2012) Transforming fusions of FGFR and TACC genes in human glioblastoma. *Science* 337: 1231–1235
- Stine ZE, Walton ZE, Altam BJ, Hsieh AL, Dang CV (2015) MYC, metabolism and cancer. *Cancer Discov* 312: 2668–2675
- Tcga (2014) Comprehensive molecular characterization of urothelial bladder carcinoma. *Nature* 507: 315–322
- Tomlinson DC, Knowles MA, Speirs V (2012) Mechanisms of FGFR3 actions in endocrine resistant breast cancer. *Int J Cancer* 130: 2857–2866
- Tsai W-B, Aiba I, Long Y, Lin H-K, Feun L, Savaraj N, Kuo TM (2012) Activation of Ras/PI3K/ERK pathway induces c-Myc stabilization to upregulate argininosuccinate synthetase, leading to arginine deiminase resistance in melanoma cells. *Can Res* 29: 997–1003
- Vivanco I, Sawyers CL (2002) The phosphatidylinositol 3-Kinase AKT pathway in human cancer. *Nat Rev Cancer* 2: 489–501
- Wada M, Canals D, Adada M, Coant N, Salama MF, Helke KL, Arthur JS, Shroyer KR, Kitatani K, Obeid LM et al (2017) P38 delta MAPK promotes breast cancer progression and lung metastasis by enhancing cell proliferation and cell detachment. *Oncogene* 36: 6649–6657
- Walz S, Lorenzin F, Morton J, Wiese KE, von Eyss B, Herold S, Rycak L, Dumay-Odelot H, Karim S, Bartkuhn M et al (2014) Activation and repression by oncogenic MYC shape tumour-specific gene expression profiles. *Nature* 511: 483–487
- Wang J, Mikse O, Liao RG, Li Y, Tan L, Janne PA, Gray NS, Wong KK, Hammerman PS (2015) Ligand-associated ERBB2/3 activation confers acquired resistance to FGFR inhibition in FGFR3-dependent cancer cells. *Oncogene* 34: 2167–2177
- Wang L, Sustic T, Leite de Oliveira R, Liefink C, Halonen P, van de Ven M, Beijersbergen RL, van den Heuvel MM, Bernards R, van der Heijden MS (2017) A functional genetic screen identifies the phosphoinositide 3-kinase pathway as a determinant of resistance to fibroblast growth factor receptor inhibitors in FGFR mutant urothelial cell carcinoma. *Eur Urol* 71: 858–862
- Williams SV, Hurst CD, Knowles MA (2013) Oncogenic FGFR3 gene fusions in bladder cancer. *Hum Mol Genet* 22: 795–803
- Witjes JA, Palou J, Soloway M, Lamm D, Kamat AM, Brausi M, Persad R, Buckley R, Colombel M, Bohle A (2013) Current clinical practice gaps in the treatment of intermediate- and high-risk non-muscle-invasive bladder cancer (NMIBC) with emphasis on the use of bacillus Calmette-Guerin (BCG): results of an international individual patient data survey (IPDS). *BJU Int* 112: 742–750
- Wu Y-M, Su F, Kalyana-Sundaram S, Khazanov N, Cao X, Lonigro RJ, Vats P, Wang R, Lin S-F, Cheng A-J et al (2013) Identification of targetable FGFR gene fusions in diverse cancers. *Cancer Discov* 3: 636–647
- Yeh E, Cunningham M, Arnold H, Chasse D, Monteith T, Ivaldi G, Hahn WC, Stukenberg PT, Shenolikar S, Uchida T et al (2004) A signalling pathway controlling c-Myc degradation that impacts oncogenic transformation of human cells. *Nat Cell Biol* 6: 308–318



License: This is an open access article under the terms of the Creative Commons Attribution 4.0 License, which permits use, distribution and reproduction in any medium, provided the original work is properly cited.

RÉSUMÉ

Le cancer de la vessie est le quatrième cancer le plus fréquent chez les hommes en Europe et lorsque la tumeur envahit le muscle vésical (TVIM), le pronostic est très péjoratif. Or, la prise en charge thérapeutique et la survie des patients atteints d'un cancer de vessie a peu évolué pendant de nombreuses années. Récemment, des essais cliniques évaluant l'inhibition de FGFR3 (avec un inhibiteur pan-FGFR) ont montré des effets bénéfiques chez des patients atteints d'une TVIM. FGFR3 est un récepteur à activité tyrosine kinase qui présente des mutations activatrices dans 20% des TVIM appartenant au sous-type luminal-papillaire.

L'objectif de ce projet était d'élucider le réseau de régulation de gènes impliquant FGFR3 dans le cancer de la vessie. Cette étude devrait permettre d'améliorer la compréhension du rôle de FGFR3 dans le développement et la progression du cancer de vessie, d'interpréter les résultats des essais cliniques (réponse et résistance au traitement) et d'ajuster la stratégie thérapeutique actuelle (à travers l'identification de nouvelles cibles). Dans la première partie de mon projet, nous avons construit un réseau de régulation de gènes via un algorithme bioinformatique (H-LICORN) et des données transcriptomiques issues de : (1) lignées de cancer de la vessie exprimant un FGFR3 muté et (2) deux modèles précliniques dans lesquels l'expression de FGFR3 a été altérée.

Dans une seconde partie, le réseau prédit a été validé fonctionnellement en utilisant des données de viabilité cellulaire (criblages à large et petite échelle : CRISPR-Cas9, siRNA). Cette validation nous a permis d'identifier p63 ; déjà décrit comme impliqué dans un sous-groupe de tumeurs basales présentant un faible taux de mutations de FGFR3, en tant que facteur de transcription également impliqué dans la voie du récepteur FGFR3 altéré. Une étude plus approfondie nous a permis de confirmer que p63 contrôle la viabilité, la prolifération, la différenciation et la migration des lignées de cancer de vessie exprimant FGFR3 muté. Ainsi, ces résultats démontrent un rôle inattendu de p63 dans les TVIM luminales enrichies en mutations de FGFR3.

Parallèlement, nous avons caractérisé un modèle murin de tumeurs de vessie surexprimant la forme FGFR3 humain mutée (S249C). Grâce à ce modèle nous avons pu démontrer in vivo le rôle oncogénique de FGFR3 muté dans la vessie. Nous avons confirmé que les tumeurs murines et humaines sont comparables au niveau transcriptomique et histologique, montrant la possibilité d'utiliser ce modèle en recherche translationnelle. Par ailleurs, les résultats de l'étude murine nous ont amené à comparer l'incidence des tumeurs de vessie entre hommes et femmes, révélant un biais important avec une incidence plus élevée chez les patients hommes atteints de tumeurs de vessie exprimant un FGFR3 muté, indépendamment du sous-type tumoral. En outre, nous avons démontré que le récepteur aux androgènes est fortement activé

MOTS CLÉS

Cancer de la vessie, FGFR3, réseaux de régulation de gènes, modèle murin de tumeur, p63.

ABSTRACT

Bladder cancer is the fourth most common cancer in men in Europe and is a deadly disease once it invades the muscle (MIBC). In spite of this, it is only in the last few years that improvement has been made in patient treatment. Recent clinical trials have shown promising results for MIBC following the inhibition of FGFR3 (with a pan-FGFR inhibitor), a receptor tyrosine kinase altered in 20% of MIBC by activating mutations. These alterations are enriched in the luminal papillary subtype of MIBC.

The aim of this project was to characterize the poorly-studied FGFR3 gene regulatory network in bladder cancer, allowing for a better understanding of the role of such receptor in bladder tumorigenesis, an improved interpretation of patient outcome from clinical trials (positive response and resistance) and the identification of new therapeutic targets.

During the first part of this project we constructed a bladder-cancer-specific gene regulatory network using a data mining algorithm (H-LICORN) as well as transcriptomic data coming from: (1) bladder cancer cell lines and bladder tumors expressing a mutated FGFR3 and (2) different preclinical models where the expression or activity of FGFR3 was modulated.

Secondly, the predicted network was functionally validated through the use of large and small gene inactivation screens followed by analysis of cell viability. Such results allowed for the identification of p63, a transcription factor previously described as important in the basal aggressive subtype of MIBC that present a low rate of FGFR3 mutation. Further functional investigation allowed us to confirm that TP63 mediates cell viability, proliferation, differentiation and migration in FGFR3 mutated bladder cancer cell lines in vitro and in vivo. These findings point to a similar yet slightly different role of p63 in basal MIBC and in luminal papillary tumors mutated for FGFR3.

In parallel to the construction and validation of the FGFR3 gene regulatory network, we characterized a mutated FGFR3 transgenic mouse model of bladder carcinoma, that shows for the first time the oncogenic role of an altered FGFR3 in vivo. Reinforcing the potential use of the model for translational research, we confirmed that tumors derived from FGFR3 transgenic mice were at the histologic and transcriptomic levels close to their human counterparts. Additionally, our murine model enabled us to pinpoint a male-dominant tumor incidence in FGFR3 mutated human tumors, observed in all molecular subtypes of bladder cancer. As a possible mechanism explaining such phenomenon, we observed that the androgen receptor (AR) was more active in FGFR3-mutated human tumors (both male and female) compared to FGFR3-wildtype tumors.

KEYWORDS

Bladder cancer, FGFR3, gene regulatory networks, murine bladder tumor model, p63.